Exploring Mechanical Niches Identified by Hair Follicle Compression and How These Transduce Proliferation and Differentiation Cues in Epidermally Derived cells.

JOHNSON, SIMEON,RICHARD

Exploring Mechanical Niches Identified by Hair Follicle Compression and How These Transduce Proliferation and Differentiation Cues in Epidermally Derived cells.

by Simeon Richard Johnson (BSc, MSc)

A thesis submitted at Durham University for the degree of Doctor of Philosophy

SCHOOL OF BIOSCIENCES
DURHAM UNIVERSITY
November 2019

Acknowledgements

I would like to give thanks to my supervisor's Dr Arto Maata and Dr Tim Hawkins for providing guidance and advice throughout this endeavour. I'd also like to thank Mrs Christine Richards and Mrs Helen Grindley for support with electron microscopy and to Mrs Joanne Robson for help with confocal microscopy. I'd like to also thank Dr Mathilde Pele, Dr Nicola Fullard and Mrs Pamela Ritchie for providing advice and guidance on various techniques and experimental designs throughout my program. I'd like to extend a special thankyou to my good friend Dr Patrick Ducknee for his continual and unwavering support throughout this entire process. Finally, I would like to thank our industrial sponsors at P&G for their support throughout the project.

Abstract

In this study the hair follicle structure and surrounding tissue was investigated before, during and after the shaving process in order to better characterise the hair follicle hysteresis (lag in response) observed during the shaving process. Individual hair shafts were loaded with weights designed to mimic the forces generated during the shaving process and deformations in nuclear morphology were used as an indicator of force transduction. Upon identifying distinct mechanical compartments corresponding to regions consistent with the infundibulum, isthmus and suprabulbar regions the study then focussed on elucidating how dermal collagen may facilitate this. Multiphoton microscopy was utilised to interrogate the extrafollicular collagen and the subsequent images were analysed to reveal distinct differences in collagen bundling at the infundibulum, isthmus and suprabulbar regions. To model how heterogeneities in collagen bundling could impact upon epidermal and follicle homeostasis collagen hydrogels were constructed and characterised. Assessment of involucrin and Ki67 levels in HaCaT cells by confocal microscopy revealed elevated proliferation rates in cells on high density (HD) matrices compared with those on low density (LD) matrices which also correlated with increased nuclear volume. HD matrices have smaller collagen bundles and therefor represent a less stiff matrix compared with the low density LD matrices. ERK1/2, JNK and p38 MAPKs have been well reported as effectors on keratinocyte proliferation and differentiation rates in response to mechanical cues and so inhibitors of each were used to identify if these MAPKs were also important in transducing matrix density/stiffness cues that impact upon proliferation and differentiation rates. P38, ERK1/2 and JNK were all found to be important in mediating the proliferation advantage derived from the HD matrices, with JNK being a potential candidate in linking nuclear dynamics with collagen density-mediated proliferation and differentiation rates. JNK was further demonstrated as being the dominant player in transducing the proliferation advantage conferred by the HD matrix.

Contents

List of Figures 1

List of Tables 5

List of Abbreviations 6

1. Introduction 8

1.1 The structure of the Anagen Hair Follicle 10

1.1.1 Overview 10

1.1.2 The Hair Follicle Matrix 14

1.1.3 The Inner Root Sheath Cells 14

1.1.4 The Companion Layer 14

1.1.5 The Outer Root Sheath 15

1.1.6 The Dermal Papilla 16

1.2 Biomechanical Implications of Hair Follicle Organisation 16

1.3 The Hair Follicle Growth Phase: Anagen 17

1.4 An Overview of Skin: Composition, Morphology and Homeostasis 20

1.4.1 Epidermal Homeostasis During Adult Life 20

1.5 An Overview of the Extracellular Matrix 23

1.5.1 Collagen 23

1.5.2 Elastin 24

1.5.3 Fibrillins 24

1.6 An Overview of Mammalian Map Kinase Signalling 25

1.6.1 General Functions of MAPKs 26

1.6.2 MAPKs in Keratinocyte Differentiation 26

1.6.3 MAPKs in Keratinocyte Proliferation 27

1.6.4 An Overview of Integrin Mediated MAPK Signalling 28

1.6.5 Integrins Transduce Via MAPK Signalling Cascades 29

1.6.6 Transduction of Matrix Stiffness in Keratinocyte Derived Cells 30

1.8 The Effects of Mechanical Force on Cell Nuclei....34
1.7 Overall Aims and Goals....36
2.0 Materials and Methods....37
2.1 Chemicals and reagents....37
All chemicals and reagents used are of analytical grade and supplied from Sigma Aldrich UK or BDH Laboratory Supplies unless otherwise stated. 37
2.2 Human Facial and Scalp Skin Preparation for Histological Analysis 37
2.2.1 3-D Printed Support for Biomechanical Studies....37
2.2.2 The Compressive Force Generating Rig....39
2.3 Histology of Human Skin 40
2.3.1 Sample Preparation 40
2.3.2 Image Acquisition....41
2.3.3 Image Analysis....42
2.4 Immunofluorescence of Human Skin 43
2.4.1 Sample Preparation 43
2.4.2 Image Acquisition....43
2.4.3 Image Analysis....44
2.5 Multiphoton Microscopy of Human Skin....45
2.5.1 Sample Preparation 45
2.5.2 Image Acquisition....46
2.5.3 Novel Image Analysis of SHG Signal 46
2.6 Polymerisation of Collagen 3D Gels 48
2.7 Scanning Electron Microscopy (SEM) of Collagen Models. 50
2.7.1 Fixation 51
2.7.2 Dehydration, Critical Point Drying and Sputter Coating....51
2.7.3 Image acquisition....52
2.7.4 Image Analysis....53

2.8 Cell Culture and Treatment of HaCaT Cells....54
2.8.1 Culture of HaCaT Cells....54
2.8.2 Notes on Choice of System to Evaluate Proliferation and Differentiation Rates in Response to Changes in Collagen Density....55
2.8.3 Treatment of HaCaTs With Inhibitors....55
2.9 Immunofluorescence of Collagen Models Seeded with HaCaTs....57
2.9.1 Sample Preparation....57
2.9.2 Image Analysis....58
3.0 Exploring Mechanical Niches Within the Pilosebacious Unit....60
3.1 Keratin and Actin as Mediators of Mechano-Transduction to The Nucleus....60
3.1.1 Keratins, Hemidesmosomes and the ECM....60
3.1.2 Cell-Cell Junctions: Desmosomes and Adherens Junction....62
3.1.3 Keratins, Actin and Nuclear Dynamics....64
3.1.4 The Effect of Mechanical Force on Cell Nuclei....66
3.2 The Effects of Pulling Force on Nuclear Morphology....68
3.2.1 Differential Pull Times Demonstrate Attenuation of Force within the ORS 69
3.2.2 K14 Staining Reveals Changes in The Tissue Architecture of The Outer Root Sheath.....69
3.2.3 Quantification of Nuclei Dimensions (x,y and z) Indicates a Recovery of Nuclear Morphology with Increased Duration of Pull Within the Infundibulum....71
3.2.4 K14 Labelling Reveals Pronounced Wave-Like Compressions Within the ORS of the Isthmus Region Compared with the Infundibulum Region....73
3.2.5 Changes in Nuclear Morphology Implicate the ORS of the Isthmus Region as The Most Compressed Region of The Follicle.....75
3.2.6 K14 Labelling Reveals a Lack of Compression and Thickening of the ORS within the Suprabulbar Region....78
3.2.7 Attenuation of Nuclear Compression Within the Suprabulbar Region of The Follicle....80

3.2.8 Differential Response to Pull Times Demonstrate Differences in Response to Compression Between Undifferentiated ORS Cells and differentiated ORS and IRS cells 82

3.2.9 Increased Pull Duration Widens the IRS Within the Infundibulum Region of the Hair Follicle. 82

3.2.10 Nuclei of the Infundibulum Are Compressed During Pulling 84

3.2.11 Involucrin Labelling Indicates the Isthmus of the IRS Reveals a Lack of Wave-Like Compressions 87

3.2.12 Compression of The Isthmus Region Within the IRS 89

3.2.13 Involucrin Labelling Shows a Homogenous IRS within the Suprabulbar Region of the Follicle 92

3.2.14 Compression within the IRS of the Suprabulbar Region is Alleviated During the 10min hold Indicative of an Opposing Pull During Follicular Compression. 94

3.2.15 Multiphoton Microscopy Reveals Attachments to the Bulb Region of the Follicle 96

3.3.1 The Outer Root Sheath Has Mechanically Distinct Compartments Corresponding to the Infundibulum, Isthmus and Suprabulbar Region 100

3.3.2 The Outer Root Sheath May Help Protect against Nuclear Deformation 104

3.3.3 Cell Stretching Within Suprabulbar Region Could Drive Both Proliferation and Differentiation 106

3.3.4 Continuity between Nuclear Dynamics of the ORS and IRS within The Suprabulbar Region 107

3.3.5 Follicular Compression Could Provide A Route to Propagate Anagen 107

4.1 An Introduction to Collagen and Multiphoton Microscopy 109

4.1.1 Second Harmonic Generation in Collagen 109

4.1.2: Characterisation of Collagen Structures by SEM and MP Microscopy 112

4.2 Interrogation of Collagen Matrices and Human Scalp Skin Using Non-Linear Optical Microscopy Techniques 115

4.2.1 SHG Generates a Signal Intensity Profile Distinct from TPEF 115

4.2.2 Spectral Analysis of Skin Allows for Distinction of Fibrillar Collagens from other Dermal Proteins 122

4.2.3 The Ratio of Collagen to Non-collagenous proteins Implies Differential Collagen Densities within the Dermis Adjacent to Hair Follicles 132

4.2.4 Distances between Intensity Peaks Implies a Reduction in Collagen Fibre Density along the Region of Dermis Corresponding to the Infundibulum to Suprabulbar Region of the Follicle 134

4.2.5 Temperature of Gelation and Concentration of Collagen in Suspension Affect the Density of the Resultant Collagen Matrix 137

4.3 Discussion 147

4.3.1 Analysis of Intensity Peaks Generated by SHG Provides a Novel Means of Assessing Collagen Matrix Density 147

4.3.2 Identification of Collagen Gradient within the Dermis Elucidates Potential Roles for Collagen in Skin Homeostasis and Follicle Homeostasis 148

4.3.4 Putative Elastin Opposes Follicle Elongation-implications in follicle homeostasis and the propagation of anagen..... 150

5.0 Manipulating Collagen Matrices to Provoke Changes in the Proliferation and Differentiation Potential of HaCaT Cells 151

5.1 Introduction to Collagen-Integrin Signalling Mediated by MAPKs; ERK1/2, JNK and p38 151

5.2 Investigating the Role of MAPKs in Communicating Collagen Derived Proliferation and Differentiation Cues 158

5.2.1 Reduced Ki67 Expression in HaCaTs on Low-Density Matrices Implicates Collage Density as a Mediator of Proliferative Cues..... 158

5.2.2 Collagen Reduced Terminal Differentiation Independently of Collagen Density 161

5.2.3 Inhibition of Either p38, ERK or JNK Reduced Ki67 Expression 163

5.2.4 High-Density Matrices Produce an Increase in Nuclear Size and a Reduction in Nuclear Circularity 172

5.2.5: MAPKs Inhibition Impacts Upon Nuclear Morphology 174
5.3 Discussion 180
5.3.1 Collagen Matrix Density Spatially Restricts HaCaTs-Implications in proliferation and differentiation rates 180
5.3.2 p38 Inhibition Suggest Roles Maintenance of the Proliferative Advantage Conferred by High-Density Collagen Substrate in HaCaT Cells 182
5.3.4 ERK Signalling Could Drives the Proliferative Advantage Gained from High-Density Collagen Matrices 183
5.3.5 JNK Signalling Could Counteract ERK1/2 Mediated Proliferation in HaCaTs 184
6 Conclusions and Future Outlook 186
7 References 191

List of Figures

List of Figures

1.1: A schematic overview of an anagen hair follicle ……..…….p11

1.2: The hair follicle cycle……...….p13

1.3: FGF and BMP signalling during the telogen to anagen transition ……..….p19

1.4: Junctional and keratin changes of the epidermis……..….p22

1.5: Canonical Wnt signalling……p32

1.6: Integrin-mediated MAPK signalling that transduces proliferative cues……p33

2.1: CAD design of the skin cassette……...p38

2.2: Hair-pulling rig……p39

2.4: Intensity plots for Masson's trichrome staining……..p42

2.5: Imaging follicle dynamics by multiphoton microscopy……..p45

2.6: Analysis of SHG images……p47

2.7: Micrographs processed by the AnalyzeSkeleton plugin in imagej…….p53

3.1: Disorders associated with defects in hemidesmosomes……..p61

3.2 Desmosomes and adherens junctions……...p62

3.3: Defining the x, y and z axis of the follicle……..p68

3.4: Confocal images of ORS within the infundibulum…….p70

3.5: Dimensional changes of nuclei within the ORS of the infundibulum…….p72

3.6: Confocal images of the ORS within the isthmus……p74

3.7: Nuclear deformations within the ORS of the isthmus……p76

3.8: Confocal images of the ORS within the suprabulbar region……..p79

3.9: Nuclear deformations within the suprabulbar region of the ORS……..p81

3.10: Confocal images of the IRS within the infundibulum…….p83

3.11: Nuclear morphology changes within the IRS of the infundibulum…….p86

3.12: Confocal images of the IRS within the isthmus region…….p88

3.13: Changes in nuclear morphology within the isthmus region of the HF……..p91

3.13: Confocal images of the IRS within the suprabulbar region……..p93

3.15: Nuclear morphology changes within the IRS of the suprabulbar region……..p95

3.16: MP images of whole mount skin……...p96

3.17: Follicular displacement during loading…….p97

3.18: MP images of a follicle under tension……...p98

3.19: MP images of pre-pull vs maximum pull……..p99

3.20: 3D representations of changes in nuclear morphology for the infundibulum.....p100

3.21: 3D representations of changes in nuclear morphology for the isthmus…..…p102

3.22: 3D representations of changes in nuclear morphology for the suprabulbar region...p104

4.1: Depiction of constructive and deconstructive interference……...p112

4.2: Micrographs of collagen hydrogels…….……..p116

4.3: Average pixel intensities for collagen hydrogels…….…….p119

4.4: Pixel correlation analysis of collagen hydrogels……..….p121

4.5: MP spectral scans of scalp skin…….……....p123

4.6: MP intensity plots for a region of dermis……..…p125

4.7: Heat maps illustrating pixel intensity (i.e.0-255) from MP micrographs...…p127

4.8: MP intensity profiles of dermal collagen fibres abutting the follicle……..p129

4.9: Pixel correlation analysis of dermal collagen…….……..p131

4.10: Masson’s trichrome staining of human scalp skin…….p132

4.11: The ratio of SHG to TPEF in extrafollicular dermis……..p133

4.12: Example intensity plots for dermal tissue excited at 840 nm…….p135

4.13: Average distances between collagen bundles adjacent to the follicle……p136

4.14: 3D reconstructions of SHG in collagen hydrogels……..p138

4.15: SHG micrographs taken 50 μm from the surface of each collagen matrix….p139

4.16: The average SHG intensity over a 200 μm depth……...…p140

4.17: SHG signal decay in collagen hydrogels……p141

4.18: SEM micrographs of collagen hydrogels……p142

4.19: Arch-chord characteristics of collagen fibres……..p143

4.20: High magnification SEM micrographs of collagen fibres……..p145

4.21: Average width of collagen fibre bundles.....p145

5.1: A depiction of how substrate stiffness affects integrin-mediated signalling....p153

5.2: MAPKs roles in governing proliferation and differentiation for keratinocytes.....p156

5.3: HaCaTs 24h and 120h after seeding onto LD or HD hydrogels.....p159

5.4: Average Ki67 expression in HaCaTs on LD and HD matrices.....p160

5.5: HaCats 24h and 120h after seeding onto LD or HD hydrogels.....p161

5.6: Average involucrin expression in HaCaTs on LD and HD matrices.....p162

5.7: HaCaT cells labelled for Ki67 post treatment with MAPK inhibitors.....p165

5.8: Average Ki67 expression in HaCaTs post MAPK inhibition.....p166

5.9 HaCaT cells labelled for involucrin post treatment with MAPK inhibitors.....p169

5.10: Average involucrin expression in HaCaTs post MAPK inhibition.....p170

5.11: Nuclear morphology descriptors for cells cultured on HD and LD matrices.....p173

5.12: Nuclear morphology descriptors for cells after 24h MAPK inhibition.....p175

5.13: Nuclear morphology descriptors for cells after 120h MAPK inhibition.....p177

5.14 Phenotypic outputs manifested in HaCaTs as a result of LD and HD collagen.....p181

List of Tables

Table 2.6.1: Recipe for the production of 100ml of reconstitution buffer as described in Artym & Matsumoto, 2010…….....……p48

Table 2.6.2: Constituents of HD and LD collagen matrices…**…….....…..**…p49

Table 2.7.1: Recipe for 0.2M phosphate buffer with a pH of 7.4……..…p51

Table 4: Characterised autoflurofores and their peak excitations and emissions…p124

List of Abbreviations

ADP-Adenomatosis polyopsis coil

BP-Bullous pemphigoid antigen

BMP-Bone morphogenic protein

CD-cluster of differentiation

CK-Caesin kinase

Cp-Companion layer

CtBP- C-terminal binding protein

DS-Dermal sheath

ECM-Extra cellular matrix

ERK-Extra cellular signal regulated kinases

FGF-Fibroblast growth factor

FZD-Frizzled

GSK-Glycogen synthase kinase

HFSC-Hair follicle stem cell

IRS-Inner root sheath

JNK-c-Jun N-terminal kinases

KASH-Klarsicht, ANC-1, Syne homology

LEF-Lymphoid enhancer-binding factor

LINC-Linker of nucleoskeleton and cytoskeleton

LRP-Lipoprotein receptor-related

MAP-Mitogen activated protein

MAPK-Mitogen activated protein kinase

MP-Multiphoton

NADPH-Reduced nicotinamide adenine dinucleotide phosphate

Nesprin-nuclear envelope with spectrin repeats

NP-No pull

ORS-Outer root sheath

PIK-Phosphoinositide kinase

PYK-proline-rich tyrosine kinase

SEM-Scanning electron microscopy

SHG-Second harmonic generation

SHH-Sonic Hedge Hog

SRF-serum response factor

SUN-Sad1p UNC-84

TCF-Transcription factor

TPEF-Two photon excitation fluorescence

TPM-Two photon microscopy

1. Introduction

This thesis is the product of a project with industrial collaboration. The applied questions relate to advancing understanding how the different components of the follicle and extra follicular collagen behave during and after a force has been applied to the follicle. This study also aims to further our understanding of how collagen can act as an extracellular cue to keratinocyte derived cells. To understand the biological implications of these forces it is therefore important to understand how cells mechanically sense and how such sensing could be linked to changes in cellular events.

Our industrial sponsors approached us with a model for how a hair shaft at the surface responds to the shaving process and were interested in understanding the hysteresis of the follicle with respects to the three-stage retraction process; extension of the shaft prior to fracture, followed by an initial rapid retraction (<1 second), followed by a slower retraction (several minutes) before coming to rest. Magnetic resonance images were provided that demonstrated an attachment to the follicle beneath the skin surface, however this revealed little about the dynamicity or composition of the structure.

With limited information available the most logical point to begin with was to address a question that would aid in the modelling of follicular response during the shaving process and providing insight on how such a process may go beyond simple physical ramifications and extend into eliciting biological responses. The first results chapter (3.2) poses a new method for identifying variations in force transduction along the hair follicle through assessment of change in nuclear morphology within three-dimensional space. To understand more about the dynamics of the shaving process and the roles of different tissue compartments in generating the hysteresis observed by P&G, human scalp skin was assessed before follicles were mechanically loaded and after follicles were mechanically loaded for differing times. Recovery of nuclear morphologies to a native conformation suggested both the existence of mechanically distinct regions along the follicle and an opposing pull.

Identification of distinct mechanical units prompted enquiry into uncovering what biological structures could achieve this and what implication this may have for cells within the locale. With collagen being the principle component of the dermis, the

decision was made to interrogate the structure of collagen using multiphoton microscopy techniques as detailed in 4.2. This label-free imaging technique has been used in the past to image collagen via the elicitation of second harmonic generation (SHG). Collagen comprises repetitive units of non-centrosymmetric molecules making it an ideal candidate for SHG. The first obstacle was to establish and identify the SHG signal ensuring the theory reported in the literature married up with the practical application. Following this a novel type of analysis was developed to identify variations in collagen bundling adjacent to the dermal sheath (methods 2.5.3).

Identification of correlation between heterogeneities in collagen bundling (adjacent to the follicle) and localised differences in the level of nuclear deformation produced in response to mechanical loading (4.2), highlighted a clear link between matrix density and nuclear deformation. A recent study addressed how restriction of available substrate drove terminal differentiation with ample substrate producing elevated proliferation rates. Importantly it was noted that the substrate composition with respects to collagen I, fibronectin and laminin was also inconsequential to the experimental outcome. The key factor was the area of available substrate (Gadhari et al. 2013; Connelly et al. 2010; Gupta et al. 2016). It therefore stands to reason that the outcome is derived from changes in cellular tensegrity as a product of substrate restriction (in the context of area available). What is not considered across the many studies is how the stiffness of a substrate and by proxy, cellular tensegrity, could impact upon proliferation and differentiation rates.

As the stiffness of a micropatterned plate would be constant irrespective of the number of ligands adhered to the surface it was important to address how substrate stiffness may impact upon proliferation and differentiation rates. It was therefore essential to first develop and characterise collagen matrices that would exhibit differing stiffness (chapter 5.0). Although the stiffness was not quantified by atomic force microscopy there is sufficient evidence from other studies that demonstrates how increased bunding of collagen fibres leads to increased stiffness (Gosline et al. 2002; C.-K. Hsu et al. 2018; Voorhees et al. 2015; O. V. Kim et al. 2017; S. C. Wei et al. 2015; Chaudhuri et al. 2014; Wen et al. 2014; Hofmann et al. 1984). Two matrices referred to as LD and HD were generated using controlled conditions. LD matrices are indicative of fewer fibres per unit area but increased bundling and therefore increased stiffness with HD matrices being the opposite. Ki67 and Involucrin were

then used as markers to assess the impact of substrate derived stiffness on proliferation and differentiation rates and this data was then correlated against changes in nuclear morphology. This posits a possible biophysical link between changes in nuclear morphology and proliferation/differentiation rates demonstrating the biological significance of mechanically distinct regions along the follicle and how substrate derived tissues tensegrity can impact upon proliferation and differentiation rates, governing tissue homeostasis.

1.1 The structure of the Anagen Hair Follicle

1.1.1 Overview

Hair follicles are comprised of two principal regions; an upper non-cycling portion and a lower cycling portion. Longitudinally the hair is divided into four regions; the bulb, suprabulbar, isthmus and infundibulum (figure 1.1). The cycling portion of the follicle is represented by the bulb and suprabulbar regions whilst the non-cycling region i.e. from the bulge cells upward, comprises the isthmus and infundibulum 1(Langbein & Schweizer 2005, Sperling 1991). During catagen the cells of the bulb and suprabulbar regions undergo a programme of cell death allowing the dermal papillae to move upward, eventually abutting the bulge cells (Stenn et al. 1996; Müller-Röver et al. 2001).

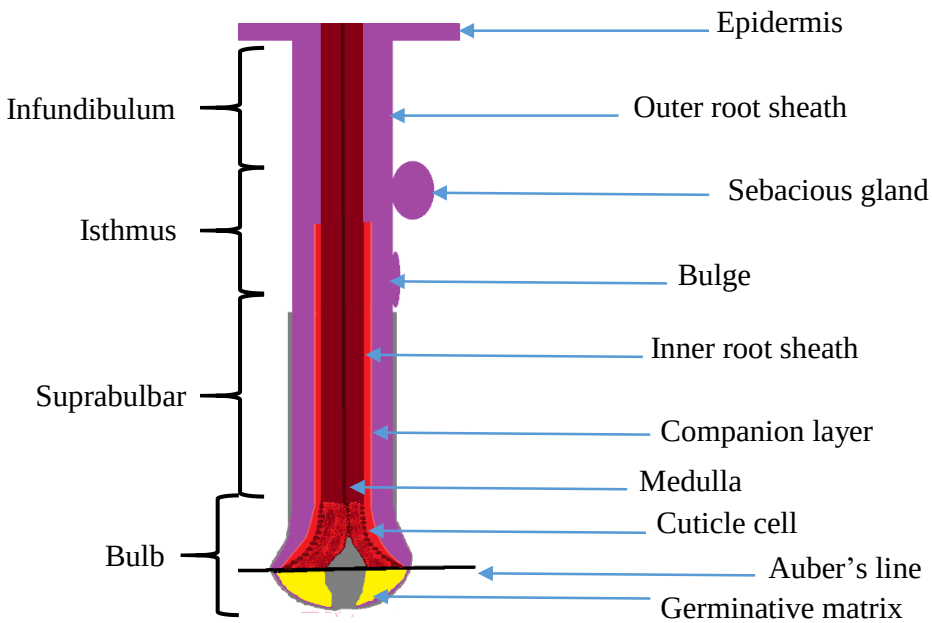

Figure 1.1: A schematic overview of an anagen hair follicle. The infundibulum region spans from the epidermis to the upper most part of the sebaceous gland. The infundibulum then follows on from the top of the sebaceous gland down toward the base of the bulge. The suprabulbar region extends from the base of the hair follicle bulge cells to the upper most part of the bulb region. The bulb region is composed of undifferentiated multipotent cells (germinative matrix) and cells that have entered programmes of terminal differentiation i.e. those above the line of Auber. The cells of the matrix receive cues from the dermal papilla (grey), instructing lineage. The cycling portion of the follicle is encased by the collagen rich dermal sheath (grey) that is continuous with the basement membrane.

The cycling portion of the follicle undergoes morphological changes as it passes through phases of growth (anagen), apoptosis (catagen) and metabolic quiescence (telogen) (figure 1.2) (Rebecca J Morris et al. 2004; Y.-C. Hsu, Pasolli, and Fuchs 2011b; Millar 2002; L Li et al. 1992). During anagen, cells from the hair follicle stem cell niches (bulge and secondary hair germ), are stimulated by the dermal papillae to produce transit amplifying cells that migrate down the outer root sheath, into the matrix of the hair bulb where they form the hair germ and undergo proliferation (within the germinative matrix) and eventual differentiation to produce the hair shaft, inner root sheath and companion layer (figure 1.1). The cells of the proliferative matrix form micro-niches as a result of morphogen gradients generated by the SHH produced from the K6 positive cells of the matrix and both BMPs and FGFs form the dermal papillae and surrounding fibroblasts and adipocytes. The proportion by which these cues converge on the undifferentiated cells will dictate the lineage resulting in the differentiation of the concentric layers of the hair follicle (Reddy et al. 2001; Huelsken et al. 2001; L.-H. Gu and Coulombe 2007a; J. Zhang et al. 2006; Chiang et al. 1999; V. Levy et al. 2005; Vidal et al. 2005; Y.-X. Su, Hou, and Yang 2014; Blanpain and Fuchs 2006a; Legué and Nicolas 2005; Rompolas, Mesa, and Greco 2013). The outer root sheath is derived directly from the bulge cells (Cotsarelis, Sun, and Lavker 1990; Vidal et al. 2005; Merrill et al. 2001; Jaks et al. 2008; P. Wong and Coulombe 2003; Füllgrabe et al. 2015; Rompolas and Greco 2013). The three central lineages; the medulla, cortex and cuticle cells form the hair shaft itself, and undergo differentiation above ‘the line of Auber’; an imaginary line that extends through the widest portion of the dermal papillae below which cells are largely undifferentiated (Auber 2012; Rompolas and Greco 2013; Folgueras et al. 2013; Snippert et al. 2010; Langbein et al. 2010). The basement membrane resides at the mesenchymal-epithelial interface, providing a strong substratum that confers mechanical strength to the dermis while protecting the underlying mesenchyme. Continuous with the dermal papillae is the dermal sheath that encases the bulb and suprabulbar components of the follicle.

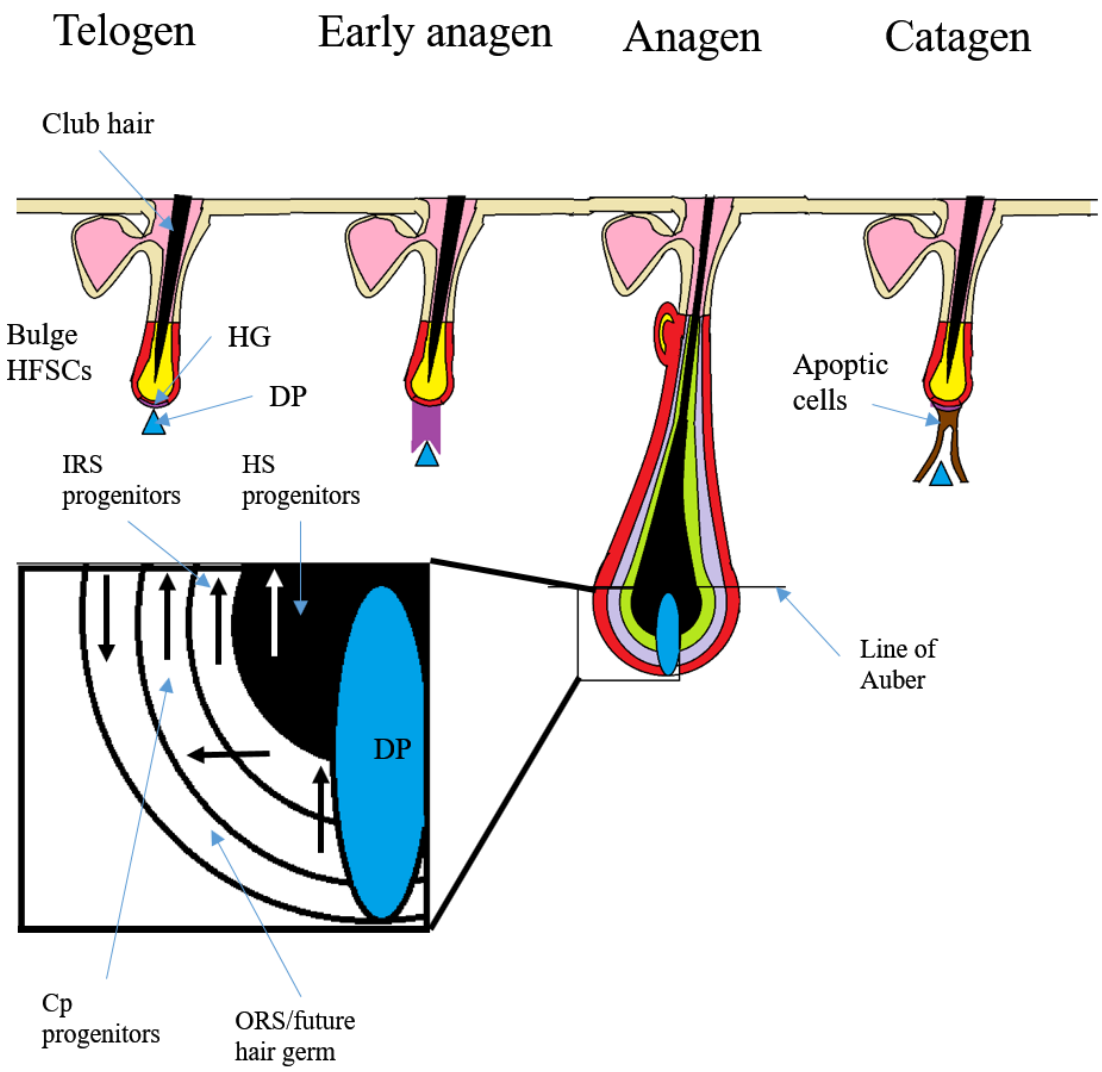

Figure 1.2: The hair follicle cycle. HFSC-hair follicle stem cells, HG-hair germ, DP-dermal papilla. Red-ORS, Purple-CL, Green-IRS, Black-hair shaft.

During telogen bulge cell HFSCs are in a state of quiescence maintained by K6 positive bulge cells and surrounding adipocytes and fibroblast that signal via diffusible BMPs to retain quiescence. The dermal papillae produce BMP inhibitory cues known as FGFs which cause entry into anagen as bulge HFSCs become Wnt high causing symmetric division and down-growth of the ORS (red) and hair germ (purple). This pushes the DP further from the bulge HFSC niche. Multipotent HFSCs within the germinative matrix still receive BMP inhibitory cues from the DP causing the growth of the hair bulb and propagation of anagen. As cells migrate further from the DP, they undergo programmes of cellular differentiation. forming the concentric layers of the follicle (IRS-green, Cp-purple, and ORS-red). Signalling cues (BMPs)

from the surrounding adipocytes and fibroblasts counterbalance SHH production within the germinative matrix resulting in programmed cell death and entry into of catagen. BMP inhibitory cues from the dermal papillae become proximal to the bulge HFSCs once again triggering anagen.

1.1.2 The Hair Follicle Matrix

The matrix cells comprise seven lineages that terminally differentiate to produce the hair shaft; medulla, cortex, hair cuticle and the inner root sheath cuticle, inner root sheath (Huxley and Henle layers) and companion layer. These multiple lineages can be simplified into two larger groups, the hair shaft, and the inner root sheath-companion layer complex. The length of the hair fibre is determined by the duration of the anagen cycle and its width is proportional to the diameter of the dermal papilla (Van Scott and Ekel, 1958; Ibrahim and Wright, 1982; Elliott, Stephenson and Messenger, 1999).

1.1.3 The Inner Root Sheath Cells

Above Auber's line the medulla, cortex, and hair cuticle cells are encased by the inner root sheath which can be subdivided into three further layers; the inner root sheath cuticle, Huxley and Henley layers (Sengel and Mauger 1976; Langbein et al. 2010). During anagen the three layers of the inner root sheath terminally differentiate, exhibiting extensive desmosomal remodelling and unique expression of keratins (Nanba, Hieda, and Nakanishi 2000; Donetti et al. 2004). The inner root sheath undergoes proteolytic separation by matriptase action at the level of the isthmus to enable the hair shaft to grow into the hair canal, emerging from the skin without becoming ingrown (K List and Haudenschild 2002; Karin List et al. 2006).

1.1.4 The Companion Layer

The outermost matrix derived layer is the companion layer, derived from the upper most matrix cells (Paus et al. 1999; Müller-Röver et al. 2001). The companion layer is heavily anchored to the Henley layer via an array of desmosomes. Both the Henley and companion are further anchored to the growing hair follicle via cytoplasmic extensions generated in the Henley that extend through all three layers to create the inner root sheath complex. The more expansive complex, referred to as the Flügelzellen, was identified as a barrel structure using electron microscopy (Clemmensen, Hainau, and Hansted 1991). The inner root sheath-companion layer

complex moves with the hair until it reaches the isthmus where the cells are apoptosed and sloughed off within the follicle canal (M Ito 1986, 1988; Langbein et al. 2002; Z. Wang et al. 2003). The companion layer is also anchored to the outer root sheath via desmosome that undergo dynamic reorganisation to effectuate migration of matrix cells from the bulb region up the follicle i.e. As the matrix cells terminally differentiate to form the hair shaft they migrate upward. The associated inner root sheath cells must therefore move in line with the matrix cells requiring junctional rearrangement (Hanakawa et al. 2004; M Ito 1986; Winter et al. 1998). Desmogleins 1 and 3 have been demonstrated as crucial components of the desmosomes of the companion layer in mice that creating a linkage to the outer root sheath and inner root sheath with loss of these resulting in loss of anagen hairs (Hanakawa et al. 2004). Hanakawa also found that the separation between the outer root sheath and inner root sheath occurred at a level where loss of the anagen hair preserved proliferating matrix keratinocytes within the follicle.

1.1.5 The Outer Root Sheath

Derived directly from bulge cells, the outer root sheath is the outermost epithelial compartment. Isolated outer root sheath cells from the suprabulbar and bulbar region have been cultured to form “autologous epidermal equivalents” (Tausche et al. 2003). Additional studies demonstrated that label retaining cells can be found migrating along the outer root sheath to form the germinative matrix of the bulb region (Cotsarelis, Sun, and Lavker 1990; Ohyama et al. 2006; L.-H. Gu and Coulombe 2007b; Heidari et al. 2016; Takeo, Lee, and Ito 2015; Aragona et al. 2017). In this context the outer root sheath appears to behave as a highway for cells to move between the bulge and matrix to regenerate the hair follicle at the onset of anagen. The high colony forming capacity of the outer root sheath cells demonstrate how this epithelial compartment is utilised for the trafficking of transit amplifying cells to form the matrix while the ability to form epidermis *in vivo* suggests this layer also provides a highway to the epidermis to aid in maintenance of the interfollicular epidermis (Oshima et al. 2001; Alexandrescu, Kauffman, and Dasanu 2009; Tausche et al. 2003; Commo, Gaillard, and Bernard 2000; Heidari et al. 2016; Aragona et al. 2017). The bimodal functionality of the outer root sheath cells is also likely to play a role in wound healing, where the properties of proliferation and stemness contribute toward the replacement of lost epidermis and epidermal homeostasis (Argyis and Trimble,

1964; Coulombe, Kopan and Fuchs, 1989; Guo, Degenstein and Fuchs, 1996; Ito *et al.*, 2005). More recent lineage tracing studies and Cre-inducible systems have shown outer root sheath cells to migrate outward from the pilosebaceous unit and into the epidermis upon wounding, contributing to the regeneration of the interfollicular epidermis. However, they are not essential for epidermal homeostasis nor reepithelialisation of wounds as illustrated in absence of this function. In this sense the outer root sheath cells can be seen as providing a recovery advantage and source of progenitors in the event of wounding. Absence of stem cells within the ORS has been demonstrated as causing delayed re-epithelisation after wounding (S Werner et al. 1994; Ansell et al. 2011; Tscharntke et al. 2007; Garcin and Ansell 2017; Lough et al. 2013).

1.1.6 The Dermal Papilla

The dermal papilla is a derivative of the dermal condensate that is a key player in the epithelial-mesenchymal interactions during morphogenesis. It is pivotal in orchestrating placode formation via its interaction with the overlying epithelium providing BMP inhibitory cues (SHH), resulting in eventual down growth of the epithelial placode cells into the primitive mesenchyme (putative dermis) (Tsai et al. 2014; Y. Zhang et al. 2008; Millar 2002). Many of the inductive properties observed by the dermal condensate during development are also evident postnatal; in particular the ability to propagate anagen via stimulation of the secondary germ and bulge cells (Kulessa, Turk, and Hogan 2000; J. Zhang et al. 2006; Oshimori and Fuchs 2012).

The dermal papilla is closely associated with the bulge derived matrix cells, separated only by a basement membrane, enabling for easy passage of diffusible cues that in part mediate the differentiation of the various terminal lineages of the hair follicle. Extending out from the dermal papilla and encasing the bulbar/suprabulbar region of the follicle are the trichogenic dermal sheath cells, so called due to their capacity to enhance follicular regeneration in the event of damage to the lower cycling portion of the follicle i.e. can produce follicles *de novo* (Yamao et al. 2015).

1.2 Biomechanical Implications of Hair Follicle Organisation

Throughout anagen the inner root sheath is anchored to the outer root sheath via an interface with the companion layer. This interface is known to exhibit dynamic changes in adhesion with respect to anagen, catagen and telogen for the cycling

portion of the follicle. The dynamic nature of this anchorage was investigated via the ablation of cell-cell junctions known as desmosomes. It was shown that the co-expression of desmogleins 1 and 3 at the IRS-Cp-ORS interface was responsible for hair shaft anchorage during anagen (Langbein et al. 2010).

Cuticle ruffling has been observed on plucked hairs that would coincide with a level consistent with the infundibulum. It has been proposed that this highly keratinized layer could provide a degree of elasticity or dampening to the retraction of the shaft back into the follicle (Chapman 1997). However, the study that inferred this lacked any form of imaging that could capture the dynamics that might imply this relationship. These studies do not however consider the role of the abutting tissues, namely type 1 collagen in hair follicle anchorage and hysteresis. Neither do they consider the structural difference of the different follicular compartments.

A key feature at the onset of anagen is the down-growth of the proliferative matrix to reform the bulb and suprabulbar regions. Pulse chase experiments show cells initially migrating down into the hypodermis along the outer root sheath, reforming the matrix of the hair follicle. The cells then proliferate, differentiate and migrate in the opposite direction to produce the mature hair shaft (Y.-C. Hsu, Pasolli, and Fuchs 2011a; Lough et al. 2013; Rompolas and Greco 2013). Much attention has been given to diffusible cues as being key governing factors in this morphological event. However, it must be considered that the physical environment plays a role in governing the polarity of cells during this morphogenic event as cellular tensegrity could be affected by changes in extracellular matrix composition and tensioning. For example, different collagen environments within the skin may be a factor in establishing polarity for cells within the follicle.

1.3 The Hair Follicle Growth Phase: Anagen

Anagen is the process in which the cycling portion of the follicle is regenerated from multipotent stem cells found within the bulge stem cell niche. These cells are stimulated to divide symmetrically by the dermal papilla (DP) resulting in expansion of the outer root sheath (L.-H. Gu and Coulombe 2007b; Rabbani et al. 2011; V. Levy et al. 2005; Paus, Stenn, and Link 1989; J. Zhang et al. 2006; Z. Wang et al. 2003). As a consequence, the DP is pushed further from the bulge HFSC niche preventing signalling between the DP and bulge. Cells within the bulge become quiescent whist

HFSCs in contact with the DP are continually stimulated by the DP resulting in growth of the hair bulb and establishment of the germinative matrix from which all components of the hair shaft, IRS, Cp are derived (Y.-C. Hsu, Pasolli, and Fuchs 2011b; Füllgrabe et al. 2015; Rompolas and Greco 2013; Tsai et al. 2014; Huelsken et al. 2001; Schmidt-Ullrich and Paus 2005; R J Morris and Potten 1999; Cotsarelis, Sun, and Lavker 1990). Before this process can begin the stem cells of the follicle must first be stimulated to exit quiescence (telogen) (figure 1.3.1).

Quiescence in HFSCs within the bulge is retained by BMP6 produced by K6 positive HFSCs in addition to BMP4 from fibroblasts and BMP2 from adipocytes (Clavel et al. 2012; Kobielak et al. 2003; Deng et al. 2015; Huelsken et al. 2001; Song et al. 2018). At the onset of anagen FGF7 and FGF10 produced by the dermal condensate derived DP cells eventually counterbalance BMP signalling from the K6 positive bulge cells and surrounding adipocytes and fibroblasts resulting in the production of Wnt-high HFSCs within the bulge SC niche (Guo, Degenstein, and Fuchs 1996; Richardson et al. 2009; Sheen et al. 2015; Petiot et al. 2003; Oshimori and Fuchs 2012). Wnt-high cells produce SHH further stimulating the DP to produce FGFs counterbalancing the BMP signalling promoting symmetric division of HFSCs and growth of the ORS/germinative matrix. This feedback loop is demonstrated in figure 1.3. However, Wnt-high cells are not susceptible to SHH themselves ensuring they retain their stemness allowing the germinative matrix to persist during anagen (Ouspenskaia et al. 2016; Tsai et al. 2014; Rabbani et al. 2011; Merrill et al. 2001).

The proliferating HFSC of the ORS cause downgrowth of the ORS into the hypodermis which also has the effect of moving the DP signalling centre further from the bulge HFSC niche, preventing signalling between the DP and bulge HFSCs. This allows the bulge cells to return to a quiescent state but retains the proliferative capacity of the HFCS that have remained proximal to the DP (Nowak et al. 2008; Ouspenskaia et al. 2016; Chang et al. 2003; Tsai et al. 2014). As cells divide away from the DP they are exposed to a ratio of FGFs from the DP and BMPs from the surrounding adipocytes and fibroblasts and matrix HFSCs. These signals are believed to be central in governing the specification of the concentric layers of the follicle via canonical Wnt signalling (Tsai et al. 2014; Xing et al. 2011; Cribier et al. 2004).

Once the cells have divided laterally and formed the germinative matrix of the bulb region of the follicle, the cells begin will divide asymmetrically to retain the germinative matrix (propagating anagen) while producing terminally differentiating progeny that specify as the move above the line of Auber, forming the concentric layers of the follicle and hair shaft(Ouspenskaia et al. 2016; Y.-C. Hsu, Pasolli, and Fuchs 2011b; Glover et al. 2017) . What is still unclear however, is what gives cells polarity as there are three directions of migration/division. The first is the symmetric longitudinal division/migration that promote the down-growth of the ORS. The second is the lateral divisions that establish and retain germinative matrix. The third is the vertical divisions/migration away from the germinative matrix to produce the differentiated components of the follicle (hair shaft, IRS and Cp).

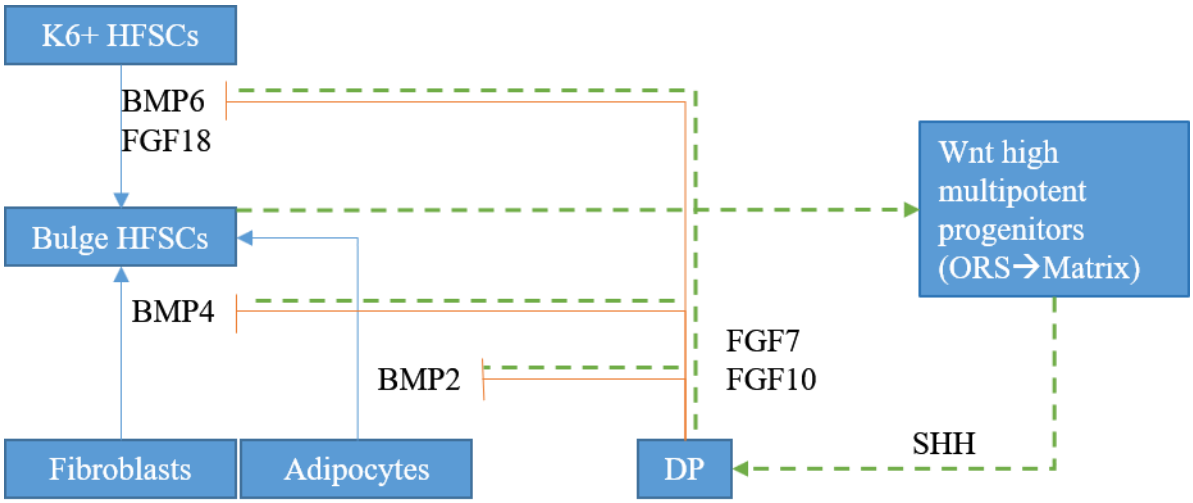

Figure 1.3: FGF and BMP signalling during the telogen to anagen transition. BMPs retain quiescence which are counterbalanced by FGFs from the DP. The results in the formation of Wnt-high HFSCs that will produce SHH stimulating symmetric division of Wnt-low HFSC and growth of the ORS/germinative matrix. In a feedback loop (green) SHH signalling increases FGF signalling from the DP, retaining the population of Wnt high HFSCs proximal to the DP. The Wnt-high cells remain slow cycling since they are resistant to SHH.

1.4 An Overview of Skin: Composition, Morphology and Homeostasis

The structure of skin can be simplified into three principal layers; the epidermis, dermis and subcutaneous fat (hypodermis). The epidermis is an essential barrier to the external environment, with the dermis and subcutaneous fat acting as supporting tissues that provide key nutrients and inductive cues driving regeneration of damaged tissue and retention of the epidermal barrier. The dermis comprises a rich extracellular matrix (ECM) which serves as a bioactive scaffold, composed predominantly of collagen and elastin. (Xu et al. 2014; X. Li et al. 2014; Hao et al. 2014).

1.4.1 Epidermal Homeostasis During Adult Life

The epidermis is subject to continual physical and chemical assault throughout its life and has evolved accordingly to renew itself whilst retaining its barrier function. This is achieved by the careful balance of quiescence and proliferation for epithelial stem cell and that of the subsequent transit amplifying cells that will undergo a programme of differentiation as they separate from the basal membrane and migrate in a columnar fashion through the suprabasal (or spinous) transition (Hohl 1990; Azuara-Liceaga et al. 2004; Merrill et al. 2001; Sabine Werner and Smola 2001; Ghazizadeh and Taichman 2001; Lechler and Fuchs 2005). It is imperative that for each cell lost another is ready to take its place in a way that the supply must match the demand without over supplying. Cells dividing uncontrollably become malignancies whilst those not dividing sufficiently will result in tissue degradation and eventual necrosis (see Blanpain & Fuchs 2009 for review). Central to this process is epidermal stem cells from which transit amplifying cells are derived as a result of asymmetric cellular division (Lechler and Fuchs 2005). All subsequent derivations are derived from the transit amplifying to form the various epidermal skin compartments (Merrill et al. 2001; Blanpain et al. 2006; Watt 2002; Beck and Blanpain 2012). The ability of stem cells to transition between a proliferative state and a quiescent state poses many questions as to how this can be achieved. Further to this what cues promote proliferation of transit amplifying cells and subsequent differentiation.

Cells at the basement membrane express genes encoding the intermediate filament proteins keratin 5 and 14 (K5 and K14) which link via plectin to integrin subunit $\alpha 6\beta 4$ creating the cell-extracellular matrix attachment. Such markers are associated with cells of the stratified squamous epithelial pertaining a proliferative potential i.e. cells of the epidermis directly adjacent to the basement membrane (E. Fuchs and

Green 1980; Pierre A Coulombe and Lee 2012; Seltmann et al. 2013; de Pereda, Lillo, and Sonnenberg 2009). As cells lose adhesion with the basement membrane and migrate through the spinous layer, they undergo a programme of terminal differentiation characterised by a shift in gene expression (S.-H. Kim, Turnbull, and Guimond 2011; Borradori and Sonnenberg 1999; Lechler and Fuchs 2005). This is manifested as a change in protein expression profile e.g. intermediate filament expression of K5 and K14 is lost and instead genes encoding the intermediate filaments K1 and K10 are expressed (Judah et al. 2012) which form strong connections with desmosomes providing structural integrity to the skin barrier (figure 1.4) (Santos et al. 2002; Tsuruta, Hopkinson, and Jones 2003a; Pierre A Coulombe and Lee 2012; Seltmann et al. 2013).

As keratinocytes undergo a programme of differentiation, they eventually transform into granular cells that deposit proteins beneath the plasma membrane that cross-linked forming a strong scaffold for specialised lipid bilayers from the lamellar granules to extrude into (figure 1.4). This phase of terminal differentiation leads to the production of a well-oiled stratum corneum, protecting the differentiating spinous cells and dividing basement cells from chemical, biological and physical damage while retaining tissue and interstitial fluids and oils (Blanpain et al. 2006; M. I. Koster and Roop 2007; Candi, Schmidt, and Melino 2005).

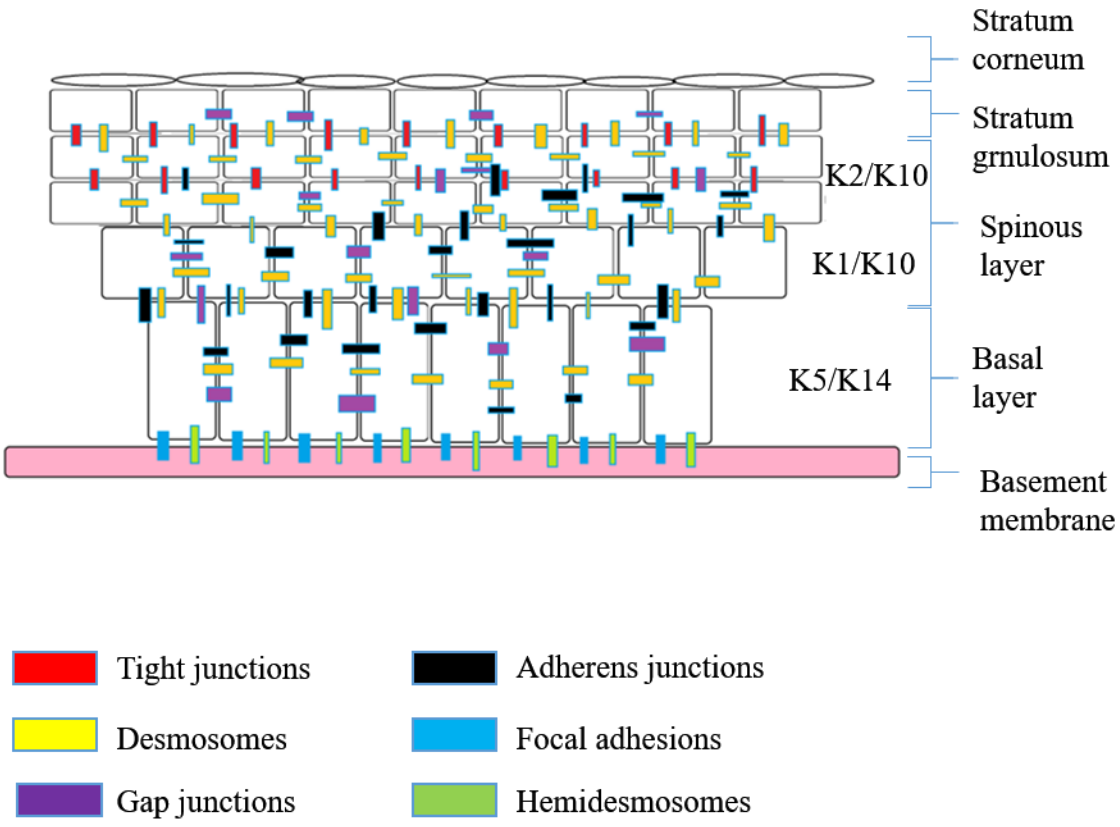

Figure 1.4: Junctional and keratin changes of the epidermis. Cells attach to the basement membrane via hemidesmosomes and focal adhesions. The basal cells express K5/K14 indicative of their proliferative potential and are adjoined to adjacent cells by desmosomes and adherens junctions. As the basal cells migrate upward and undergo a programme of terminal differentiation their keratin profile changes in favour of highly branched keratin dense networks that confer structural strength. Cells in the stratum granulosum form tight junctions and hemidesmosomes forming strong cell-cell contacts and loose adherens junctions.

1.5 An Overview of the Extracellular Matrix

Collagens and elastin are the primary structural constituents of the ECM: Collagens produce fibrillar networks that resist plastic deformation of elastic fibres (Gosline et al. 2002). As the name suggests elastin fibres confer elasticity to tissues enabling them to resist rupture from repetitive mechanical stress (Rauscher and Pomès 2012). However as previously alluded, their role is not only to resist mechanical forces but also as a mechano-sensing and mechano-transducing network. In part achieved through their interaction with cell membrane receptors such as integrins, linked to the cells actin cytoskeleton (S.-H. Kim, Turnbull, and Guimond 2011). This cellular-extracellular interface enable the ECM to influence diverse cellular processes including proliferation, differentiation, migration, adhesion and apoptosis (Connelly et al. 2010; S. A. Ibrahim, Hassan, and Götte 2014; Bonni 1999; S. Y. Li, Mruk, and Cheng 2013; Goetsch, Kallmeyer, and Niesler 2011; Watt 2002; S.-H. Kim, Turnbull, and Guimond 2011).

Interspersed between the collagen and elastin fibres of the ECM are a plethora of growth factors, cytokines, glycosaminoglycans (GAGs), proteoglycans (PGs), proteases and chemokines (Gattazzo, Urciuolo, and Bonaldo 2014; Culav, Clark, and Merrilees 1999; Kozel et al. 2006). The hydrophilic regions within PGs and GAGs sequester water molecules to this rich proteinaceous milieu, giving rise to a protective cushion that resists impact damage (Culav, Clark, and Merrilees 1999).

1.5.1 Collagen

Collagen is the most abundant protein within animals (~30%) and features heavily as a connective tissue, conferring tensile strength to tissues and in some cases, such as in tendons, a degree of elasticity (Shadwick 1990). Connective tissue acts as a supportive network as exemplified in bone, tendons and dermis (Shadwick 1990).

Collagens form a conserved superfamily of proteins characterised by the triplet repeat Gly-x-y for which Gly represents glycine and x and y can be any other amino acid but in most cases are proline and hydroxyproline respectively (Brodsky and Persikov 2005; Bella et al. 2006). Collagens are a tripartite structure of three α-chains that align in a helical register to generate fibrils. The composition of the α-chains is how a collagen is classified, however the α-chains may contain non-collagenous regions that produce breaks within the helical register, enabling the formation of more

geometrically diverse and tissue specific structures as in the case of the bone, tendons and dermis). The structural heterogeneities of collagens enable their participation in a variety of cellular processes such as migration, adhesion, proliferation, tumour suppression and molecular filtration (see Wess 2005 for review).

1.5.2 Elastin

The primary function of elastin is to allow tissues to undergo repetitive stretching while returning to its original dimensions (Gosline et al. 2002). This protein evolved in conjunction with the close loop circulatory systems, to accommodate for the high pressures of pulsatile blood flow, meaning it is only present within the ECM of vertebrates, with the exception of lamprey and hagfish (Gordon and Hahn 2010). Elastins exhibit an extremely low turnover under normal conditions and so must be capable of withstanding thousands of cycles of elongation and contraction (Muiznieks and Keeley 2013). It is not known if increased cycling or deformation of elastic fibres stimulate elastin neogenesis within the ECM or if collagen has a role in sensing this plastic deformation in a feedback loop that regulates neogenesis of both itself and elastin.

Elastin is encoded by a single gene in mammals, bird and reptiles, containing 34 exons and is secreted from the cell in its monomeric from, tropoelastin. Tropoelastin is a 60KDa alternately spliced, hydrophobic protein. The primary structure of elastin is characterised by alternating hydrophobic and cross-linking domain. Crosslinking regions typically comprise lysine residues in one of two arrangements: 1) KA-type domains where the lysines are flanked mostly by valines; 2) KP-domain where lysine residues are arranged within a proline-glycine rich region (Muiznieks and Keeley 2010; Chung et al. 2006; Gosline et al. 2002).

Hydrophobic regions contain high proportions of glycine, proline, valenine and alenine arranged in tandem repeats of: GV, GVA and PGV (Chung et al. 2006; Tamburro, Bochicchio, and Pepe 2003; Lonsdale-Eccles et al. 1984; Muiznieks and Keeley 2010; Itoh and De Camilli 2006; Rauscher and Pomès 2012).

1.5.3 Fibrillins

Fibrillins are a family of large extra cellular glycoproteins (~350KDa) that form the primary constituent of multiprotein microfilaments (typically 10% elastin). Three isoforms (fibrillin-1,-2,-3) exist in humans which are expressed within embryonic

tissues (Sabatier et al. 2011), however only fibrillin-1 persists at notable level throughout adulthood (Sabatier et al. 2011; Corson et al. 2004). These proteins are composed of over 30 tandem calcium-binding EGF domains, infrequently interspersed by TGFβ-binding proteins that are rich in cysteine (Hubmacher, Tiedemann, and Reinhardt 2006). This arrangement makes this protein a good candidate as a potential mechano-sensor and transducer.

Fibrillin rich microfibrils associate with a range of proteins during elastic fibre formation, including elastin, latent transforming growth factor-β binding proteins (LTBPs), matrix-associated glycoproteins (MAGPs), members of the fibulin family and PGs (Baldock et al. 2001; Sabatier et al. 2009; Yadin et al. 2013; RITTY et al. 2003; Vehviläinen, Hyytiäinen, and Keski-Oja 2009). With the capacity to interact with such an array of proteins, fibrillin acts as a structural organiser of elastic fibres in addition to its role in the regulation of tissue maintenance through interactions with TGFβ growth factor (Baldock et al. 2001; RITTY et al. 2003; Ramirez and Sakai 2010; Massam-Wu et al. 2010; Chaudhry et al. 2007; Qian and Glanville 1997).

1.6 An Overview of Mammalian Map Kinase Signalling

Mitogen-activated protein kinases (MAPKs) are a highly conserved group of enzymes unique to eukaryotic cells that aid in the transduction of extracellular stimuli to affect key regulatory targets within cells. Such stimuli include receptor-mediated, adhesion-mediated, chemical and physical stress induced. These stimuli impact upon tissue-homeostasis by altering proliferation, differentiation and apoptosis rates. This ability to transduce information of the physical environment to the nucleus allows for epigenetic control over cellular behaviour, allowing for cells and tissues to respond to changes within their physical environment.

The MAPK cascade comprises three tiers of regulatory kinases; a MAPK, a MAPK kinase (MAPKK) or MEK kinase (MEKK) and a MAPKK kinase of MEK kinase (MAPKKK or MEKKK) (English et al. 1999). These can be activated by either small heterotrimeric GTP-binding proteins (G-proteins) or STE20 kinases (putative yeast MAPKKKK) (S. J. Gutkind 2000; Dan, Watanabe, and Kusumi 2001). Kinases that MAPKs are targeted to specifically are collectively known as MAPK-activated protein kinases (MAPKAPK) and are inactivated by MAPK phosphatases (Martín et al. 2005; Keyse 2010).

Yeast models have been exploited for their ease of genetic analysis to uncover much about the function and regulation of the MAPK pathways (Herskowitz 1995). However, with the advent of genetically modified mice, specific antibodies and inhibitors, the functionality of the MAPK pathways within mammals has been dissected. What is abundantly clear is that the MAPK pathways regulate almost all cell processes from proliferation and differentiation through to adhesion and migration.

1.6.1 General Functions of MAPKs

Regulation of gene expression by extracellular signals is mediated by MAPK signalling modules (Treisman 1996). MAPKs in the main phosphorylate Ets transcription factors that are linked to induction of *fos* genes, whose products heterodimerise with Jun proteins to form activation protein 1 (AP-1) complexes (Treisman 1996). JNKs phosphorylate Jun proteins causing them to adopt an active conformation enabling heterodimerisation with c-Fos to form the AP-1 complex. Phosphorylation allows for activation without effecting DNA binding (Tuula Kallunki et al. 1996). The p38 proteins have a catalytic effect on MEF2C (MADS box transcription factors) and related family members (Tuula Kallunki et al. 1996). In all of these cases the MAPKs are targeted to transcription factors pre-bound to DNA demonstrating how cell surface receptor activation can exert epigenetic control over cellular behaviour. ERKs in general are involved in the regulation of mitosis.

However, it is not only through direct action on transcription factors that the MAPKs are able to regulate gene expression. Only part of the active MAPK module is translated to the nucleus whilst other parts remain within the cytoplasm where they are targeted to post-transcriptional mechanisms. For example JNK is important in stabilising messenger RNA of IL-2 in activated T-cells (C. Y. Chen et al. 2000). p38 has also been found to be important in stabilising specific messenger RNAs (Winzen 1999; Lasa et al. 2000).

1.6.2 MAPKs in Keratinocyte Differentiation

The p38 MAPK isoforms p38α,β and δ are expressed in keratinocytes (Dashti, S R et al 2001). Although information regarding the different isoforms is limited it has been found that p38δ is in abundance in keratinocytes (Dashti, Efimova, and Eckert 2001). Ocadaic acid has been used to stimulate p38δ specifically through its potent inhibition

of protein phosphatases 2A, 1, and 3 (A H Schönthal 1998). Ocadaic acid binds the catalytic subunit of phosphatase 2A supressing its enzymatic activity (Bialojan and Takai 1988). The inhibition of phosphatase activity in keratinocytes results in accumulation of hyper phosphorylated p38 proteins which leads to stimulation of the signalling cascade which in turn produces alteration in gene expression (Axel H. Schönthal 1995; Haystead et al. 1989; Sassa et al. 1989; Connelly et al. 2011; Kramer et al. 1996).

Efimova et al, 2003 demonstrated not only that p38δ is specifically stimulated by ocadaic acid but provide the first evidence that p38 is co-precipitated with ERK1/2. Not only this but how increased p38δ activation leads to reduced ERK1/2 activity and vice versa. This was also linked increased binding of AP1 and CAATT enhancer binding protein factors to the involucrin (hINV) promotor. These responses are maintained in the presence of SB203580 that inhibits p38α and β suggesting a central role for the p38δ isoform (Kumar et al. 1997; Cuenda 1997). This evidence suggests that p38δ directly regulates ERK1/2 activity via formation of the p38δ-ERK1/2 complex and is the major regulator driving suprabasal hINV gene expression. It is also worthy to note however that the increased phospho-ERK1/2 was also accompanied by increased phosphor c-Jun which suggests increased JNK1/2 activity.

1.6.3 MAPKs in Keratinocyte Proliferation

The ERKs have been shown as an important regulator of cellular proliferation. ERK 1/2 phosphorylates the rate limiting enzyme carbamoyl phosphate synthetase II which is essential for pyrimidine nucleotide biosynthesis (Graves et al. 2000). Further to this ERKs have also been found to promote cell-cycle progression through inhibition of the cell-cycle inhibitory kinase MYT1 (Palmer, Gavin, and Nebreda 1998). By contrast ERKs have also been implicated in stalling of meiotic cells at metaphase II by activating a cytostatic factor (Bhatt et al. 1999; Gross et al. 1999). ERKs can also stimulate proliferation indirectly through upregulation of the AP1 activity with the concomitant induction of cyclin D1 (Treinies et al. 1999; Connelly et al. 2011; Barnum and O'Connell 2014; Arai, Kanda, and Miura 2002). Independently this pathway is insufficient to stimulate DNA synthesis and so it requires the synergy of phosphatidyl-inostol-3-OH kinase (PIK). Incidentally this kinase is activated by autocrine growth factors whose expression is ERK responsive (Treinies et al. 1999). Autocrine factors are important responders of MAPK signalling (Wasserman,

Freeman, and Matthew 1998), enabling for a single MAPK cascade to elicit multiple signalling pathways simultaneously (Minden, Lin, McMahon, et al. 1994).

A study into squamous cell carcinomas by Masatoshi *et al* (2013) demonstrated how ERK1/2 upregulation was the cause of abnormal rates of proliferation. The increased ERK1/2 levels were found to correspond with increased rates of proliferation with attenuation by siRNAs targeted specifically to ERK1/2 returning proliferation rates to a normal level.

1.6.4 An Overview of Integrin Mediated MAPK Signalling

Integrins provide a physical connection between extracellular matrix components and the cell cytoskeleton. Integrin binding has been demonstrated as influential over cell behaviour with respects to proliferation, differentiation, motility and apoptosis. The integrin family of cell surface receptors have been well established as integral to cell adhesion being the principal recipients of extracellular matrix ligands such as collagen, lamins and fibronectin (Watt 2002; Gullberg and Lundgren-Akerlund 2002; Y. Chen et al. 2017; Raghavan, Vaezi, and Fuchs 2003; Borradori and Sonnenberg 1999). Integrins function as bridges that connect the ECM with the actin-cytoskeleton. Complex mechanisms govern the integrin-actin interaction of which the Rho family of Ras-related GTP-ases play a large part in transducing (Buhl et al. 1995; Tapon and Hall 1997; Nobes and Hall 1999; Westwick et al. 1997). The ability of integrins to bind ECM components is regulated not only by Rho and Ras family members but by a plethora of other proteins found within the cell membrane such as the caveolin integral membrane proteins (Y. Wei et al. 1999; Wary et al. 1998, 1996). Regulation of these interactions has profound impacts upon cytoskeletal organisation, cell cycle progression, pro-apoptic cues, and cell motility.

These cellular changes are mediate by integrin signalling that can be broadly categorised as direct or indirect signalling. Direct signalling is the product of the association of several integrins with the concomitant activation of cytoplasmic tyrosine kinases such as focal adhesion kinases (FAK) and serine threonine kinases (such as those in the mitogen activated protein kinases), which induce ionic transients (e.g. Ca^{2+}, $Na^{+}/H^{+)}$, and stimulate lipid metabolism (e.g. phosphatidylinositol-4,5-bishphosphate (PIP_2) synthesis) (Aplin et al. 1998; K.-J. Lee et al. 2017; Raghavan, Vaezi, and Fuchs 2003; Gadhari et al. 2013). Activation of kinases allows for the

physical extracellular environment to exert control over cellular behaviour via the MAPK cascades for example. The indirect signalling is a form of collaborative signalling in which the integrins modulate signalling cascades elicited by other cell surface receptors, in particular by receptor tyrosine kinases (RTKs). Evidence would suggest that signalling originating from the cell surface is dependent upon association with integrin complexes (Y.-X. Su, Hou, and Yang 2014; Gahmberg et al. 2009; X. Chen et al. 2014).

The cytoplasmic tails of integrins lack enzymatic activity and hence transduce signals via associated adaptor proteins that connect the integrin with cytoplasmic kinases, membrane associated growth factor receptors and the cytoskeleton (Judah et al. 2012; Wary et al. 1996; D D Schlaepfer, Broome, and Hunter 1997). Integrins have an intimate relationship with the actin cytoskeleton inducing formation of actin stress fibre formation from focal adhesion sites and linking ECM substrates (e.g. collagen) with keratins (Watt 2002; Raghavan, Vaezi, and Fuchs 2003; Gullberg and Lundgren-Akerlund 2002; Greiner et al. 2013; Walko, Castañón, and Wiche 2015). Integrins will bind to the ECM forming lateral connections with adjacent integrins to form an adhesion complex. This complex promotes the polymerisation of actin from the site of clustering (Machesky and Hall 1997; Burridge and Chrzanowska-Wodnicka 1996b; Lyman et al. 1997). The organisation of actin into larger stress fibres promotes further integrin clustering increasing integrin adhesion with the ECM (Burridge and Chrzanowska-Wodnicka 1996a). In this regard integrins are a means for cells to detect and interact with the cells ECM. A recent study demonstrated how availability of G-actin impacts upon proliferation rates via its negative influence over the serum response factor activity (Gadhari et al. 2013; Koegel et al. 2009). This suggests that increased F-actin as a result of increase integrin-collagen binding could sustain a proliferation advantage in keratinocyte derived cells.

1.6.5 Integrins Transduce Via MAPK Signalling Cascades

There is evidence for both integrin-mediated stimulation of MAPK however it is still ambiguous as to how this is mediated with three models currently being proposed. The first model suggests the clustering of integrins at the membrane signal via FAK, to SH2-domain adaptor proteins, to guanine nucleotide exchange factors, to Ras which activates downstream MAPK cascades (Elbediwy et al. 2016). This model is analogous to that proposed for the stimulation of MAPK cascades by growth factors,

with FAK replacing RTK. In support of this hypothesized model is the auto phosphorylation of FAK as a product of integrin mediated adhesion. This in turn leads to the recruitment of Src, further tyrosine phosphorylation of FAK and p130CAS and the binding of SH2-domain proteins including Shc and the Grb2/Sos adapter protein-exchange factor complex (David D. Schlaepfer et al. 1994; David D. Schlaepfer and Hunter 1997; Polte and Hanks 1997; Vuori et al. 1996). The formation of this adapter with FAK might suggest further signalling to MAPKs. More direct evidence was provided when the overexpression of FAK led to Src- and Ras-dependent activation of MAPKs (David D. Schlaepfer and Hunter 1997).

However, such overexpression studies posit cause for concern as such artificially high levels of expression can alter the function of kinases. The ability of MAPK cascades to elicit different responses is in part reliant upon the ability to stimulate cascades in an analogue fashion. FAK may only be stimulating MAPK as a result of this overexpression and not directly as a result of integrin mediated adhesion. Contrary to the direct involvement of FAK other studies argue that FAK is not involved in stimulation of MAPK as no activation was observed when FAK was constitutively expressed in epithelial cells (Frisch 1996). Again, this illustrates how artificial expression of kinases involved in multiple pathways can trigger a change in function and produce an entirely different outcome. Another mechanism postulates that FAK is in fact redundant in the activation of MAPK, instead proposing the activation of Ras-Raf by the caveolin-Shc-Grb2-Sos complex upon engagement of integrin-ligand interaction (Samarakoon and Higgins 2018).

1.6.6 Transduction of Matrix Stiffness in Keratinocyte Derived Cells

The epidermis and anagen hair follicle are maintained under homeostatic conditions; the follicle reaches a maximum length during anagen from which a hair shaft is differentiated whilst the skin continually replaces cells that are sloughed off at its surface. Many molecular mechanisms have been detailed that govern these processes but what is still unclear is how this homeostasis is achieved. One such mechanism that would enable for rapid communication between cells is a physical link mediated by the cell-cytoskeleton-cell-ECM interactions. Alterations in this via loss of tension could act as a means of providing instructive cues to cells on both the need for proliferation and on the plane within which the division is needed (providing polarity).

Many studies looking into the impact of mechanical transduction on cellular behaviour focus on long term exposure to a force for example by cyclic stretching or exposure to pressure over several hours (Y. Li et al. 2011; Greiner et al. 2013; Yano et al. 2004; O. V. Kim et al. 2017). With varied effects from cell type to cell type there is no straightforward relationship between physical forces and cellular outputs. However, a theme that persist throughout is how alterations in stress/strain values across a cell over prolonged periods produces biological outputs with respects to alterations in proliferation, differentiation and migration (Gupta et al. 2016; Y. Wang et al. 2012; Greiner et al. 2013; Moriya et al. 2011; S Kippenberger et al. 2000; Y. Li et al. 2011).

Mechanical loading has been shown to elicit changes in cellular proliferation rates, differentiation, protein expression and gene expression. The outcome of the physical output appears to be the product of both the cellular context and the source type. For example, cyclic stretching of fibroblasts can propagate the production of MMPs, type I collagen and proliferation whilst prolonged stretching has the opposite effect in keratinocytes producing a reduction in proliferation rates (Barkhausen et al. 2003; Greiner et al. 2013; K. Zhang et al. 2016; Voorhees et al. 2015; Ruiz and Jarai 2011; JH-C Wang and Thampatty 2006; S Kippenberger et al. 2000). Considering that the forces generated by shaving are dissipated over a matter of seconds/minutes it is not likely that these forces will produce the biological outputs reported on and so what is more interesting is to consider the roll of different established physical environments and how these could impact upon hair follicle homeostasis and epidermal homeostasis with respects to governing proliferation and differentiation.

HaCaT cells have been shown to exhibit elevated proliferation rates in response to an increased substrate stiffness. MTT assays and flow cytometry were used to evaluate cells cultured on high stiffness (Youngs modulus=1.6 MPa) and low stiffness (Young's modulus 0.05 MPa) polydimethyl siloxane (PDMS) substrates. The key findings from this study were that the stiffness mediated proliferation was independent of Wnt/β-catenin pathway but dependent on FAK-ERK 1/2 pathway. In addition to this nuclear transduction was noted via the increased expression of Lamin A/C (Gupta et al. 2016). These findings are additive to earlier findings that recorded elevated β-catenin levels to coincide with increased proliferation rates suggesting that although β-catenin is capable of eliciting increased proliferation rates via the

canonical Wnt pathway (figure1.5) it is not the dominant means by which proliferation is driven in keratinocyte derived cells (Novak et al. 1998; Andl et al. 2004; Kobielak et al. 2007; Van Mater et al. 2003).

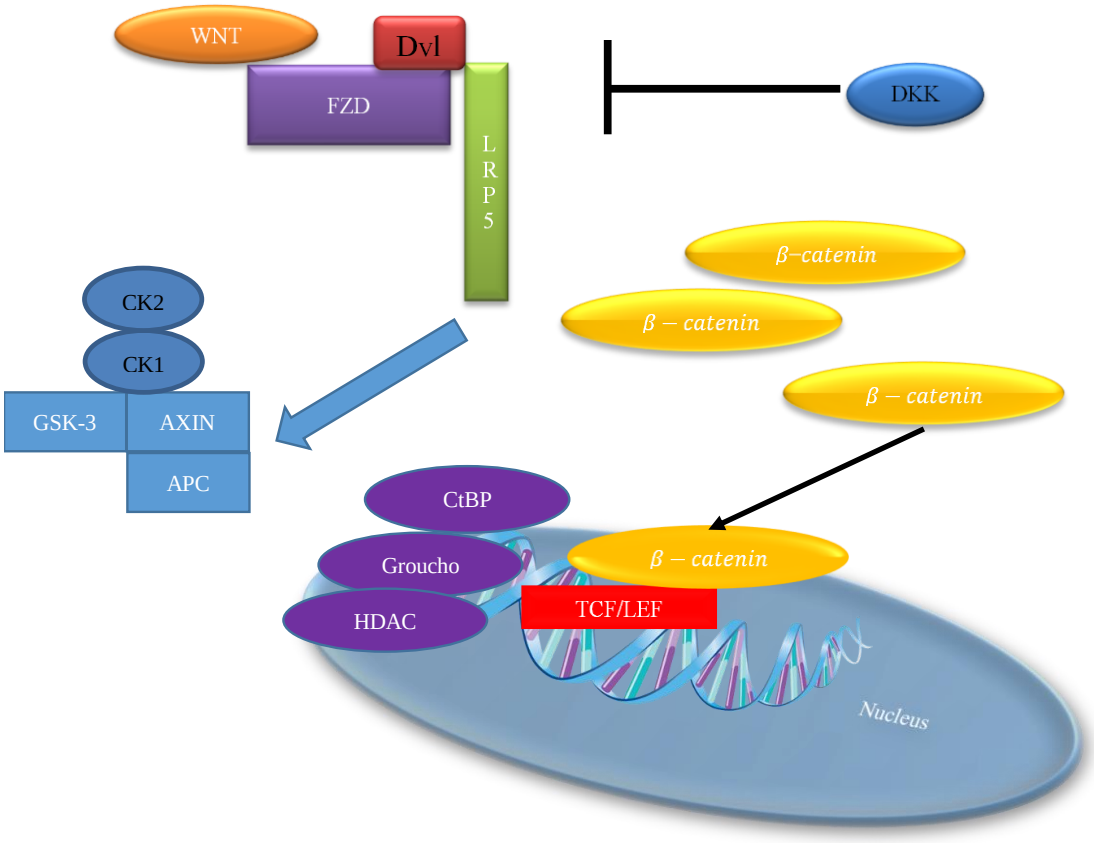

Figure 1.5: Canonical Wnt signalling**.**

Wnt binds to the G-protein coupled receptor frizzled (FZD) causing recruitment of the AXIN complex (APC-AXIN-GSK-3) via Dvl. The kinases GSK-3 and CK1 then phosphorylates the receptor LRP5 of the membrane which in turn sequesters additional AXIN causing further phosphorylation of LRP5. This amplification step results in receptor-AXIN complex clusters forming at the membrane, blocking ubiquitination and subsequent proteosomal degradation of β-catenin. β-catenin will therefore accumulate in the cytoplasm where is will eventually be translocated to the nucleus. Once in the nucleus β-catenin binds to and activates the TCF/LEF transcription factors. CK1 and CK2 have been postulated as kinases that prepare β-

catenin for interaction with GSK-3 (G. Wu et al. 2009; Tsai et al. 2014; Rao and Kühl 2010; Lim et al. 2016; Ding and Dale 2002; Gwak et al. 2012) . Wnt signalling has also been linked to the activity of Groucho (a family of transcriptional regulators), CtBP (a transcriptional corepressor) and HDACs (histone deacetylases) which form a complex network of factors that contribute to the epigenetic modification of DNA (see MacDonald et al. 2009 for review).

In the FAK-ERK pathway the integrin associated FAK is autophosphorylated in a matrix dependent manner (figure 1.6). The phosphorylation of the FAK modulates the catalytic activity and physical association with Src homogy 2 (SH2)-containing proteins including the Grb2-Sos complex (Schaller et al. 1994; J. G. Wang et al. 2005; F. Liu, Sells, and Chernoff 1998; Hanks and Polte 1997). The Grb2-Sos complex is a key regulator of Ras which has downstream impacts on both JNK and ERK1/2 activity, both of which have been shown to be involved in transducing proliferation cues in keratinocytes (Lamarche et al. 1996; D'Souza-Schorey, Boettner, and Van Aelst 1998; Clark and Hynes 1996; Brenner et al. 1996; Mishima, Inoue, and Hayashi 2002; Sun et al. 2015; Ip and Davis 1998).

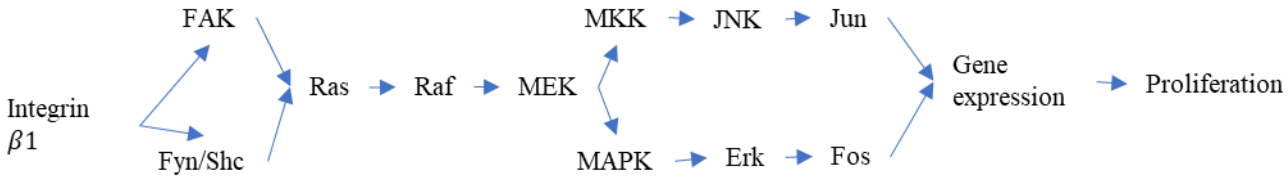

Figure 1.6: Integrin-mediated MAPK signalling that transduces proliferative cues. This figure is a simplified break down of how an ECM interaction with an integrin could elicit cellular proliferation via MAPK signalling.

As the autophosphorylation of FAK is ECM dependent there is a potential source of modulation whereby increased access to substrate would enable increased integrin clustering which in turn produces increased FAK activity with down-stream activation of JNK and ERK eliciting proliferation Earlier studies have shown how increased integrin clustering leads to increased phosphorylation of p125fak which has also been reported to signal via Ras eliciting increased ERK1/2 activity (Bauer et al. 1993).

β-Catenin is known for its involvement in intercellular adhesion structure called adherens junctions and was later found to be a key member in the Wnt signalling pathway. Wnt signalling causes it's translocation to the nucleus where it transactivates transcription of

target genes together with members of the Tcf/Lef1 transcription factor family (Huber et al. 1996; Behrens et al. 1996). However, Posthaus *et al.* has already showed that β-catenin is not required for proliferation of mouse epidermal keratinocytes suggesting although this pathway has capacity to induce proliferation in keratinocytes, it is not essential (Posthaus et al. 2002). Within the Gupta 2016 study β-catenin nuclear localisation was not found to alter, with only changes at the cell periphery being noted leading to the conclusion that stiffness induced proliferation was independent of this pathway. The increase pERK1/2 suggests the FAK-ERK pathway to be more important in transducing stiffness cues.

These findings were observed in an earlier study by Wang et al 2012 whom again used PDMS substrates of differing Young's moduli (stiffness) to investigate the relationship between substrate stiffness and proliferation/differentiation rates and cells migration. The group similarly found that an increased stiffness generated a proliferation advantage and promoted cell spreading. Flourescence flow cytometry suggested this increased proliferation to correlate with increased integrin-β1 which signals via the FAK-ERK pathway (Y. Wang et al. 2012).

The literature surrounding the mechanotransduction of matrix stiffness all agree that increased stiffness leads to increased proliferation and most likely via FAK-ERK1/2 signalling. To understand better how substrate stiffness could be used to retain functionally distinct environments, the hair follicle provides an ideal model since the infundibulum, isthmus and suprabulbar regions are all abutted by structurally different dermal environment that will be investigated within this study. The follicle also retains both stem cell niches, transit amplifying cells and differentiating cells. Insight into substrate stiffness may point to new sources of tissue governance not previously considered.

1.8 The Effects of Mechanical Force on Cell Nuclei

In HaCaT cells the LINC complex has been found to impact upon nuclear size via interaction with both microtubules and F-actin. Disruption of F-actin resulted in shrunken and disfigured nuclei whilst disruption of microtubules caused enlarged nuclei. However, when both were disrupted the same phenotype as when F-actin alone is disrupted was returned implying F-actin and actin binding domains within the LINC complex to be dominant in nuclear dynamics. It is also well documented that

cells in interphase and S-phase exhibit an increase in nuclear volume (Black L 2019, Li Yang 1997, 23, 24).

There is growing evidence that physical properties of the ECM modulate nuclear shape. The actin-myosin cytoskeleton transmits mechanical force from focal adhesions at the cell membrane/ECM junction to nuclear LINC complexes and the lamina (Friedl, Wolf, and Lammerding 2011), and the actin cytoskeleton was also shown to be important in coordinating nuclear shape with cell shape (Versaevel, Grevesse, and Gabriele 2012). Substrate stiffness on which NIH 3T3 cells were cultured modulated nuclear shape. Malleable substrates produced cells with round nuclei while stiff substrates led to flattened nuclei (Lovett et al. 2013).

Intriguing interactions between lamin A levels, ECM stiffness, and cell differentiation have also recently emerged (Swift et al. 2013), as well as a novel role for keratin filaments in regulating nuclear shape (C.-H. Lee et al. 2012). K14 was recently shown to impact upon nuclear shape of cultured keratinocytes. K14 was noted to concentrate around the nucleus with K5 via a disulphide linkage. K14 knockdown produced severe nuclear aberrations. As K14 is only present in basal keratinocytes this could suggest a possible link between keratins, nuclear dynamics and chromatin remodelling. However, is more relevant to this study is that this study demonstrates a physical link between K14 and nuclear morphology and therefore forces transduced from the cell periphery can reach the nucleus via K14.

Within this study, nuclear morphologies will be evaluated to delineate how forces generated during the shaving process are distributed along the hair follicle to understand how mechanically distinct environments within the dermis could have functional roles in follicle homeostasis. For example in regions where progenitors are known to be found it would be beneficial to ameliorate compressive forces while providing a low stiffness environment which have been shown to produce increased proliferation and terminal differentiation (Y. Li et al. 2011; Greiner et al. 2013; Raymond et al. 2005; Xu et al. 2014; Engler et al. 2006; Y. Wang et al. 2012).

1.7 Overall Aims and Goals

This study aims to characterise how forces are distributed along the hair follicle by assessment of nuclear deformation (in the context of shaving), to reveal mechanical niches generated by collagen adjacent to the hair follicle using a combination of high-resolution confocal microscopy and multiphoton microscopy. Once these collagen niches have been identified and characterised, they will be modelled *in* vivo using collagen hydrogels produced from isolated type 1 rat tail collagen. This will allow correlations to be drawn between matrix density, changes in nuclear morphology and proliferation/differentiation rates. This will inform upon the significance of differential collagen environments abutting the hair follicle and how these may aid in follicle homeostasis with respects to the propagation of anagen, and in epidermal homeostasis.

2.0 Materials and Methods

2.1 Chemicals and reagents

All chemicals and reagents used are of analytical grade and supplied from Sigma Aldrich UK or BDH Laboratory Supplies unless otherwise stated.

2.2 Human Facial and Scalp Skin Preparation for Histological Analysis

Human scalp and facial skin were supplied by Procter and Gamble and sourced by Caltag Medsystems. All tissues were stored and discarded in accordance with the Human Tissue Act 2004. All skin was screened for a panel of infectious diseases before receipt.

2.2.1 3-D Printed Support for Biomechanical Studies

To capture the dynamics of the follicular compression a custom rig was designed using free, open source compute aided design software (FreeCad: https://www.freecadweb.org/). Multiple iterations were tested until the platform below was produced. 0.5cm by 3cm sections of skin were cut from frozen skin explants, to avoid compression of structures. The skin would be left at room temperature to thaw for 30 minutes. During this period string would be glued to individual hair shafts and passed through the apertures of the skin cassette. The epidermis would run parallel to the apertures to ensure the force applied was perpendicular to the skin surface. The apertures were sufficiently small to prevent the prolapse of the tissue but large enough to ensure the natural movement of the skin surrounding the follicle during compression without the structures providing support to the follicles being pulled. This ensured the dynamics of the epidermis, dermis, hypodermis and pilosebaceous unit could be captured during the pull with the tension generated by the pull being distributed in a native manner i.e. without artificial support.

For dynamic imaging the chamber is then filled with PBS to prevent drying out of the specimen. A glass coverslip would then be placed over the skin and held in place by the coverslip clamp (figure 2.1). The strings would be tensioned once the specimen was in place within the microscope. For non-dynamic imaging i.e. pull then fix, no coverslip is required. The cassette was place within a chamber filled with PBS and the string was tensioned for the required durations. After the allotted tensioning the PBS would be substituted for 4%PFA and left for a 24h period. Although a skin tensioner

was incorporated into the design it was too larger source of variability to use e.g. It wouldn't be possible to accurately tension all the skin with the equipment available.

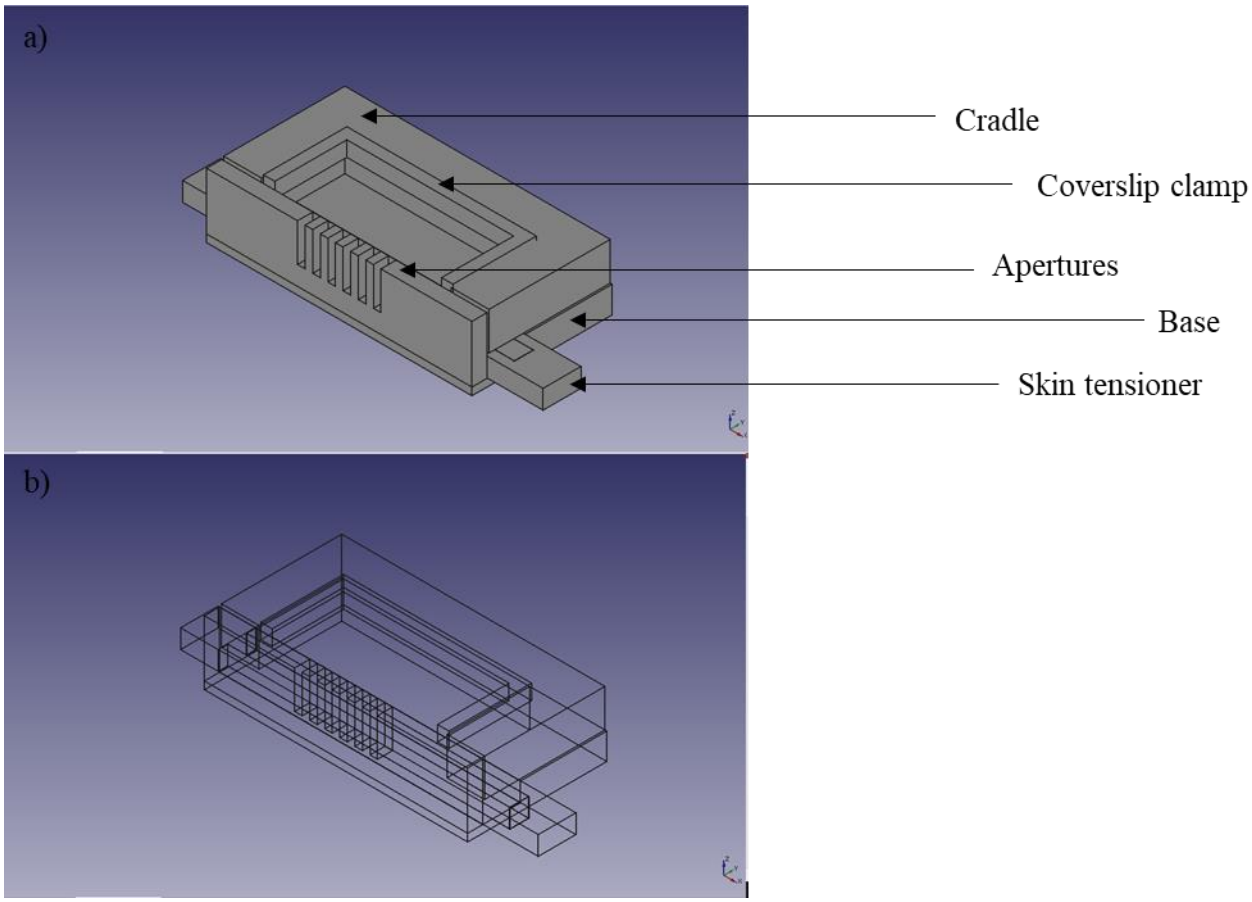

Figure 2.1: CAD design of the skin cassette. a) 3D padded model. b) 3D Wire frame model

2.2.2 The Compressive Force Generating Rig

To simulate the forces generated as a result of shaving a 2g weigh was applied to individual follicles as pictured below (figure 2.2). The string was attached to individual hairs using a hot glue gun, and the weight gently loaded to prevent depilation. For static pulls (i.e. pull-hold-fix/ 0 min) the skin would be secured within the cassette which would then be anchored into a secondary chamber that would later be filled with 4% paraformaldehyde: 0.2% Glutaraldehyde made up in PBS and left for 24 hours. The weight would be applied prior to addition of the fixative to capture the dynamics of the pull.

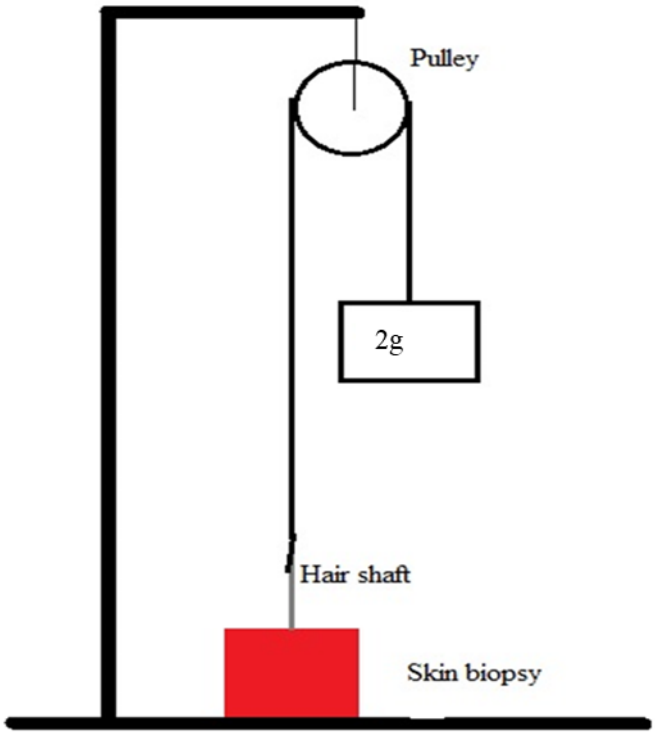

Figure 2.2: Hair-pulling rig. A retort stand was used to hold the low-friction pulley in place. The string that was pre-attached to the hair shafts was then passed over the pulley. Finally, a weight of 2g/follicle would be added.

2.3 Histology of Human Skin

2.3.1 Sample Preparation

Skin sample were fixed in 4% paraformaldehyde: 0.2% Glutaraldehyde: 95.8% PBS v/v/v. Samples were then taken through a dehydration series of 10%, 30%, 70%, 95%, 100%, 100% ethanol: deionised water at 1h intervals. This would then be left over-night followed by a further 6h for the final 100% ethanol. Samples would then be transferred to 100% xylene for 24h then 50% xylene:50% paraffin wax for 24 hours. Upon the addition of paraffin samples would be stored in a 50℃ oven. Finally, the sample would be incubated twice for 24 hours in 100% paraffin. Samples were then cooled to room temperature and stored. Specimens were sectioned to ~10μm using a rotary microtome. Thin sections were then floated onto 37℃ water prior to mounting on poly-L-lysine coated slides (Thermo Fisher). The slides were then heated to 40℃ and incubated overnight to drive off moisture encourage adherence and decompress of the section. Samples would then be deparaffinized using xylene followed by a rehydration series of 100%, 100%, 95%, 70% 30%, 10%, 0%, 0%, ethanol: deionised water at 5-minute intervals. Following this samples were mordanted by heating to 56℃ in Bouin's solution to achieve better contrasts as a result of staining. Samples were then cooled to room temperature using a large water bath as opposed to running water to prevent loss of sections.

For the Masson's trichrome slides were first stained for 5 minutes in Weigert's haematoxylin solution (mix equal parts of solution A: 5g haematoxylin in 500ml CH_3CH_2OH, and solution B: 5.8g $FeCl_3$, 5ml HCl (concentrated), 495ml H_2O) followed by a 5-miute wash in deionised water. Samples were then transferred to Scarlet-Biebrich acid Fucshin for 5 minutes followed by another wash in deionised water. Slides were then transferred to analine blue solution for 5 minutes followed by clarification in 1% acetic acid for 2 minutes. Slides were then be dehydrated by 10%, 30%, 70%, 95%, 100%, 100% ethanol: deionised at 5-minute intervals. Finally, samples were cleared in xylene for 10 minutes and mounted in DPX-mounting media.

For haematoxylin and eosin staining slides were deparaffinized and mordanted as in the Masson's trichrome technique. After this the slides were placed in working Mayer's haematoxylin solution (50g $KAl(SO_4)_2 \cdot 12H_2O$, 1000ml dH_2O, 1g haematoxylin) for 5 minutes followed by a further 5-minute wash in deionised water.

Samples would then be differentiated for 5 minutes using 1% HCl:40% CH_3CH_2OH:59% H_2O. After this samples would be washed for 3 minutes in deionised water followed by a 2-minute incubation in eosin solution. The sample would then be dehydrated and be mounted as described in Masson's trichrome staining.

2.3.2 Image Acquisition

Images were acquired using a Leica DMI3000 B DIC fitted with a Panasonic 3CCD 1080p HD Colour camera this allowed for the acquisition of 16-bit RAW images that could be analysed using imageJ.

2.3.3 Image Analysis

Images were imported into ImageJ as RAW files for which intensity plots were generated for regions of collagen adjacent to the follicle that coincided with the infundibulum, isthmus and suprabulbar region. An average of the pixel intensity for each box was calculated based on the blue channel to select for collagen staining (figure 2.3). Increased blue intensity would indicate increased fibres per unit area as the average intensity of each box was generated. The same size box was used to analyse collagen for each area excluding the dermal sheath and follicle. Values range from 0-256 as the images acquired were 8-bit (i.e. 2^8 possible variables). Parameters were adjusted to ensure only blue was analysed. Other channels were stripped away and images were compared against the original to ensure only the red features had been removed.

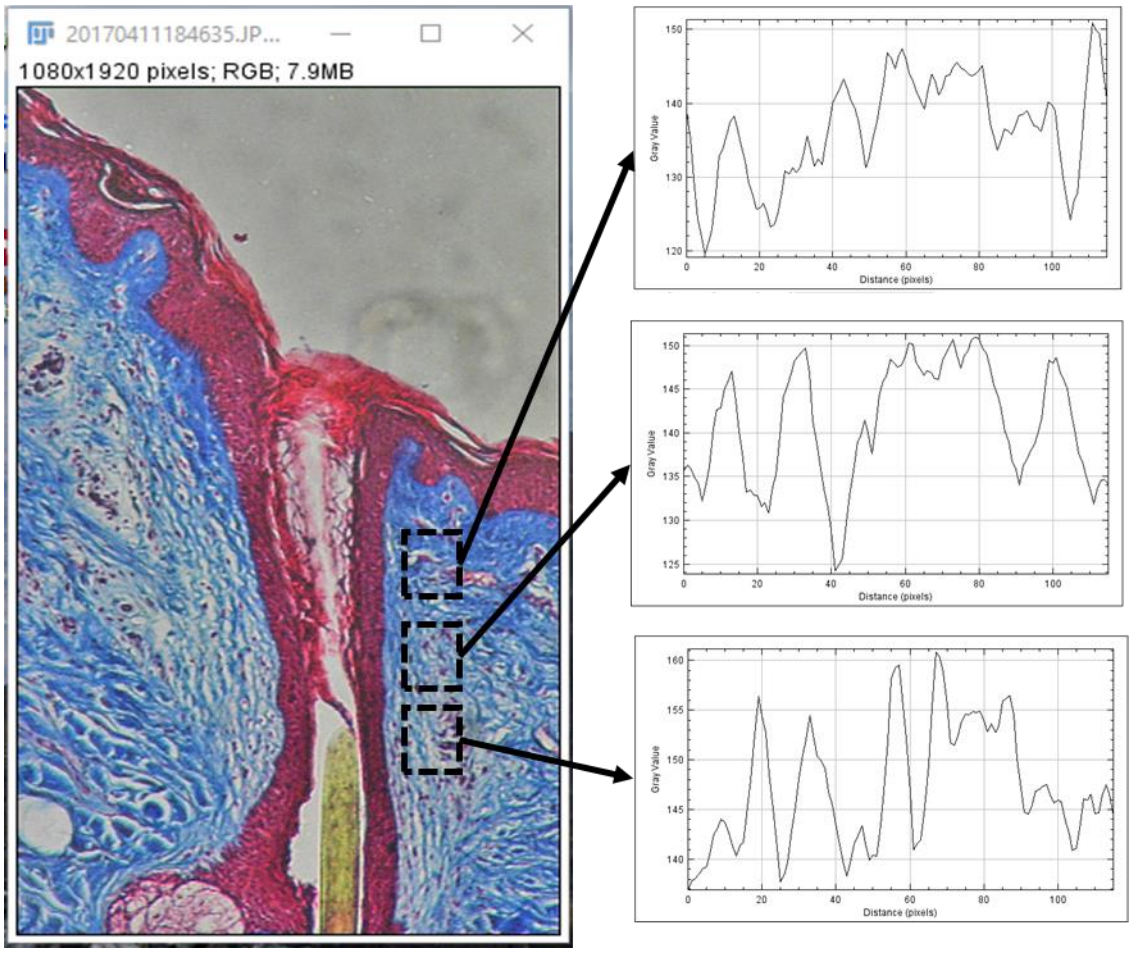

Figure 2.3: Intensity plots for Masson's trichrome staining. Representative of the infundibulum region of the follicle.

2.4 Immunofluorescence of Human Skin

2.4.1 Sample Preparation

Tissue was fixed as described in 2.3.1 then snap frozen in liquid nitrogen. Tissue was then transferred to a -15℃ cryomicrotome for 30 minutes before being embedded in optimum cutting temperature (O.T.C) compound before sectioning to 8 µm thick sections. Sections were then placed onto poly-L-lysine coated slides and brought to room temperature. Samples were then washed 3×10 minutes in 1X PBS followed by permeabilization in 0.2% triton x-100 for 30 minutes. Following this samples were blocked for 1 hour using 0.1% fish skin gelatine: 2% bovine serum albumin made up in PBS. Samples were then incubated overnight at 4℃ with either rabbit polyclonal anti-involucrin (ABCAM) or rabbit polyclonal anti cytokeratin-14 (ABCAM) at 1:100 dilution made up in blocking buffer. For dual labelling samples would be incubated sequentially with each primary antibody at room temperature for 1 hour. After each primary antibody incubation samples were washed 3×10 minutes in PBS. After an overnight incubation samples would be permeabilised a second time followed by 3×10 minutes in PBS. Samples were then incubated with AlexaFluor secondary antibodies (ABCAM) at a 1:500 dilution in blocking buffer for 1 hour. Samples were then washed for 10 minutes in PBS followed by a 40 minute incubation with 0.5ug/ml DAPI:PBS solution. Finally, samples were washed for 2× 10 minutes in PBS then mounted in VectaShield H-1000 (Vector Laboratories) soft set mounting solution before imaging. Slides were sealed using TiPex and kept in opaque containers prior to imaging to preserve fluorescence.

2.4.2 Image Acquisition

Images were acquired using a Zeiss LSM 880 with Airyscan. Image were exported as uncompressed CZI files. Identical filter sets, exposure times, gains, magnification, excitations, z-intervals were used for acquisition of images to ensure comparability between samples prepared at the same time and recorded to meta data for each image file.

The zeiss 880 excites the specimen with lasers tuned to the excitation wavelength of the flurophores being analysed (DAPI: 405 nm, phalloidin: 488 Alexa Fluor: 594 nm/488 nm). The laser was scanned across the specimen in rows with line averages taken to increase the signal to noise ratio with emissions being captured at

wavelengths 10 nm greater than the excitation wavelength. Emission spectre were prevented from overlapping through restricting detection using a dichroic mirror minimising excitation of non-target flurophores.

2.4.3 Image Analysis

Images were split into their composite channels and regions of interest created to enable analysis of nuclei corresponding to either involucrin positive cells (IRS) or K14 positive cells (ORS). Data relating to nuclear morphology was extracted from the images using the shape descriptors plugin built into the imagej (fiji) software. The image would be split into its composite channels and cropped to include only nuclei of either the IRS or ORS. Running the ‘particle analysis’ plugin within imagej would return information relating to the height (y-dimension), width (x-dimension) and depth (z-dimension).

To ensure the orientation of the follicle does not impact this data all images were oriented such that the hair follicle trajectory would be perpendicular to the x-axis. To ensure only pulled hairs are quantified all hairs within the region to be analysed would be loaded with a 2g weight.

2.5 Multiphoton Microscopy of Human Skin

2.5.1 Sample Preparation

Skin was prepared as described in 2.3.1 and loaded into the cassette. The cassette was then placed under the objective and clamped in place (figure 2.5). The hair follicle pulling rig was used to generate the pulling force. Images were taken before the pull, at maximum pull and upon release of tension by unloading the weight. The length of skin used was great enough to prevent leakage of moisture through the apertures retaining the hydration of the skin during imaging. The epidermis of the biopsy was effectively still providing the barrier function to the dermis and hypodermis.

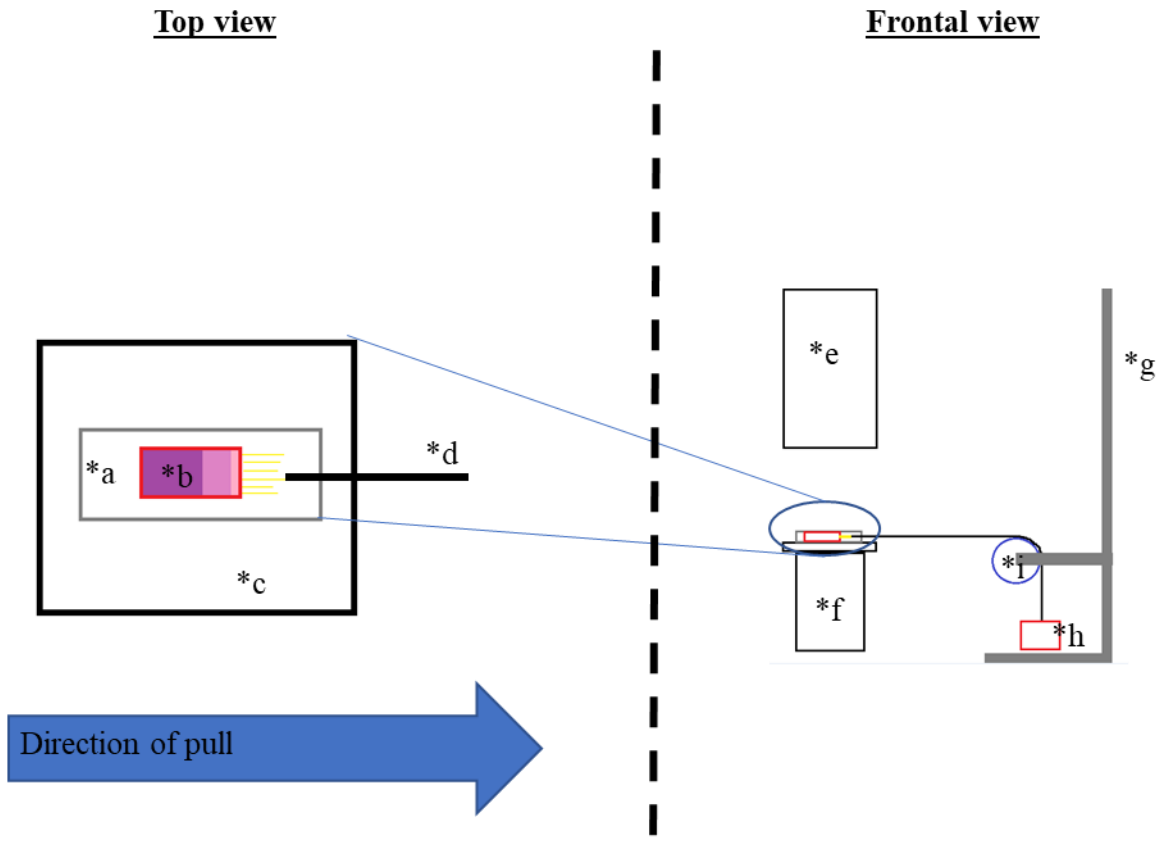

Figure 2.5: Imaging follicle dynamics by multiphoton microscopy: ***a**-skin anchorage cassette, ***b**-skin biopsy, ***c**-microscope stage, ***d**-Sting, ***e**-objective, ***f**-stage, ***g**-retort stand, ***h**-weight, ***i**-pulley.

2.5.2 Image Acquisition

Images were acquired using a BioRad Microradiance 2000MP by a direct detection system equipped with a bandpass filter that allowed for signal detection within the range of 410 nm to 490 nm. Images were stored as 8-bit TIFFS.

2.5.3 Novel Image Analysis of SHG Signal

SHG is only possible in structures comprising molecules that are non-centrosymmetric and arranged in highly repetitive arrays placing collagen as an ideal generator. Chapter 4 documents how it was possible to delineate a collagen derived SHG signal from any other form of SHG (e.g. background signals from smaller micromolecular structures) or TPEF. Once parameters to generate SHG of collagen had been established it was possible to use intensity plots to identify changes in collagen bundling. It was assumed that each peak represents the mid-point of a fibre i.e. the thickest and therefore brightest part of a bundle, the distances between peaks will therefore represent distances between collagen fibre bundles. As distance between peaks are being assessed the height of the peak is irrelevant ensuring all fibre thicknesses are considered. This will provide a good indication of collagen density. As each pixel will generate a value it is important to only retain peaks and the corresponding pixel number (figure 2.6). This can be carried out manually using the pixel profile plots generated in imagej (fijij) or by this novel logic argument in excel i.e. =IF(AND(C5>C4,C5>C6),C5,FALSE). This bespoke argument ensures that values are only retained if they are greater than the values of the pixels directly abutting ensuring only peaks are retained i.e. maxima. Values that fall on inclines (figure 2.6) will only be as large as one of the adjacent pixels. Once the maxima intensities and corresponding pixel location have been identified, the pixel location values can be subtracted to return the distances between each of the peaks. These can then be averaged to give the average distance between fibres that intersect the line (figure 2.6). Pixel values can be later converted into microns in accordance with the pixel ratio used e.g. 4.3px/μm. The pixel ratio was calculated using a graticule as this data was not provided within the meta data of the images obtained.

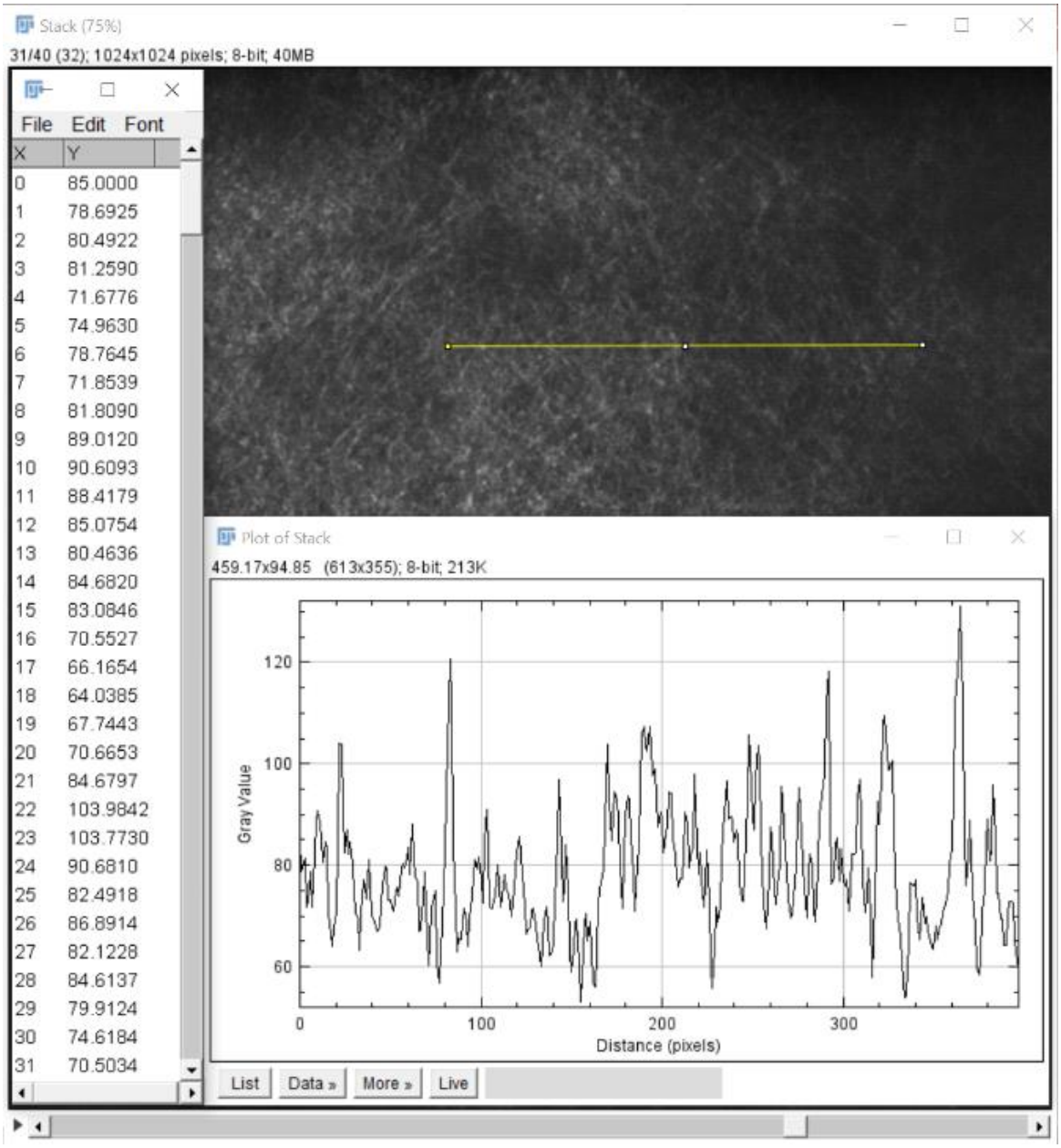

Figure 2.6: Analysis of SHG images. An intensity plot (bottom) generated from an SHG sourced image (top). The yellow line drawn will generate a value at each pixel along the line producing both a line graph and a table of raw values corresponding to each of the pixels and its location on the line.

2.6 Polymerisation of Collagen 3D Gels

To prevent premature polymerisation all solutions were placed on ice for 30 minutes before use. All pipette tips, plates and inserts were cooled in the -20°C freezer 30 minutes ahead of use and only removed from the freezer as required. All steps were executed on ice using sterile reagents inside a tissue culture hood.

Collagen gels were polymerised from chloroform treated, isolated rat tail type I collagen, solubilised within a solution of acetic acid (First Link UK Ltd).

In accordance with Artym & Matsumoto, 2010 collagen was neutralised by first adding 10X DMEM that ammounts to 1/6th the total volume of collagen inside a sterile pre-cooled 50ml falcon tube. The 10X DMEM contained phenol red to enable for approximation of pH. The collagen would then turn a straw yellow coulour indicative of an acidic pH.

This was followed by the addition of 10X reconstitution buffer (table 2.6.1) that ammounted to 1/6th the total volume of collagen solution to be used.

Table 2.6.1: Recipe for the produciton of 100ml of reconstitution buffer as described in Artym & Matsumoto, 2010. All solutions were filter sterilised using a 0.2um poresize filter to ensure removal f any microbial contaminants.

Chemical	Quantity
Sodium carbonate (Na_2CO3)	2.2g
HEPES ($C_8H_{18}N_2O_4S$)	4.8g
Distilled Water (H_2O)	100ml

Post additon of reconstitution buffer, collagen was mixed by pipetting as described above. A 1µl sample was then taken and applied to indicator paper to gain a more accurate indication of pH. Finally 2 molar sodium hydroxide is added dropwise with mixing between drops until a pH of 7.4 was achieved. The phenol red should turn from a yellow to a light pink as pH 7.4 is reched. To ensure both solutions have an equal pH frequent testing on indicator paper was carried out. The table below (table 2.6.2) lists volumes used:

Table 2.6.2: Constituents of HD and LD collagen matrices. The volumes can be scaled according to the total final volume required. I routeenly make an additional 10% to account for collagen lost during pipetting post netralisation.

Start mg/ml collagen	Volume Collagen (ml)	Volume of 10XDMEM (ml)	Volume of RC buffer (ml)	Final mg/ml of collagen solution	Total Volume of solution (ml)
2.05	1	0.2	0.2	1.46 (HD)	1.4
5	1	0.2	0.2	3.57 (LD)	1.4

Note the collagen concentration (mg/ml) can be adjusted throuhg the addition of PBS however adjusting the salt level including potassium chloride (a component of PBS) has been shown to impact upon the stability of α-helices which may impact upon the structures formed (Kohn, Kay, and Hodges 1997). Therefore two batches of collagen were utilised to ensure the salt levels for each solution were equal with respects to potassium chloride levels. One at 2.05mg/ml and the other at 5mg/ml.

Once a pH of 7.4 is reached the solution was left for a further minute to ensure equibrilum had been reached and a final reading would be taken. The tube would then be sealed and placed in a centrifuge pre-cooled to 2°C and centrefuged at 300RCF for 1 minute. This final step is essential to ensure there are no bubles left within the solution to prevent structural heterogeneties produced by air bubbles during polymerisation.

While samples were centrifuged the required number of 6-well plates were removed from the -20°C freezer. It was essentail that the plates were cooled to prevent premature polymerisation at room temperature (22°C) ensuring even spreading across the dish and structural consitency from one model to the next. 1.5ml of collagen was pipetted into each well using pre-cooled tips. The plates were tilted in order to evenly spread the solution across the base of the well and then sealed using micropore tape. The plates were then immediately placed at there target polymerisation temeperature for 24h. After a 24h period 2ml of 1X DMEM, pre-heated to 37℃ would be added. At this point models were ready to be seeded as needed.

2.7 Scanning Electron Microscopy (SEM) of Collagen Models.

SEM microscopy utilises a focussed beam of thermionically produced electrons from a tungsten cathode to generate information regarding surface topology and composition of a specimen. In this instance, it is the topological information that is required. As the beam of electrons is scanned across the surface of the specimen electrons will either be; inelastically scattered, incoherently elastically scattered, elastically scattered or transmitted. The inelastic and incoherent scattering result in the production of secondary electrons that are detected and amplified to generate a readable signal. The intensity of the secondary emitted electrons is converted into a grey scale. The secondary electrons emitted from a specific location within the sample will therefore be mapped onto a single pixel as a product of grey. In this way, the topological information can be translated into a 2D grey-scale image.

As electrons are utilised instead of a light source a high vacuum was required for beam operation to prevent electrons being scattered or absorbed by atoms in the path of the beam that are not attached to the surface of the specimen. Therefore, the specimen needed to be completely devoid of water and substances that will evaporate or sublimate in a high vacuum. This presents significant issues in biological specimens since water is actively involved the structural integrity of many proteins including collagen (Brodsky and Ramshaw 1997; Rich, And, and Crick 1961; Brodsky and Persikov 2005). Specimens must therefore be well fixed prior to dehydration.

2.7.1 Fixation

The first fixation was carried out using a 2% solution of glutaraldehyde made up in Sorenson's buffer (table 2.6.1) for 2 hours. Glutaraldehyde is a fast-acting fixative that will keep components in their native positions during the secondary fixation. Sorenson's buffer meanwhile offers far superior buffering capacity compared with PBS reducing the number of artefacts within the sample.

Table 2.7.1: Recipe for 0.2M phosphate buffer with a pH of 7.4: 40.5ml of solution X was added to 9.5ml of solution Y to make to produce 50ml of 0.2M phosphate buffer with a pH of 7.4.

Solution X		Solution Y	
$Na_2HPO_4.2H_2O$	35.61g	$NaH_2PO_4.H_2O$	
dH_2O	1000ml	dH_2O	1000ml

Post primary fixation the specimen was washed for 3×15mins and then a secondary fixative of 0.1% Osmium tetroxide (OsO_4) made up in Sorenson's buffer was applied for 1 hour. Osmium both heavily cross-links proteins and confers electron dense properties to organic components. This aided in the transmission of incoherently scattered electrons through the specimen reducing the noise produced by secondary emitted electrons resultant from incoherent inelastic interactions.

2.7.2 Dehydration, Critical Point Drying and Sputter Coating

Collagen models were taken through a dehydration series of 10%, 30%, 70%, 95%, 100%, 100% ethanol for 15 minutes per concentration. Samples were then critical point dried to avid formation of artefacts or structural alterations as a result of surface tension. This process perfectly preserves collagen in its native configuration provided superficial fluid conditions are met. This required extreme pressure and high temperatures during the exchange of liquid dry ethanol for liquid carbon dioxide.

Dehydrated collagen was then sputter coated with 4nm of chromium to give optimum resolution during secondary electron capture. Thinner coatings proved inadequate to prevent surface charging while thicker coating generated artefacts. Samples were stored under low vacuum prior to imaging to reduce oxidation and production of artefacts.

2.7.3 Image acquisition

Images were acquired using a Hitachi S-5200 with a resolution limit of 0.5nm at 30kV. Secondary electron mode was utilised to gain topological information of the collagen matrices. High magnification images were acquired at a voltage of 30kV with a focus depth of 2µm. These settings were optimised to reduce charging preventing deformation of the collagen structure during imaging. Quantification of collagen matrices at a higher resolution was impractical as the high kVs produced rapid surface charging resulting in movement and deformation of the specimen after only a few minutes of imaging.

2.7.4 Image Analysis

The AnalyzeSkeleton plugin for imageJ (fiji) is an implementation of the 3D thinning algorithm by Lee et al, 1994. The program uses the algorithm to iteratively erode the surface of an object symmetrically to retain the medial points along the skeleton (T. C. Lee, Kashyap, and Chu 1994) . It will therefore retains the midline of every collagen bundle.

Voxels/pixels composing the skeleton are classified into one of three categories; endpoint, junction and slab. End-point voxels have less than two neighbouring voxels, junctional voxels have more than two neighbouring voxels and slab voxels have exactly two adjacent voxels. With these criteria the program was able to render a skeletal image from in which voxels were color-coded and quantified. End-point voxels are blue, slab voxels are orange and junctional voxels are purple (figure 2.7).

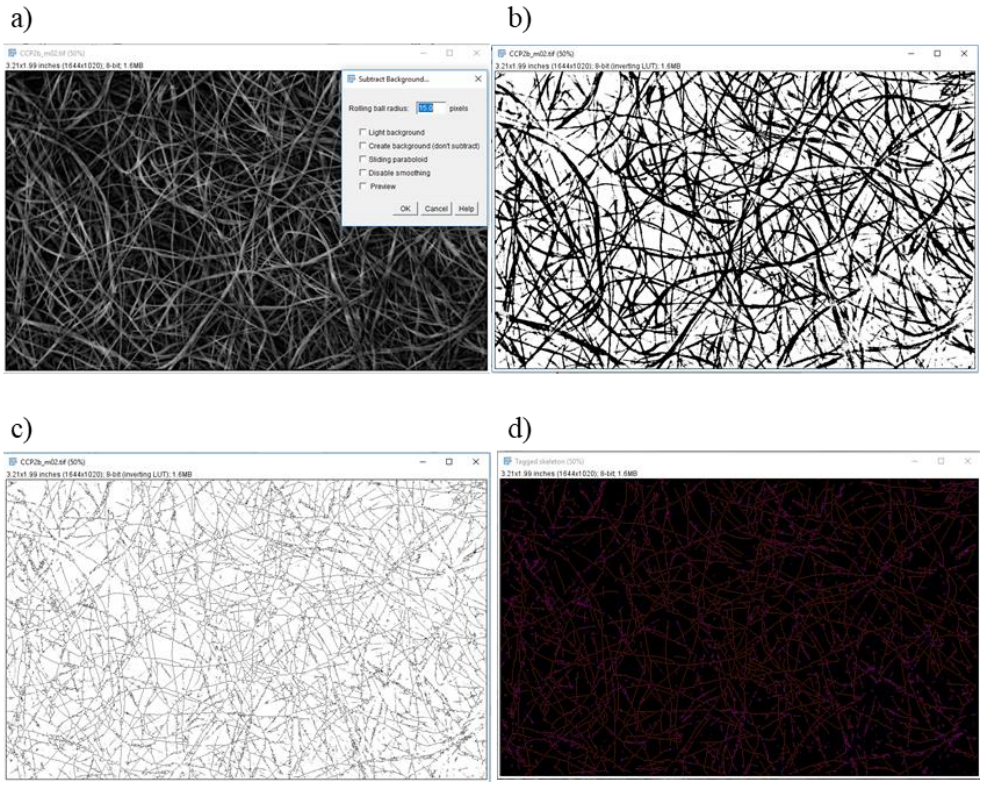

Figure 2.7: Micrographs processed by the AnalyzeSkeleton plugin in imagej. a) Is an SEM images of a collagen matix after removal of background using the rolling ball algorithm set to a pixel radius of 15 (i.e. larger than the larges fibre diameter). b) Is the binarization of the image in a). Pixels no longer have bit depth. They are simply 1 (black) or 0 (white) now. c) The binarized image is then thinned using the plugin written by Ignacio Arganda-Carreras, 2008 ImageJ(fiji) (Valente et al. 2017). d) The

analysed skeleton returning colour coded branches; end-point voxels are blue, slab voxels are orange and junctional voxels are purple.

The table of results displayed the number of branches (slab segments), the number of voxels of every type (slab, end, and junction), the number of actual junctions, the number of triple points (exactly three branches) and quadruple points (exactly four branches), and finally the average and maximum length of branches in corresponding units. This could have been problematic for a matrix in which the skeleton derived may have many interconnected loops and branches as the program may not be able to distinguish one branch from another. This could result in several branches being quantified as one. To overcome this cycle detection and pruning were implemented. In this instance where loops are detected pruning has been calibrated to sever the shortest branches.

Within the plugin there is also options to provide detailed information producing a separate table of results detailing 3D coordinates of the extremes of the branch (vertices V1 and V2) and the Euclidean distance between those extreme points. Using the average of the Euclidean distances and average length of each branch it was possible to generate a value that indicated the tortuosity of the matrix. The arc-chord method is the simplest mathematical method for estimating tortuosity and can be applied to the data outputs from imageJ (fiji). Further to this the number of branch points and distances between branch points were assessed. Fibre widths were manually quantified using the line drawing tool.

2.8 Cell Culture and Treatment of HaCaT Cells

2.8.1 Culture of HaCaT Cells

HaCaT cells were cultured between passage 8 and passage 40 in Dulbecco's modified Eagle's medium supplemented with 10% foetal calf serum (Boukamp et al. 1988). Cells were obtained from a verified stock and cultured without antibiotics to allow for early identification of infection. Cells were passaged weekly and not allowed to grow beyond 70% confluency to ensure cells were retained within the $\log_{10}$ phase of growth. Cells were passaged typically at a 1:25 split ratio upon reaching 70% confluency in a T75 flask with filterer caps (SARSTEDT). Cells were passaged using a 1X trypsin solution of 1:250 made up in sterile 1X phosphate buffered saline (PBS; 137 mM NaCl; 2.7 mM KCl; 10 mM Na_2HPO_4; 1.8 mM KH_2PO_4). The 1:250

designation indicates the tryptic activity based on standardized testing. This ratio indicates that one-part trypsin will digest 250 parts casein in the United States Pharmacopeia activity assay. Cells were seeded at 10,000 cells per well in a 6 well plate to allow for the behaviour of individual cells to be studied at 24h prior to colony formation observed after a 5-day incubation period.

2.8.2 Notes on Choice of System to Evaluate Proliferation and Differentiation Rates in Response to Changes in Collagen Density

Primary keratinocytes culture in vitro at a low calcium concentration retain a basal phenotype, while addition of calcium (>0.1mM) triggers their differentiation, shifting the keratin profile expression pattern from basal (K5 and K14) to suprabasal (K1 and K10) with the concomitant production of involucrin (P. A. Coulombe, Kopan, and Fuchs 1989; Lloyd 1995; Ryle et al. 1989; Micallef et al. 2009; Murthy et al. 1993). There are two major draw backs regarding primary keratinocytes. The first is the need for large amounts of growth factors and the second is that once a cell undergoes a programme of terminal differentiation they rapidly die, preventing analysis of long-term differentiation signals (Hennings et al, 1980).

HaCaT cells however exhibit a capacity to switch freely between a differentiated and basal state depending on the calcium concentration. Critically the cells do not die and detach upon entering a programme of differentiation, they simply express elevated involucrin, K1 and K10 (Deyrieux and Wilson, 2007). To ensure the media was not the driving cause for differentiation low-calcium DMEM (<0.3 μM) was used which has been shown to retain HaCaT cells within a basal, undifferentiated state provided cells are retained in a sub-confluent state. Therefore, any increase in differentiation potential would be attributed to changes in substrate and not as a result of media-induced calcium signalling.

2.8.3 Treatment of HaCaTs With Inhibitors

Inhibitors were purchased from SelleckChem. All drugs were made up in 200X stocks (i.e. 200x working concentration) in dry DMSO such that a final concentration of 0.5% DMSO with inhibitor could be achieved to control for cytotoxicity conferred by DMSO. DMSO was found to have no cytotoxic effects on HaCaT cells below 1% DMSO as determined MTT assay (P. Walsh, 2016).

Erk inhibition was carried indirectly by PD98059 (Erki) through inhibition of the upstream MAPK kinase MEK1. ERKi is a non-ATP competitive inhibitor with an IC-50 of 2uM. It inhibits MEK1 specifically with no inhibition of either p38 or JNK MAPKs. Its effects have been noted after 1h at 10 uM in MCF-7 cells and 1h hour in HepG2 cells at 10 uM after one hour (Cybulsky and McTavish 1997; Gazel et al. 2008; Zu et al. 1998). To ensure adequate levels of inhibition cells were continually exposed during each time course.

SP600125 (JNKi) is a broad-spectrum JNK inhibitor for JNK1, JNK2 and JNK3 with IC50 of 40 nM, 40 nM and 90 nM in cell-free assays, respectively; 10-fold greater selectivity against MKK4, 25-fold greater selectivity against MKK3, MKK6, PKB, and PKCα, and 100-fold selectivity against ERK2, p38, Chk1, EGFR (Bennett et al. 2001). Cells were treated with a with 10uM continually for each time course. The concentration was deemed non-cytotoxic by MTT assay (P. Walsh, 2016).

The p38 inhibitor PD98059 (p38i) inhibits basal MEK1 produced by mutation of serine at residues 218 and 222 to glutamate (MEK-2E) with IC50 of 2 μM. p38i does not inhibit the MAPK homologues JNK and P38. p38i is highly selective against MEK, as it does not inhibit several other kinase activities including Raf kinase, cAMP-dependent kinase, protein kinase C, v-Src, epidermal growth factor receptor kinase, insulin receptor kinase, PDGF receptor kinase, and phosphatidylinositol 3-kinase. p38i inhibits PDGF-stimulated activation of MAPK and thymidine incorporation into 3T3 cells with IC50 of ~10 μM and ~7 μM, respectively (Dudley et al. 1995). p38i potently prevents the activation of MEK1 by Raf or MEK kinase with IC50 of 4 μM, and weakly inhibits the activation of MEK2 by Raf with IC50 of 50 μM. p38i does not inhibit the activation of MEK homologues MKK4 and RK kinase that participate in stress and interleukin-1-stimulated kinase cascades in KB and PC12 cells, and the activation of p70 S6 kinase by insulin or epidermal growth factor in Swiss 3T3 cells (Alessi et al. 1995).

2.9 Immunofluorescence of Collagen Models Seeded with HaCaTs

2.9.1 Sample Preparation

Collagen models were fixed in a 4.0% paraformaldehyde: 0.2% glutaraldehyde PBS solution for 1 hour. Collagen models were then washed 3×10 minutes in 1X PBS followed by permeabilization in 0.2% triton x-100 for 30 minutes. Following this samples were blocked for 1 hour using 0.1% fish skin gelatine: 2% bovine serum albumin made up in PBS. Samples were then incubated at room temperature with either rabbit polyclonal anti-involucrin (ABCAM) or mouse polyclonal anti Ki67 (ABCAM) at 1:100 dilution made up in blocking buffer. For duel labelling samples would be incubated sequentially with each of the primaries at room temperature for 1h. After each primary incubation samples would be washed 3×10 minutes in PBS. After an overnight incubation samples would be permeabilised a second time followed by 3×10 minutes in PBS. Samples were then incubated with alexa fluor secondary antibodies at a 1:500 dilution in blocking buffer for 1 hour. Samples would then be washed for 10 minutes in PBS followed by a 40-minute incubation with 0.5ug/ml DAPI dissolved in PBS. Finally, samples would be washed for 3× 10 minutes in PBS then mounted in vectashield H-1000 (Vector Laboratories) soft set mounting solution before imaging. Slides were sealed with TipEx and kept in opaque containers prior to imaging to preserve fluorescence. Images were acquired as outlined in 2.4.2.

2.9.2 Image Analysis

Ki67 expression was analysed by averaging the average pixel intensity of Ki67 per nuclei. Images were first separated into their composite channels then a mask was created from the blue channel (corresponding to DAPI) using the following macro constructed in imageJ (fiji):

```
macro "MakeMask [F1]" {

run("Subtract Background...", "rolling=150");

run("Smooth");

run("Make Binary");

run("Dilate");

run("Fill Holes");

run("Median...", "radius=9");

run("Watershed");

run("Analyze Particles...", "size=0-infinity circularity=0.00-1.00 show=Masks exclude");

run("Create Selection");

roiManager("Add");

roiManager("Split");

roiManager("Select", 0);

roiManager("Delete");

}
```

In summary the macro subtracts all background based on the size of the largest nuclei using the rolling ball algorithm. This means that a continuous signal larger than the size of a nucleus would be removed, leaving only nuclei as active pixels. The nuclei would then be converted to a binary image and have the spaces within the nuclei filled to return a solid nucleus. The macro is then able to create a perimeter for each nucleus which is then converted into a mask which can then be overlaid onto the red channel (corresponding to Ki67) ensuring only Ki67 within the nuclei was quantified. The following macro constructed in imagej (fiji) was then applied to quantify the pixel intensity for each nucleus within the image:

```
{
run("Subtract Background...", "rolling=90");
roiManager("Select", 0);
n = 1
roiManager("Select", n);
for (i=0; i<=n; n++) {
        roiManager("Select", n);
        run("Measure");
}
}
```

The macro used the mask of nuclei stored within the ROI (region of interest) manager to remove background signal and quantify only Ki67 foci within the nuclei.

3.0 Exploring Mechanical Niches Within the Pilosebacious Unit

To understand the biological significance of mechanical niches along the follicle it was important to consider how mechanical forces were transduced from cell to cell and cell to ECM.

3.1 Keratin and Actin as Mediators of Mechano-Transduction to The Nucleus

Cytoskeletal filaments provide tissues with the structural support required to cope with mechanical stress. However, their role extends well beyond this, being implicated in stimulation of MAPK cascades linked to modulating cellular proliferation and differentiation. These relationships posit questions surrounding the impact of compressive forces exerted along the length of the hair follicle during the shaving process. To understand the biological implication of these forces it is first worthwhile exploring the physical connections that enable the transduction of force from the external environment to the nucleus.

3.1.1 Keratins, Hemidesmosomes and the ECM

Cell-matrix adhesion is crucial to the governing of many biological processes including epidermal homeostasis, wound healing, inflammation and malignant cell progression (Ridley 2003). For epidermal cells, matrix adhesion is maintained by both actin-associated focal adhesions and keratin-associated hemidesmosomes. Much has been elucidated regarding the formation of focal adhesions and the interplay between actin, focal adhesions and MAPK signalling (S. Y. Li, Mruk, and Cheng 2013; Descot et al. 2009). Through the study of mutations and disease, increasingly more is understood surrounding the role of keratin in the formation of the stable, keratin-associated hemidesmosomes and what implications keratin destabilisation and force transduction has on desmosomal formation, stability and signalling to elicit changes in cellular behaviour.

Disruption of the keratin-associated hemidesmosome gives rise to a plethora of chronic diseases including epidermolysis bullosa (figure 3.1). This disease can arise as result of mutation in integrin-linked keratins K5 and K14 or mutations within the genes encoding hemidesmosomal proteins such as the linker protein plectin and transmembrane protein integrin α6β4 (Fine 2010; Sawant et al. 2018; Seltmann et al. 2013; Litjens, de Pereda, and Sonnenberg 2006). The stability of hemidesmosomes is believed to be attributed to the stable interaction of integrin $\alpha 6\beta 4$ with the linker-

protein plectin, which in turn connects the integrin cluster to the keratin intermediate filaments K14 and K5 (de Pereda, Lillo, and Sonnenberg 2009).

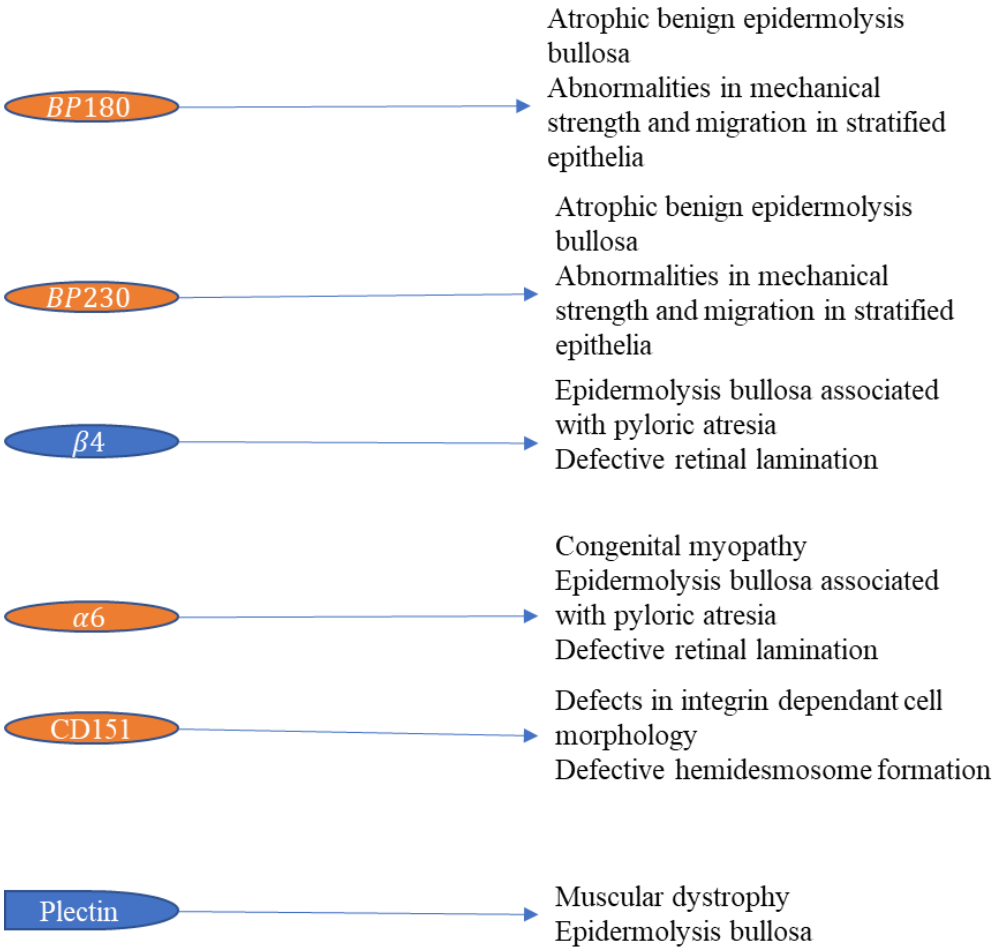

Figure 3.1: Disorders and structural cellular changes associated with defects in the hemidesmosome-mediated ECM-cytoskeleton bridge (McGrath et al. 1995; Walko, Castañón, and Wiche 2015; Hamill et al. 2009; J. Koster, van Wilpe, et al. 2004; Valencia et al. 2013; Berditchevski et al. 2001; Spinardi et al. 1993; L. M. Sterk et al. 2000).

Plectin is able to interact with at least three sites to $\alpha 6\beta 4$ mainly through actin-binding domains within the N-terminal domain of the protein (J. Koster, Van Wilpe, et al. 2004). Binding to keratin is mediated via the C-terminal plakin repeat domain imparting plectin with a duality where it can mediate both focal adhesion (actin-associated) and hemidesmosomal (keratin-associated) dynamics (Andrä et al. 2003; Ozawa et al. 2010; Tsuruta et al. 2011). The association of $\alpha 6\beta 4$ integrin with plectin is essential for hemidesmosomal assemble (J. Koster, Van Wilpe, et al. 2004). The

transmembrane proteins BP130 and CD151 link to plectin and BP230 which act as adaptor proteins, connecting with keratin intermediate filaments, linking the keratin intermediate filament network to the extracellular ligand laminin-332 (Jones, Hopkinson, and Goldfinger 1998; Borradori and Sonnenberg 1999; L. M. T. Sterk et al. 2000).

3.1.2 Cell-Cell Junctions: Desmosomes and Adherens Junction

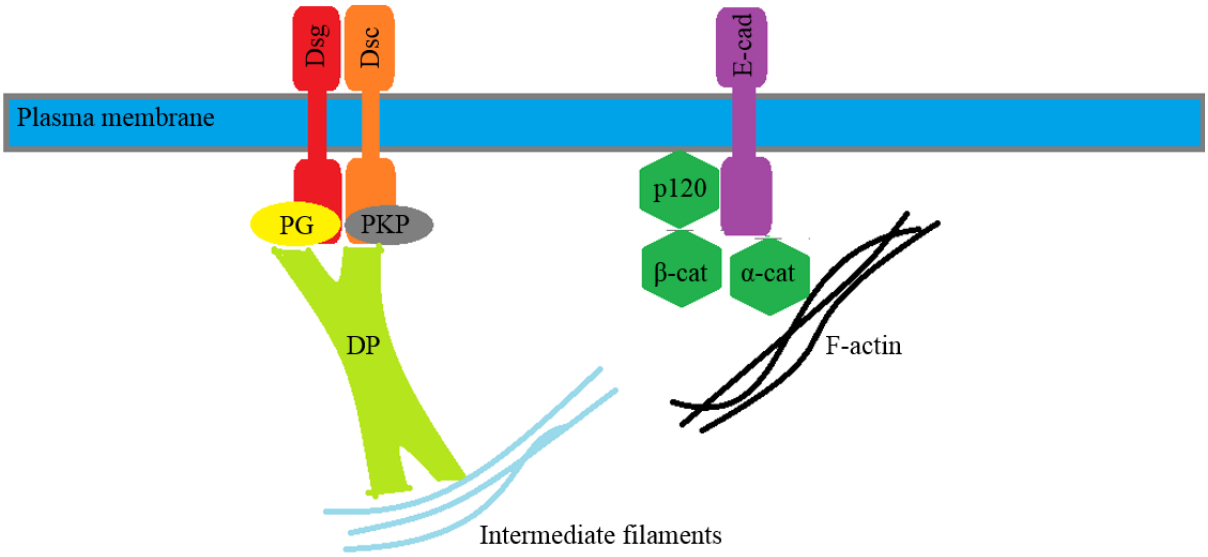

Figure 3.2: Desmosomes (left) and adherens junctions (right): DP, desmoplakin; Dsg, desmoglein; Dsc, desmocollin; PKP, plakophilin; PG, plakoglobin; E-cad, E-cadherin; p120, p120 catenin; β-cat, β-catenin; α-cat, α-catenin.

Adherens junctions are vital cell-cell junctions that have roles in cell-cell adhesion, intracellular signalling and transcriptional regulation, and regulation of actin cytoskeleton dynamics. These junctions are therefore in a position to facilitate the transduction of mechanical cues to inform upon transcriptional changes that govern epidermal homeostasis. In addition adherens junctions establish cell-cell contacts prior to the formation of the stronger and more stable desmosomes and tight junctions. The transmembrane component is comprised by the cadherin superfamily, such as E-

cadherin whilst the cytosolic components are made up from the catenin family members including p120 catenin, α-catenin and β-catenin.

E-cadherin is a classical cadherin that mediates epithelial cell-cell contacts in a calcium (Ca^{2+}) dependent manner similar to Dsc and Dsg (Gooding, Yap, and Ikura 2004). Classical cadherins have five transmembrane repeats that mediate cadherin-cadherin interactions and initiate weak cell-cell contacts leading to the formation of adherens junctions (Nanba, Hieda, and Nakanishi 2000). The formation of intracellular contact imitates clustering of cadherins which spread laterally increasing the strength of the contact (Adams et al. 1998; Ehrlich et al. 2002; Vaezi et al. 2002). Within they cytoplasmic domain there are two defined catenin binding domains that bind p120-catenin and β-catenin (Ferber et al. 2002; Aberle et al. 1994) with α-catenin complexing with β-catenin.

The catenins connect the cadherin complex the actin cytoskeleton and signal transduction pathways (figure 3.2). p120-catenin (p120) is suggested as a stabiliser of E-cadherin at the plasma membrane during the formation of cell-cell contact as disruption of the p120-catenin-E-cadherin interaction using siRNA and mutational analysis (knock down and competitive expression of catenins) results in a loss of retention of the cadherin complex at the membrane (W. Zhang et al. 2006; Thoreson et al. 2000; Jamora et al. 2003; Birchmeier 1995). More recently however, the Src-dependent phosphorylation of p120 catenin was shown to reduce E-cadherin at the membrane promoting cellular migration during wound healing. Inhibition of Src kinases greatly impeded cellular migration and retention of E-cadherin-p120 at the membrane. In this way p120 is more a regulator of E-cadherin having a capacity to both stabilise the complex and bring about its endocytosis and subsequent proteosomal degradation.

The regulation of E-cadherin at the membrane can impact upon the proliferation and differentiation rates of cells through increasing the cytosolic pool of β-catenin and p120 catenin (Thoreson et al. 2000; Ferber et al. 2002). Regulation of the E-cadherin complex poses potential to affect proliferation and differentiation rates since the loss of E-cadherin would increase the pool of cytosolic β-catenin which would in turn produce an upregulation of the Lef/TCF transcription factor promoting proliferation. Further to this p120 depletion has been shown to result in overexpression of the

pluripotency factors Nanog, Oct4 and Sox2 (Li Li, Bennett, and Wang 2012; M. Lee et al. 2014). p120 has been shown to have an overlap in function with β-catenin through interaction with the Kaiso transcriptional repressor. It is believed that the interaction of p120 with Kaiso allows the β-catenin activated transcription factors to bind their targets (Park et al. 2005; del Valle-Pérez et al. 2016).

A key member imparting tissue integrity for tissues that experience physical stress i.e. compression, expansion and torsion, is the desmosome (figure 3.2). Desmosomes bridge the plasma membrane, creating physical connections with adjacent cells via the desmoglein-desmocollin interactions in a calcium dependent manner (Garrod and Chidgey 2008). Desmogleins (Dsc) and desmocollins (Dsg) are in turn connected to desmoplakins via the linker proteins plakoglobin and periplakin (Kowalczyk et al. 1998; Getsios, Huen, and Green 2004; Garrod and Chidgey 2008). It is the c-terminus of the desmoplakins that associate with the intermediate filaments allowing for the intercellular connection of intermediate filaments via desmosomal junctions (Broussard et al. 2017; Choi and Weis 2016; Favre et al. 2018). Dsc and Dsg are also classical cadherins that can associate with p120 and so the establishment of desmosomal junctions may well be a factor in attenuating β-catenin activation of transcription factors promoting quiescence over proliferation in cells.

3.1.3 Keratins, Actin and Nuclear Dynamics

The nuclear envelope links the cytoskeletal components to structural elements of the nucleus with implications in nuclear reorganisation, chromosome remodelling, cell-cycle check points, apoptosis and cytoskeleton remodelling. This intrinsic connection between cell surface receptors, cytoskeletal components (actin and keratin) and nuclear architecture demonstrate the means by which the external environment of a cell could impact directly upon nuclear architecture which provides a pathway for the transmission of physical cues such as compressive forces to exert potential epigenetic control over cellular behaviour.

The current model for the link between the cell cytoskeleton and nuclear cytoskeleton posits that KASH (Klarsicht, ANC-1, and Syne/Nesprin homology) proteins of the outer nuclear membrane link with the SUN (Sad1 and UNC-84) proteins of the inner nuclear membrane to form the linker of nucleoskeleton and cytoskeleton (LINC) complex (Crisp et al. 2006; Haque et al. 2010, 2006; McGee et al. 2006; Ostlund et al.

2009; Padmakumar et al. 2005; Khatau et al. 2009). This complex acts as a physical bridge between the cell cytoskeleton and nuclear lamins at the inner nuclear membrane.

The giant mammalian proteins nesprin-1 and nesprin-2 are anchored to the outer nuclear membrane via a highly conserved C-terminal KASH domain whilst their N-terminal domains bind F-actin (Daniel A. Starr and Fridolfsson 2010; Volk 1992; Nery et al. 2008; Schneider, Noegel, and Karakesisoglou 2008). Phenotypic analysis has shown Syne/Nesprin-1 and -2 anchor nuclei within the cell (Yu et al. 2006; D. A. Starr 2003; D A Starr et al. 2001; X. Zhang et al. 2007). There are currently two hypothesis suggesting the function of these large KASH proteins; 1) They form long filamentous extension for F-actin to associate with, tethering the outer nuclear membrane to actin filaments 2) They form filamentous, spectrin-like baskets surrounding and supporting the outer nuclear membrane (Sosa et al. 2012; Daniel A Starr 2011).

Intermediate filaments have been long established as effectors of nuclear positioning and morphology. Vimentin is often associated with the nucleus with mutations in vimentin producing defects in nuclear architecture (Toivola et al. 2005). The plakin family protein plectin that crosslinks actin to intermediate filaments was found to interact with the KASH domain of nesprin-3 suggesting a physical link between actin, intermediate filaments and nuclear morphology (Wilhelmsen et al. 2005). An observation especially relevant to the study conducted here was the reorganisation of the nucleoplasm as a result of the mechanical pulling of beads attached to cells via adherens junctions (Maniotis, Chen, and Ingber 1997). This reorganisation demonstrates a clear link between cell junctions, actin and nuclear dynamics leading to the hypothesis that KASH and SUN proteins function in the mechanotransduction of physical inputs from the extra cellular matrix directly to chromatin (Jaalouk and Lammerding 2009; N. Wang, Tytell, and Ingber 2009).

More recently a study demonstrated how the SUN protein UNC-84 is required only in force bearing cells to maintain nuclear envelope architecture (Cain et al. 2014). Large deletions within the luminal domain of the protein did not result in distortion in nuclear envelope for hypodermal and pharangeal cells of L1 *C.elegans*. Further to this UNC-84 mutant nuclei were indistinguishable from wild type nuclei of *C.elegans*

embryos. The authors propose that either the LINC complex is not required for nuclear envelope architecture or that the majority of tissues do not experience sufficient force to disrupt the envelope in the absence of the LINC complex. Muscle cells revealed significant distortions of the outer nuclear membrane as a result of disruption of the LINC complex by mutations in UNC-84. These data would suggest that the nucleus its self is important in intermediate filament anchorage and by proxy, force transduction across the cell. In some ways this complex may be critical to providing cells with tensegrity.

3.1.4 The Effect of Mechanical Force on Cell Nuclei

In HaCaT cells the LINC complex has been found to impact upon nuclear size via interaction with both microtubules and F-actin. Disruption of F-actin resulted in shrunken and disfigured nuclei whilst disruption of microtubules caused enlarged nuclei. However, when both were disrupted the same phenotype as when F-actin alone is disrupted was returned implying F-actin and actin binding domains within the LINC complex to be dominant in nuclear dynamics (Lu et al. 2012). It is also well documented that cells in interphase and S-phase exhibit an increase in nuclear volume (Black L 2019, Li Yang 1997). The intrinsic relationship between adherens junctions, actin dynamics and nuclear shape make it pertinent to probe the relationship between nuclear dynamics and proliferation. But first it must be identified if mechanical forces are able to manifest as alterations in nuclear morphology within the hair follicle to establish if such a relationship would be relevant in the context of shaving.

There is growing evidence that physical properties of the ECM modulate nuclear shape. The actin-myosin cytoskeleton transmits mechanical force from focal adhesions at the cell membrane/ECM junction to nuclear LINC complexes and the lamina (Friedl, Wolf, and Lammerding 2011), and the actin cytoskeleton was also shown to be important in coordinating nuclear shape with cell shape (Versaevel, Grevesse, and Gabriele 2012). Substrate stiffness on which NIH 3T3 cells were cultured modulated nuclear shape. Malleable substrates produced cells with round nuclei while stiff substrates led to flattened nuclei (Lovett et al. 2013).

Intriguing interactions between lamin A levels, ECM stiffness, and cell differentiation have also recently emerged (Swift et al. 2013), as well as a novel role for keratin filaments in regulating nuclear shape (C.-H. Lee et al. 2012). K14 was recently shown

to impact upon nuclear shape of cultured keratinocytes. K14 was noted to concentrate around the nucleus with K5 via a disulphide linkage. K14 knockdown produced severe nuclear aberrations. As K14 is only present in basal keratinocytes this could suggest a possible link between keratins, nuclear dynamics and chromatin remodelling. However, is more relevant to this study is that this study demonstrates a physical link between K14 and nuclear morphology and therefore forces transduced from the cell periphery can reach the nucleus via K14.

This chapter evaluated nuclear morphologies to delineate how forces generated during the shaving process were distributed along the hair follicle to identify the hypothesized mechanical niches. The emergence and characterisation of the mechanical niches posited new insight into how different mechanical microenvironments could potentially support homeostasis within different regions.

3.2 The Effects of Pulling Force on Nuclear Morphology

Individual hair shafts within skin explants were loaded with a 2g weight as described in the materials and methods. To ensure only pulled follicle were evaluated post pull, all hairs within an explant would be loaded. While under tension the explant was submerged in a mixture of glutaraldehyde and formaldehyde to produce a "snap-shot" representative of the start of the hysteresis. This allowed for comparison of morphological changes occurring within the pilosebaceous unit and the surrounding dermis/hypodermis during follicular compression. From this it was possible to identify mechanically distinct units within the follicle. Alterations in nuclear morphology (figure 3.3) were used to visualise and quantify changes within the hair follicle. Nuclei were sampled from follicles in the anagen stage of the hair follicle cycle. Follicles were also imaged in real time by multiphoton microscopy to understand the more global changes occurring e.g. the interplay between the follicle, dermis and hypodermis during the pulling event.

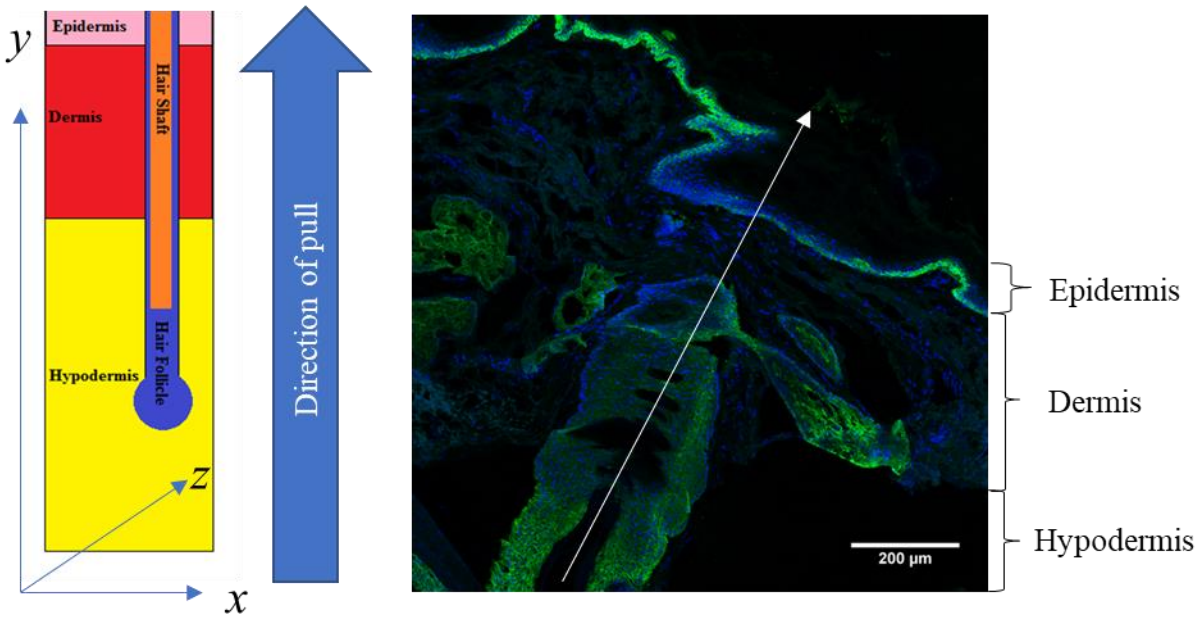

Figure 3.3: Defining the x, y and z axis of the follicle. (Left) A schematic of the hair follicle cross section with respect to the x, y and z dimensions. (Right) Shows a follicular compression in the direction of the white arrow by a 2g weight. All measurements were taken relative to the y-dimension determined by the longitudinal axis of the follicle.

3.2.1 Differential Pull Times Demonstrate Attenuation of Force within the ORS

A 2g weight was loaded onto the follicle for an immediate 'Release', a 1-minute hold or a 10-minute hold to evaluate the impact of force on follicle morphology. The 'Release' time point was executed by loading a 2g weight followed by an immediate release. The 0-minute (release) time point was utilised to illustrated how the follicle was able to recover while the latter time points formed the impression of how forces generated during the pull were distributed along the follicle, and the extent to which localised recovery can take place i.e. regions that will adjust to compensate for the increase in loading. Differences in nuclear compression would indicate potential heterogeneities within the extrafollicular dermis.

3.2.2 K14 Staining Reveals Changes in The Tissue Architecture of The Outer Root Sheath.

K14 labelling was utilised to delineate the ORS from the abutting tissues as it is not expressed in the adjacent dermal sheath (DS) or companion layer (CL) nor in the indirectly abutting inner root sheath (IRS) (Langbein and Schweizer 2005b; Langbein et al. 2010; L.-H. Gu and Coulombe 2007b) Compressive forces acting upon the ORS produced wave-like compression within the infundibulum region as is evident from the K14 labelling (figure 3.4) indicating a reduction in length of the follicle due to compression. Interestingly the largest number of wave-like compressions was produced within the ORS of the infundibulum during the 1-minute hold and not the 10-minute hold suggesting the tissues were compressing further down the follicle post pull after a 10-minute hold. The No Pull (NP) (figure 3.4) images exhibited increased homogeneity in nuclear morphology compared with the subsequent time points which appear to exhibit a shift in morphology. The nuclei post 1-minute hold appear to become more elongated in the x-dimension and return to a more rounded morphology post the 10-minute hold time point which indicted alleviation of compression acting on the cells of the outer root sheath within the infundibulum. There also appeared to be a reduction in the y-dimension (i.e. along the direction of the pull) from NP to 1-minute hold and then an increase from 1-minute hold to 10-minute hold. Upon visually seeing deformation of the ORS the next step was to quantify to what extent nuclei within this region are being deformed.

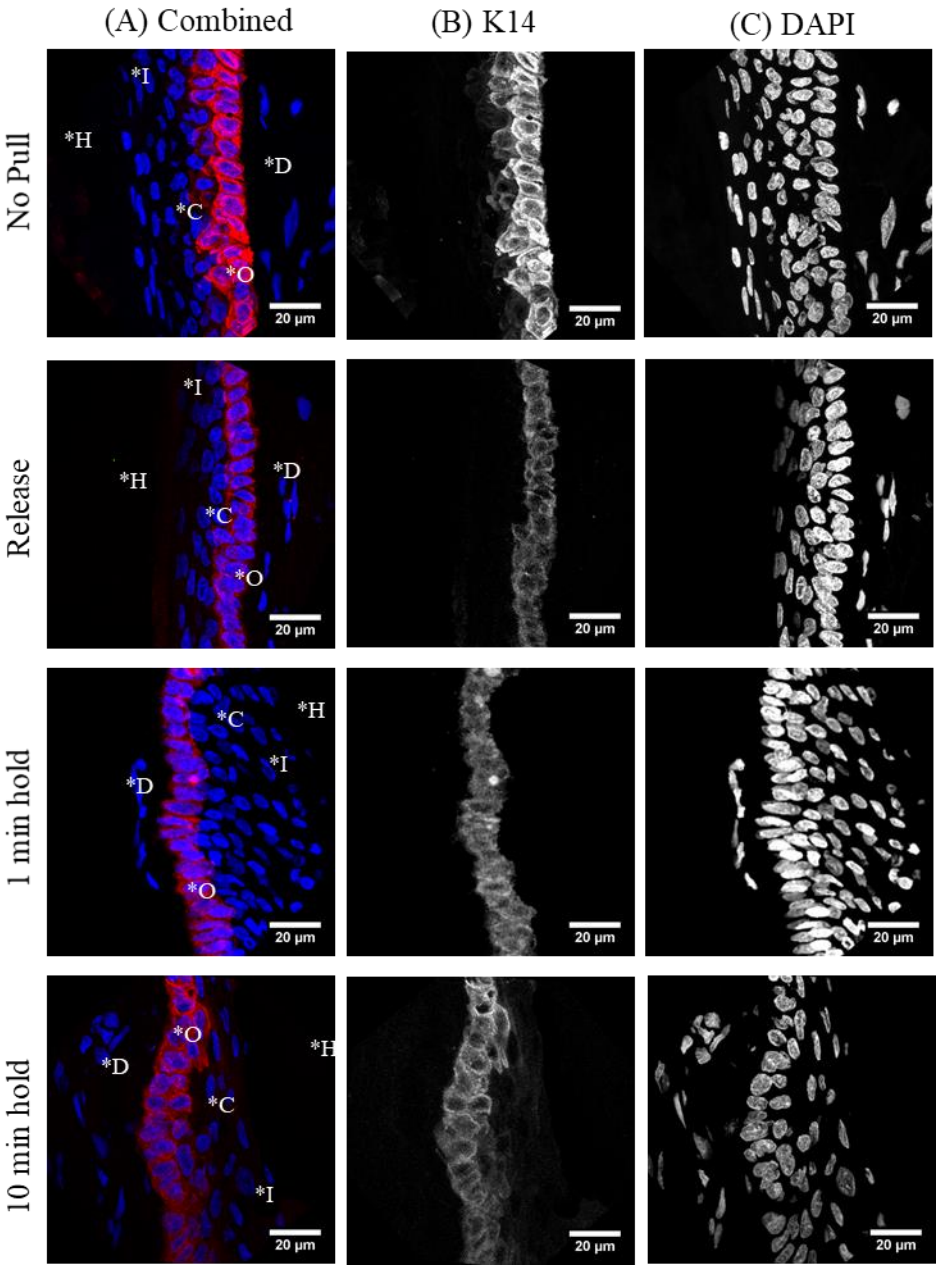

Figure 3.4: Confocal images of infundibulum. Representative of the 'Release', 1-minute hold and 10-minute hold. Scale bars represent a 20 µm distance. The merged images (A) show both DAPI (blue) and K14 staining (red). K14 is a keratin specific to the ORS of the hair follicle. It is not expressed within the adjacent DS, CL or the indirectly adjoining IRS. (A) H-hair shaft; I-inner root sheath; C-companion layer; O-outer root sheath; D-dermal sheath. (B) and (C) are images generated from excitation at 488nm and 405nm respectively.

3.2.3 Quantification of Nuclei Dimensions (x,y and z) Indicates a Recovery of Nuclear Morphology with Increased Duration of Pull Within the Infundibulum

There was a significant increase in the x-dimension at the 1-minute hold and 10-minute hold (figure 3.5) compared with the NP time point, indicative of nuclei being compressed. There was no significant increase from the 1-minute hold to the 10-minute hold suggesting the level of x-deformation has reached a maximum or that there is a lessening in the forces being exerted on cells in the outer root sheath of the infundibulum between 1-minute and 10-minute holds. The 0-minute (release) time point exhibited no significant difference indicating sufficient elasticity for the structures to return to their native conformation.

The y-dimension (figure 3.5) exhibited the converse trend with both the 1-minute hold and 10-minute hold having a significantly lesser y-dimension indicative of nuclear compression along the direction of the pulling force. However, the greatest difference in this instance is not between the 10-minute hold and the NP. It is instead between the 1-minute hold time point and the NP. Again, this suggested a reduction in the forces acting on the nuclei within the ORS of the infundibulum region from 1min hold to 10-minute hold duration. The significant decrease from NP to 0-minute (release) was greater than the decrease from 0-minute (release) to 1-minute hold indicating that the effects of the hair pull on nuclear morphology diminished with increased pull duration. This suggested a lessening of the intra follicle compression within the ORS of the isthmus region as pull duration was increased.

The data for the z-dimension (figure 3.5) shows and initial increase at 0-minutes followed by a decrease from 0-minutes to 10-minutes. The initial increase followed by a decrease was again indicative of a lessening the forces acting on the nuclei within the outer root sheath of the isthmus as the duration of the compression was increased. Interestingly the 1-minute hold time point does not produce a significant deformation in the z-direction as is the case for the x-, and y-dimensions indicating the presence of two forces acting independently of one another. One acting longitudinally along the follicle and the other acting laterally to the follicle (figure 3.5).

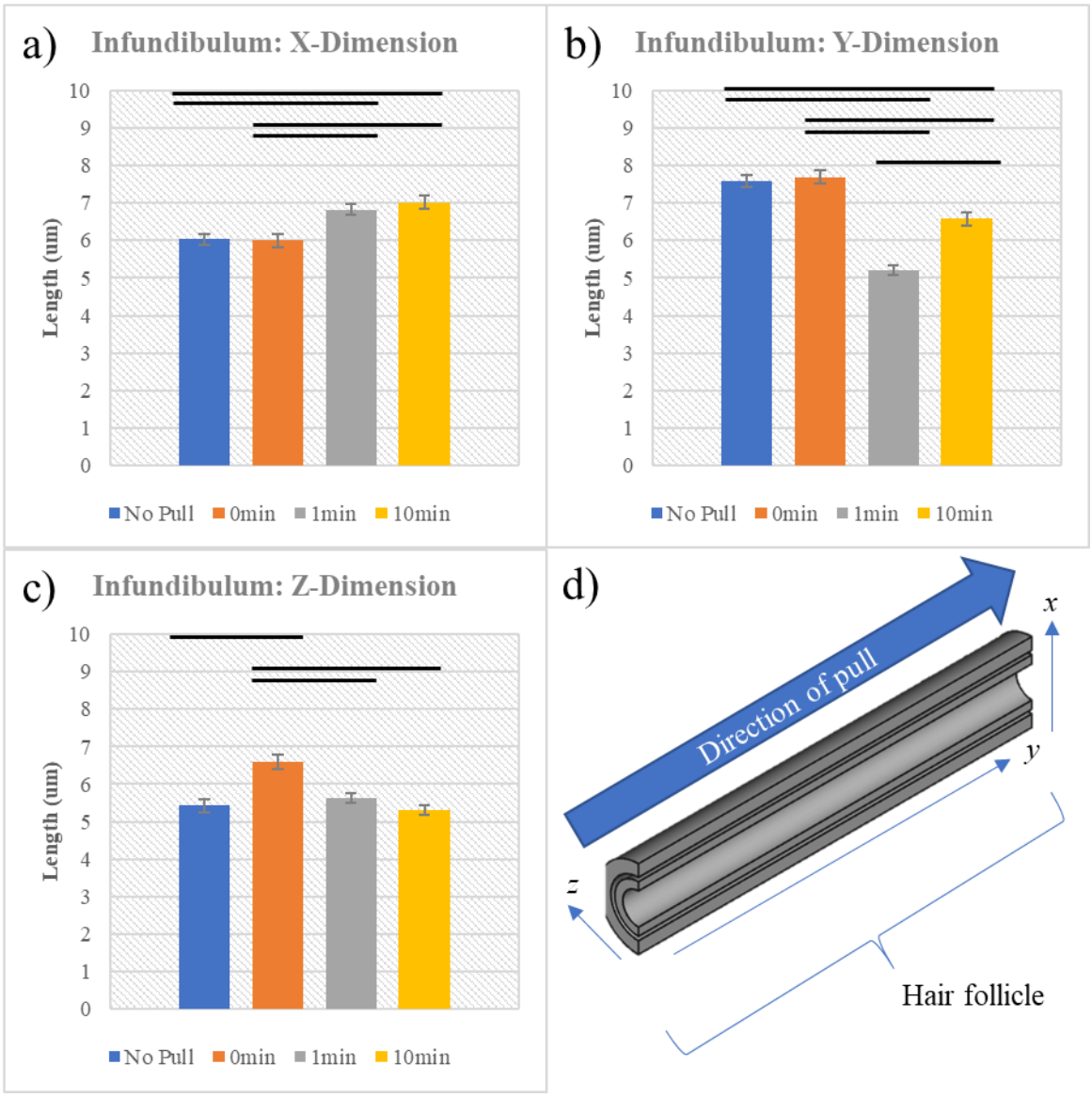

Figure 3.5: Dimensional changes of nuclei within the ORS of the infundibulum. a-c) Mean changes in length of the x-, y- and z-dimension with increased duration of pull. d) Illustrates how these dimensions translate to the follicle with x and y forming the cross-section plane and z extending through the cross-section plane, perpendicular to the direction of the pull and x-dimension. The error bars represent the standard error of mean with black bars highlighting groups significantly different from one another (n=10, $P \leq 0.0167$) as determined by anova and post hoc t-test. >30 nuclei per region analysed for each repeat.

Anova data for x-, y- and z-dimensions for nuclei within the ORS of the infundibulum region returned P-values of 1.68×10^{-6}, 1.98×10^{-32} and 1.86×10^{-8} respectively. All were statistically significant (≤ 0.05) demonstrating that the duration of the pull had a significant effect on nuclear morphology with respects all three dimensions. To better resolve where these differences are a Tukey's test was conducted with an adjusted critical value of 0.0167 to reduce the chances of a type-1 error occurring. These significant differences are highlighted within the respective graphs.

3.2.4 K14 Labelling Reveals Pronounced Wave-Like Compressions Within the ORS of the Isthmus Region Compared with the Infundibulum Region

Visually the isthmus region (figure 3.6) exhibited a similar pattern of ORS deformation to that of the infundibulum with the highest degree of ORS 'ruffling' evident at the 1-minute hold time point, and the 10-minute hold appearing to resemble the NP and 'Release' more closely than the 1-minute hold. The nuclei adopted a flattened morphology at the 1-minute time point and return to a more oval morphology at the 10-minute time point. This suggested that the tissue is able to readjust itself during a longer pull duration. The lack of deformation at 0-minutes (release) again could have been attributed to inherent elasticity within the system that enabled the nuclei to return to their native morphology. A notable difference between the infundibulum images occurred at the 1-minute time point where significant deformation in the form of ruffling was evident.

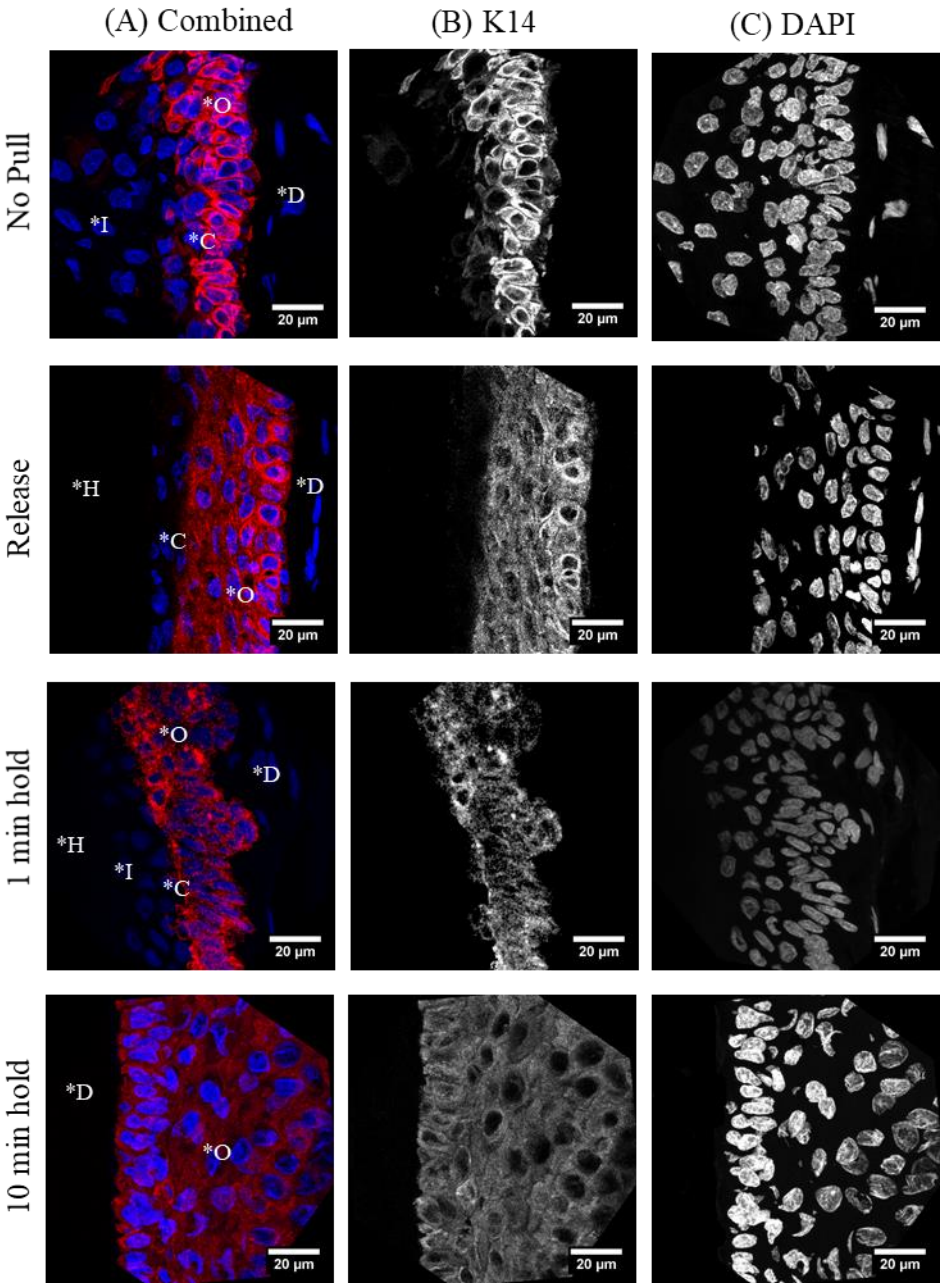

Figure 3.6: Confocal images of the ORS within the isthmus. Representative images of release, 1-minute and 10-minute pull durations. Scale bars span a 20 µm length. (A) Represents the combined image of (B) and (C) with K14 (red) and DAPI (blue) labelling; H-hair shaft; I-inner root sheath; C-companion layer; O-outer root sheath; D-dermal sheath. Columns (B) and (C) represent images obtained from excitation at 488nm and 594nm respectively.

3.2.5 Changes in Nuclear Morphology Implicate the ORS of the Isthmus Region as The Most Compressed Region of The Follicle.

The x-dimension exhibited a significant increase after a 1-minute hold and a 10-minute hold compared with NP as was also the case for the infundibulum region (figure 3.8). This suggest the nuclei adopted a more flattened morphology due to compressive forces acting along the follicle length. 1-minute and 10-minute holds similarly produced a significantly longer x-dimensions compared with the 'Release' time point. This again supported observations made within the infundibulum region. Thus, as the duration of the pull increased so did deformation in the x-direction. There was no significant reduction in the x-dimension at the 10-minute hold time point compared with the 1-minute hold time point. The average x-length at 10-minute hold was less than the 1-minute hold which supported observations made in the infundibulum that compressive forces acting along the follicle are attenuated with time when a 2g weight is applied.

Interestingly, the most profound change was evident in compression of nuclei along the direction of the pull (y-dimension) (figure 3.7). This was key as it implied a greater force acting within this region compared with the infundibulum resulting in immediate morphological deformation that was not present until the 1-minute hold time point for the infundibulum. The largest difference was observed for the 1-minute time point as was the case for the infundibulum. The 10-minute hold time point exhibited the least difference from the NP further supporting this lessening of compression acting on those specific cells between 1-minute hold and 10-minute hold. However, an important difference to note between the infundibulum and isthmus was the significant difference between the 'Release' and 10-minute hold that was absent in the infundibulum region. The 10-minute hold produced a significantly longer y-dimension (figure 3.7) compared to the 1-minute hold which adopted a morphology more like the NP morphology indicative of a reduction in compressive forces acting on cells within the isthmus region of the ORS.

The z-dimension implied an initial increase in follicle diameter at 0-minute (release) with subsequent decrease toward 10-minute hold (figure 3.7), not unlike the infundibulum. However, unlike the infundibulum the 10-minute hold produced a significantly lower z-length than the NP. The infundibulum returned to its original z-length whilst the isthmus retreated further achieving a lesser z-length.

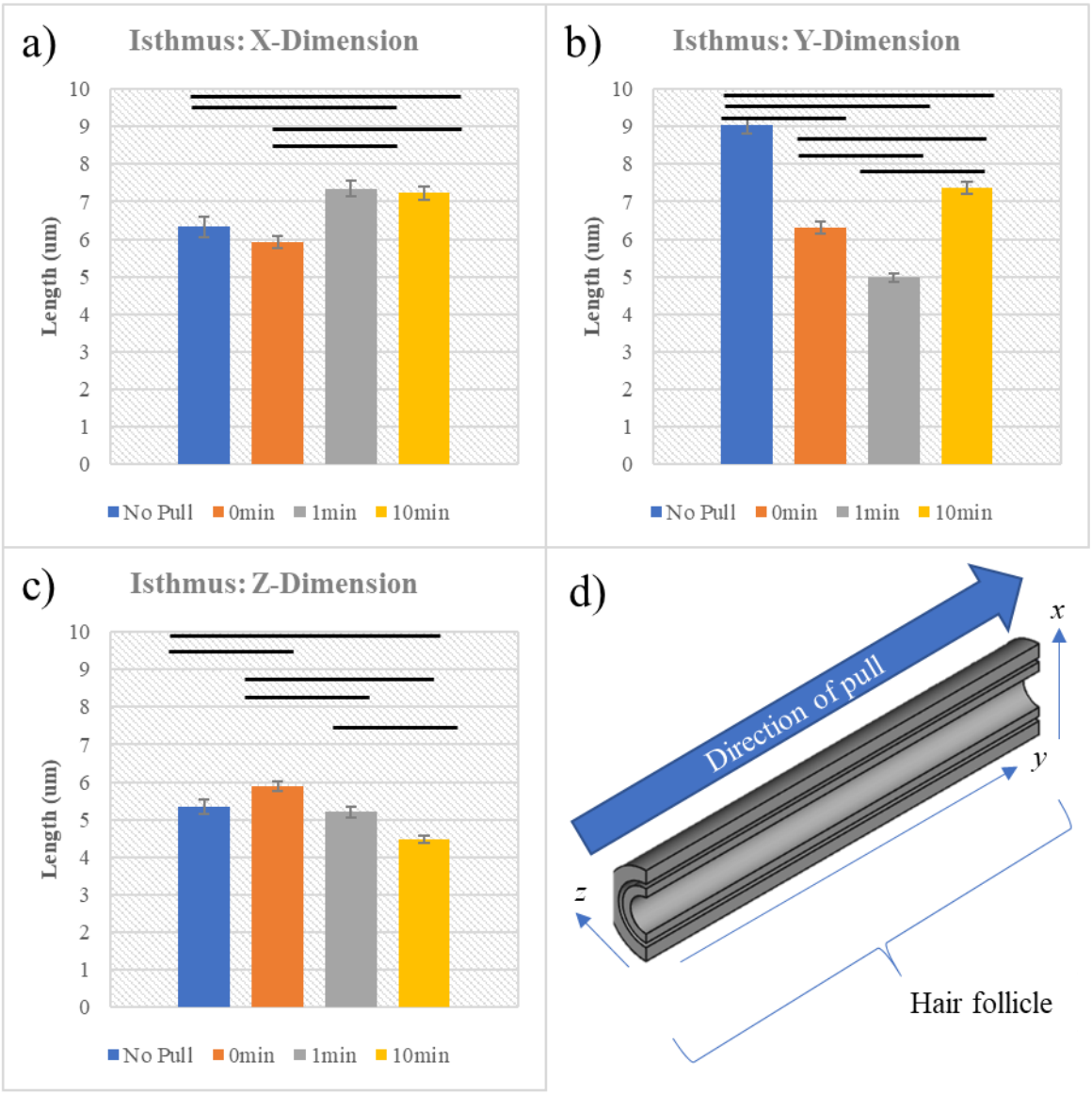

Figure 3.7: Nuclear deformations within the ORS of the isthmus generated by varying pull times a-c) Changes in length of the x-, y- and z-dimension of nuclei. d) Illustrates how these dimensions translate to the follicle with x and y forming the cross-section plane and z extending through the cross-section plane. The error bars represent the standard error of mean with black bars highlighting groups significantly different from one another (n=10, $P \leq 0.0167$) as determined by anova and post hoc t-test. >30 nuclei per region analysed for each repeat.

Anova data comparing all three dimensions of the nuclei within the ORS returned P-values of 2.05×10^{-8} $3.69\times10^{-40}$and 3.59×10^{-15} respectively. As was observed in the infundibulum region of the ORS, all were statistically significant (≤ 0.05) demonstrating that the duration of the pull had a significant effect on nuclear morphology.

3.2.6 K14 Labelling Reveals a Lack of Compression and Thickening of the ORS within the Suprabulbar Region

There was a distinct lack of deformation within the ORS of suprabulbar region (figure 3.8) with the ORS showing a straight conformation versus the undulating conformations produced in the infundibulum and isthmus regions by the 2g pull. Further to this the ORS appeared thicker in this region compared with the two preceding regions. These images indicated the compressive forces acting along the follicle were more strongly resisted or dissipated in the suprabulbar region compared with the two preceding regions.

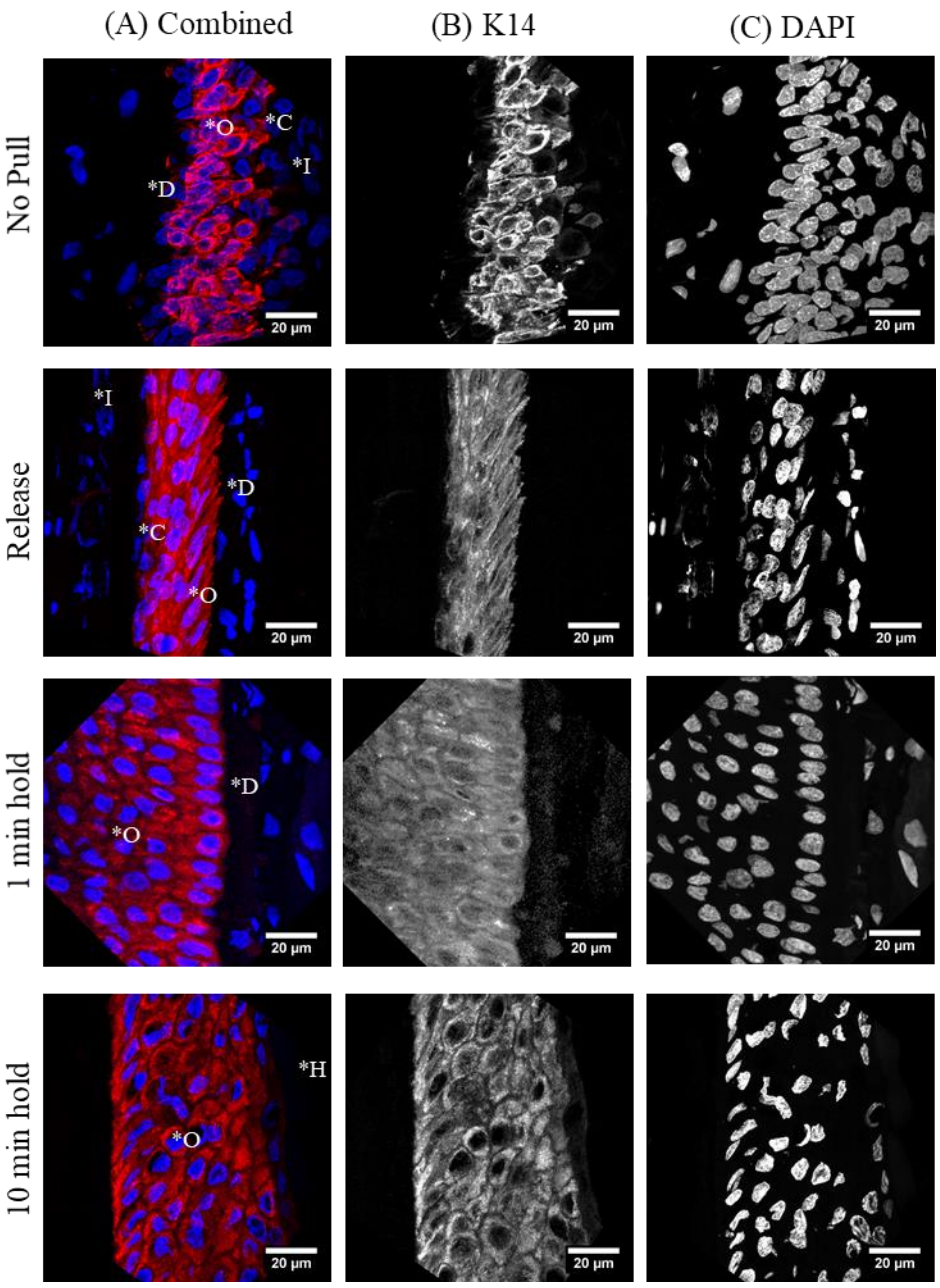

Figure 3.8: Confocal images of the ORS within the suprabulbar region. Images representative of 'release', 1-minute and 10-minute pull durations. Scale bars are 20 µm long. (a) The merged images show both DAPI (blue) and K14 staining (red). Columns (b) and (c) are images generated by laser excitation at 488 nm and 405 nm respectively. (a) H-hair shaft; I-inner root sheath; C-companion layer; O-outer root sheath; D-dermal sheath.

3.2.7 Attenuation of Nuclear Compression Within the Suprabulbar Region of The Follicle

A significant increase in the x-direction post 1-minute hold and a 10-minute hold (figure 3.9) was indicative of nuclear compression. There was also a significant decrease in x-length from 1-minute hold to 10-minute hold indicating attenuation of compression. The 0-minute (release) time point also exhibited no significant variation from the NP indicative of elastic properties of the ORS within this region which were also observed for both the infundibulum and isthmus regions of the follicle.

Numerical analysis of nuclei within the suprabulbar region revealed a difference in nuclear compression between the cycling (suprabulbar region) and non-cycling portion of the follicle (infundibulum/isthmus). There was an initial increase at 0-minute hold in the y-dimension suggesting the nuclei were being elongated along the length of the follicle (figure 3.9). The subsequent decrease from 0-minute (release) to 1-minute hold showed the nuclei had become compressed as a result of the increased pull duration, in affirmation with the effects of the longer pull duration in both the infundibulum and isthmus region. The 10-minute time point exhibited a significantly longer y-length than the NP suggesting the nuclei were elongated again after the 1-minute hold time point. The key difference here is the elongation aspect that occurs which pointed to an opposing pull acting on the base of the follicle.

The z-dimension exhibited an initial increase at 0-minute followed by a decrease from 0-minute hold to 10-minute hold. There was a significant reduction from 0-minute to 1-minute hold and a lesser but still significant decrease from 1-minute hold to 10-minute hold. These significant reductions indicated a reduction in follicle diameter with increased pull duration as was evident for finding in both the infundibulum and isthmus.

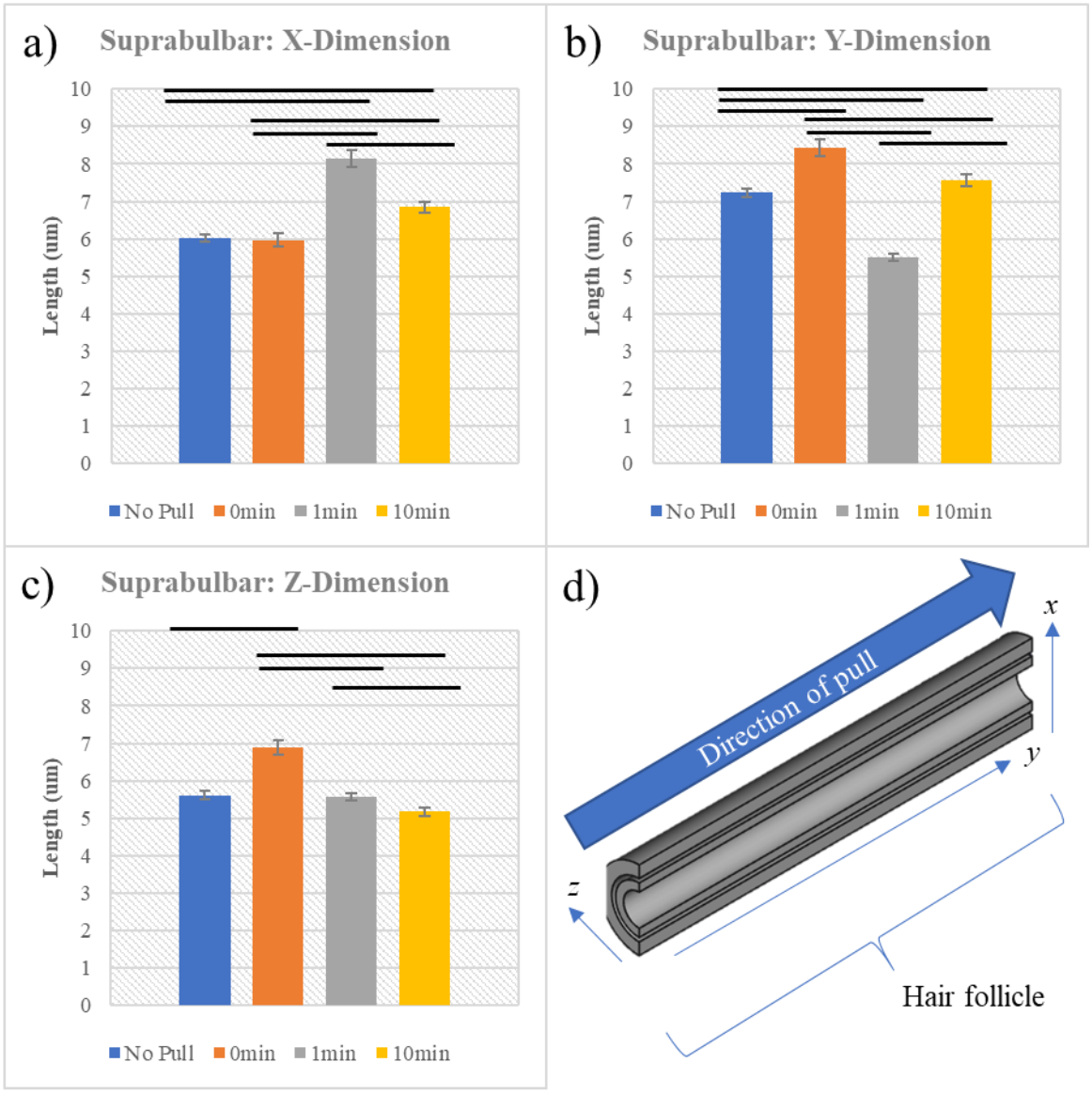

Figure 3.9: Nuclear deformations within the suprabulbar region of the ORS. a)-c) Changes in length of the x-, y- and z-dimension with increased duration of pull. d) Illustrates how these dimensions translate to the follicle with x and y forming the cross-section plane and z extending through the cross-section plane. The error bars represent the standard error of mean with black bars highlighting groups significantly different from one another (n=10, $P \leq 0.0167$) as determined by anova and post hoc t-test. >30 nuclei per region analysed for each repeat.

Anova data for x-, y- and z-dimensions for nuclei within the ORS of the isthmus region returned P-values of 5.55×10^{-21}, 8.23×10^{-23} and 2.65×10^{-14} respectively. All were statistically significant (≤ 0.05) demonstrating that the duration of the pull had a significant effect on nuclear morphology with respects to the x-, y- and z-dimensions.

3.2.8 Differential Response to Pull Times Demonstrate Differences in Response to Compression Between Undifferentiated ORS Cells and differentiated ORS and IRS cells

Having developed an understanding of the mechanics of the ORS it was interesting to investigate the IRS and differentiated cells of the ORS. This is the second thickest layer of the follicle after the ORS and directly abuts the hair shaft. It is separated from the ORS by a duel layer of cells that comprise the CL layer (Birbeck & Mercer 1957, Langbein & Schweizer 2005).

3.2.9 Increased Pull Duration Widens the IRS Within the Infundibulum Region of the Hair Follicle.

Increased pull duration caused cells within the IRS of the infundibulum to bunch as indicated by an increased region of involucrin expression (figure 3.10). Visually it was evident that as the compression within the ORS increases the bunching of nuclei within the IRS increased also. The level of bunching within the IRS of the infundibulum was less post the 10-minute hold compared with the 1-minute hold (figure 3.10). This was in accordance with observations within the infundibulum of the ORS. However, a difference can be seen in the orientation of nuclei. The nuclei did not appear to be changing shape i.e. going from a sphere to an ovoid and *vice versa*.

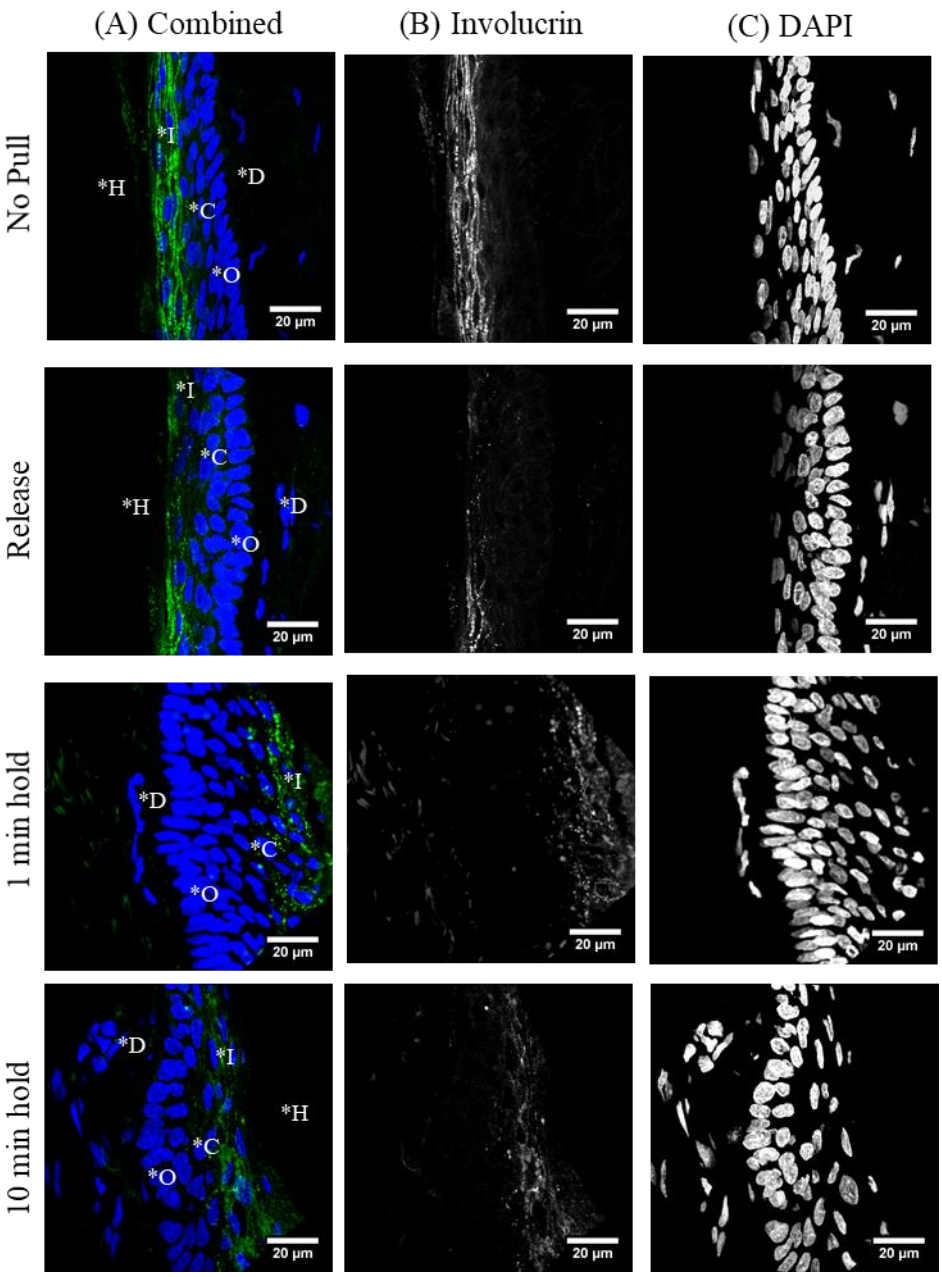

Figure 3.10: Confocal images of the IRS within the infundibulum. Scale bars set to 20 µm long. (a) Illustrates an overlay of involucrin (b) and DAPI (c) with green indicating involucrin and blue indicating nuclei. Note that involucrin occupies a broader cross section at 1min hold. (a) H-hair shaft; I-inner root sheath; O-outer root sheath; D-dermal sheath.

3.2.10 Nuclei of the Infundibulum Are Compressed During Pulling

The x-dimension exhibited a significant increase after the 1-minute hold compared with the NP which was complimented by a significant decrease in the y-dimension for the corresponding time point indicating the nuclei were becoming compressed with respect to the z-axis (figure 3.11). Although a decrease within the z-dimension was observed, this was not found to be significant. This indicated a reduction of retraction of the hair shaft post the 1-minute hold and is also aligned with observations made within the ORS for the same timepoint further supporting the ORS and IRS work in unison up until the 1-minute hold. The conical shape of the hair shaft may be the driving force behind the latent retraction. There was also no significant change in the x-dimension compared with NP after the 0-minute (release) (also observed within the ORS) solidifying the unified relationship between the IRS and ORS up until the 1-minute hold at the level of the infundibulum (figure 3.11,). Where the x-dimensional changes within the IRS differentiated from those within the ORS was post the 10-minute hold, where within the IRS the x-dimensions returned to the unloaded length unlike nuclei within the ORS that retained an elongated x-dimension.

When considering the y-dimensional changes in relation to the x- and z-dimensions it appeared the nuclei were being rearranged around the z-axis (figure 3.10). There was a transition from an elongated conformation to a flattened conformation from 0-minute to 1-minute hold and then a return to a longitudinal conformation not significantly different from the NP (figure 3.11). This mode of action was similar to the ORS in that after a 10-minute hold the nuclei within the IRS also achieved an unloaded conformation.

Changes within the z-dimension were similar to those made within the ORS of the infundibulum region which also demonstrated a significant increase after 0-minute hold followed by return to a resting z-length post the 0-minute hold supporting the premise that the ORS and IRS operate in unison as far as the 1-minute hold. The increase in z-length from the 1-minute hold to the 10-minute hold is again where this similarity ceased as although not statistically significant there was a notable increase in the z-dimension of nuclei within the IRS of the infundibulum post the 10-minute hold. This was the converse of what had been observed within the ORS suggesting the IRS and ORS behave independently of one another post the 10-minute hold.

Combined these findings implicate the IRS and ORS as co-operators until the 1-minute hold as the changes in nuclear orientation within the IRS correspond to nuclear morphological changes within the ORS until this time point. After the 10-minute hold there was evidence that the IRS behaved independently of the ORS. The effects of pull duration on nuclear morphology were substantiated by the anova ($P \leq 0.05$) outcomes: x-dimension $P=7.22\times10^{-11}$; y-dimension $P=7.08\times10^{-11}$; z-dimension $P=1.61\times10^{-7}$. The post hoc t-test (Tukey's test) illustrated how only two dimensions are being significantly altered in support of a rotation around an axis as opposed to compression and loss of volume which was observed for nuclei of the ORS (figure 3.11)

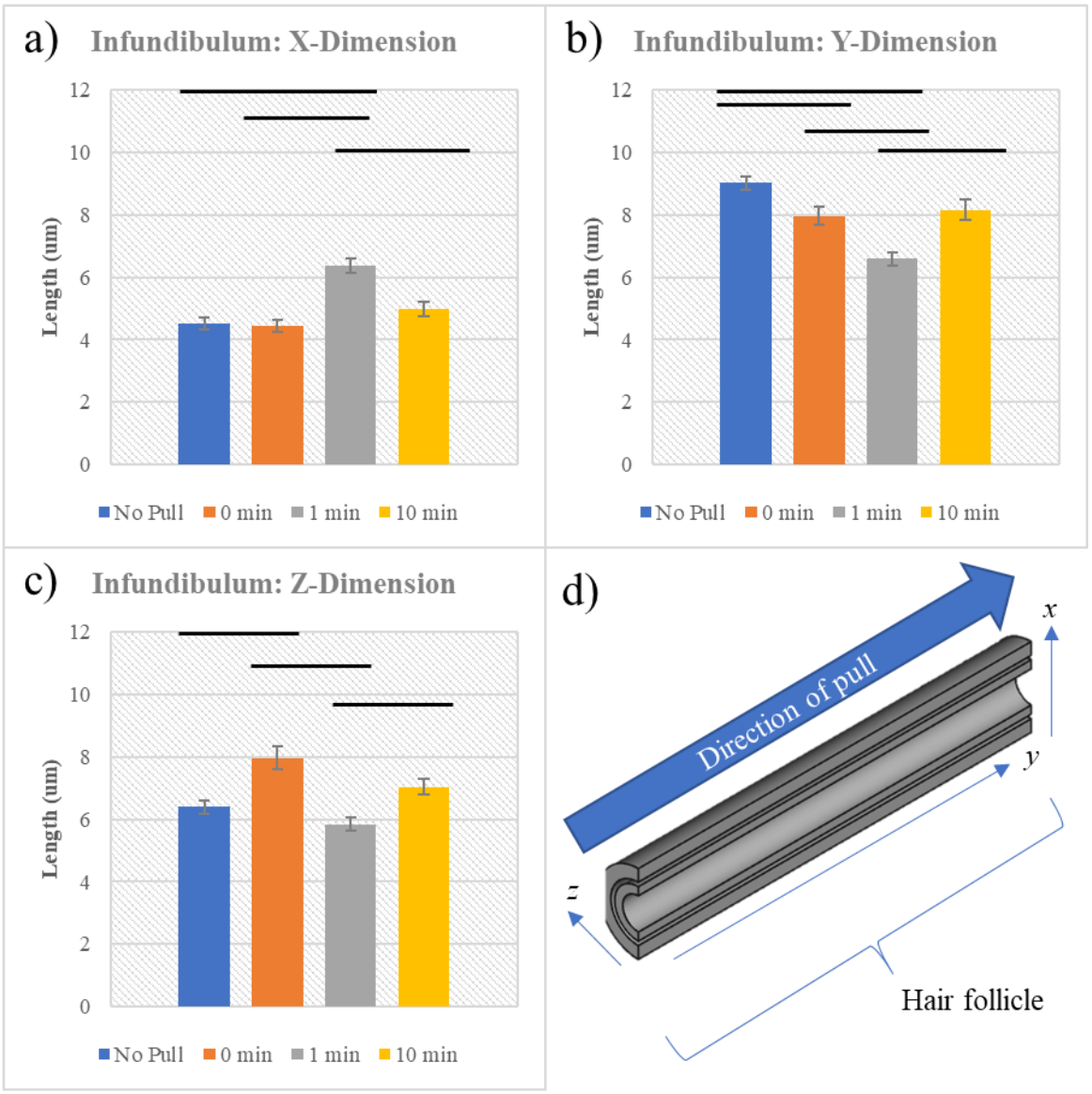

Figure 3.11: Nuclear morphology changes within the IRS of the infundibulum. (a)-(c) represent changes in nuclear morphology in the x-, y- and z-dimension respectively which can be interpreted in relation to the pull direction and follicle orientation (d). The error bars represent the standard error of mean with black bars highlighting groups significantly different from one another (n=10, $P \leq 0.0167$) as determined by anova and post hoc t-test. >30 nuclei per region analysed for each repeat.

3.2.11 Involucrin Labelling Indicates the Isthmus of the IRS Reveals a Lack of Wave-Like Compressions

The nuclei within the isthmus exhibited a more spherical morphology across all time points compared with those of the infundibulum making it is difficult to visually discern any changes in orientation or morphology (figure 3.12). A striking difference between the infundibulum and isthmus region was that the crumpling of the ORS within this region was not mirrored by the IRS (figure 3.12). This suggested the IRS to be more resistant to compressive forces or that these forces were attenuated by the properties of the ORS.

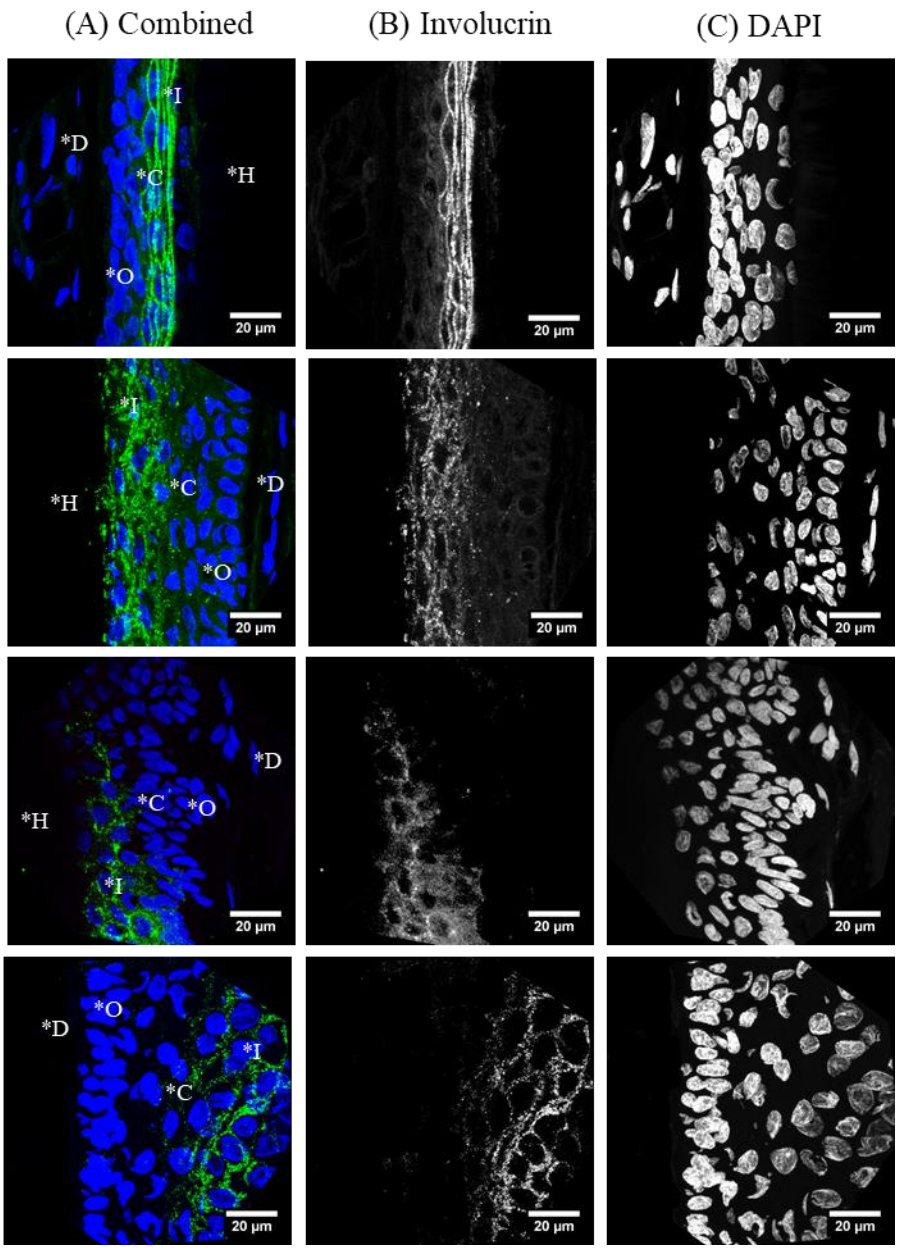

Figure 3.12: Confocal images of the IRS within the isthmus region of the follicle for the respective time points and the control (NP). Scale bars set to 20µm long. (a) Is the product of a two-channel overlay produced by excitations at 488nm (b) and 504nm (c) indicative of involucrin and nuclei. (a) H-hair shaft; I-inner root sheath; C-companion layer; O-outer root sheath; D-dermal sheath.

3.2.12 Compression of The Isthmus Region Within the IRS

The nuclei within the isthmus region of the IRS exhibited volumetric changes as indicated by significant changes across all three dimensions for both the 0-minute (release) and 10-minute holds. The outcome of the anova demonstrated the duration of the pull to have a significant impact upon the morphology of the nuclei within the IRS of the isthmus region for the x-, y- and z-dimension.

During the 0-minute timepoint the initial increase in x-length length showed a significant decrease (figure 3.13) suggesting the nuclei were becoming elongated. However, the corresponding y-value was significantly less (figure 3.13) indicting the nuclei were not stretching along the y-axis but instead are being stretched around the circumference of the hair shaft. The significant increase in z-length produced by the 0-minute time point (figure 3.13) supported this model of change. Combined these three data points indicated an increase in diameter of the IRS within the isthmus region which was also observed within the ORS of the isthmus region demonstrating these two layers behave as one during the 0-minute time point.

The significant decrease in the y-dimension after the 1-minute hold combined with an increased z-dimension suggested the nuclei to be rotating around the x-axis. (figure3.13). This indicated the compressive forces were attenuated during the 1-minute hold which was also observed within the ORS as a lessening of change in both the x- and z-dimension. However, there was a clear difference in that the nuclei within the ORS experienced considerable deformation post the 1-minute hold whilst those of the IRS exhibited only a change in orientation. This suggested that the ORS and IRS behave independently of one another post the 1-minute hold or that the compressive forces within the IRS were ameliorated by conformational changes within the ORS.

The 10-minute hold revealed a significant increase in the x-dimension combined with a significant reduction in both the y- and the z-lengths (figure 3.13). This implied the nuclei were being flattened along the x-axis. This same pattern of deformation was observed for nuclei within the isthmus region of the ORS suggesting the expansion of the ORS in the x-direction accommodates for expansion of the IRS in the x-direction. It should also be noted that expansion in the x-dimension within the IRS was delayed compared to that of the ORS demonstrating the IRS and ORS behaved independently while still having a functional impact upon one another.

When the findings here are considered in relation to those of the ORS a parallel can be drawn as the isthmus region also exhibits the highest degree of nuclear deformation suggesting this region may act as a force dissipation region, relieving the compressive forces experienced by nuclei within the infundibulum and suprabulbar region of the follicle. Both the IRS and ORS exhibited significant compression within the isthmus region.

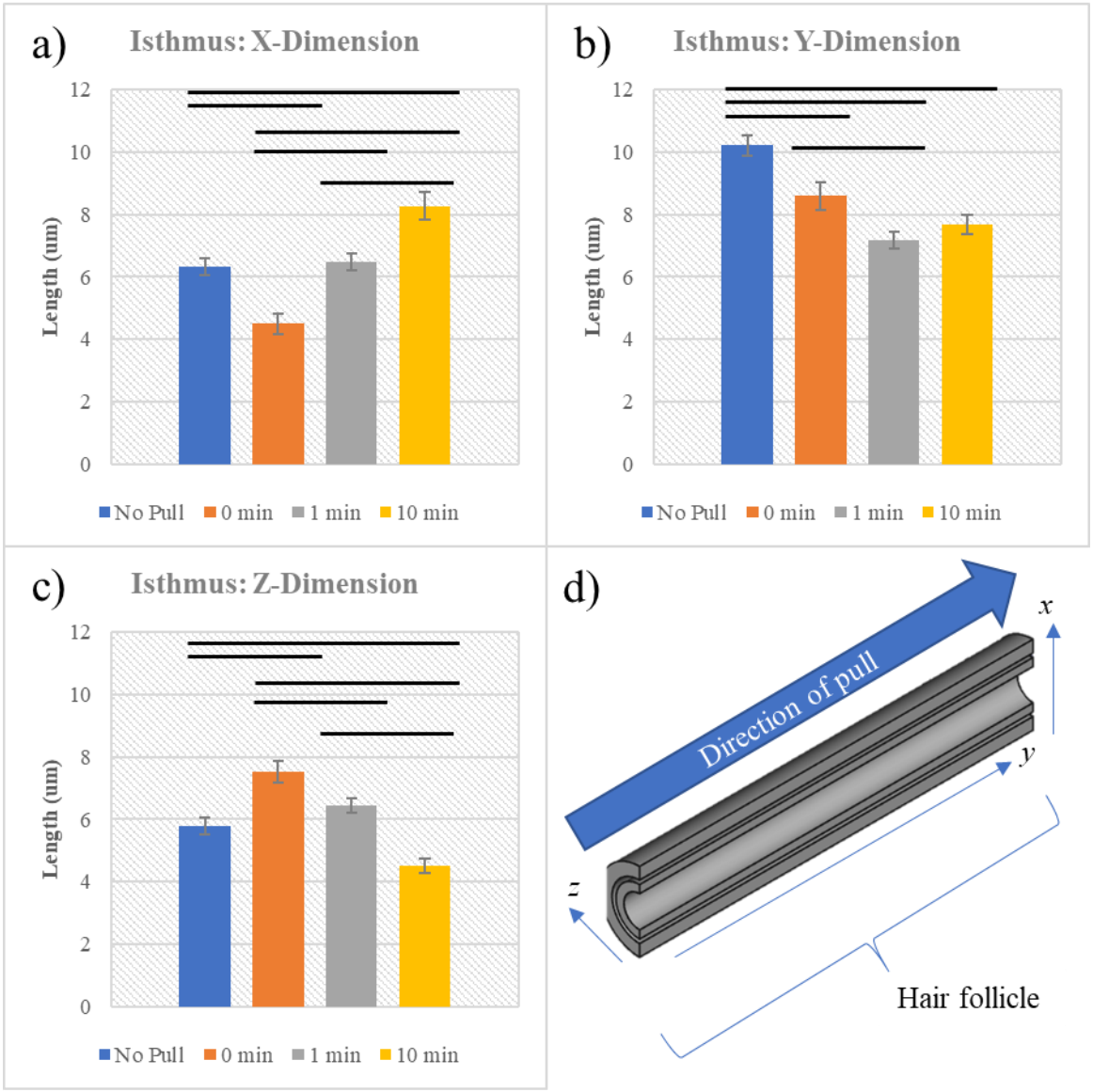

Figure 3.13: Changes in nuclear morphology within the isthmus region of the HF. Average change in the x- (a), y- (b) and z-direction (c) for each time point indicate clear volumetric changes occurring within the isthmus region. The schematic in (d) shows how change in the x-, y- and z-direction relate to the direction of the pull and follicle orientation. The error bars represent the standard error of mean with black bars highlighting groups significantly different from one another (n=10, $P \leq 0.0167$) as determined by anova and post hoc t-test. >30 nuclei per region analysed for each repeat.

3.2.13 Involucrin Labelling Shows a Homogenous IRS within the Suprabulbar Region of the Follicle

Involucrin staining revealed no obvious differences between the different pull durations and the NP (figure 3.14) indicating the nuclei were subjected to a lesser compression compared with the previous regions. This further supports the idea of the isthmus region as a force-dissipating region, alleviating compressive forces acting within both the infundibulum and suprabulbar region. This could also point to possible forces opposing the pull generated via dermal and hypodermal attachment to the follicle.

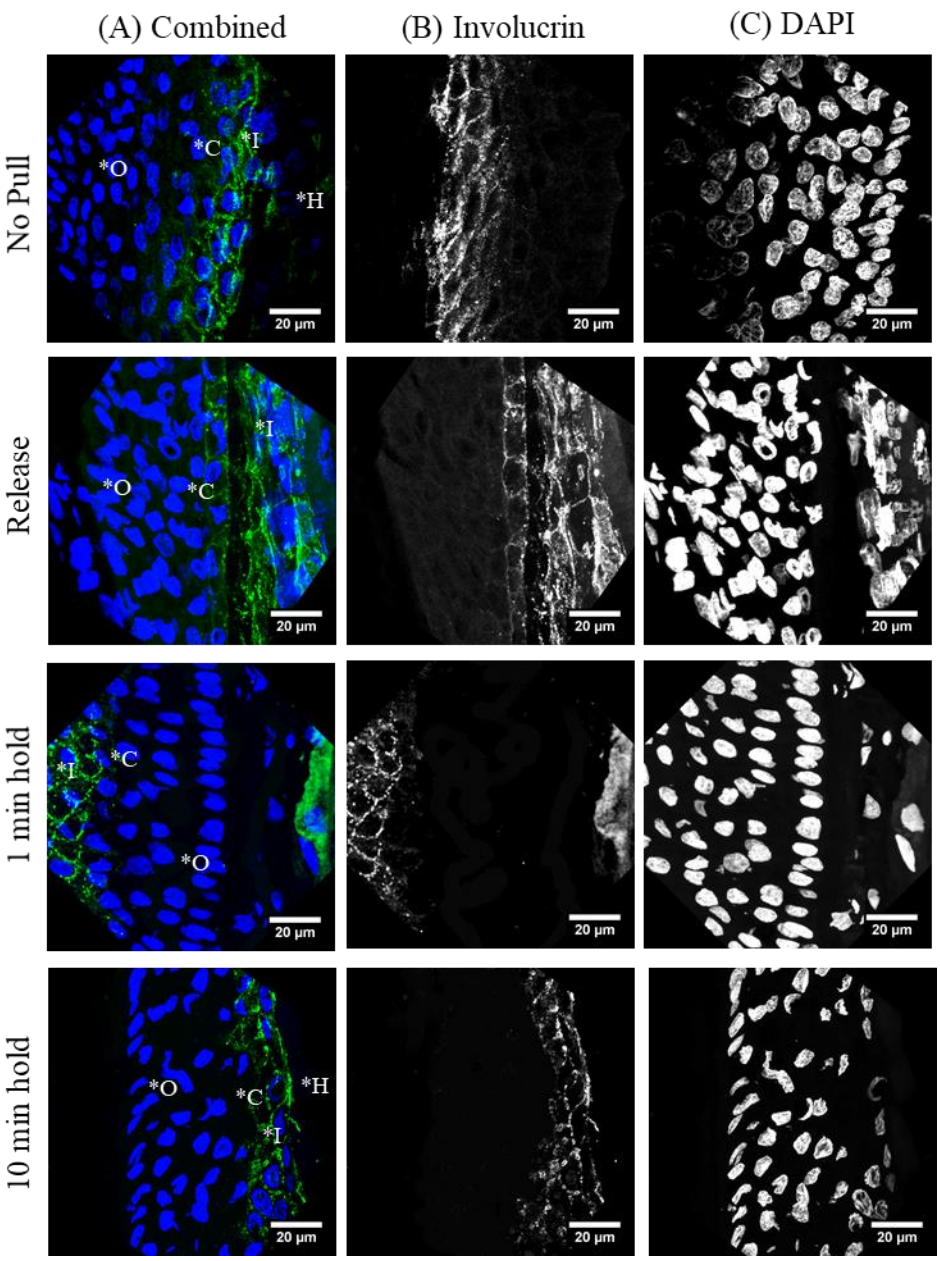

Figure 3.14: Confocal images of the IRS within the suprabulbar region. Combined images (a) produced by an overlay of channels (b) and (c), indicate a far greater proportion of ORS to IRS when compared with the above isthmus and infundibulum. (c) Illustrates a lack of ruffling within the IRS of the suprabulbar region. Scale bars set to 20µm length.

3.2.14 Compression within the IRS of the Suprabulbar Region is Alleviated During the 10min hold Indicative of an Opposing Pull During Follicular Compression.

The anova data indicated that the duration of the pull had significantly impacted upon the x-, y-, and z-dimension. However, the post hoc t-tests demonstrated a significant recovery from the 1-minute hold to the 10-minute hold, manifested as an increase within the y-dimension and a decrease in both the x- and z-dimensions, indicative of nuclear elongation (figure 3.15). The preceding 1-minute hold produced a clear nuclear compression as indicated by a sharp increase in x- and z-length and a decrease y-length. The transition from the compression to elongation suggested an opposing pull. The source of this pull cannot be determined from changes within the follicle and so it must be considered that attachments between the follicle and surrounding dermis/hypodermis could be responsible for an opposing pull.

The lack of compression at 0-minute as indicated by no significant changes in x-length or y-length compared with NP (figure 3.15) supports the earlier conclusion of the isthmus region acting as a compression relief region.

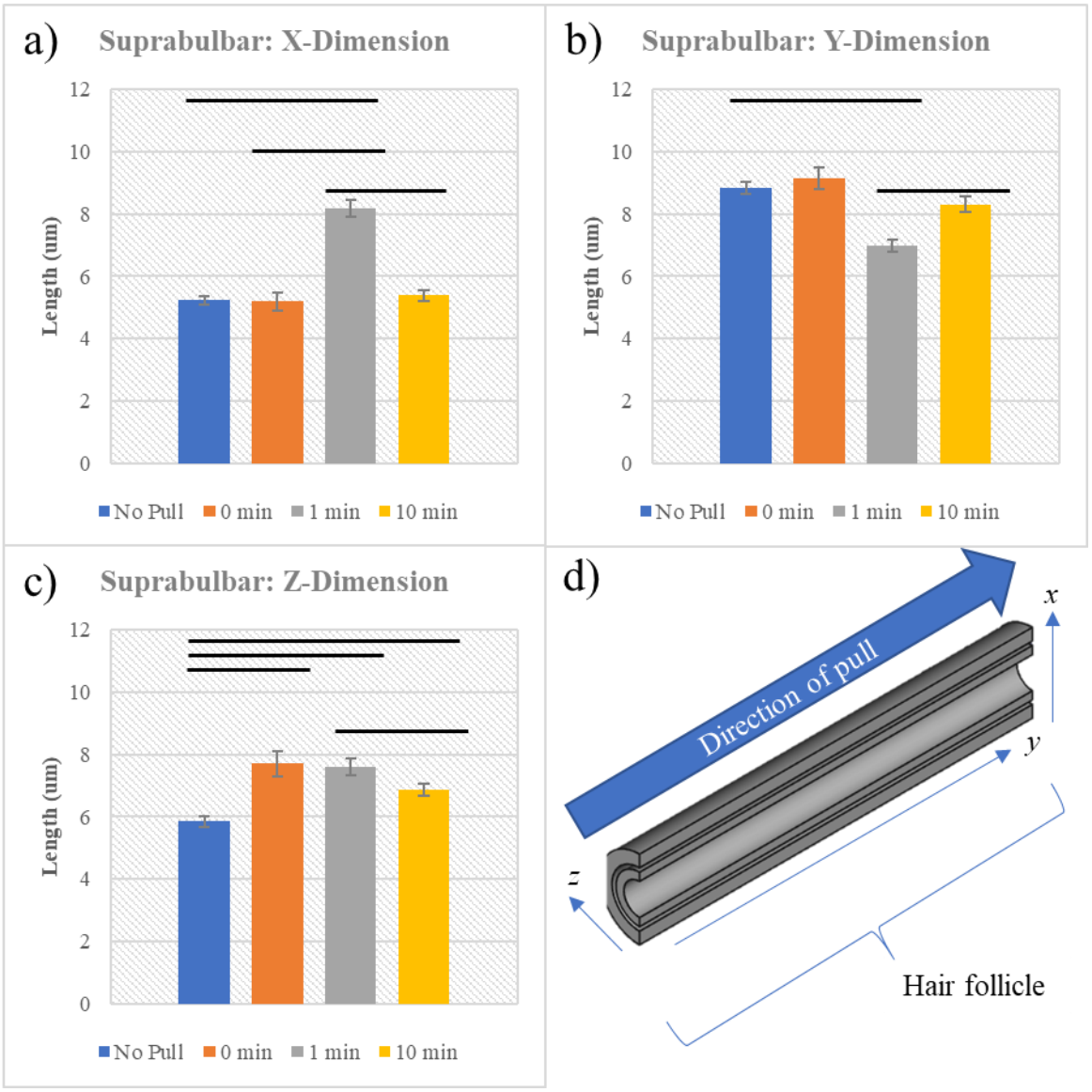

Figure: 3.15: Nuclear morphology changes within the IRS of the suprabulbar region. a)-c) Show the average changes of nuclei shape in response to different pull durations for the x-, y-, and z-dimension respectively. The error bars represent the standard error of mean with black bars highlighting groups significantly different from one another (n=10, $P \leq 0.0167$) as determined by anova and post hoc t-test. >30 nuclei per region analysed for each repeat.

3.2.15 Multiphoton Microscopy Reveals Attachments to the Bulb Region of the Follicle

The opposing pull indicated by the elongation of nuclei within the suprabulbar region of the follicle and the return of nuclei to an NP-like morphology with increased pull duration prompted investigation into the dynamics of the surrounding dermis/hypodermis during a pull. The MP approach allowed for a non-invasive means of imaging the dermal and hypodermal structures of non-fixed, whole mount skin in a pre-pull and maximum pull conformation (Figure 3.16).

Initial images illustrated a fibrous attachment at the base of the follicle that extends into the hypodermis (figure 3.16). At maximum pull with a 2g weight the follicle reaches a peak extension that coincided with invagination of the collagenous attachment further into the hypodermis in the direction of the pull (figure 3.16). This highlighted a clear point of attachment to the basement membrane within the hypodermis preventing follicular prolapse during loading of the hair shaft.

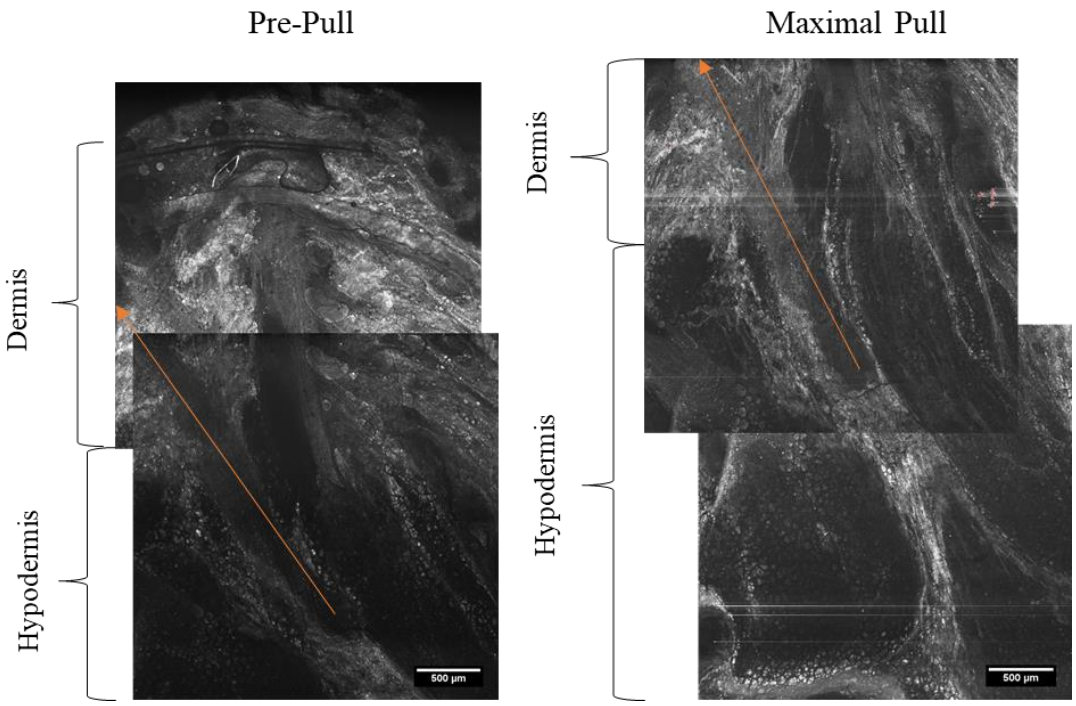

Figure 3.16: MP images of whole mount skin. Scale bars are 500 µm. The orange arrow indicates both the follicle and direction of the pull. The maximal pull clearly demonstrates attachment as implied by the strong signal generated.

Of the 35 hairs assessed during a 2 g pull none exceeded a movement of over 2200 µm with a range of movement from 1300 um to 2200 µm prior to depilation of the follicle (figure 3.17). The depilation beyond this was not due to failure of the fibrous attachment which was retained in post pull images. This suggesed a failure within the follicle as indicated by delamination between the ORS and IRS through putative failure of the CL. When the maximum extension is reached it is possible for regions within the compressed follicle to also experience extension, such as those within the suprabulbar region for which crumpling of both the IRS and ORS was absent. In addition, nuclear elongation was observed supporting this hypothesis.

Considered in conjunction with morphological changes occurring within the infundibulum, isthmus and suprabulbar region of the follicle with time, this fibrous anchorage could explain the elongation of nuclei with increased pull duration. However, it does not explain how the nuclei appeared to return to an NP conformation post the 10-minute pull nor does it explain how the hair shaft retracted back into the follicle post pull.

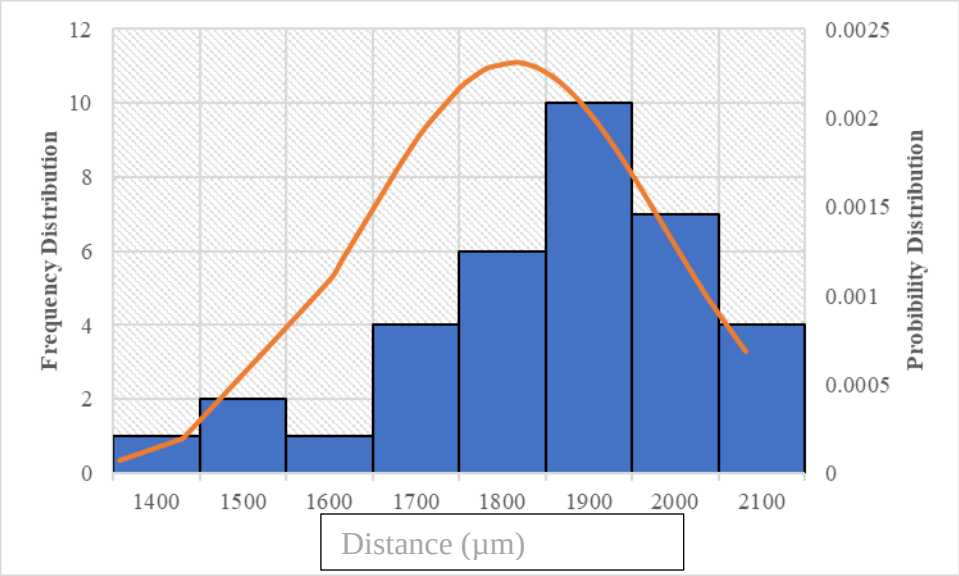

Figure 3.17: Follicular displacement during loading. The histogram shows the distanced moved by follicles pulled with a 2g weight. The overlying normal distribution illustrates the parametric nature of the distribution as well as the average (apex) and standard deviation (point of inflection). n=35.

To better understand other components involved in retraction of the follicle scans at an excitation wavelength of 740 nm were also performed to identify regions rich in elastin (figure 3.18). At higher magnifications and different z-depths through the cross-section of the follicle. A rich collagen matrix that sheaths the follicle with filamentous attachments emanating from the bulb of the follicle out into the hypodermis was identified (figure 3.18).

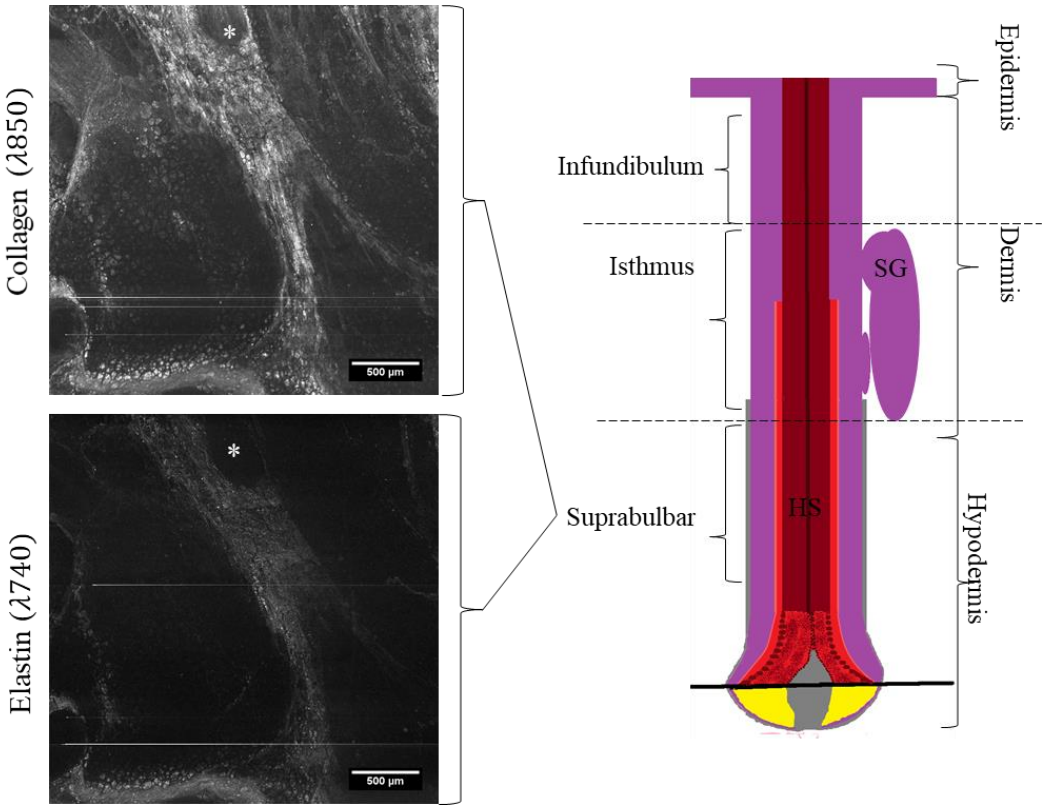

Figure 3.18: MP images of a follicle under tension. Putative collagen and elastin composite attachment was evident at the base of the follicle. The asterisks mark the hair shaft. HS-hair shaft, SG-sebaceous gland.

The excitation of the fibrous attachments perpendicular to the follicle could provide the kinetic energy required to retract the follicle post pull (figure 3.19). Figure 3.19 demonstrates how the fibrous structures become taught upon loading of the follicle indicative of their role in follicular anchorage.

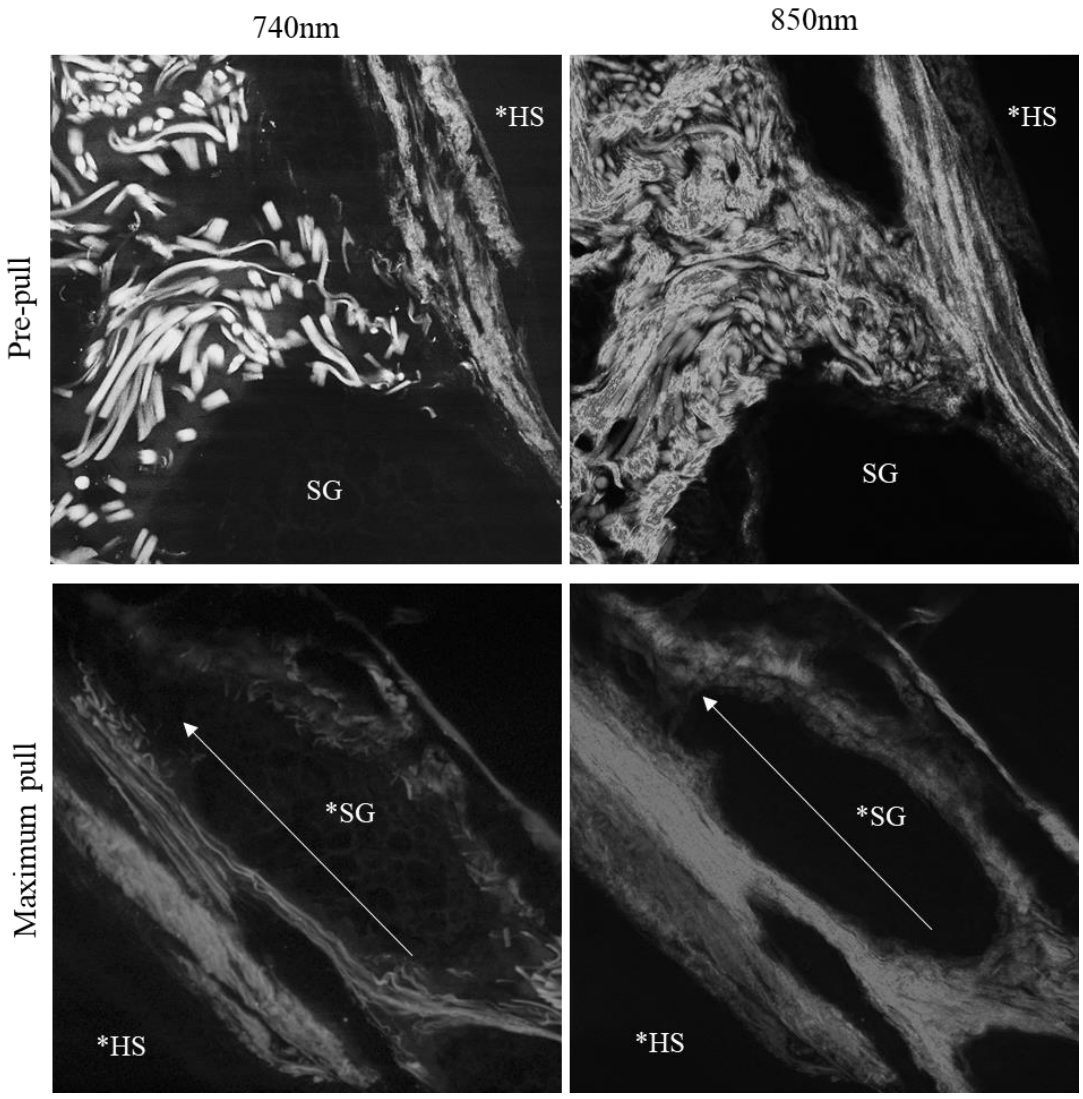

Figure 3.19: MP images of pre-pull vs maximum pull. An example of how collagenous and elastin fibres change conformation during loading, transforming from loose undulating fibres to taught compact fibres aligned with the pull vector. Images taken at an excitation wavelength of 720 nm excite putative elastin while those taken at 840 nm generate SHG within collagen bundles. HS-hair shaft; SG-sebaceous gland.

3.3.1 The Outer Root Sheath Has Mechanically Distinct Compartments Corresponding to the Infundibulum, Isthmus and Suprabulbar Region

Nuclei within the isthmus experienced a reversal of pulled morphology to NP-like morphology post the 10-minute pull indicative of a force acting in the opposite direction to the pull (figure 3.20). From 0-minutes to 1min hold there was a reduction in the y-dimension and an increase in the x-dimension. At 0-minutes the nuclei become more flattened and broader. This is then followed by an increase in the y-dimension and a reduction in x-dimension from 1-minute hold to 10-minute hold indicative of a reduction in compressive forces acting on nuclei within the ORS of the isthmus region.

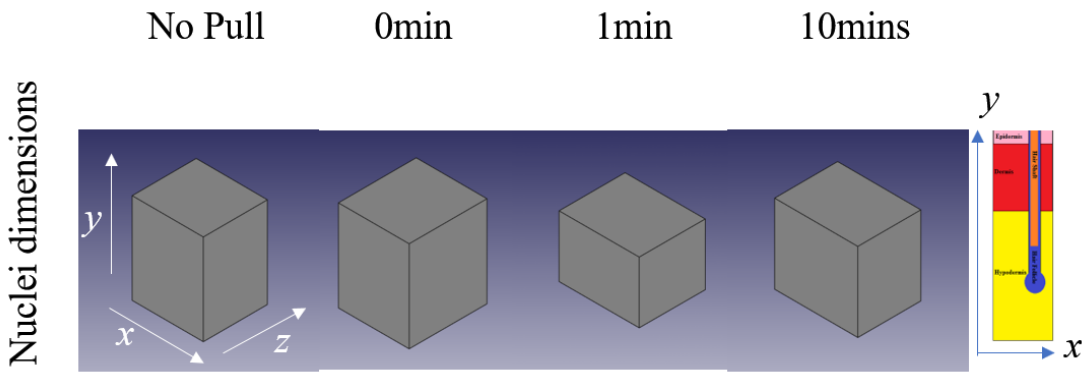

Figure 3.20: 3D representations of changes in nuclear morphology for the infundibulum. The boxes are the average x, y, and z length for a nucleus after each of the pulls carried out using a 2g weight. the x, y plane forms the cross-sectional area for the follicle spanning the epidermis (pink) dermis (red) and hypodermis (yellow).

The graphical interpretation of the numerical data obtained for the nuclei within the ORS of the isthmus clearly shows how the nuclei exhibited an increasingly flattened morphology up until 1-minute hold followed by a return to an NP-like morphology at 10-minute hold (figure 3.21). The z-dimension exhibits an initial expansion at the 0-minute hold followed by a compression from the 1-minute hold to 10-minute hold. Both trends have also been found to be present within the infundibulum with two key differences. The first is a lesser return to an NP-like morphology within the isthmus at the 10-minute hold time point with respects to the x- and y-dimension. The second is the reduction in z-length to below that of the NP. This would suggest the nuclei are elongating along the y-axis i.e. in-line with the direction of the follicle. The observations are similar to that of the infundibulum in that increased duration of pull

diminished the level of compression experienced by cells within this region. These changes suggest there are forces acing within the isthmus region that resist the compressive forces generated by the 2g weight.

The crucial factor is the length of time after pulling that changes in nuclear morphology are observed. If there were a linear distribution of force along the follicle the changes in nuclear dynamics should correlate with respects to timing. The segregation observed leads to the conclusion that the follicle comprises mechanically distinct units. Thus far it would seem the isthmus region behaves as a shock-absorber that allows for the dissipation of compressive forces acting on nuclei within the infundibulum.

Interestingly this characteristic is restricted to the permanent part of the follicle i.e. the non-cycling portion. The biological significance of this could be to preserve cellular tensegrity in stem cell niches. Alterations in nuclear tensegrity via mutational analysis and mechanical manipulation has been shown to produce alterations in cellular behaviour with respect to proliferation, differentiation, migration and apoptosis (Greiner et al. 2013; Plikus et al. 2008; Stefan Kippenberger et al. 2005; Yano et al. 2004; Sawada et al. 2001). In the case of stem cells slow-cycling would be beneficial in preservation of genomic fidelity reducing the probability of developing deleterious mutations and pre-cancerous lesions that would be inherited by all subsequent progeny.

For mechanically distinct regions to exist there must be structural heterogeneities that exist between the different regions of the follicle. These could be derived from the cells that make up the ORS or from the tissues that abut the ORS. Intracellular aspects to consider would be keratin expression profiles for cells of the different regions since different keratins confer different structural integrities to cells which in turn have epigenetic ramifications (Pierre A Coulombe and Lee 2012; Russell 2004; L.-H. Gu and Coulombe 2007b; L. Levy et al. 2000). For example basal keratinocytes express high levels of cytokeratin-14 which is important in cell-cell and cell-extracellular matrix adhesion at the basement membrane (Seltmann et al. 2013). Mutations and knockouts of K14 cause a variety of skin blistering disorders and also depletion of epidermal stem cell niches (Chan et al. 1994; Pierre A Coulombe and Lee 2012; Loschke, Homberg, and Magin 2016; Waikel et al. 2001; Alam et al. 2011). A more

recent study utilising siRNAs demonstrated the epigenetic ramifications of K14 knockdown in epithelial cells which exhibited reduced proliferation and delayed cell-cycle progression with the concomitant increase of involucrin and K1 indicative of terminal differentiation (Alam et al. 2011).

Although this data cannot pinpoint the specific biological significance of these observations it is abundantly clear that extracellular forces are transferred cell-to-cell via the nuclear lamin network as indicated by the altered nuclear morphologies. This network is critical for dissipating forces across a tissue and could be instrumental in preservation of cellular integrity and tissue homeostasis. Lamin staining revealed no differences along the length of the follicle for cells of the ORS. This would suggest extrafollicular collagen to be an important factor in generating the mechanically distinct environments. If cells experience tension from cell-to-cell via the nuclear lamins this could be a potential route by which cells can sense changes in their physical environment. In the same way that cells at the leading edge of a closing wound migrate toward the area of high-tension cells of a basement membrane could similarly detect when a cell need replacing via the same mechanism. The mechanism by which they sense this could present new target for combatting hyperproliferative epidermal disorders and skin cancer (see Ge & Fuchs 2018 for review).

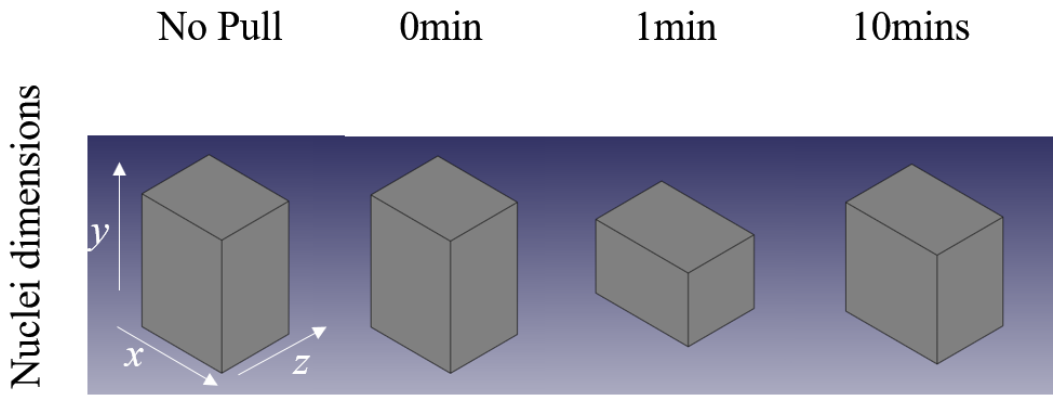

Figure 3.21: 3D representations of changes in nuclear morphology for the isthmus. Boxes representing the average x,y and z dimensions for nuclei after each pull.

To summarise the morphological changes of nuclei within the ORS of the suprabulbar region, there is an initial expansion at 0-minute followed by a compression at 1-minute hold. The nuclei then return to an NP-like morphology at the 10-minute time point with more elongated nuclei (figure 3.22). The increase at 0-minute suggested there to be an opposing force acting in the direction of the pull which may well be attributed to the dermal collagen attachment identified at the base of the follicle. This would also explain the return to an NP-like morphology after a 10-minute pull. However, if there was an opposing pull it seems unusual that nuclei within this region would still exhibit a compressed morphology at the 1-minute mark.

This can be explained by considering the nuclear dynamics with the infundibulum and isthmus regions. First it must be assumed that at the instance of force application the compressive forces are distributed linearly along the follicle. This is evident from time point 0-minutes where all regions experience a mild compression of nuclei. Upon extending the pull to a 1-minute duration there was a divergence in nuclear morphological changes through to the 10-minute pull duration. The wave-like compressions within the isthmus becomes evident at 1-minute and 10-minute pulls and were more pronounced after a 10-minute long pull. When combining these findings, it would appear that prior to the wave-like compression within the isthmus region, forces are transferred in a more linear fashion from the infundibulum, through the isthmus and into the suprabulbar region.

These observations converge upon a new hypothesis that postulates the ORS within the infundibulum is a means to limit nuclear deformation of cells in a region where stem cells important for follicle regeneration, wound healing and epidermal homeostasis can be found (Snippert et al. 2010; Lough et al. 2013; Mayumi Ito et al. 2005, 2004; Heidari et al. 2016; Lin and Yang 2013).

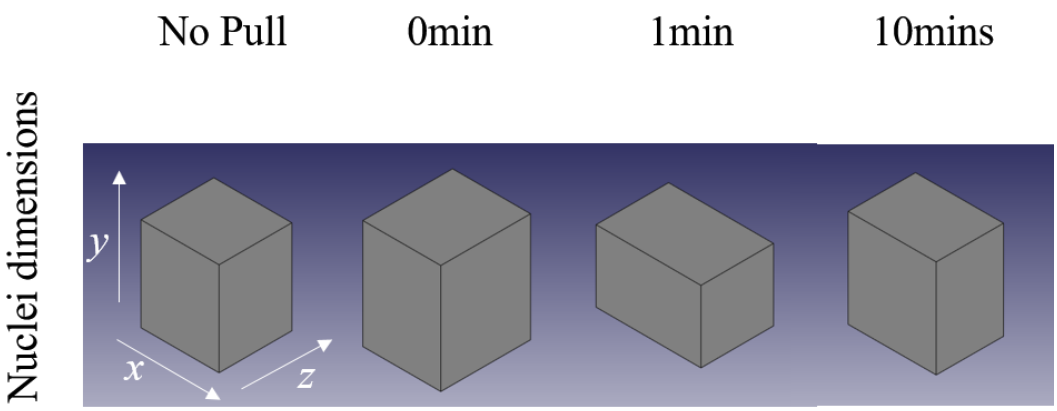

Figure 3.22: 3D representations of changes in nuclear morphology for the suprabulbar region. Boxes representing the average x, y and z-dimensions of nuclei within the suprabulbar region of the follicle after each pull.

3.3.2 The Outer Root Sheath May Help Protect against Nuclear Deformation

As already outlined, the nuclei within the ORS all exhibited a return to the NP morphology after a 10-minute pull indicative of the mechanical protections evolved to prevent nuclear deformation. The biological significance of the location of wave-like compressions is that it corresponds with a region where LGR-5 and LGR-6 positive cells can be found (Lough et al. 2013; Snippert et al. 2010; Jaks et al. 2008). LGR-5 stem cells have been identified as crucial for the regeneration of the follicle after catagen (Lough et al. 2013; Jaks et al. 2008), whilst LGR-6 cells have been identified as important during the wound repair of the interfollicular dermis (Jiang et al. 2017; Snippert et al. 2010). There is much debate as to whether or not the LGR-6 positive cells also contribute to epidermal homeostasis with a recent paper using lineage tracing as a means of demonstrating the incorporation of LGR-6 derived cells into the interfollicular epidermis (Füllgrabe et al. 2015). Contrary to this an earlier paper showed how ablation of LGR-6 had no effect on intermolecular epidermal homeostasis (Jiang et al. 2017).

Links between mechanical compression of nuclei have been shown to elicit apoptosis, mediate by upregulation of ERK1/2 signalling while in another study the upregulation of ERK1/2 signalling was related to increased rates of proliferation (Z. Zhang et al. 2018; García Lopez et al. 2009; X.-J. Wu et al. 2014). This highlights the highly analogue nature of ERK signalling with different degrees of stimulation producing very different outcomes. To this end attenuating the effects of compression may well

have links with reducing ERK1/2 stimulation below the threshold necessary for an apoptotic phenotype to manifest. As the ORS cells are epidermally derived it may be possible to investigate the relationship between ERK, nuclear morphology and proliferation rates using epidermally derived cells. In particular this could look at how structural properties (considering mechanically distinct niches) could impact upon nuclear morphology and how this correlates with proliferation and differentiation rates. Before this can be addressed it is first necessary to identify and characterise these hypothesized niches.

The intrinsic relationship between the cytoskeleton, nuclear morphology and nuclear lamins mean that forces experienced at the cell membrane will be transmitted to the nucleus via intermediate filaments and microfilaments. It must therefore be considered that protecting against nuclear deformation will similarly safe-guard against cellular compression and potential destabilisation of intermediate keratin filaments and F-actin which in turn could result in dissociation of these filaments from focal adhesion, hemidesmosomes and the nuclear LINK complex. Such large-scale cytoskeletal organisation can have an array of implications on cellular proliferation, differentiation and apoptosis.

Cyclic strain experiments have been shown to induce proliferation in keratinocytes through stimulation of ERK1/2 via activation of EGFR by a calcium influx (Yano et al. 2004). Protecting against such cell-cycling cues is essential in regions where stem cells reside to retain slow cycling. The isthmus region of the ORS has adapted to limit nuclear deformation within this region while also reducing nuclear deformation in the adjacent suprabulbar region.

Protecting against nuclear deformation would also protect against chromatin remodelling and potential large transcriptional changes. Within the nucleus heterochromatin appears to be anchored at the periphery with euchromatin being free within the nucleoplasm (Kourmouli et al. 2000). Nuclear envelope transmembrane (NET) proteins have been well documented as anchors of heterochromatin with lamin-B receptor (LBR) being implicated in the anchorage of heterochromatin to lamin-A (Solovei et al. 2013). This intrinsic link of chromatin anchorage with the cell cytoskeleton poses a potential means for epigenetic modification of the functional chromosome pool by physical force transduction. However, it is still unclear whether

chromosomal dissociation from the inner nuclear membrane drives transcriptional changes or if it is the result of stimulation of transduction cascades though other means such as calcium signalling and filament reorganisation during compression. The specific phenotypes observed by nuclear envelopathies may suggest a dysregulation of normal cellular processes through chromosomal disruption as has been postulated for nuclear envelopathies such as Familial partial lipodystrophy (Tu et al. 2016; Vouillarmet and Laville 2016). As the mutations within these laminopathies produce such global protein dysregulation it is strikingly interesting how tissue specific these disorders can be. This may well be explained by the mutations coinciding with regions essential for binding euchromatins containing genes relevant to the tissue.

3.3.3 Cell Stretching Within Suprabulbar Region Could Drive Both Proliferation and Differentiation

Hemidesmosomes mediate the cell-cell connection of cytoskeletal components allowing for the transfer of force from one cell to the next via the nucleus as has been demonstrated though atomic force microscopy (Haase and Pelling 2015; Vielmuth et al. 2018). The opposing force is presumably generated by the hypothesized elastin and collagen fibres that produce stretching of nuclei within the suprabulbar region. This would suggest that cells within the bulb region would also experience stretching. This stretching could elicit stimulation of the ERK1/2 via Ras activation through EGFR elicitation by Ca^{2+} influx (Centuori et al. 2016; Hong et al. 2014; Raymond et al. 2005; Greiner et al. 2013; Gazel et al. 2008) as has been documented in systems studying the effects of cyclic strain.

Further to elicitation of ERK1/2 and propagation of proliferation, force induced nuclear deformation has been linked to increased nuclear stiffness through changes in lamin A architecture. The wider effects of this are induction of matrix driven differentiation via chromatin remodelling (Solovei et al. 2013; Y. Li et al. 2011; Ostlund et al. 2009). It is interesting that stretching of nuclei is observed within a region of the follicle where cells are terminally differentiating i.e. above the line of Auber. In this respect follicular compression could be a potential means of driving terminal differentiation of hair matrix derived cells.

3.3.4 Continuity between Nuclear Dynamics of the ORS and IRS within The Suprabulbar Region

The changes in nuclear morphology observed within the suprabulbar region of the IRS closely mirrored those of the ORS for the same region with an initial elongation, followed by a compression with a return to an NP-like morphology after a 10-minute pull. Without repeating what has already been mentioned the transmittance of physical force to the matrix derived cells could drive proliferation through induced calcium influx and subsequent stimulation of the ERK1/2 cascade while driving differentiation by the opposing forces generated by the collagen/elastin attachment at the base of the follicle (Yano et al. 2004; Centuori et al. 2016; Micallef et al. 2009).

3.3.5 Follicular Compression Could Provide A Route to Propagate Anagen

A recent study highlights how TGFβ2 can propagate anagen through transient stimulation of the hair follicle stem cells, bulge cells (Oshimori and Fuchs 2012). Two observations from this study have particular relevance when considering the impact of follicular compression on hair growth cycles: 1) TGFβ2 acts in a proximal manner i.e. its stimulatory effects and hence propagation of anagen are diminished exponentially with distance; 2) That TGFβ's are able to influence how a stem cell responds to stimulation from BMP's (Oshimori and Fuchs 2012; Peters et al. 2005).

TGFβs are generated by the dermal papilla and are able to diffuse into the surrounding tissue. The immediate environment of this protein is rich in fibrillins that pertain TGFβ binding sites (Yadin et al. 2013) that could act as a reservoir for the molecule that when mechanically stimulated, undergo conformational changes that cause their release (Robertson et al. 2015; Hyytiäinen, Penttinen, and Keski-Oja 2004) . This could allow for attenuation of the BMP signalling within the bulge cells, driving the anagen phase in place of either catagen or telogen (Kobielak et al. 2003; Oshimori and Fuchs 2012). Binding of TGF-βs to fibrillins can occur directly via an 8-Cys domain of via latent TGF-β binding proteins which similarly contain the 8-Cys domains (Massam-Wu et al. 2010; Ramirez and Rifkin 2009). In this way follicular compression could cause spiking of TGFβ molecules within the dermis which may provide sufficient signalling to counterbalance BMP signalling within the bulge stem cells or bulge derived stem cells that form the matrix cells that eventually differentiate into the concentric layers of the follicle (Clavel et al. 2012; Ming Kwan et al. 2004).

In support of this hypothesis a recent study has demonstrated how mechanical compression of dermal papillae via head massages resulted in upregulation of hair follicle cycling genes NOGGIN, BMP4 and SMAD4 and a decreased in hair-loss genes including IL6 as identified by RT-PCR and microarray analysis (Koyama et al. 2016). The upregulation of pro-cycling genes was accompanied with an increased hair follicle density across the massaged region, indicative of increased anagen follicles. Upregulation of NOGGIN is particularly important in propagation of anagen over telogen as it antagonises BMP2 signalling through its 15 fold affinity for the BMP2 receptor BMPR1 which in turn blocks phosphorylation of SMADS 1/5/8 preventing their complex with SMAD4 and subsequent translocation to the nucleus allowing for cell cycle progression in follicle stem cells (Lange et al. 1998; Takeda et al. 2004; Yang, Wang, and Yang 2009).

4.1 An Introduction to Collagen and Multiphoton Microscopy

In the first results chapter collagen was implicated as a potential effector of cellular tensegrity and has also been suggested as important in explaining the pattern of nuclear deformation observed within the follicle during compression. This pointed to potential heterogeneities within the extra follicular collagen. Taking this further it was therefore essential to probe the collagen structures abutting the follicle to identify if mechanically distinct compartments existed at levels consistent with the infundibulum, isthmus and suprabulbar region. This chapter lays the foundations to model the heterogeneities and investigate how the varying collagen matrices impacted upon cellular behaviour identifying new roles for collagen in follicle homeostasis and potentially epidermal homeostasis.

Collagen hydrogels offer a solution to study how matrix stiffness impacts cell behaviour. By controlling the conditions under which the hydrogels are polymerized from the purified rat tail type 1 collagen it is possible to generate matrices of different stiffness and density (Roeder et al. 2002). The resultant matrices provided a defined substrate against which novel multiphoton microscopy technique can be calibrated against before being applied in more in vivo unknown systems such as human skin. This system ultimately provided the foundations required to evaluate collagen bundling within intact human skin.

Once conditions had been established that allow for the reliable reproduction of two structurally distinct matrices it was then possible to observe the effects of a stiff vs a less stiff matrix on nuclear morphology and to correlate this against proliferation and differentiation rates (chapter 5). Many earlier approaches focussed on dynamic forces that produced alterations in nuclear morphology. A static system allowed for assessment of a more *in vivo* like scenario, accounting for how the ECM derived tensegrity governs the overlying and adjacent cells. This aided with understanding the biological significance of different collagen environments abutting the follicle.

4.1.1 Second Harmonic Generation in Collagen

Non-linear microscopy techniques emerged as a powerful optical tool that allowed for optical interrogation far beyond the limits of conventional linear techniques (e.g. confocal microscopy). This technique enabled for label free imaging to depths well beyond those achievable by linear techniques in optically turbid samples. Non -linear

microscopy also lends a high degree of spatial resolution in both the x, y and z plane without the need for a pinhole. Second harmonic generation (SHG) and two photon excitation fluorescence are two such techniques for which our microscope can perform. The ability to deliver high-resolution information regarding biological structures at depth make this an ideal technique to image collagen matrices and human scalp skin.

Two photon emission occurs when two photons are absorbed by a fluorescent molecule in the same quantum event. The photons can only interact with the fluorophore if their sum energy is identical to the energy gap between the molecules ground state and a vibrational level of the excited electronic state (Göppert-Mayer 1931). This means visible light and UV fluorescence can be elicited with far red light reducing the effects of photobleaching by the incident light beam and enabling for deeper penetration of the incident beam (So et al. 2000).

The necessity for photons to combine enables for optical sectioning through excitation of sub-femto litre volumes of the sample at any one time. This characteristic also removes the need for a pinhole as only light within the focal plane will produce excitation of the fluorophore (Roth and Freund 1979; Cicchi et al. 2013; Mazza et al. 2008). This restriction is due to the lack of convergent photons above and below the focal plane preventing two photons being incident on fluorophores outside of the plane within one quantum event. The time restriction of the quantum event is dictated by the time-energy uncertainty principle which in our system translates to 10^{-16} seconds (Aharonov and Bohm 1961).

Conventional microscopy methods encompass linear phenomena such as reflection, absorption, fluorescence and scattering. In these instances, the relationship between the strength of the electrical field of incoming light and the induced polarisation of the object is linear. In the instance of an incoming oscillating field with a non-resonant frequency (such that it is not of a frequency absorbed by the molecules of the material), the optical response can be approximated to be a first-order response:

$\tilde{P}(t)=\epsilon_0 X^{(1)} \tilde{E}(t)$

$\tilde{P}(t)$ is the laser power, ϵ_0 is the dielectric constant of the vacuum, $X^{(1)}$ is the linear susceptibility of the specimen and $\tilde{E}(t)$ is the electric field strength. Non-linear phenomena elicited by high power intensity, are not linearly dependent on the applied

electric field. SHG is one such phenomenon in which light is coherently scattered at twice the optical frequency (Kirsch et al. 2008). The non-linear response can be written as:

$\tilde{P}(t)=\epsilon_0 (X^{(1)} \tilde{E}(t)+X^{(2)} \tilde{E}^2+X^3 \tilde{E}^3\ldots)$

The first left term relates to the linear scattering (i.e. two-photon excitation fluorescence, the second to SHG and the third to third harmonic generation and so on. Because fields are vectors in the above equation (i.e. they have both magnitude and direction), each atom will oscillate in a dipole radiation pattern (So et al. 2000). The radiation phase among an enormous number of atoms, such as those comprising collagen, must be in sync with one another to induce constructive interference (Denk, Strickler, and Webb 1990; Bancelin et al. 2014). Constructive interference is when one or more waves matched the phase of another, thus creating the effect of one wave that is the sum of the two or more waves in magnitude (figure 4.1). Deconstructive interference is when the waves are out of phase resulting in the reduction of magnitude or in the case of a Pi shifted wave (figure 4.1) one would cancel out the other. This constructive interference is the reason why only molecules that exhibit a specific symmetry (e.g. non-centrosymmetric materials such as collagen) can originate SHG (Roth and Freund 1979).

SHG can therefore only occur if certain criteria are fulfilled. First there must be the presence of electron donors and electron acceptor moieties connected by a π-conjugated system, enabling for the vibrational excitation of electrons to higher energy states. The second is the structural organisation of the molecular emitters within the focal volume. Both conditions are achieved in anisotropic molecules such as collagen making this technique well suited to the imaging of collagen and probing of its organisation (So et al. 2000; Tilbury et al. 2014; ‘Second Harmonic Generation’ 1990; Roth and Freund 1979).

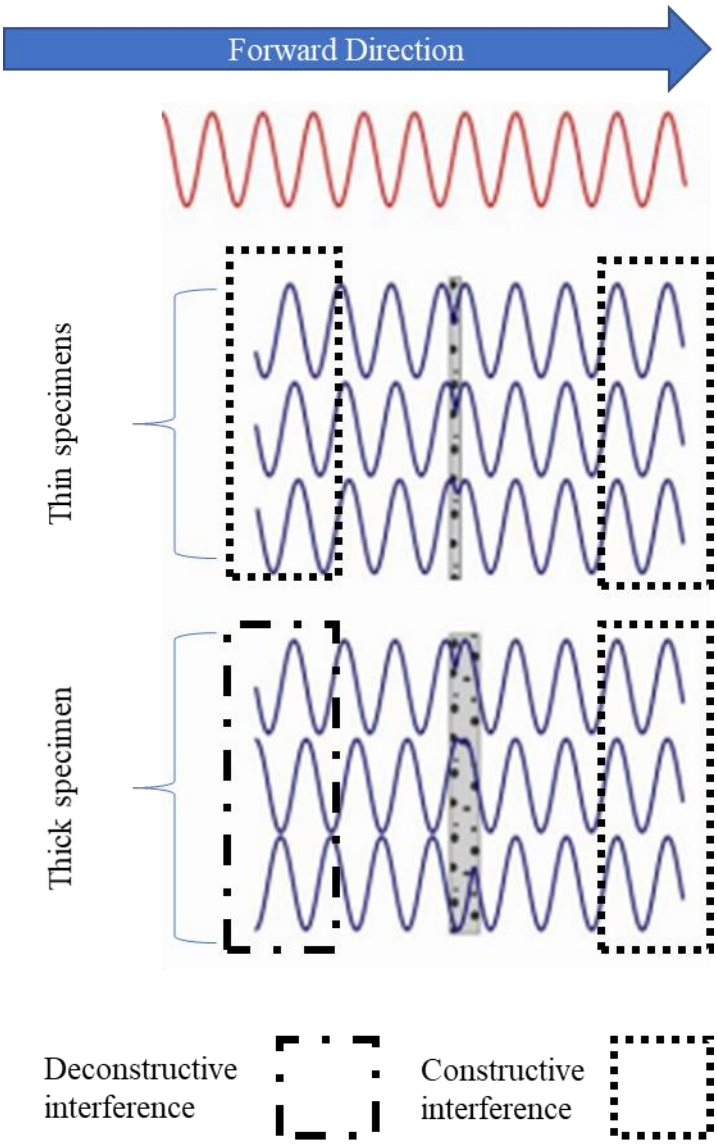

Figure 4.1: Depiction of constructive and deconstructive interference. The red wave represents the squared fundamental excitation with the blue waves representing SHG from thin and thick specimens. The forward waves show faze matching and thus produce constructive interference whilst the backward waves illustrate loss of phase in thick specimen procuring deconstructive interference.

4.1.2: Characterisation of Collagen Structures by SEM and MP Microscopy

Advanced imaging techniques enable the interrogation of protein macromolecular assemblies including collagen fibrils. Scanning electron microscopy provides a means to asses properties of structures that go beyond the resolution limit of light; a light wave can only be used to visualise something that is greater than the half the wavelength of the incident wave which for visible light is 0.4-0.7 μm . However, that is not to say light-microscopy is not capable of imaging below this limit as techniques

have been developed (super resolution microscopy) to achieve resolutions on the angstrom scale. Super resolution microscopy was available to use for this study but was deemed not necessary since the Hitachi SEM produced superior resolution to asses collagen fibres with fewer complications.

SEM principally involves illuminating the surface of a desiccated specimen, coated with an electron dense material, by a beam of electrons, emitted from a tungsten filament. The electrons are funnelled into a beam by a series of powerful orbital magnets with the whole process taking place in an ultra-low vacuum to ensure the path of the electrons is not affected by air molecules. As electrons exhibit particle-wave duality, as a wave they exhibit a far lesser wavelength compared with light and can therefore produce a resolutions less than a nanometre (see Frank Krumeich for review). For this reason, SEM will be used to characterise collagen fibre diameter and bundling against which variations in MP signal will be compared allowing mapping of MP signal properties onto collagen matrix properties.

The electron beam incident upon the specimen will interact either elastically or inelastically with the specimen. The former interaction is the foundation for SEM image generation. As electrons penetrate an electron cloud they are attracted by the positive potential of the nucleus while simultaneously being repelled by the electron cloud, and its path is deflected toward the nucleus as a result. The closer the electron travels to the nucleus the greater the deflection and in the most extreme cases, electrons are deflected back toward the electron source. These are known as back scattered electrons and their angular distribution can be used to calculate the topography of the specimen. For this reason, it is beneficial to coat specimens in chromium or carbon. These electron dense materials increase the production of back scattered electrons versus uncoated biological material which may not be sufficiently electron dense to produce an image (Kuo 2008; Stick and Goldberg 2010).

The disadvantage of scanning electron microscopy is that it only enables for topological analysis making it difficult to analyse specimens in an in vivo like environments. To overcome this issue light microscopy techniques come into play, specifically multiphoton microscopy which allows for the imaging of specimens in a label free manner to depths exceeding 10,000 μm (Yuryev, Molotkov, and Khiroug 2014; Heuke et al. 2013; Jing Chen et al. 2014). However, increased depth of imaging

comes at the expense of resolution as light waves are increasingly scattered. For the same reason we cannot look through a 1 mm slice of ham nor can we image 1 mm into a slice of ham using visible light. To overcome this problem and mitigating lengthy and costly processing of specimens (fixation, clearing, sectioning etc) scientists began experimenting with femtosecond-pulsed lasers that excite specimen within the far-red end of the spectrum. The result is a light wave that does not interact with the specimen outside of the focal plane, allowing for signals to pass through several millimetres of turbid tissue.

Scanning electron microscopy and multiphoton microscopy offer two very different ways of assessing collagen micro-structure and organisation. These techniques were used to complement each other with SEM acting as the gold standard against which a novel MP analysis was verified against. Upon Establishing how to interpret the MP signal using SEM data and defined collagen matrices, the MP technique was applied to evaluate collagen environments adjacent to the follicle within intact skin explants. The goal was to understand how established distinct mechanical environments abutting the follicle and epidermis may govern the homeostasis or functionality of different regions. Adding onto what has already been investigated this broadened our understanding of how the extrafollicular collagen also impacted upon the hair follicle mechanics during the shaving process and potential roles in governing tissue homeostasis. Ultimately this data allowed the development of an in vitro system to test how different collagen environments could impact upon proliferation and differentiation rates within keratinocyte derived cells.

4.2 Interrogation of Collagen Matrices and Human Scalp Skin Using Non-Linear Optical Microscopy Techniques

Two-photon microscopy is a non-linear imaging technique that enables for the label-free imaging of structures composed from repeating units of non-centrosymmetric molecules including collagen. By characterising how variations in signal amplitude and intensity varied with changes in collagen density it was possible to use the technique to evaluate differential collagen environments abutting the hair follicle. Differences here demonstrated the discrete mechanical compartments of the follicle allowing us to hypothesize as to possible biological functions.

4.2.1 SHG Generates a Signal Intensity Profile Distinct from TPEF

To verify the generation of SHG purified rat tail type I collagen hydrogels were produced from either a 1.46mg ml^{-1} solution or a 3.54 mg ml^{-1} solution of purified rat tail type I collagen (Carlson et al. 2008; Stark et al. 2004)(figure 4.2). Collagen was excited using a mode-locked femtosecond-pulsed laser from 710 nm to 910nm excitation wavelength at 10nm intervals. For SHG signal generation occurs at exactly half the wavelength of the excitation wavelength allowing for discrete detection at a single wavelength (Roth and Freund 1979; Bancelin et al. 2014; Williams, Zipfel, and Webb 2005; Tilbury et al. 2014; Yew, Rowlands, and So 2014; Heuke et al. 2013; Cicchi et al. 2013; Bauman et al. 2014). Therefore, SHG should only be visible from 820nm to 910nm in our system which detects all wavelengths between 410nm and 490nm. As the MP system used had a broad-spectrum detector it was essential to investigate signals that were not SHG but exhibited overlap in emissions spectrum to identify where the cut off for TPEF occurred and what characteristics the different signals exhibited.

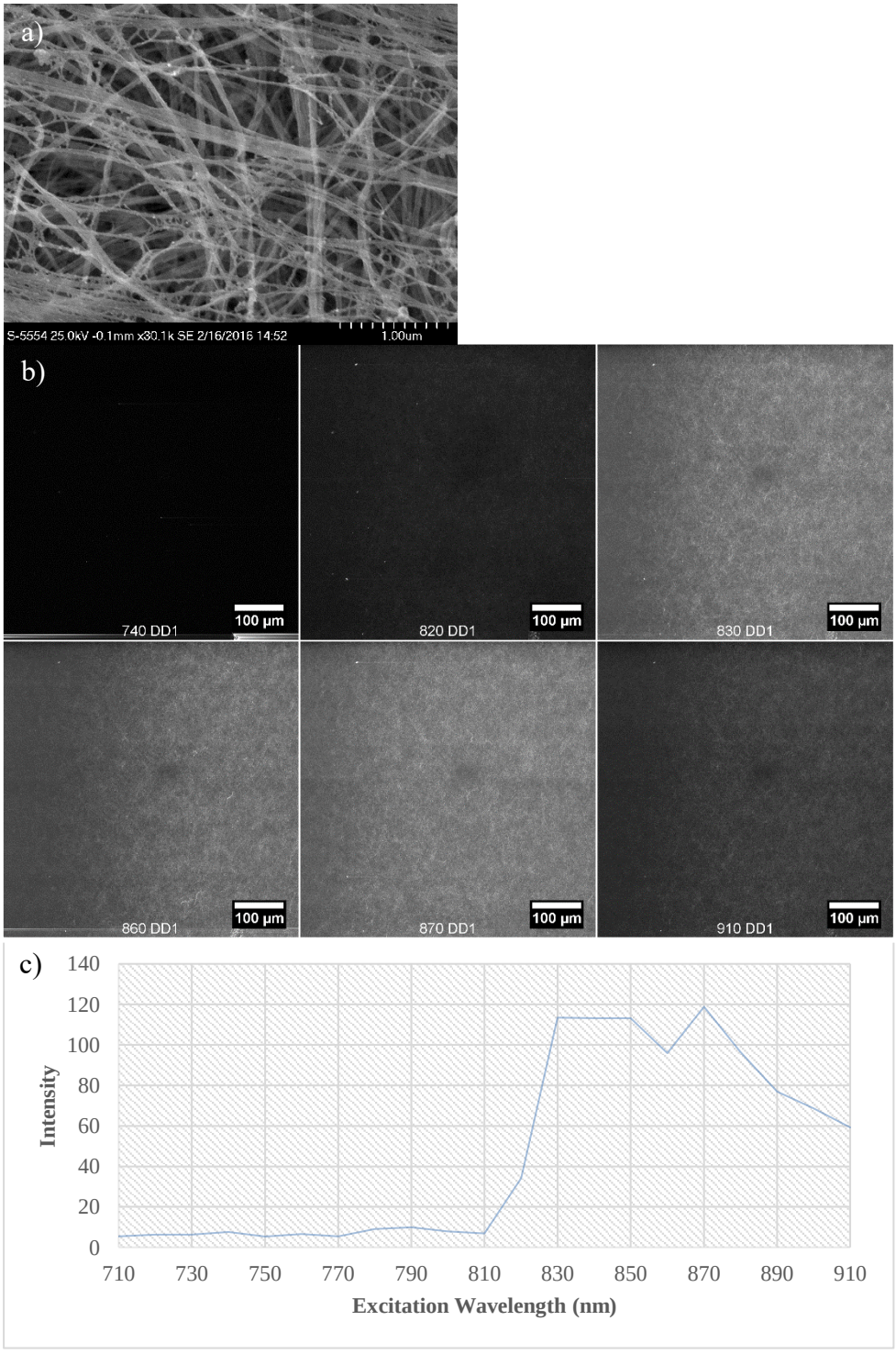

Figure 4.2.: Micrographs of collagen hydrogels a) Scanning electron micrographs of a collagen hydrogel illustrates fibril formation. Scale bar set to 1 µm b) Micrographs at key excitations where the switch from two-photon excitation fluorescence to second harmonic generation can be seen i.e.810 nm to 830. Scale bars set to 100 um c) The intensity plot for unlabelled, polymerised collagen, whole mounted and imaged via two-photon microscopy within the range of 410 nm-490 nm.

A characteristic of the plot in figure 4.3 that would not be the case if this was attributed to autofluorescence, was the sudden increase of intensity from 810nm to 830nm. Fluorescence emission plots produce bell curves with a peak emission and an infinite number of variable emissions within the excitation range. Therefore, there should be multiple intensities between the peak emission and ground state which was absent from the plots generated. Further to this, at wavelengths above 830 nm there was a sustained plateau at the peak emission which again is uncharacteristic of fluorescence emission which should exhibit clear peaks and troughs suggesting the signal was SHG (figure 4.2).

Detectable emission was first produced at 820 nm excitation at a much lower intensity compared with subsequent emissions produced from 830nm to 910nm excitations (figure 4.3). Within the 410nm-490nm detection range the optimal operating excitation wavelength was found to be at 840nm as this provided a good compromise between signal strength and laser power required. Excitations over 870nm required considerable increase in laser power to achieve an image of equal signal causing heating and eventual damage of the specimen. No signal was collected in the detection range 500nm-530nm for any of the trialled excitation wavelengths indicating demonstrating the detection of SHG only.

When intensity profiles across a range of excitation were considered there was a clear separation between those generated from excitation at 710nm-810nm and those generated from excitation at 820nm-910nm (figure 4.3). Those generated from 710nm-810nm exhibited only background levels of intensity indicating the lack of TPEF elicited in the collagen that is detectable between 410nm and 490nm. Any residual background was most likely attributed to autofluorescent amino acid residues within collagen and possibly by autofluorescent species that have been trapped by the collagen matrix. These include paraformaldehyde, glutaraldehyde, co-purified collagen binding proteins, NADH and FAD. Therefore, signal produced at a level that is greater than the background must be SHG. The average intensity of profiles generated by excitation from 710nm-810nm was subtracted from each individual profile generated by excitation in the range of 820nm-910nm. All intensities remained positive further supporting the signals produced by the excitation range 820nm-910nm as SHG when detecting within the 410nm-490nm detection range.

Figure 4.3 illustrate the average y-pixel intensity for each x-coordinate over a 30um^2 area within the image. The average intensity per column showed differences of intensity between the different SHG signals (excitation ≥820 nm) across the entire collagen lattice. The greatest intensity within the 820nm-910nm range was elicited by excitation at 870nm and the least at 820nm as was shown by the average intensity per image. This again suggest a lack of SHG emission between the excitations 710nm-810nm as only basal intensities are generated for this range. The lack of peaks and troughs within the average y-pixel trace indicate a high degree of homogeneity within the collagen matrix. Large variations in fibre diameter and void sizes would be manifested as peaks and troughs across the y-pixel average. Although it is possible that large fibres and small fibres could effectively mask one another as a result of the averaging of y-pixels the consistency across the x-dimension suggests this not to be the case.

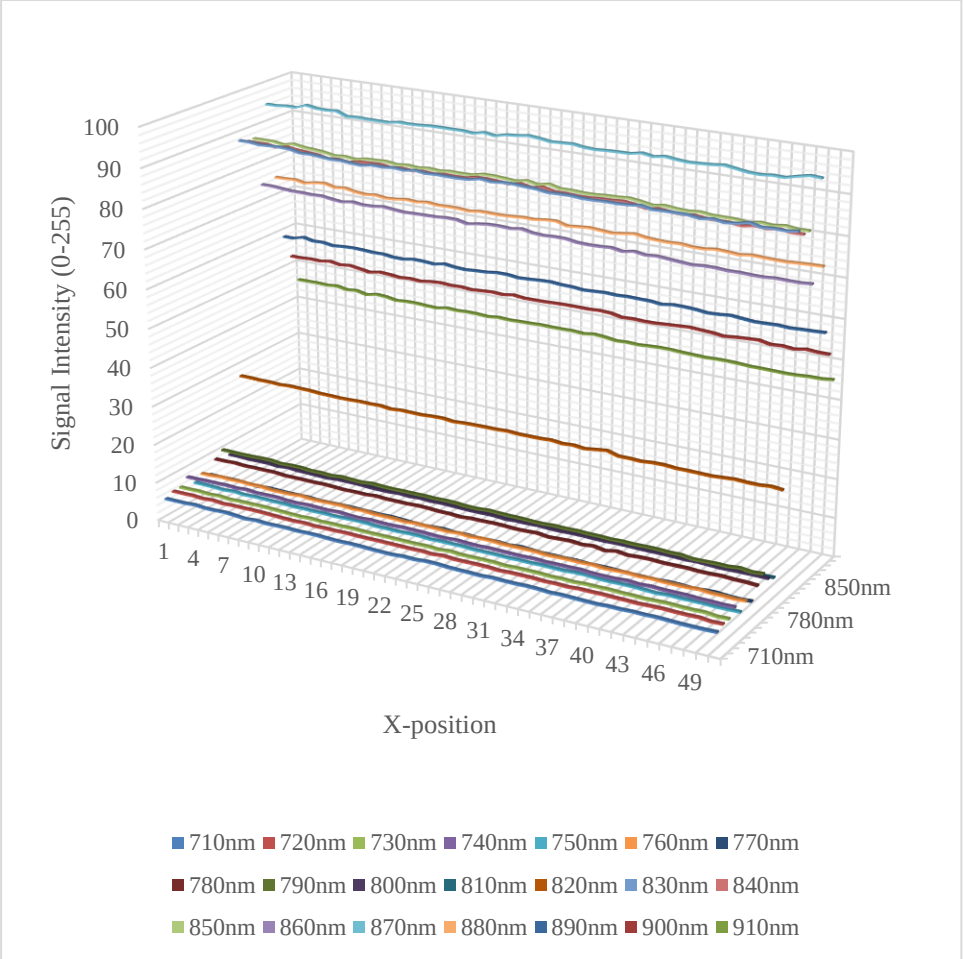

Figure 4.3: Average pixel intensity (8-bit) for collagen hydrogels. Each average is calculated at a different x-position on a constant y,z vector across three identical collagen matrices excited at range of wavelengths. This illustrates the TPEF to SHG transition and the homogeneity of collagen matrices.

A second set of intensity profiles was generated to identify individual variations in pixel intensity resulting from different excitation wavelengths. This allowed for a clearer distinction between SHG and TPEF as in SHG the same pixels should illuminate with slight variation in pixel intensity as indicated by the y-pixel averages and frame averages (figure 4.3). TPEF however should illustrate variations due to the varying autoflurofores excited from 710 nm-810 nm. This method of analysis also clarified the excitation ranges that produced TPEF and SHG.

If the wavelength is altered autofluorescent species would be expected to exhibit a peak at a specific wavelength, producing a maximum intensity peak, with all subsequent excitations being of lower intensity the further from the excitation maxima

the wavelength moves. For this specific reason a pixel that represents an autofluorescent species was hypothesised to exhibit greatly reduced intensity for excitations that do not match the peak excitation. Therefore, if the intensity of that pixel for a given wavelength is plotted against the pixel intensity for the same pixel from an image of the same sample excited at a different wavelength, each subsequent wavelength will show a reduced correlation as the excitation wavelength moves either side of the peak excitation (i.e. the position illuminated at a different wavelength will produce a variation in intensity for TPEF). SHG excitation produces a plateau at emission as depicted earlier and thus intensity values will correlate almost perfectly as the wavelength is altered within the SHG generation range. This analysis more definitively shows the TPEF and SHG ranges.

Correlation analysis was carried out comparing pixels from the same locations in each image to those generated by each excitation wavelength for the three collagen gels (figure 4.4). A value of 1 indicates an identical pixel profile i.e. matched intensities across different excitations, and values less indicating divergence. Excitation at 820 nm generates a profile with a correlation greater than 0.8 with pixel intensities resulting from excitations above 820 nm. This suggests the 820 nm intensity profile is at the intersection of SHG and TPEF generation since TPEF wavelength typically share a correlation of 0.2 or less with the putative SHG profiles. In summary the profiles generated by excitations from 820 nm to 910 nm share a 0.8 and over correlation coefficient with one another. This correlation demonstrates SHG since the pattern of excitation i.e. where each bright pixel falls, is close to identical for profiles generated by excitation wavelengths of 820 nm and over. Slight decay in correlation within the SHG range may be explained by subsequent images produce heating of the specimen causing movement of fibres meaning the pixel position intensity is affected by the. As a result, a slightly different region of collagen is excited which results in the slight deviations of intensity.

TPEF profiles (<820 nm excitation) only exhibit a correlation of 0.8 with profiles generated within +/-20 nm of the lowest wavelength of the comparison. i.e. The profile of 780 nm has a correlation of over 0.8 with those generated by 760 nm and 800 nm but considerably less for those outside of this range, indicative of emission spectra produced by varying fluorophores within the collagen matrix, not SHG. If this

were SHG the same pixels would be illuminated at each excitation and as is indicated by the correlation matrix plot (figure 4.4), this is not the case.

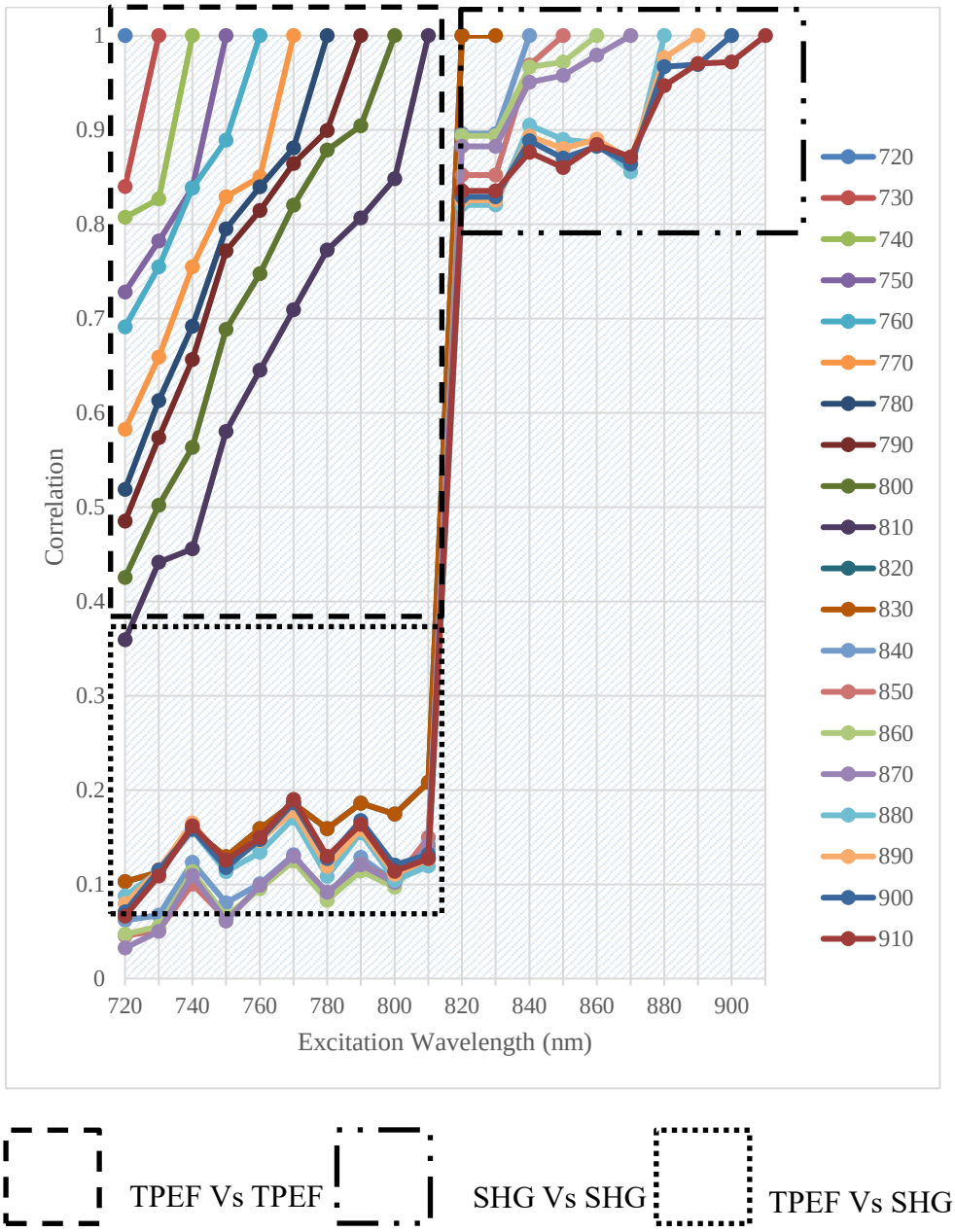

Figure 4.4: Pixel correlation analysis**.** Pixel intensities were correlated as the wavelength of the emitted beam was increased from 720 nm to 910 nm. What this matrix illustrates is a clear correlation between pixels excited via SHG and not for those excited by TPEF. This confirms the production of SHG at 820 nm-910 nm.

4.2.2 Spectral Analysis of Skin Allows for Distinction of Fibrillar Collagens from other Dermal Proteins

After establishing the imaging parameters of SHG in purified collagen and how to interpret the varying signals generated these criteria were applied to images of human skin to evaluate the collagen environments abutting the hair follicle. As human skin contains a plethora of proteins that are capable of TPEF and SHG generation a spectral scan was carried out to establish the boundaries of TPEF and SHG signal production ensuring correct intensity profiles could be analysed.

Figure 4.5 illustrates the presence of TPEF alone, TPEF and SHG, and SHG only at the longest wavelength of 900 nm. At 740 nm and 810 nm excitation of the keratinous hair shaft was evident indicative of TPEF. This structure was visible all the way to 900 nm excitation wavelength suggesting both SHG and TPEF are elicited at least between 820-900nm excitation wavelength. Figure 4.3.1 provides a summary of excitation and emission maxima for some characterised autoflurophores elicited by TPEF. Keratin produces emission spectra by TPEF with a peak excitation of approximately 725 nm tailing off at as high as 950 nm which overlaps with the SHG excitation range (Pena et al. 2005; Heuke et al. 2013; Jianxin Chen et al. 2009). Thus, both SHG and TPEF will be present.

The filter set utilised (410 nm-490 nm and 500 nm-530 nm) in the MP microscope allowed for collagen, elastin and keratins to be excited and detected simultaneously (figure 4.5). The challenge was therefore not in generating an image but generating images in which collagen and TPEF profiles can be identified, segregated and analysed to reveal information regarding collagen density.

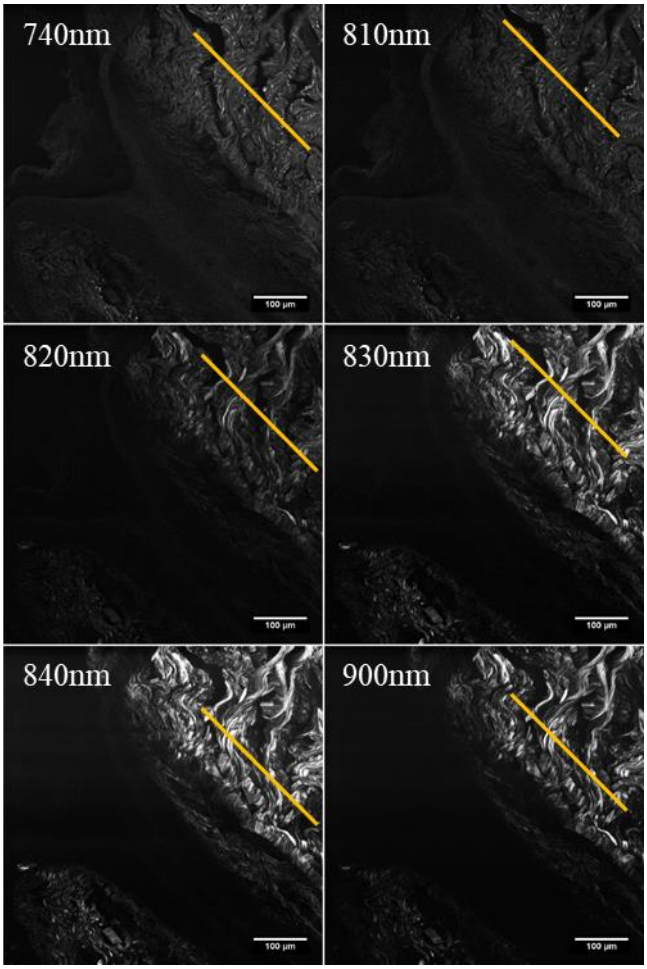

Figure 4.5: MP spectral scans of scalp skin. These illustrate the change in visible structures with changing excitation wavelengths. The orange lines illustrate the direction of the hair follicle. Excitation at 740 nm to 810 nm appears to excite keratinous structures including the medullar of the hair shaft but gradually as the wavelength is increased beyond 810nm collagen bundles become mere clearly defined until 900nm where only collagen bundles are viable. Scale bars represent 100 µm.

Table 4.3.1 Characterised autoflurofores and their peak excitations and emissions (Na et al. 2000; Tilbury et al. 2014; Laiho et al. 2005). Note that NADH, and Flavine are not likely to be present in notable amounts in the dermis due to the high ECM:fibroblast ratio. Keratin is also only weakly autofluorescent as seen in figure 4.3.1

Fluorophore	Location	Absorption maximum (nm)	Fluorescence maximum (nm)
NADPH	All layers	710	470
Elastin	Dermis, subcutis	730	495
Collagen	Dermis, subcutis	730	525
Keratin	Epidermis, hair follicle	760	475
Melanin	Epidermis	800	620
Flavine	All layers	730	525

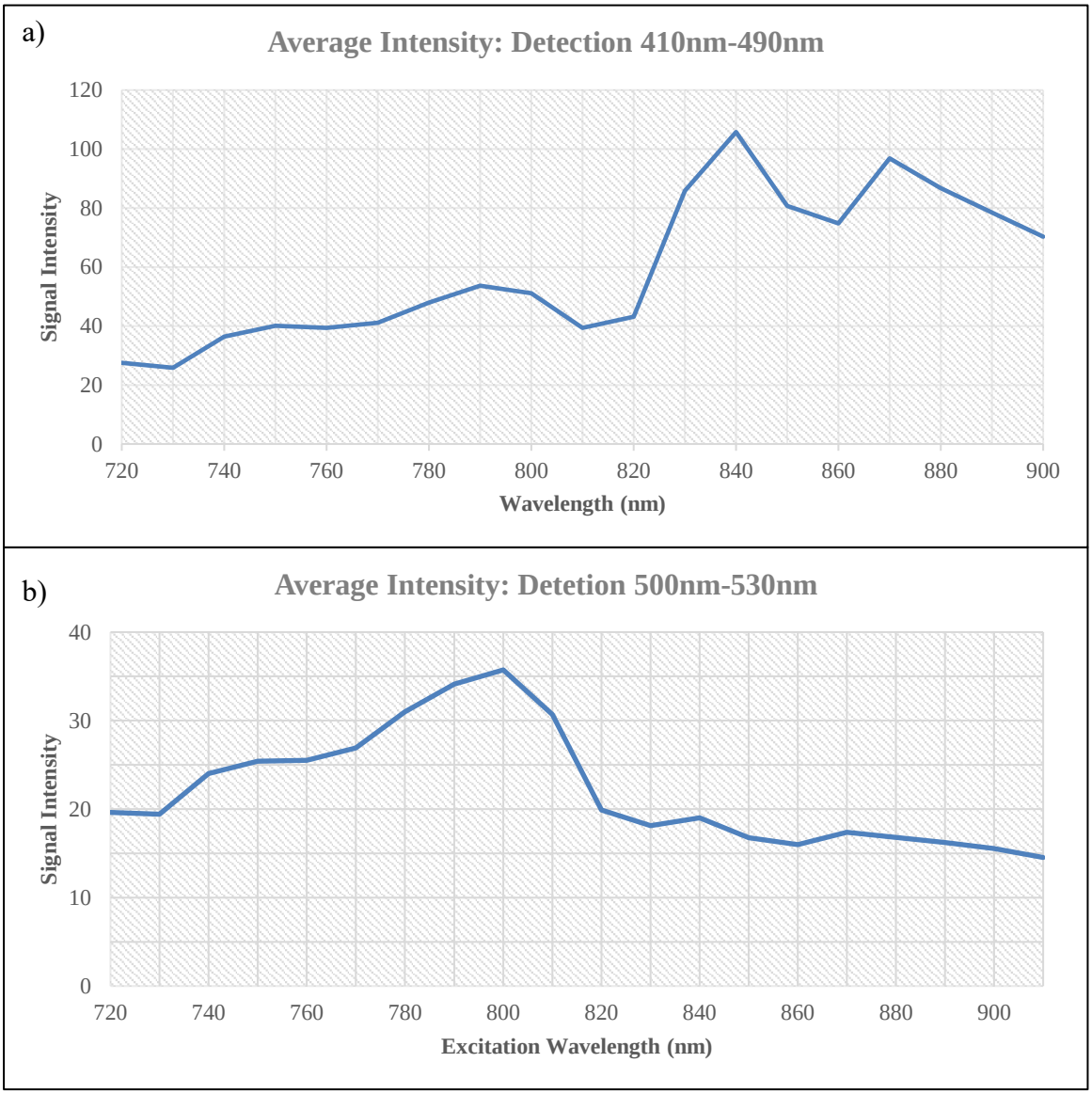

Figure 4.6: MP intensity plots for a region of dermis excited at 10 nm intervals from 720 nm to 910 nm. The two detection ranges were determined by the available filter cube sets and highlight the production of SHG from 830 nm to 910 nm with TPEF only from 720 nm to 820 nm. These figures illustrate how the 410 nm to 490 nm filter set detect SHG i.e. a signal at half the excitation wavelength whilst the 500 nm to 530 nm filter set detects only TPEF i.e. at a much lower intensity as the emission is not at a single wavelength but spread over a spectrum.

To evaluate signals derived from TPEF and SHG in human skin, intensity profiles produced from spectral scans over the 710 nm to 900 nm range at 10 nm intervals were compared (figure 4.7). The intensity maps represent a comparison of pixel intensity from the same locations within the dermis (with respect to x, y and z coordinates), excited by different wavelengths. The excitations were calculated for each pixel intersecting a line drawn from the collagen adjacent to the follicle out into the interfollicular dermis. This further supported the production of SHG in the excitation range from 820nm-900nm with TPEF being the only signal present outside of this range as the 820nm-900nm excitation exhibit a high similarity of pixel intensity across the varying wavelengths. Low correlation would be indicative of a bell curve of emission produced by fluorescent species and hence as the wavelength is altered the pixel intensity would decrease away from the peak emission. SHG however produces a plateau emission. Therefore, altering the wavelength within the SHG range should not affect pixel intensity. The peaks of excitation evident from the excitation range 750 nm-800 nm may be indicative of the presence of elastin known to have an emission peak at 780 nm (Jianxin Chen et al. 2009; Huang, Heikal, and Webb 2002; Zoumi et al. 2004).

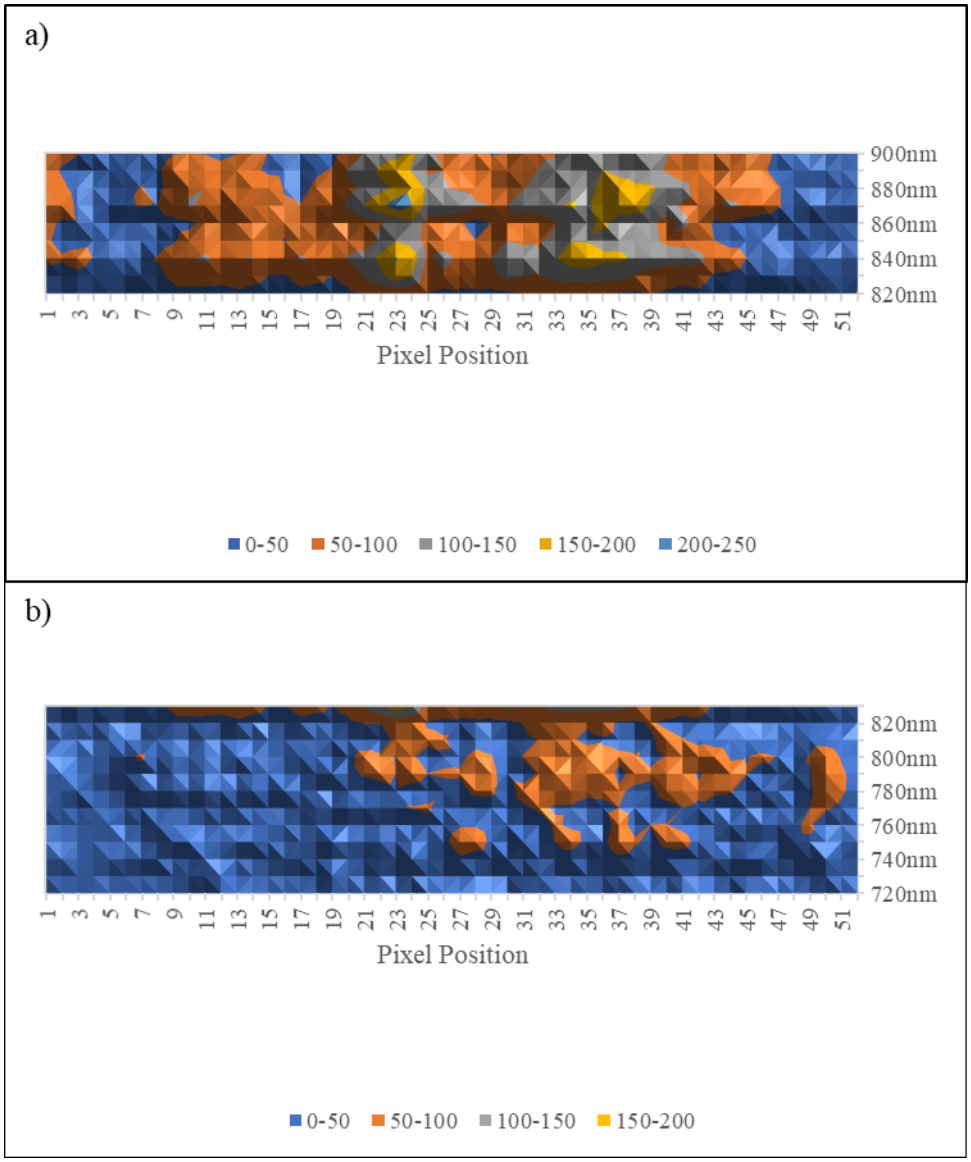

Figure 4.7: Heat maps illustrating pixel intensity (i.e.0-255) from MP micrographs. This illustrates a co-localisation between TPEF and SHG but also shows a clear increase in signal strength when SHG is elicited indicative of a collagen rich environment. Pixel positions correspond to pixels that intersect the line from the follicle into the interfollicular dermis covering a 25 µm distance. Panel a) range deomonstrates the SHG excitation range (830nm-900nm) with panel b) illustrating the TPEF range (710-820nm).

When cosidering intensity profiles directly there are two distinct profiles with peaks for each occouring at different location indicative of two biologiaclly distinct structures (figure 4.8). A line was drawn perpendicular to the direction of the collagen bundle through dermis only, avoiding follicles and non-dermal structures with pixels intersecting the line being quantified. Figure 4.8 therefore provides information relating to distances between bundles, bundle thickness and the proportion of collagen to elastin (and other fluorescent species). The TPEF intensity profiles exhibit larger varitions in profile pattern indicataive of different endogenous flurophores with different excitation peaks. The excitation wavelength of 780nm also coincides with the region of highest intensity spanning pixel lengths exceeding 2µm in the pixel intensity map further suggesting the structure to be fibrous rather than diffuse (figure 4.8). Diffuse endogenous flurophores are represented by the lower more ubiqitous intensites. Panel b) also shows the charachteristic homogenity of traces across the SHG excitation range showing the plateu of emission versus the peak emission and tailing off produced by TPEF. It was therefore possible do distinguish between SHG and TPEF. SHG traces will be of greater intensity and consistent across a range whilst TPEF traces will exhibit varying peak heights across an excitation range.

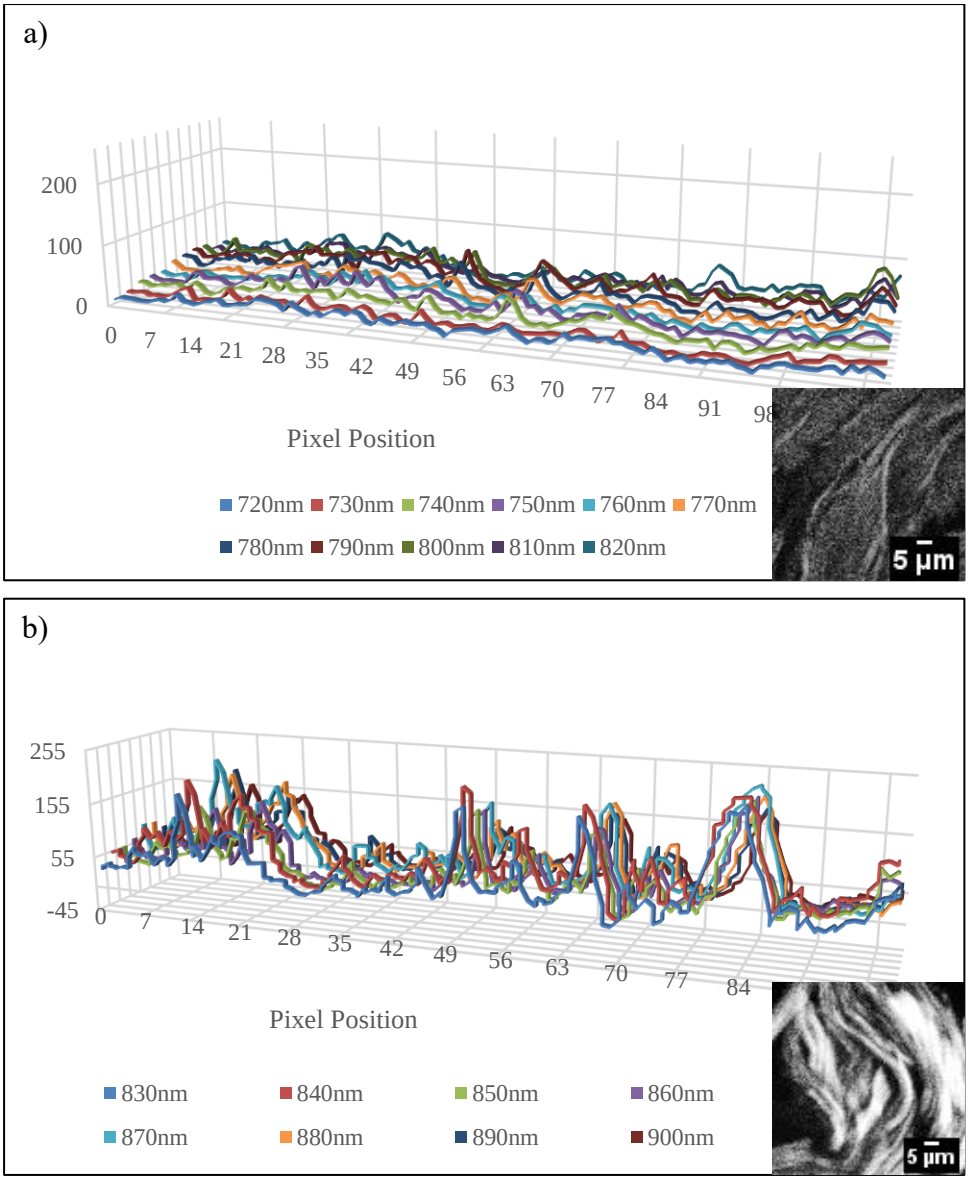

Figure 4.8: MP intensity profiles taken perpendicular to the collagen abutting the follicle (3.5 pixels μm^{-1}). a) Heterologous TPEF traces produced from a variety of colocalising flurophores. Large broad peaks imply a bundled structure such as elastin fibres whilst small shallow peaks will most likely be attributed to small ubiquitous fluorophores such as tryptophan amino acids. b) Traces derived from excitations in the SHG range. Peak widths are indicative of collagen bundle size.

To quantify the homogeneity of the SHG signal and heterogeneity of the TPEF signal correlation analysis was carried out (figure 4.9). As was the case with purified type-1 collagen the correlations fell into three major groups representing SHG, TPEF and both TPEF and SHG. The SHG signals produced by excitation wavelengths ranging from 820nm to 900nm all exhibited a correlation coefficient of $\geq$0.8 indicative of high degree of similarity in intensity profiles. Unlike isolated type I collagen there is the emergence of two further sub-categories of SHG correlation 820 nm-860 nm and 870 nm-900 nm suggesting the contribution of TPEF (although only small) in the 425 nm-475 nm emission spectrum cause variations in the lower peaks of the SHG trace.

The 710 nm-810 nm excitation range exhibited decreasing correlation indicative of spectral emission (figure 4.9). Although a flurophore may have multiple excitation peaks these peaks will correspond to multiple emissions peaks that are stokes-shifted. As detection was carried out within a range it is possible, multiple peak emission were collected for a fluorescent species. However, as a peak emission is passed or falls outside of our detection range it was hypothesized a lower intensity signal would be collected reducing the correlation between signals. Thus, each emission profile generated within the 710nm-810nm range only had a correlation coefficient of over 0.8 with intensity profiles generated at +/- 20 nm e.g. 780 nm has a reducing correlation across the wavelengths.

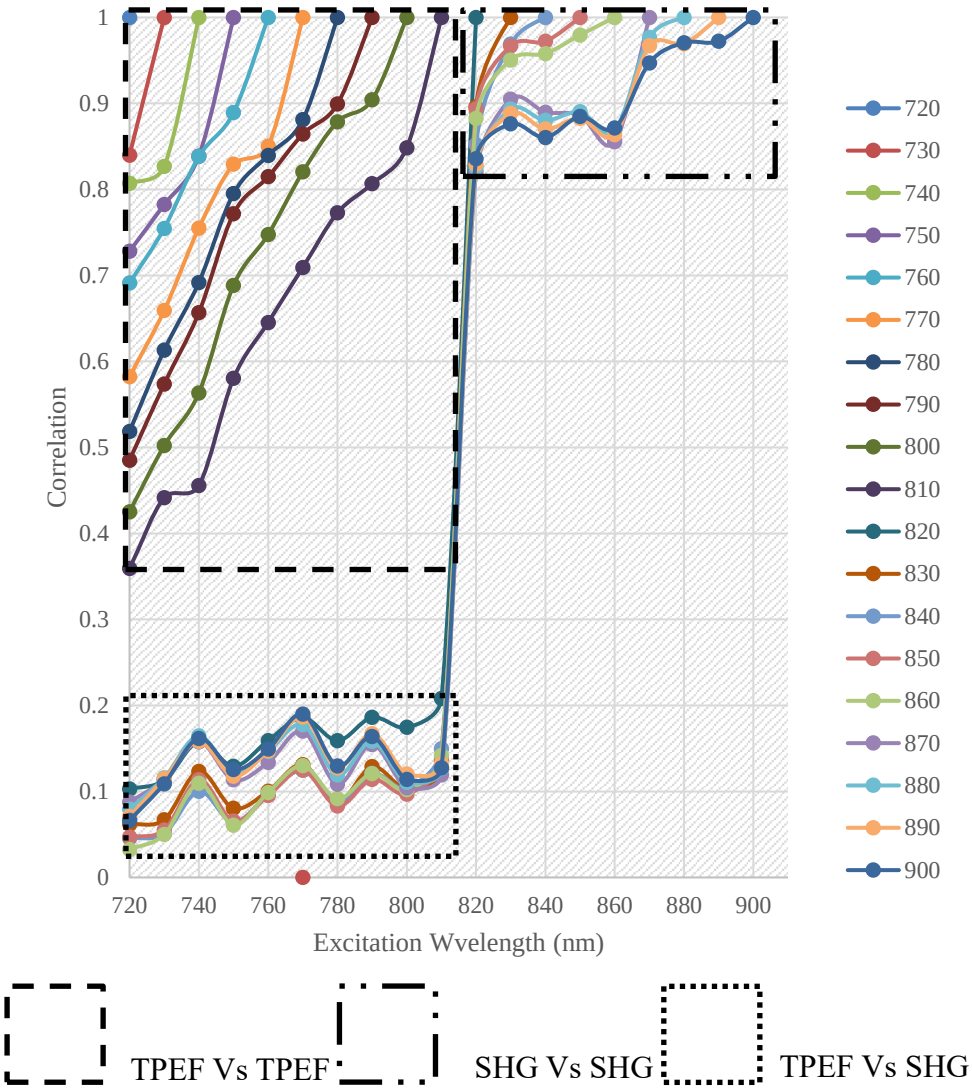

Figure 4.9: Pixel correlation analysis of dermal collagen. Correlation of signal intensities for a defined group of pixels. The pixels represent emissions as a result of excitation from 720 nm to 900 nm. The emissions generated from a defined region of the image are then compared to subsequent images of the same sample and same regions, as the excitation wavelength is altered. The correlation coefficient is an indicator of similarity between pixel intensity at one excitation wavelength to those generated by the same pixel for another wavelength. A value of 1 would indicate identical intensities. Values descending from one indicate increasingly less similarity.

4.2.3 The Ratio of Collagen to Non-collagenous proteins Implies Differential Collagen Densities within the Dermis Adjacent to Hair Follicles

The Masson's trichrome stain was utilised as histological method to visualise the collagen environment encompassing the pilosebaceous unit (figure 4.10). This was suggestive of a reduction in abundance of collagen as you pass from the infundibulum through to the suprabulbar region of the follicle prompting MP analysis to asses the ratio of collagen to elastin within the different regions.

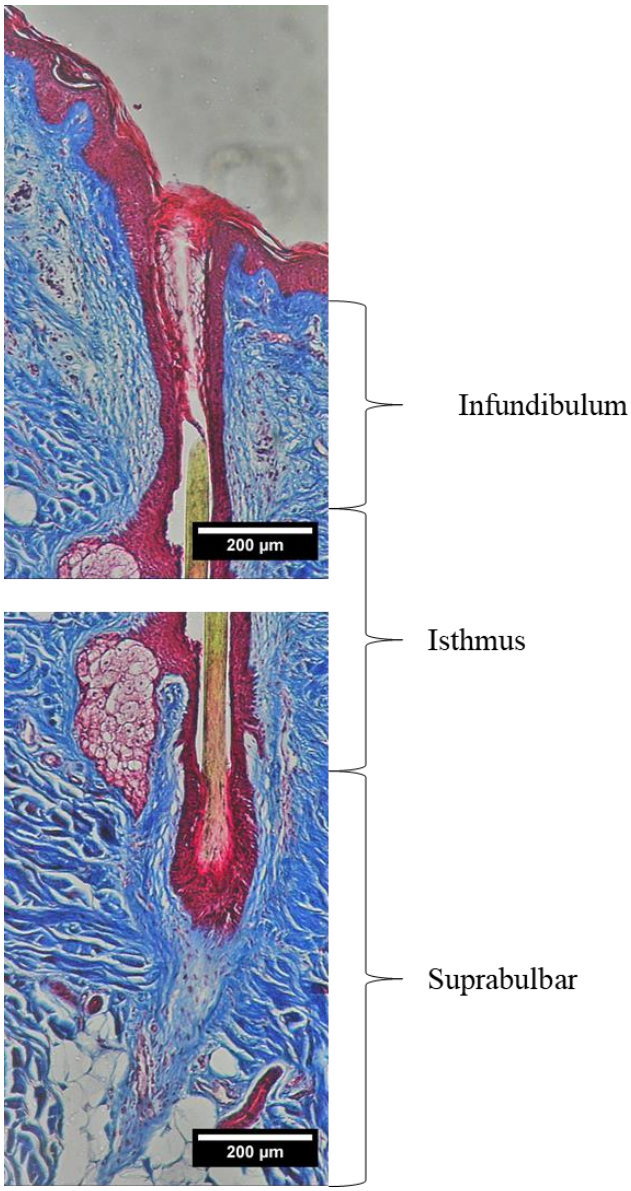

Figure 4.10: Masson's trichrome staining of human scalp skin. Fixed in 4% paraformaldehyde with 0.2% glutaraldehyde for 24h followed by snap freezing and sectioning to 8µm using a human tissue designated Leica cryostat. Blue indicates collagen and nuclei with red indicating keratins, cytoplasm and muscle.

To clarify the differential collagen environments and inspect if the change in the amount of collagen corresponded with increased non-collagenous fibrous structures, the ratio of collagen to non-collagen was evaluated (figure 4.11). To do this 8µm thick facial skin sections (unlabelled) were excited at 720nm to ensure elastin fibres were excited and at 840nm to generate SHG within collagen only. The intensity of the TPEF and SHG signal are subtracted then divided by the sum of the two. In this way we get a ratio SHG described as a single value. In this instance an increased ratio would indicate a higher proportion of collagen to non-collagenous proteins whilst a reduced ratio would indicate a more equal proportion of collagen to elastin. This suggested the isthmus region to have the highest proportion of collagen to elastin and the suprabulbar region to have the lowest proportion of collagen to non-collagenous protein.

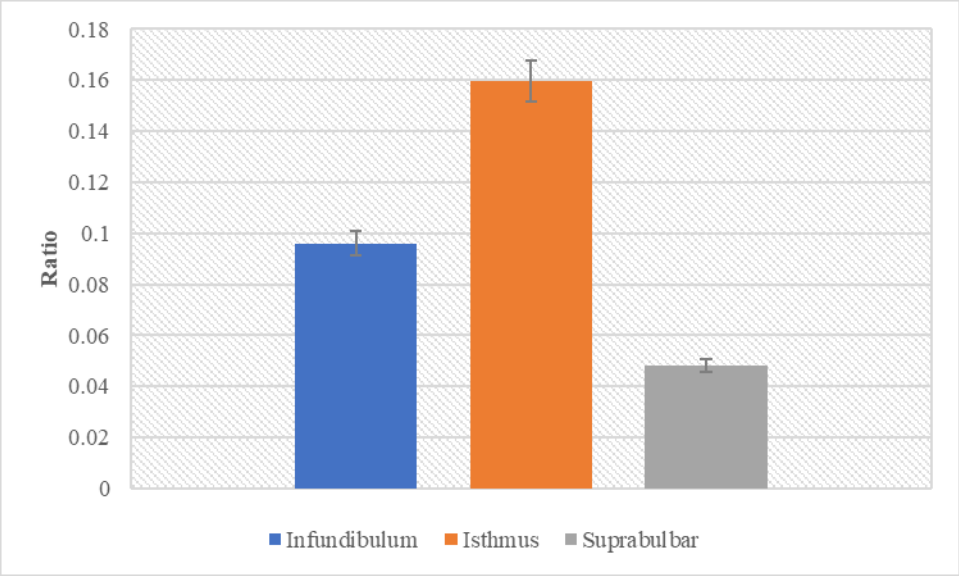

Figure 4.11: The ratio of SHG to TPEF in extrafollicular dermis. An increase ratio represents an increase in the proportion of collagen. Error bars indicate the standard error of mean, n=10.

4.2.4 Distances between Intensity Peaks Implies a Reduction in Collagen Fibre Density along the Region of Dermis Corresponding to the Infundibulum to Suprabulbar Region of the Follicle

Through use of a novel logic arguments in Microsoft Excel (e.g. IF(X)>OR=(Y)AND(Z), (X)) it was possible to calculte the distances between intensity peaks generated for pixels intersecting with lines drawn perpendicular to the follicle. As SHG is only generated in collagen the peaks generated are representative of collagen fibres with troughs being the regions between bundles (figure 4.12). Distances between peaks were therefore indicative of the density of collagen fibre bundles adjacent to the different regions of the follicle.

Figure 4.12 demonstrates two different collagen environments with the infundibulum and isthmus regions exhibiting a higher density of fibres when compared with the suprabulbar region. The traces also highlight a change in the collagen organisation from the suprabulbar region with larger broader excitations indicative of larger bundles compared with the smaller more frequent peaks of the infundibulum and isthmus. This was indiative of a finer more densly packed network of collagen fibres at a level consistent with the infundibulum and isthmus.

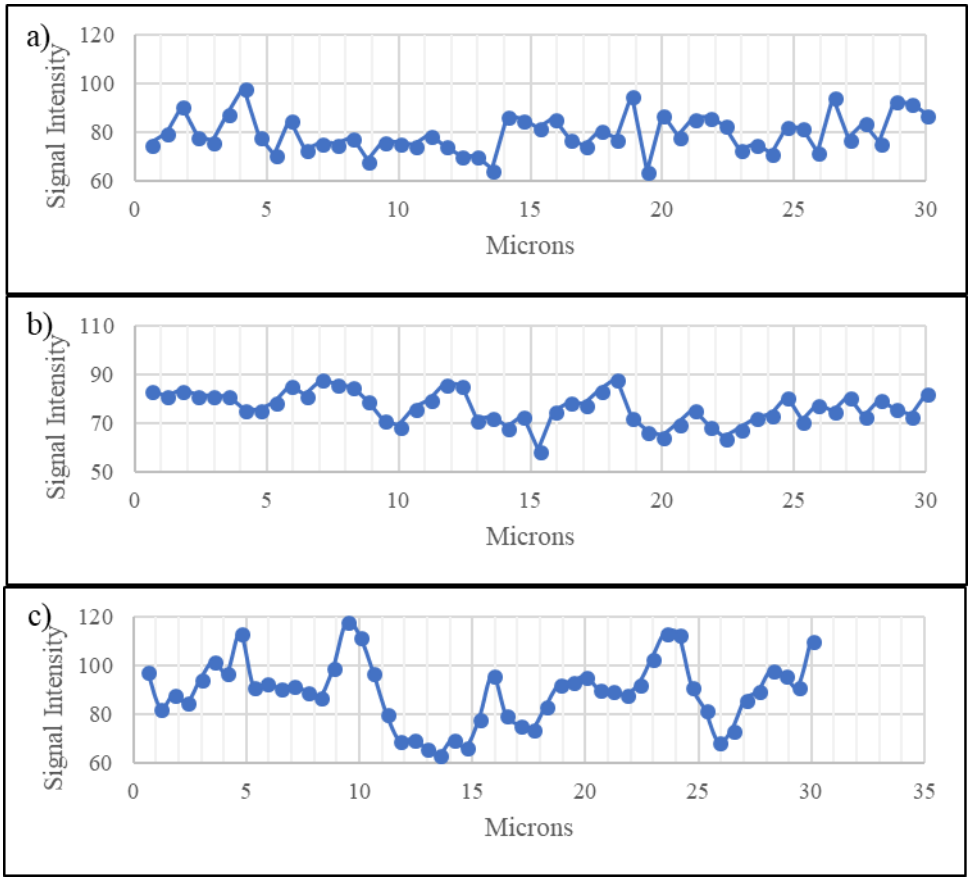

Figure 4.12: Example intensity plots for dermal tissue excited at 840 nm with subsequnet detection at 410 nm- 490 nm. Plots represent pixels intersectin lines drawn perpendicular to the direction of the follicle. a) Infundibulum b) Isthmus c) Suprabulbar

In resting skin, there was a significant diffence in density between the collagen environment at the level of the isthmus and infundibulum. However, there was no significant difference between the isthmus and suprabulbar region. Figure 4.13 would suggest there was a reduction in collagen fibre density adjacent to the follicle as you move from the infundibulum through to the suprabular region.

Post-loading of the hair shaft with a 2g weight the collagen envirmonents adjcent to the infundibulum to suprabulbar regions exhibit homogenity with one another (figure 4.13). This implies rearrangemnt as a result of loading which may be related to the function of collagen in follicle anchorage and retraction of the follicle back into the skin post relesing of the weight from the hair shaft. The homogenity of collagen identified post-pulling indicated the fibres to have become taught which suggest they

had a degree of extension capacity to accommodate for the follicular compression during loading of the hair shaft.

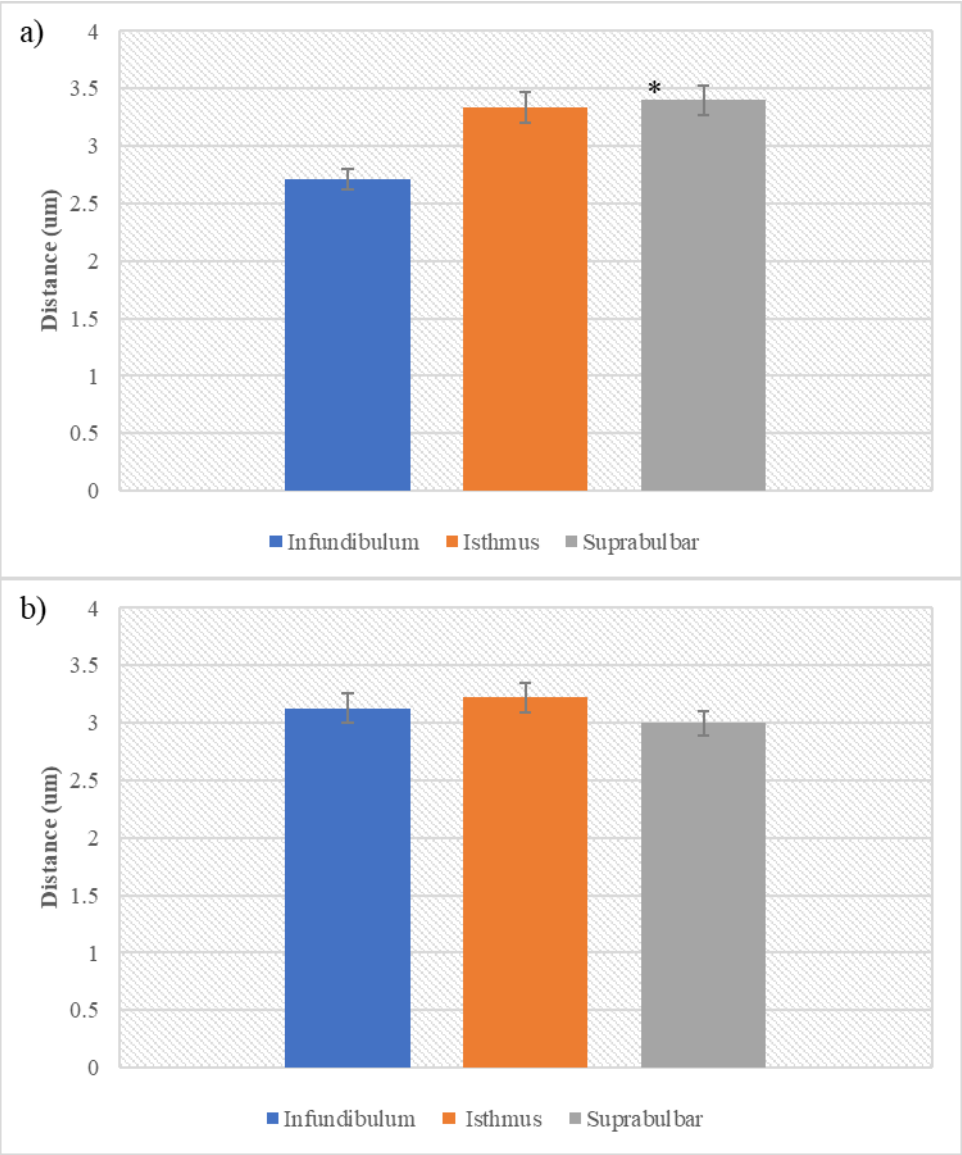

Figure 4.13: Average distances between collagen bundles adjacent to the follicle. Distances calculated from distance between intensity peaks. a) The average distance between peaks pre-loading of the follicle b) The average distance between peaks post-loading of the follicle. Error bars are +/- the standard error of mean with * denoting significant differences compared with the infundibulum ($P<0.05$ for n=10). There was no other significant difference calculated between the infundibulum and isthmus or the suprabulbar region and isthmus pre-pull. No significant differences were found post-pull.

4.2.5 Temperature of Gelation and Concentration of Collagen in Suspension Affect the Density of the Resultant Collagen Matrix

To elucidate how physical differences in collagen environments impact proliferation and differentiation rates of epidermally derived cells, high-density (HD) and low-density (LD) collagen hydrogels were developed and characterised. The matrix properties are affected by the concentration of collagen (mg ml^{-1}) and the temperature of gelation. Matrices were evaluated using a combination of SEM and MP. The MP approach allows interrogation of structures at depth in addition to assessing the overall homogeneity of the matrices produced. SEM on the other hand provides detailed topographic information to verify results obtained by MP microscopy. Combining these approaches was used to demonstrate that structural properties of the matrices can be manipulated to produce HD and LD matrices.

One of the unique properties of two-photon microscopy is that at any one time only a sub-femtolitre volume is excited sufficiently to produce either TPEF or SHG consequently giving excellent three-dimensional resolution compared with linear techniques that require pinholes and software to remove out of focus light. It is therefore possible to interrogate the three-dimensional structure with high precision identifying changes within localised volumes that can give insight into the structure's morphology and composition. In this instance back scattered SHG has been used as a means of assessing localised changes in collagen density and fibre orientation.

Initial observations of the 3D reconstruction (figure 4.14) show the increase in temperature of gelation and increased concentration of collagen used generate a brighter signal which could be indicative of increased diameter of collagen fibres. The increased fibre diameter as a result of increased concentration of collagen is illustrated in (figure 4.14). Further to this the higher concentration collagen produced larger collagen fibre nucleation sites as indicated by the large white dots spread throughout the matrices. The 3D cross-section suggests the matrices polymerised at lower temperature (4℃) form more compact matrices whilst those polymerised at the upper temperature (37℃) produce matrices with larger void sizes. This was indicated by the homogenous grey observed within the matrices polymerised at the lower temperature whilst those at the higher temperature exhibited a mottled heterogenous grey intensity.

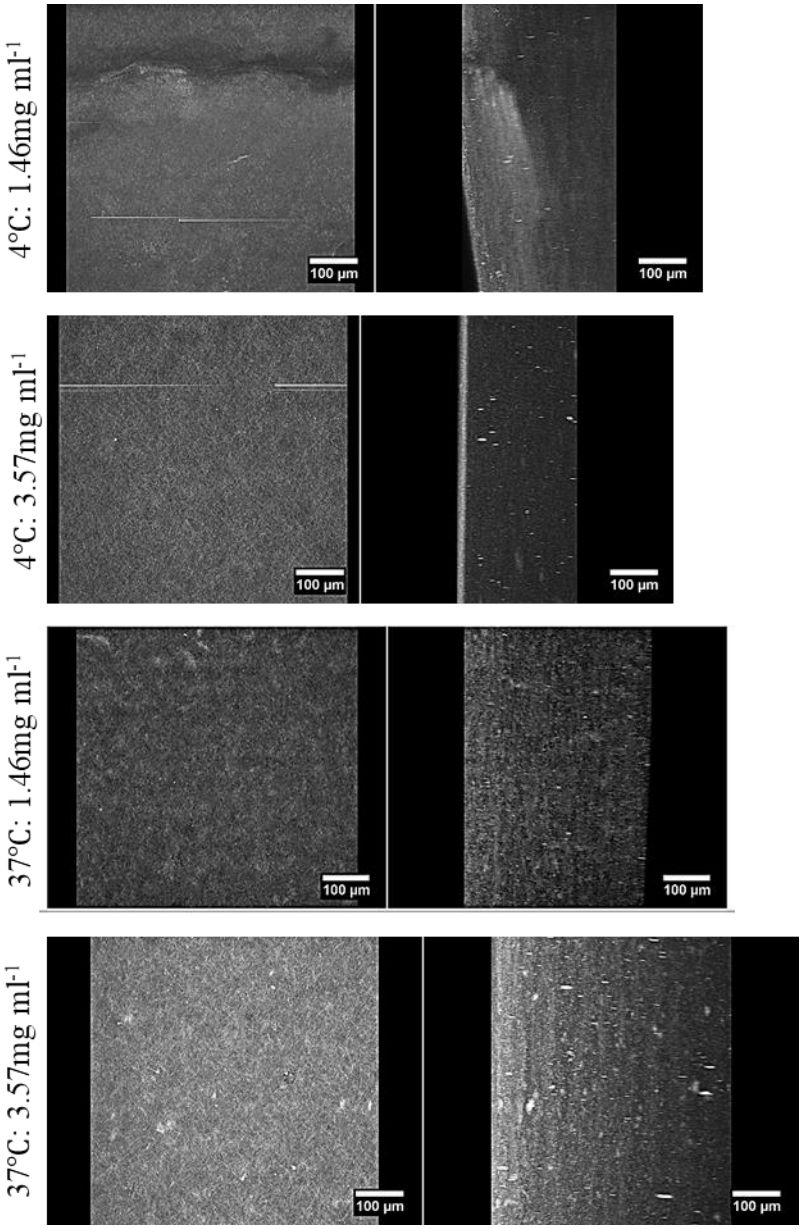

Figure 4.14: 3D reconstructions of SHG in collagen hydrogels taken at 1um intervals over a 200µm distance. The left pane represents the maximum intensity projection looking top-down whilst the right pane represents a cross-section of the z-plane. Scale bars are 100 µm.

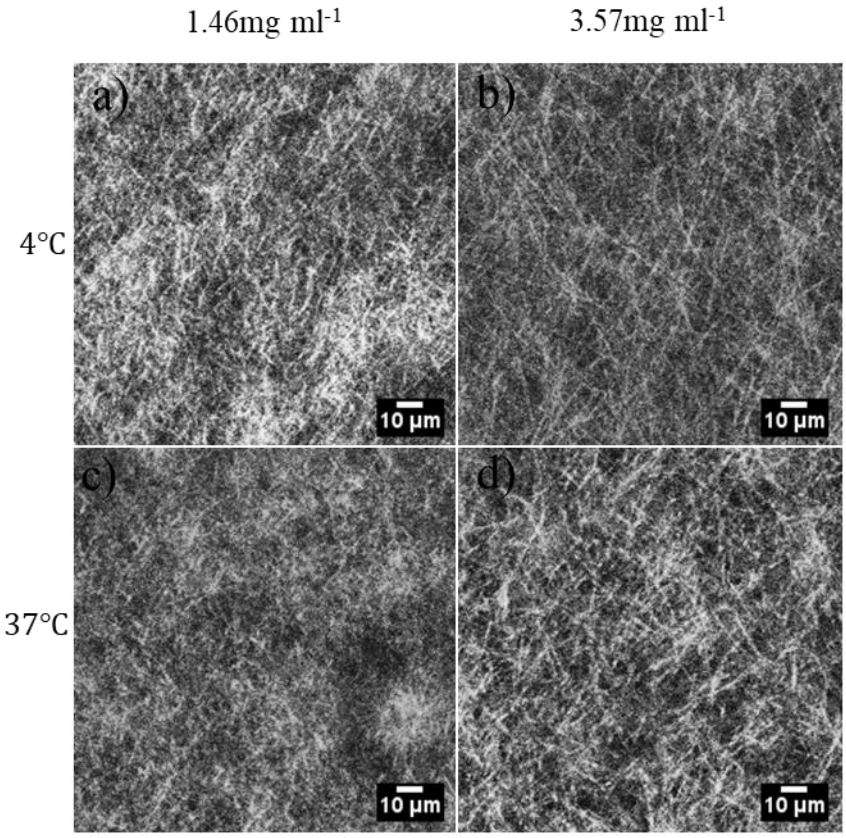

Figure 4.15: SHG micrographs taken 50 µm from the surface of each collagen matrix. The increased concentration is linked to increased void size as suggested by the larger distances observed between the white collagen fibres. Scale bars are 10 µm.

When considering how the SHG intensity changes with depth (z-axis) morphological differences become more apparent as a result of the increased temperature of gelation and increased concentration of collagen used (figure 4.16). Average intensity over a 200 µm distance would suggest the matrices polymerised at 37 ℃ to have less densely packed fibres as the signal decay is lower compared with those polymerised at 4 ℃.

However, the effect of increased concentration of collagen appeared to have two different effects depending on the temperature of gelation. At 4 ℃ the increased concentration resulted in a reduction of intensity which implied the formation of a denser matrix. The converse was the case for matrices polymerised at 37 ℃ which exhibited an increase in intensity with increased concentration of collagen suggestive of a less dense matrix. With this paradoxical situation it became imperative to consider what components comprise density. There are two key features that will affect the collagen density: 1) The thickness of the collagen fibre bundles 2) the number of collagen fibre bundles per unit area. Therefore, increased fibre size as a

result of increased temperature of gelation was hypothesized to produces a less tightly packed matrix whilst at low gelation temperatures were expected to generate a larger number of thin fibres per unit area producing a denser matrix.

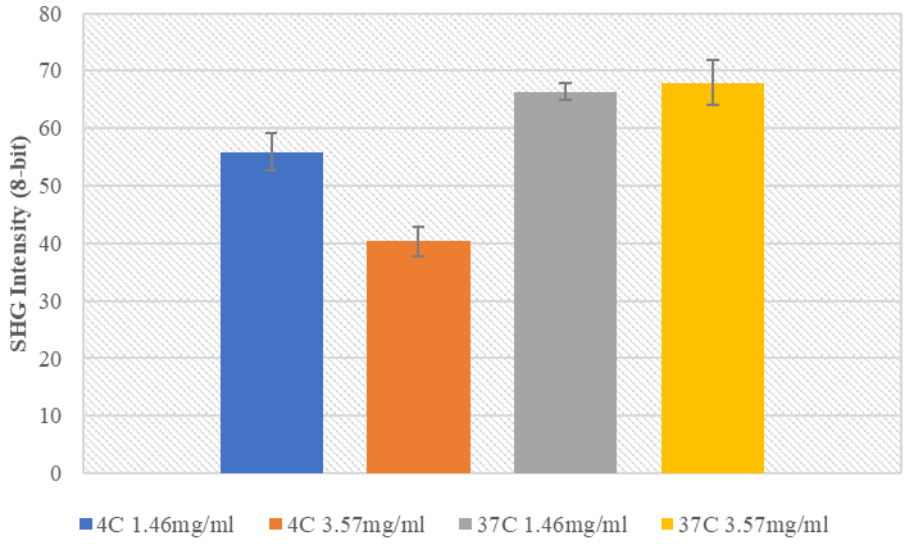

Figure 4.16: The average SHG intensity over a 200 µm depth. Error bars represent the standard error of mean.

Assuming the signal decay is a function of fibre thickness and how densely packed the fibres are the percentage change at 2 μm intervals over a 200 µm distance were analysed (figure 4.17). The largest percentage change is indicative of a more densely packed matrix (i.e. more fibres per unit area) and *vice versa*. Figure 4.17 suggests that altering the collagen concentration only impacts upon collagen density when polymerised at 4 ℃. This suggests that the temperature of gelation is the key controller of matrix density. However, this assumes that there is no difference in collagen fibre bundling as larger collagen fibre bundles would generate a greater signal but would also produce increased scattering of the backscattered SHG. Thus, the rate of change of SHG from the surface would be far greater than in a matrix with smaller bundles. The average percentage change over 200 µm depth figure 4.17 suggest that the increased concentration of collagen at both temperatures of gelation results in increased fibre bunding as indicated by a greater reduction in back scattered SHG over a 200 µm depth.

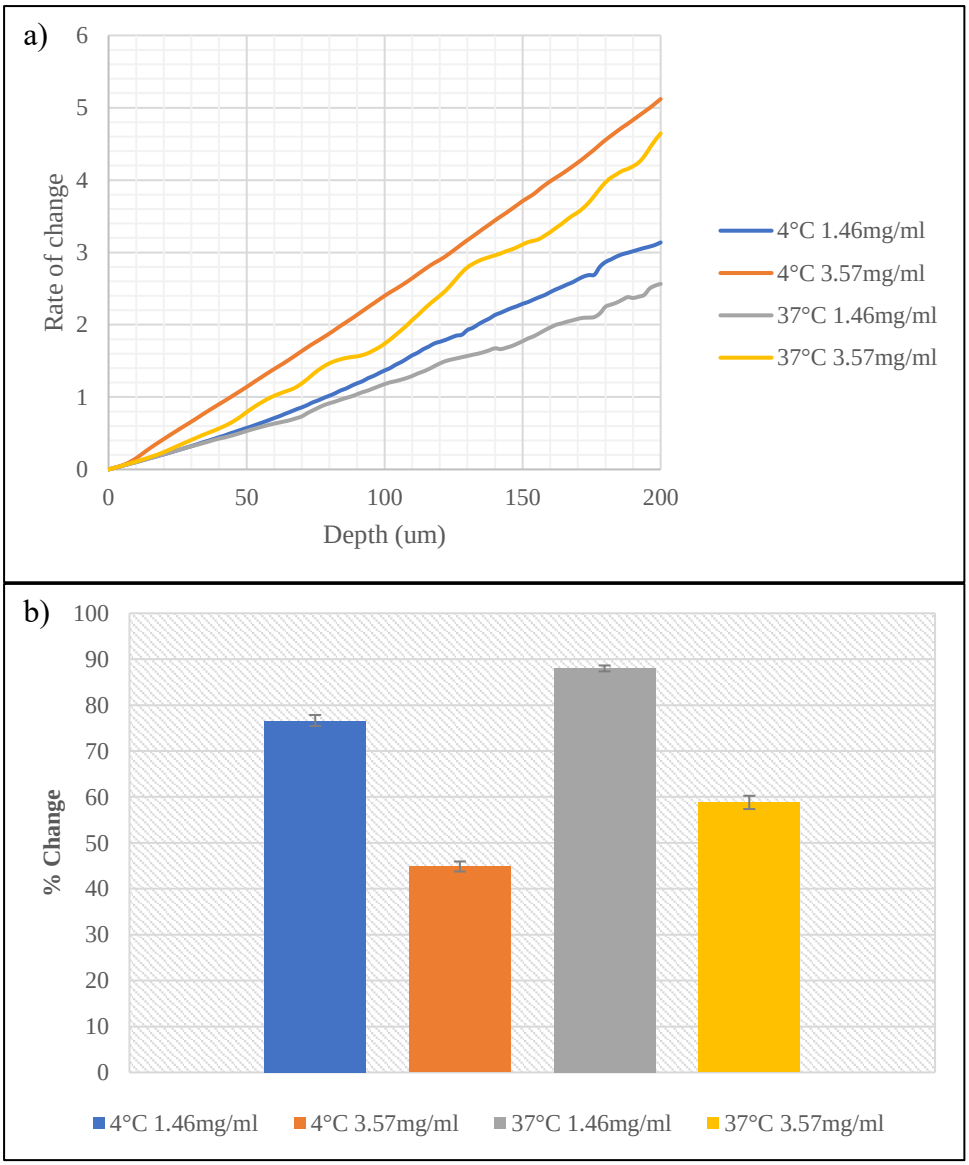

Figure 4.17: SHG signal decay in collagen hydrogels a) Rate of change over a 200 µm depth of collagen. The steeper the gradient the greater the rate of change. b) The average percentage change of SHG over 200 µm (n=3).

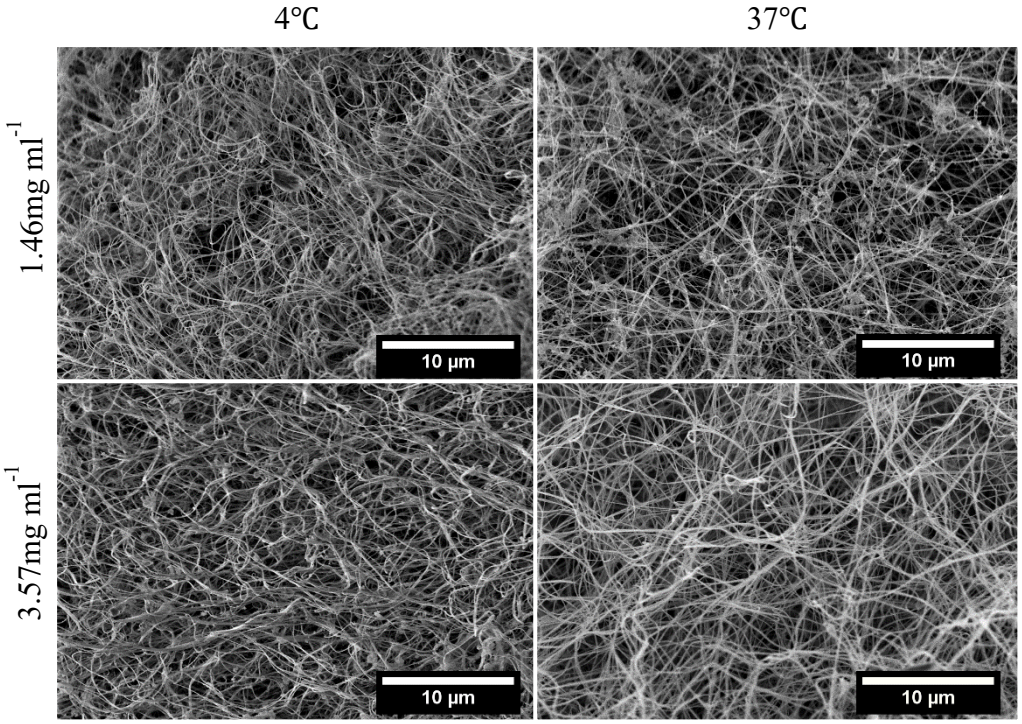

Figure 4.18: SEM micrographs of collagen hydrogels produced at varying temperatures and from different concentrations of collagen solution. 10 µm scale bars.

Figure 4.18 illustrates how the increased temperature of gelation produces matrices with fewer fibres per unit area with the increased concentration of collagen having a greater number of fibres per unit area. To quantify the number of fibres per unit area straight line distances from one intersection of a collagen fibre to the next (Euclidean distance) and the length of the region of the fibre spanning the distance between to intersections (branch length) have been quantified (figure 4.19). A denser matrix was hypothesized to have a higher number of intersections. The Euclidean distances are indicators of collagen fibre thickness with thicker fibres exhibiting less tortuosity (i.e. increased Euclidean distance and branch length). A high density (HD) matrix should exhibit a longer branch length and a low Euclidean distance which would indicate an increased length of fibre per unit area and *vice versa* for a low density (LD) matrix.

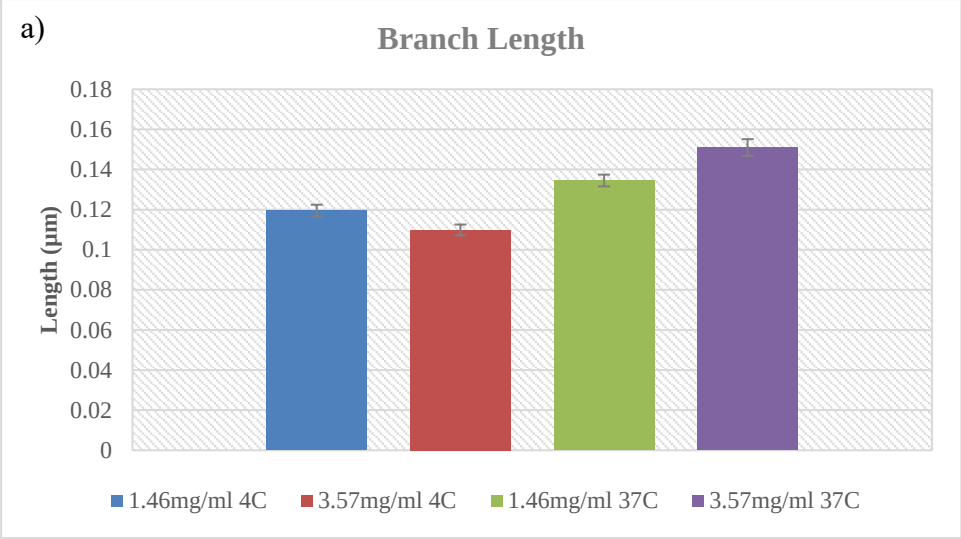

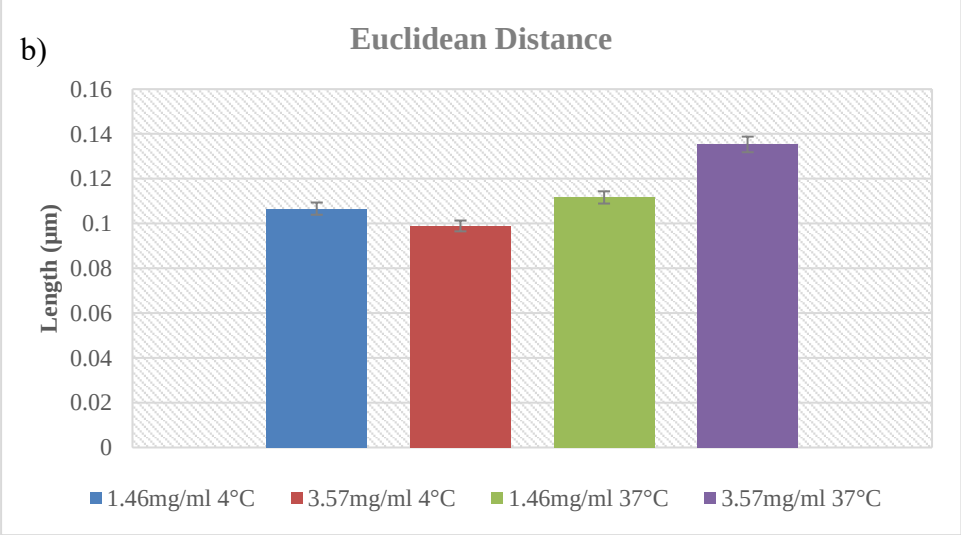

Figure 4.19: Arch-chord characteristics of collagen fibres. The Euclidean distance (a) represents the straight-line distance from one end of a collagen fibre spanning two intersections/branch points, to the other. The branch length (b) is the actual length of the collagen fibre that spans the two intersections/branch points. The error bars represent the standard error of mean (n=3).

The change in concentration had two effects dependent upon the temperature of polymerisation as was also evident from the multiphoton analysis. At 4℃ the increased concentration of collagen produced a significant increase in both Euclidean distance and branch length implicit of reduced fibres per unit area in line with findings from multiphoton analysis. Increased concentration would therefore be of a lower density.

When polymerised at 37℃ the collagen fibres exhibit a significant increase in both the Euclidean distance and branch length. The effect of increasing the concentration of collagen has the converse effect to that observed at 4℃ with concomitant increase in both Euclidean distance and branch length (figure 4.19). The increased Euclidean distance and branch length implies a reduction in the number of collagen fibres per unit area indicative of a less dense matrix as was also observed within the multiphoton study.

There was no significant change in branch length for the 1.46 mg ml^{-1} with increased temperature. However, there was a significant increase in Euclidean distance indicative of a decrease in the number of fibres per unit area and an increase in void size.

As previously demonstrated when understanding collagen density both the number of fibres per unit area and the fibre diameter must be considered. The diameter of collagen fibres and bundles of fibres have been quantified within the different matrices produced. Figure 4.21 demonstrated the increased bundling of fibres at the 3.75 mg ml^{-1} collagen matrices for gelation temperatures of both 4℃ and 37℃ compared with their 1.46 mg ml^{-1} counterparts. Increasing the temperature of gelation significantly increased the bundle width for 1.46 mg ml^{-1} matrices but not for 3.57 mg ml^{-1} matrices.

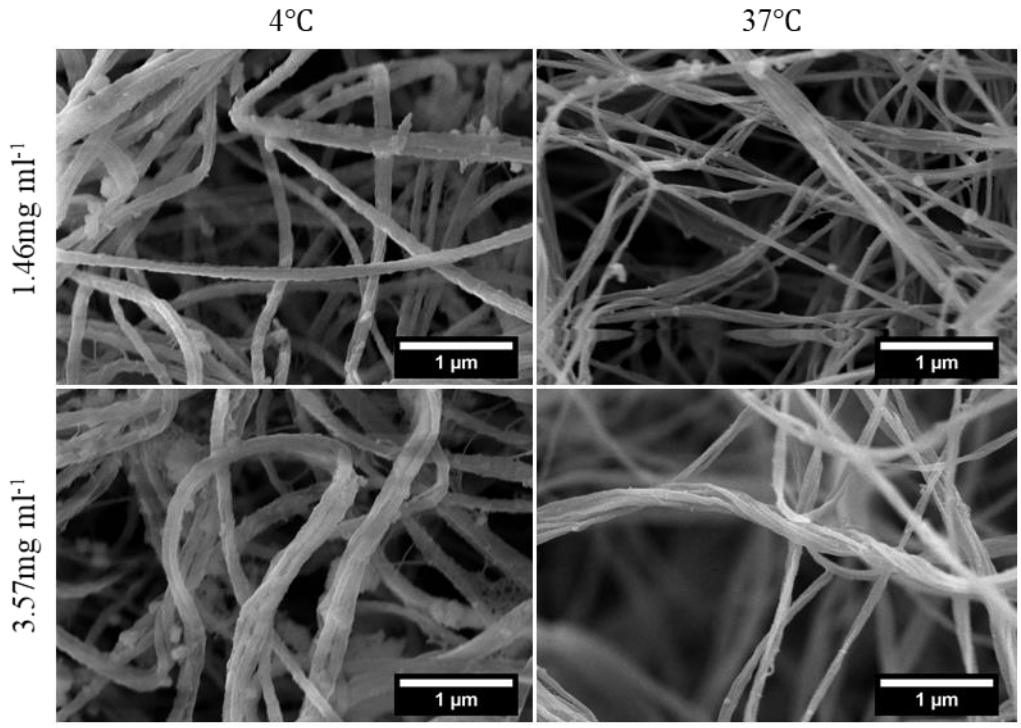

Figure 4.20: High magnification SEM micrographs of the collagen fibres produced by each of the different gelation conditions detailed. When considering fibre diameter bundled fibres have also been quantified as a single fibre since these will increase the surface area of collagen available to an overlying cell. 1 µm scale bars.

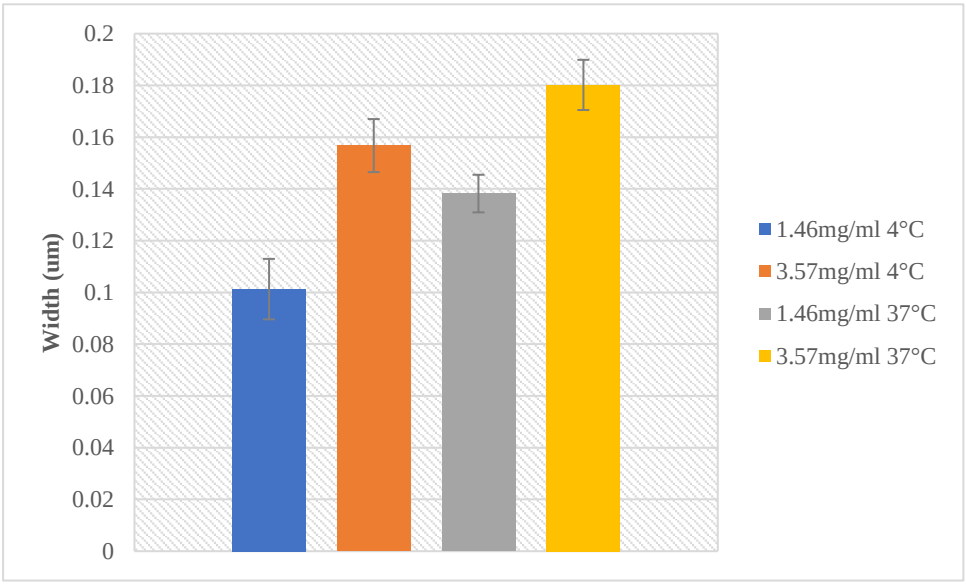

Figure 4.21: Average width of collagen fibre bundles quantified from high resolution electron micrographs. Error bars represent the standard error of mean for each condition. Error bars represent the standard error of mean (n=3).

Therefore, to achieve an equivocally high-density matrix it was deemed essential to have a high number of fibres per unit area and small bundles to reduce the void size, increasing the availability of collagen substrate to the cell. Increased fibre diameter correlated with increased void sizes as indicated by the increased Euclidean distances for unchanged branch lengths. In summary, polymerisation at 37℃ produced a high-density (HD) matrix at a lower concentration collagen and a lower density (LD) matrix with a higher concentration of collagen.

4.3 Discussion

4.3.1 Analysis of Intensity Peaks Generated by SHG Provides a Novel Means of Assessing Collagen Matrix Density

Probing collagen organisation by MP microscopy is a highly complex process requiring specialised sensors and filters capable of detecting both backward and forward emitted SHG. SHG radiation patterns are a product of the spatial extent of the emission source (Williams, Zipfel, and Webb 2005). Such methods have been able to interrogate the periodicity of collagen fibres through analysing the angular distribution of polarised light (Tiaho et al. 2007.; Su et al 2011). The real problem though is that SHG is entirely theoretical. That is to say that like all microscopy techniques it relies on theoretical physics that predicts particulate interactions (Sheppard et al. 1977; Denk, Strickler, and Webb 1990; Laiho et al. 2005). Therefore, there is a need to both characterise and verify the signal being collected when applied to a biological system. Use of a limited filter set and only capacity for only backward detection (i.e. in the direction opposite to the direction of the excitation light source) make this characterisation and verification difficult for two key reasons. The first is that there is a potential overlap between SHG and TPEF emission and the second is the inability to assess change in forward versus backward scattered SHG to inform upon collagen density.

The quantum nature of non-linear techniques requires the interactions of parcels of energy within a miniscule time scale (i.e. 10^{-16} seconds) (Tilbury et al. 2014; Vielreicher et al. 2017; Sheppard et al. 1977). To increase the chances of such an event occurring the pulsed laser is focussed into a sub-femto litre volume (i.e. less than 1 cubic micron). This allows for the defining of fine structures through analysing intensity differences between regions from one focal volume to the next. The configuration utilised to analyse skin produced a resolution limit of approximately 1 micron. This resolution allowed for the identification of collagen fibre bundles and crucially the distances between these bundles that contribute to the different collagen densities.

Recent studies identified the papillary and reticular dermis as having collagen bundle sizes of 38 um and 80um respectively. The authors posit that the smaller fibres diameter of the papillary dermis allows for tighter compaction providing a stiffer environment that confers mechanical support to the epidermis while the larger fibres

are interwoven with elastic fibres to form a microfibrillar network (Hellström et al. 2014; Naylor, Watson, and Sherratt 2011). The evidence within this study corroborates these findings and hypothesis as a high-density collagen environment has been identified adjacent to the infundibulum (which would fall within the papillary dermis) and in a low-density collagen environment has been identified in a region adjacent to the suprabulbar region (which coincides with the reticular dermis). SHG and TPEF image have also identified collagen-elastin composite structures within the reticular dermis.

4.3.2 Identification of Collagen Gradient within the Dermis Elucidates Potential Roles for Collagen in Skin Homeostasis and Follicle Homeostasis

The collagen gradient that runs from high to low from the papillary dermis to the reticular dermis may well have significance beyond just differential mechanical support. High-density collagen matrices have been identified as restricting cell migration whilst low density collagen environments have been found to promote cell migration (da Rocha-Azevedo, Ho, and Grinnell 2013). The high-density collagen surrounding the upper non-cycling portion of the follicle could have a role in polarising the directional growth of the follicle. It could be considered that if the matrix density were analogous to that of the lower cycling portion there would be potential for lateral outgrowth of the follicle into the surrounding papillary dermis. Equally the low-density papillary dermis could invite downgrowth of the anagen follicle. Evidence of cell polarisation toward regions of lesser tensegrity is evident in wound healing with cells at the edge of wounds undergoing elevated programmes of proliferation in the direction of the wound. Cells within the skin surrounding the wound do not experience elevated proliferation demonstrating the importance of physical cues (in this case cellular tensegrity) in directing cellular proliferation (Tscharntke et al. 2007; Takeo, Lee, and Ito 2015; Zeltz and Gullberg 2016).

When considering the lack of crumpling of the ORS and IRS within the infundibulum region it must also be considered that lateral opposition to follicular expansion could be conferred from the high collagen density. Further to this increased collagen density is known to promote increased integrin binding and formation of actin stress fibres that in turn produce increased cell stiffness (Barry et al. 1997; D D Schlaepfer and Hunter 1997; Dans et al. 2001; L. Levy et al. 2000; Elbediwy et al. 2016; Dupont

2016; Miralles et al. 2003; C. Gu et al. 2010; Wen et al. 2014). However, whether or not such connections would made via the dermal sheath have not been explored.

It is interesting that the stem cells of the hair follicle are also located in a collagen dense environment. The increased collagen network would be capable of binding a large number of diffusible cues such as such as TGF-β, noggin and BMP4 and BMP7 reducing the dermal papilla derived cues that promote proliferation and terminal differentiation, retaining the cells of the upper bulge in a state of quiescence. It is interesting how studies have found proliferating cells to emanate from the base of the bulge i.e. a region in lower density collagen, and not the upper (Snippert et al. 2010; Merrill et al. 2001; Rebecca J Morris et al. 2004; Greco et al. 2009; Plikus et al. 2008; Y.-C. Hsu, Pasolli, and Fuchs 2011a). Although it has been suggested that this is due to the diffusion limit of cues derived from the dermal papillae it must be considered that collagen is a limiting factor in diffusible cue migration (Vehviläinen, Hyytiäinen, and Keski-Oja 2009; Oshimori and Fuchs 2012; Foitzik et al. 1999; Philpott, Green, and Kealey 1990).

Turing back to the physical properties of collagen it has been noted that thicker fibres exhibit greater stiffness compared with thinner fibres as does increasing the number of fibres per unit area (Bauman et al. 2014; Voorhees et al. 2015; Haase and Pelling 2015). This increased stiffness has been found to increase pre-tensioning and promote exit from cell cycling through reduced histone H3 acetylation at the promotors of serum response factor genes, *FOS* and *JUNB* leading to the suppression of stem cells maintenance genes *LRIG1*, *TP63* and *ITGB1* in keratinocyte derived cells (Connelly et al. 2011; S. C. Wei et al. 2015). Increased pre-tensioning of fibroblast will also allow for faster sensing of damage though disruption of hemidesmosomes and focal adhesions causing an upregulation of ERK signalling promoting collagen biosynthesis and rearrangement (da Rocha-Azevedo, Ho, and Grinnell 2013; Pankov et al. 2000; Dutta et al. 2015; Brooks et al. 1996; Voorhees et al. 2015; Akasaka et al. 1995; Keely et al. 1997; El Azreq et al. 2016; Osmanagic-Myers et al. 2006).

Increased fibre bundling promotes increased adhesion of fibroblasts where low bundling produces reduced adhesion allowing for cells to migrate (da Rocha-Azevedo, Ho, and Grinnell 2013; Rouillard and Holmes 2012; S. A. Ibrahim, Hassan, and Götte 2014). This could effectively promote migration of fibroblast toward the

hypodermis away from the epidermis reducing physical stresses experienced by cells while protecting against deep tissue lacerations. An alternative way to consider this is the high-density collagen promotes increased integrin binding (Ilić et al. 1995; Makino et al. 2009; da Rocha-Azevedo et al. 2013; S. A. Ibrahim, Hassan, and Götte 2014) which prevents fibroblast migrating away from the upper dermis where they are needed to provide growth factor cues to the overlying epidermis to balance quiescence against proliferation in SCs.

4.3.4 Putative Elastin Opposes Follicle Elongation-implications in follicle homeostasis and the propagation of anagen.

Elastin confers the ability of skin to retain its normal morphology after deformation by external forces (Tzaphlidou 2004; Muiznieks and Keeley 2013; Tilbury et al. 2014). This study highlights a potential role for elastin in follicular retraction though attachment at the base. The significance of this is it keeps the dermal papilla proximal to the bulge region. This could be important in preventing overstimulation by diffusible cues such as the BMP2/4 antagonist noggin. Noggin has been shown to deplete bulge SC's through stabilisation of β-catenin that drives upregulation of the Lef/TCF transcription factors, that drive proliferation and differentiation (Plikus et al. 2008; Botchkarev et al. 2001; Song et al. 2018; Merrill et al. 2001; Behrens et al. 1996; Kobielak et al. 2003). It would be interesting to identify if the elastin attachment is retained through-out follicle cycling as the mechanical pulling could also be important in directing follicle down growth.

5.0 Manipulating Collagen Matrices to Provoke Changes in the Proliferation and Differentiation Potential of HaCaT Cells

To uncover more about how mechanical sensing can impact upon cellular behaviour, characterised collagen matrices were developed to evaluate how altering the number of fibres per unit area will influence the proliferation and differentiation potential of the overlying epidermically derived HaCaT cells.

5.1 Introduction to Collagen-Integrin Signalling Mediated by MAPKs; ERK1/2, JNK and p38

Keratinocytes form focal adhesions and hemidesmosomes with the ECM via integrin clusters. Integrins are transmembrane proteins that act as receptors for the ECM being able to form ligands with fibronectin, laminin and collagen (Tsuruta, Hopkinson, and Jones 2003b; Christopher S Chen, Tan, and Tien 2004; Gupta et al. 2016; Raghavan, Vaezi, and Fuchs 2003; Čabrijan and Lipozenčić; Rabinovitz and Mercurio 1997; Nikolopoulos et al. 2005). Recent studies demonstrated that the type of ligand with respects to collagen, fibronectin, laminin and PDMS substrates was inconsequential to proliferation and differentiation rates and so it would appear that integrin ECM interactions are promiscuous (Gupta et al. 2016; Connelly et al. 2010; J. G. Wang et al. 2005; Greiner et al. 2013). This is significant as it suggests that it is not the ligand composition that impacts upon proliferation and differentiation but instead the number of integrin-ECM interactions the cell is able to make based on availability of the ligand or the ability of the cell to interact with those ligands determined by substrate stiffness.

In support of this hypothesis an earlier study demonstrated how increased integrin clustering resulted from increased contact with the substrate, naming substrate stiffness as the key mediator of integrin clustering and therefore matrix derived signalling cues (Gallant, Michael, and García 2005). However, alternate studies counter that the density of substrate is not the deciding factor and instead posit that it is substrate availability that is key (Connelly et al. 2010). However, this study has one major oversight when making this claim which is not to address how variations in substrate stiffness (a product of the substrates density) could impact upon proliferation rates through altering the number of contacts the cell can make with its substrate per unit area. Secondly it is not clear whether an upper or lower boundary

for sensitivity to ligands was explored. If the lowest boundary for ligands per unit area were already above the saturation point for that matrix stiffness altering the number of ligands would be inconsequential. Combining these findings and considering the differing contexts, the former carried out on PDMS substrates and the latter on micropatterned islands with a protein resistant background, this may suggest there is a spacial limit to the number of focal adhesions able to form per unit area and so an important factor in increasing this would be the proportion of membrane that is able to contact the membrane with increased contact leading to increased proliferation. The factors affecting this could therefore be collectively described as density in the context of biological substrates such as collagen, where increasing the number of fibres per unit area would both increase the number of ligands and the matrix stiffness for a defined fibril diameter.

Collagen hydrogels offered a solution to this. As demonstrated in chapter 4 they can be manipulated to change ligands per unit area and stiffness by way of altering the level of collagen bundling. To understand how the physical properties of collagen impact upon this consider the behaviour when under tension generated by the overlying cells. It is conceivable that a less stiff matrix would form increased contacts with a cell membrane as the tension generated by the cells cytoskeleton would cause the flexible matrix to curl up around the edges of a cell more, when compared with a stiff, inflexible substrate enabling for increased integrin-ECM interactions (figure 5.1). This could in turn produce increased focal adhesion formation which accounts for elevated levels of FAK activity as one integrin binds to the collagen substrate, promoting integrin clustering at that site (L. Levy et al. 2000; Q Chen et al. 1996; Paszek et al. 2009).

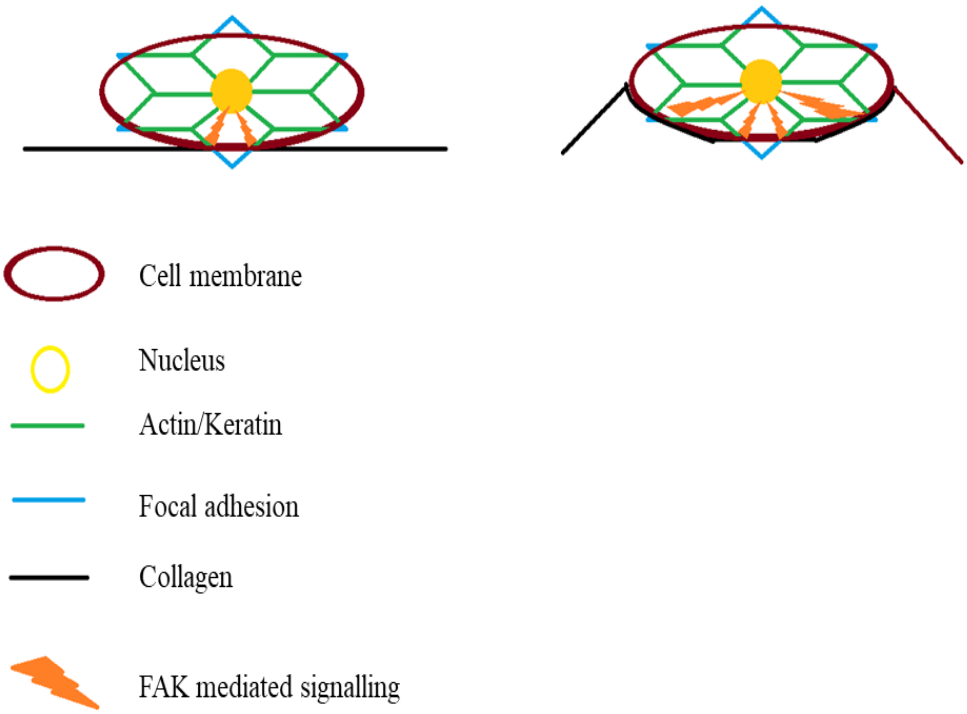

Figure 5.1: A depiction of how substrate stiffness affects integrin-mediated signalling. Matrix stiffness may also impact upon substrate availability. An increased stiffness would produce a reduced substrate area whilst a flexible substrate (right) would produce an increase in substrate availability. The tension generated by the cell cytoskeleton may draw the substrate in the direction of the nucleus which in turn produces increased FA formation resulting in increased FAK activation.

This mechanobiology could potentially be explained by the MAPKs ERK1/2, JNK and p38. Although $p130^{cas}$ phosphorylation of β-catenin has been posited as a potential route to stimulate proliferation via activation of the LEF/TCF transcription factor this was recently shown to be redundant by JNK signalling (Soucy and Romer 2009; Guasch et al. 2007; Oshimori and Fuchs 2012; Huelsken et al. 2002; Park et al. 2005; Gazel et al. 2008; Ke et al. 2010; Sun et al. 2015; Gazel et al. 2006; D D Schlaepfer and Hunter 1997). Keratinocytes have been shown to exhibit increased

rates of proliferation when cultured on stiffer PDMS substrates with the proliferation advantage being mitigated in the presence of ERK1/2 inhibitors but not in the presence of Wnt inhibitors (Yano et al. 2004; Posthaus et al. 2002). If Wnt signalling is blocked then β-catenin is phosphorylated by the CK1γ-Axin-GSK-3-APC complex, targeting it for ubiquitination, preventing its translocation to the nucleus and subsequent activation of the LEF/TCF transcription factors. In the absence of β-catenin, the transcriptional co-repressors, CTBP, HDAC and Gro bind and block the TCF/LEF transcription factor (Yano et al. 2004; Mehic et al. 2005; Zenz et al. 2005a; Behrens et al. 1996). This would suggest proliferation cues to be derived independently of the canonical Wnt signalling pathway. However, many studies have reported on elevated β-catenin and LEF/TCF activity to coincide with increased proliferation rates which suggest Wnt signalling to be redundant to integrin-mediated signalling via ERK for keratinocytes (Tscharntke et al. 2007; Zenz et al. 2005b; Clark and Hynes 1996; Gazel et al. 2008; Posthaus et al. 2002).

ERK signalling may well be an important pathway in mediating transduction of matrix stiffness and was therefore a good target for this study to address its significance in transducing differences in collagen density/stiffness to elicit a proliferation advantage. If ERK1/2 proves to be a key transducer it would suggest that substrate composition with respects to fibronectin, laminin and collagen is inconsequential to cellular behaviour and that it is the physical properties of the substrates that affect change in proliferation rates since earlier studies using PDMS substrates of varying stiffness have already shown this to be the case (Gupta et al. 2016).

Both ERK1/2 and JNK are activated by focal adhesion kinase (FAK) via the Ras-Raf-MEK pathway (S. A. Ibrahim, Hassan, and Götte 2014; Ishida et al. 1996; Clark and Hynes 1996; D D Schlaepfer and Hunter 1997; Nikolopoulos et al. 2005; Mainiero et al. 1997; Gazel et al. 2008). The literature has also shown increased ECM stiffness has produced elevated JNK signalling in conjunction with increased proliferation rates in carcinomas but reports little on keratinocytes (Schrader et al. 2011; Gallant, Michael, and García 2005; Paszek et al. 2009). Much of the literature surrounding keratinocytes elucidates only that elevated proliferation occurs in conjunction with elevated JNK (Nikolopoulos et al. 2005; Gazel et al. 2008; Sun et al. 2015; Dupont 2016; Xu et al. 2014). JNK has been shown to target the G0/G1 checkpoint proteins

p53, for ubiquitination enabling cell cycle progression. In this way JNK can signalling can be seen as instrumental in propagating proliferation but by no means is the only player (Sun et al. 2015; S. Y. Fuchs et al. 1998; Serge Y. Fuchs et al. 1998; Shi et al. 2014). JNK binds to and phosphorylates c-Jun which activates the AP1 transcription factor (T Kallunki et al. 1994; Minden, Lin, Smeal, et al. 1994). This is significant since the AP1 transcription factor is known to act upon genes important for inflammation, apoptosis, proliferation and differentiation (Mehic et al. 2005; Zenz et al. 2005a; Balasubramanian, Efimova, and Eckert 2002; Connelly et al. 2011). Further to this c-Jun activation is essential for the G1/S transition making JNK a key component in propagating cell cycle progression (Jiao et al. 2008; Sabapathy et al. 2004; Medhurst et al. 2008). Studies in keratinocytes have also shown how inhibition of JNK has led to terminal differentiation as indicated by elevated involucrin promotor activity (Gazel et al. 2006; Bennett et al. 2001; Ke et al. 2010; Efimova et al. 1998; Balasubramanian, Efimova, and Eckert 2002). The decision was hterfore taken to combine variations in collagen matrix density with JNK inhibition to discern whether JNK signalling is independent of collagen density/stiffness and to what extent JNK signalling is important in communicating matrix derived proliferation cues.

p38δ is a key regulator of hINV gene expression. Phosphorylation of p38 produced increased binding of the AP1 transcription complex to the AP1 binding site of the hINV promotor, secession of proliferation and increased formation of the cornified envelope in keratinocytes (Balasubramanian, Efimova, and Eckert 2002). However, the same study that demonstrates p38 as a regulator of hINV expression also demonstrated elevated c-Jun activity, the component of the AP1 complex that is the downstream effector or ERK1/2 and JNK signalling (J. S. Gutkind 2000; X.-J. Wu et al. 2014; E. K. Kim and Choi 2010). This could suggest an interplay between the three MAPKs with p38 opposing the effects of ERK and JNK. As all three MAPKs act upon the AP1 complex it should be noted that the MAPKs activate different composite components of the homo-/heterodimer which impacts upon its target. In this way the AP1 transcription factor can fulfil opposing roles; facilitating both proliferation differentiation.

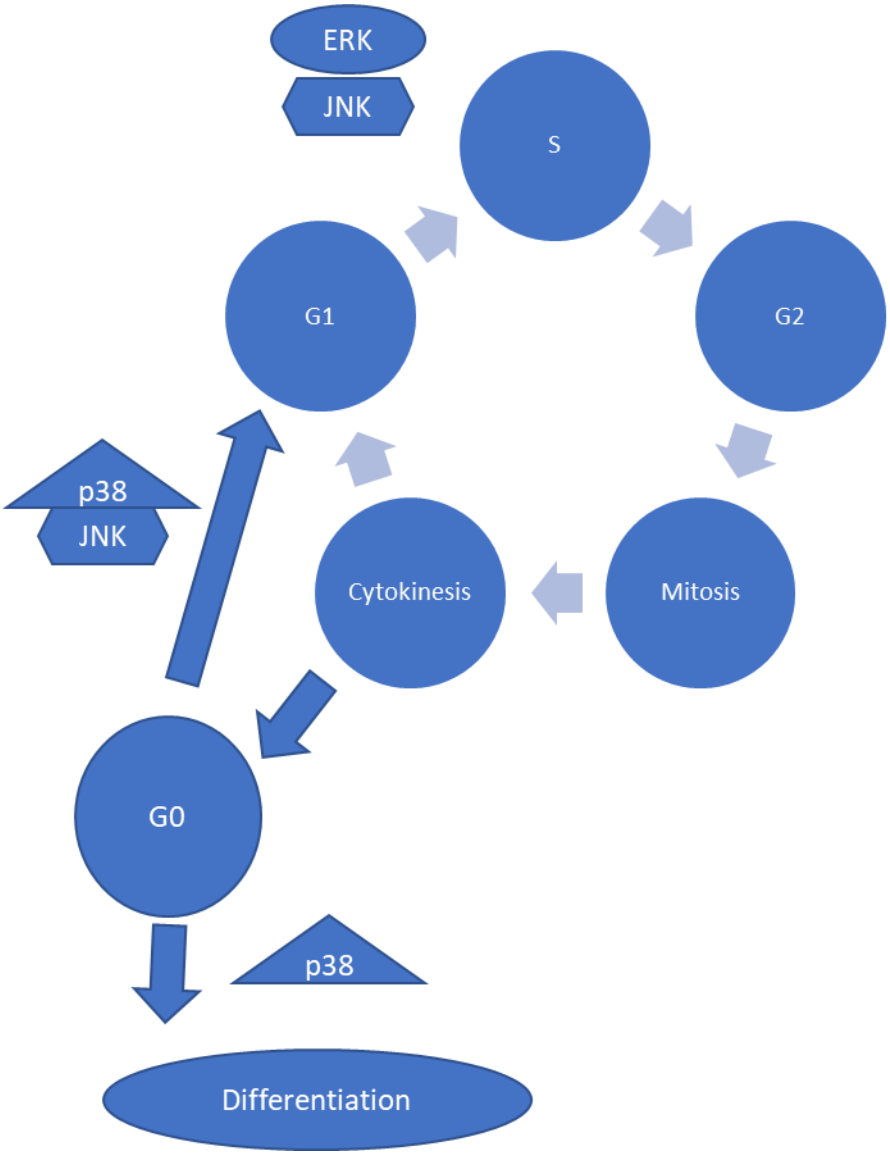

Figure 5.2: MAPKs roles in governing proliferation and differentiation of keratinocytes. ERK is essential for the G1/S transition and suppression of antiproliferative genes whilst p38 exhibits a duality being involved in both exit from quiescence (when bound to JNK) and propagation of AP-1 binding the hINV promotor, driving differentiation. JNK is essential the G0/G1 transition and has been suggested as a counterbalance to p38. Further this JNK has also been noted to facilitate the G1/S transition in keratinocytes.

Evidence from scratch assays conducted on keratinocytes has also been used to demonstrate how ERK signalling is critical to wound closure whilst p38 inhibition only leads to delayed wound closure (Balasubramanian and Eckert 2007; X.-J. Wu et al. 2014; Vollmar et al. 2002). This suggests ERK1/2 signalling to be the dominant

pathway by which cellular proliferation is instigated and may suggest the p38 signalling is important in promoting cell migration which is supported by several other studies (E. K. Kim and Choi 2010; X.-J. Wu et al. 2014; J. G. Wang et al. 2005; Mishima, Inoue, and Hayashi 2002; Sharma, He, and Bazan 2003). p38 inhibition has also been shown to prevent keratinocyte outgrowth from skin organ cultures (Stoll, Kansra, and Elder 2003). In psoriatic skin both p38 and ERK1/2 are elevated. This is perhaps a good scenario to support the opposing roles leading to thick calluses; ERKs promoting proliferation and p38 driving differentiation (figure 5.2). There is this issue of context that greatly impacts upon the function of MAPKs which imposes the importance of investigating the function of MAPKs in communicating matrix derived proliferation and differentiation cues.

A later study demonstrates the importance of JNK in retaining the proliferative potential of keratinocytes. Inhibition caused terminal differentiation evident from increased involucrin gene expression (microarray analysis) with a concomitant increase of involucrin as indicated by western blot analysis (Balasubramanian, Efimova, and Eckert 2002; Gazel et al. 2006). This may suggest that active JNK is able to negatively regulate p38 which was suggested in a later study where dimerization of JNK and p38 was evident in the presence of active JNK. This could prevent the phosphorylation of AP1 components that would target the AP1 transcription factor to the hINV instead targeting the transcription factor to genes linked with proliferation.

Involucrin is an ideal marker to use in assessment of whether or not a cell is undergoing terminal differentiation as its production is also accompanied by an exit from cell cycle progression and production of the cornified envelope as demonstrated across several studies (Balasubramanian and Eckert 2007; Watt 1983; Azuara-Liceaga et al. 2004; Eckert et al. 2004). Further to this it will inform on whether the hINV gene expression is modulated via MAPKs in the context of collagen matrices. This could potentially point to new roles for ERK, p38 and JNK in determining AP1 specificity for cell cycle promoting genes vs cell cycle exit genes.

This chapter aimed to address how collagen density and therefore stiffness impacted upon proliferation rates and differentiation rates within keratinocyte derived cells. This would then be applied to understand how differential collagen environments

identified along the hair follicle may aid in the functionality of cells within the locale, and whether MAPKs are instrumental in transducing matrix derived cues. Initially defined matrices were used to identify the relationship between collagen density/stiffness and proliferation and differentiation rates. Further to this nuclear morphology was also characterised in each scenario to see if any correlations between nuclear morphology, matrix stiffness and proliferation/differentiation rates were present. Following this the three MAPK families, ERK, JNK and p38 were inhibited individually to inform on the extent to which each is involved in propagating matrix derived cues and whether they may also influence nuclear dynamics. Combined these experiments aimed to address how static forces that exist within the epidermis and follicle drive either proliferation or differentiation.

5.2 Investigating the Role of MAPKs in Communicating Collagen Derived Proliferation and Differentiation Cues

Initially it was necessary to first establish the relationship between matrix stiffness and proliferation and differentiation rates. Once this had been established the different MAPKs were inhibited to assess their roles in communicating these cues.

5.2.1 Reduced Ki67 Expression in HaCaTs on Low-Density Matrices Implicates Collage Density as a Mediator of Proliferative Cues

To understand how cells interact on an individual basis with the different collagen substrates cells were initially cultured at low seeding volumes (1000 cells cm^{-1}). Distances between cells were anticipated to reduce the paracrine influence of surrounding cells ensuring conclusions drawn to be from cell-substrate interaction rather than cell-cell interactions.

Images in figure 5.3 demonstrate increased Ki67 expression for cells on the HD matrices compared with cells on LD matrices. This increase in Ki67 expression was accompanied by changes in cell morphology with nuclei appearing larger and elongated compared with cells on the LD matrices after a 24h period. The actin-cytoskeleton appeared to be exhibiting polarity i.e. a spread along a specific vector, on the HD matrices after 24h and return to a more globular appearance after a 120h incubation. The converse appeared to be the case for the LD matrices which appear spherical after a 24h period and exhibit a more spread morphology after120h.

The interplay between cell-cell interactions and cell-substrate interactions to produce changes in cell behaviour, was evaluated. Cells were seeded onto their respective substrates and cultured for 120h allowing for colonies to form. Initial observations showed little difference in Ki67 expression generated by cells on the different substrates (figure 5.3). However, colonies produced on collagen appeared to be smaller compared with those cultured on LD matrices. This could indicated that a reduction in substrate density affected cell cycle progression.

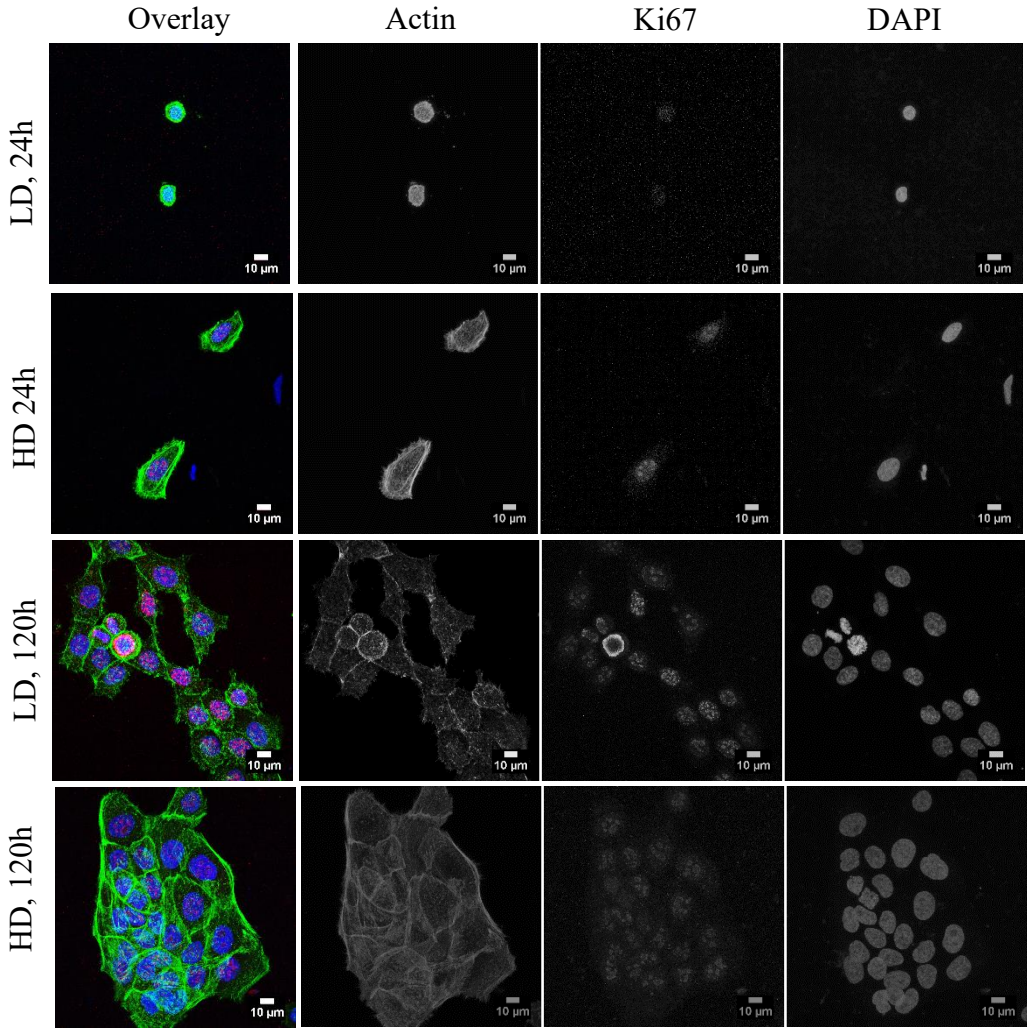

Figure 5.3: HaCaTs 24h and 120h after seeding onto LD or HD hydrogels. F-actin (green), Ki67 (red) and nuclei (blue). HD-Cells seeded on high-density collagen; LD-Cells seeded on low-density collagen. Scale bars represent 10 µm.

LD collagen hydrogels exhibited a significantly lower expression of Ki67 compared with the HD matrices after both a 24h and a 120h incubation indicative of either a proliferation advantage conferred by higher density collagen matrix. (figure 5.4).

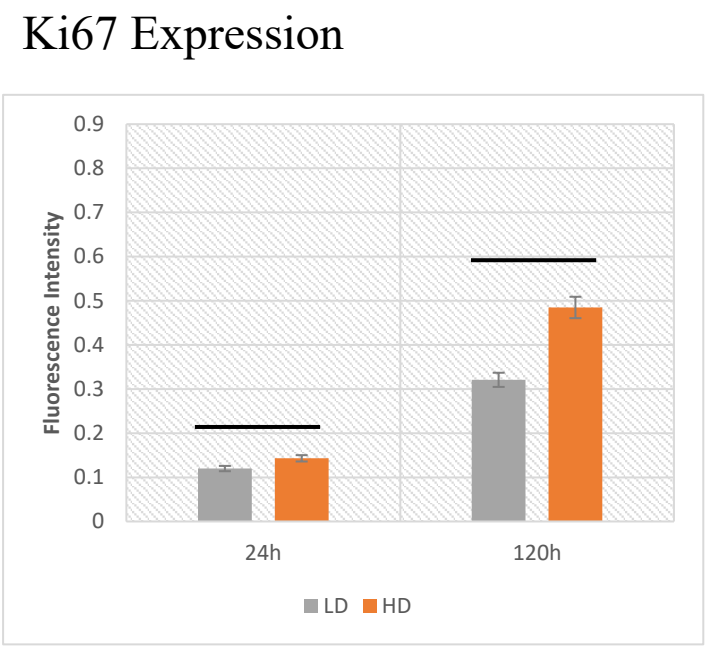

Figure 5.4: Average Ki67 expression in HaCaTs after 24h on HD and LD matrices. This was taken as a proportion of the total number of nuclei analysed for 24h (n=3, >25 nuclei/n) and 120h (n=3, >100 nuclei/n) after seeding onto the respective substrates. Error bars represent the standard error of mean. Horizontal bars represent $P<0.05$ between groups as determined by the students t-test.

5.2.2 Collagen Reduced Terminal Differentiation Independently of Collagen Density

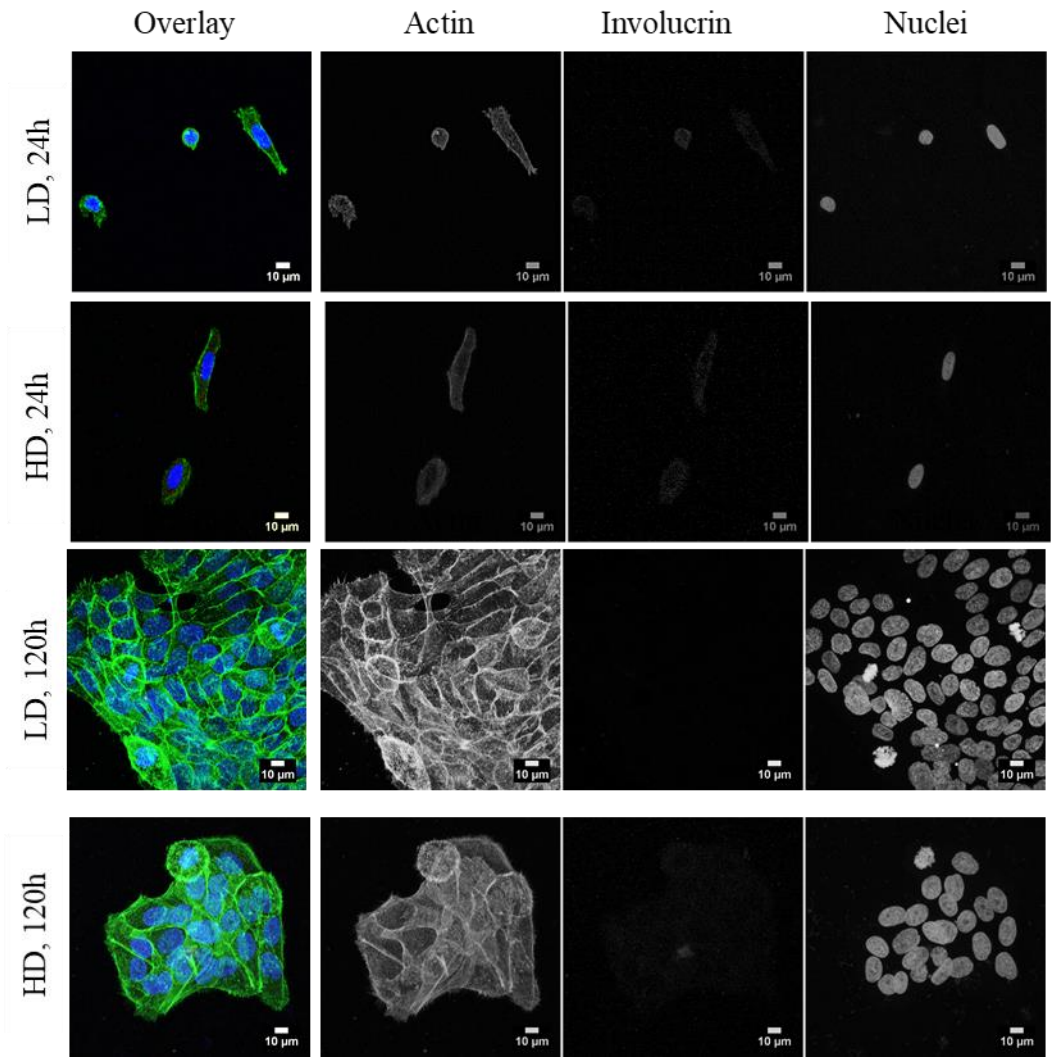

Figure 5.5: HaCaTs 24h and 120h after seeding onto LD or HD hydrogels. F-actin (green), Ki67 (red) and nuclei (blue). HD-Cells seeded on high-density collagen; LD-Cells seeded on low-density collagen. Scale bars represent 10 µm.

HaCaT cells were almost entirely devoid of involucrin expression after 120h incubation on either HD or LD matrices suggesting collagen may have been driving the observed proliferation advantage. As the availability of collagen fibres was restricted through reducing the number of fibres per unit area, cells expressed significantly lower levels of involucrin (i.e. more than 2-fold less compared with the 24h time point). There was no significant difference between levels of involucrin for cells culture on the two different densities of collagen suggesting that terminal differentiation rates are reduced by collagen substrates in a density independent manner (5.6). Involucrin levels were also evaluated after a 24h incubation to indicate if the lower levels of Ki67 expression observed on the LD matrices is attributed to cells cycle arrest or cells being driven toward terminal differentiation. Figure 5.6 shows a clear increase in involucrin expression with restriction of access to substrate; LD to HD. Visual inspection of the images suggested unconvincing expression of involucrin in cells on either density of matrices. However, analysis of fluorescence intensities would suggest the collagen to have an impact on involucrin expression though not statistically significant.

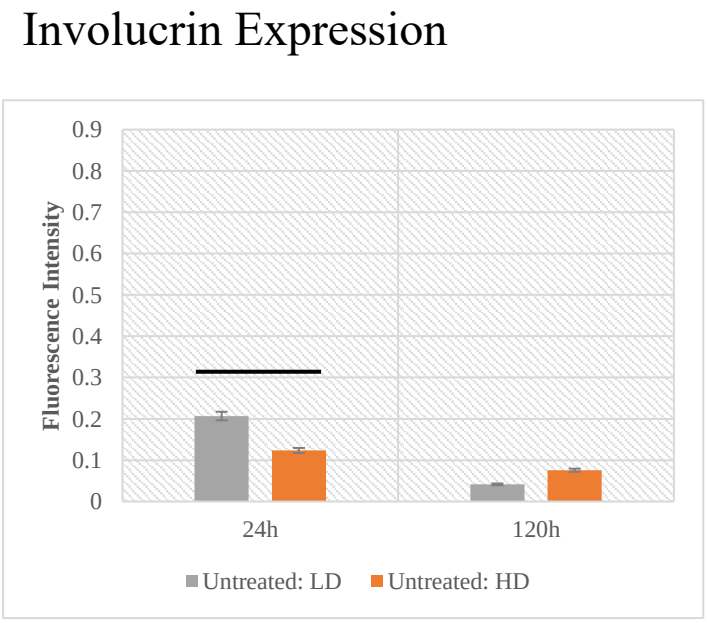

Figure 5.6: Average involucrin expression in HaCaTs 24h and 120h on LD and HD matrices. This was taken as a proportion of the total number of nuclei analysed 24h (n=3, >25 nuclei/n) and 120h (n=3, >100 nuclei/n) after seeding onto the respective substrates. Error bars represent the standard error of mean. Horizontal bars represent $P<0.05$ between groups as determined by the students t-test.

5.2.3 Inhibition of Either p38, ERK or JNK Reduced Ki67 Expression

HaCaTs exhibited a density-dependent response by way of increased density of collagen leading to elevated proliferation rates compared with its lower density counterpart. The MAPKs presented interesting targets to address, as many studies have already identified ERK and JNK signalling as being important in communicating ECM derived proliferation cues in relation to substrate stiffness (Dupont 2016; Chaudhuri et al. 2014; Schrader et al. 2011; Gupta et al. 2016). P38 although not addressed as potential transducer of ECM density/stiffness, is important in enabling cell cycle progression via its interplay with JNK and its role in cells exiting quiescence (Rodríguez-Berriguete et al. 2016; S. Liu et al. 2017). Therefore, to address the potential involvement of communicating the putative low-stiffness (HD matrices) and putative high-stifness (LD matrices) p38, ERK or JNK were inhibited for either a 24h period or a 120h period. The two timepoints also address in part the extent to which the cell-ECM and cell-cell-ECM interactions are dependent on these pathways to govern proliferation and differentiation rates.

***HaCaT cells were cultured for either a 24h period or 120h period on collagen hydrogels during which time they were exposed to one of the three MAPK inhibitors (p38i; SB203580, ERKi; PD98059 or JNKi; SB600125).

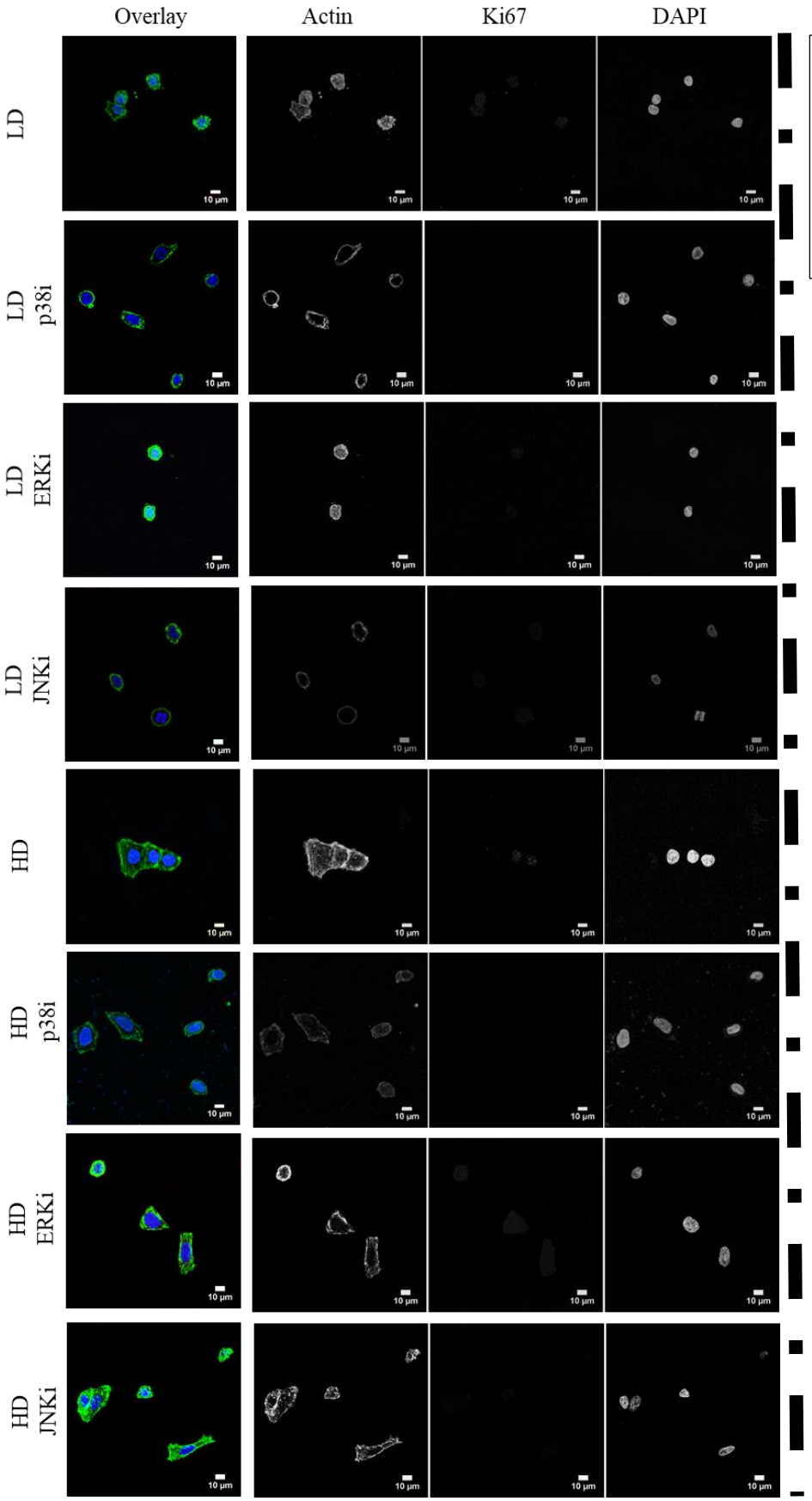

Panel A: HaCaT cells 24h after seeding on collagen.

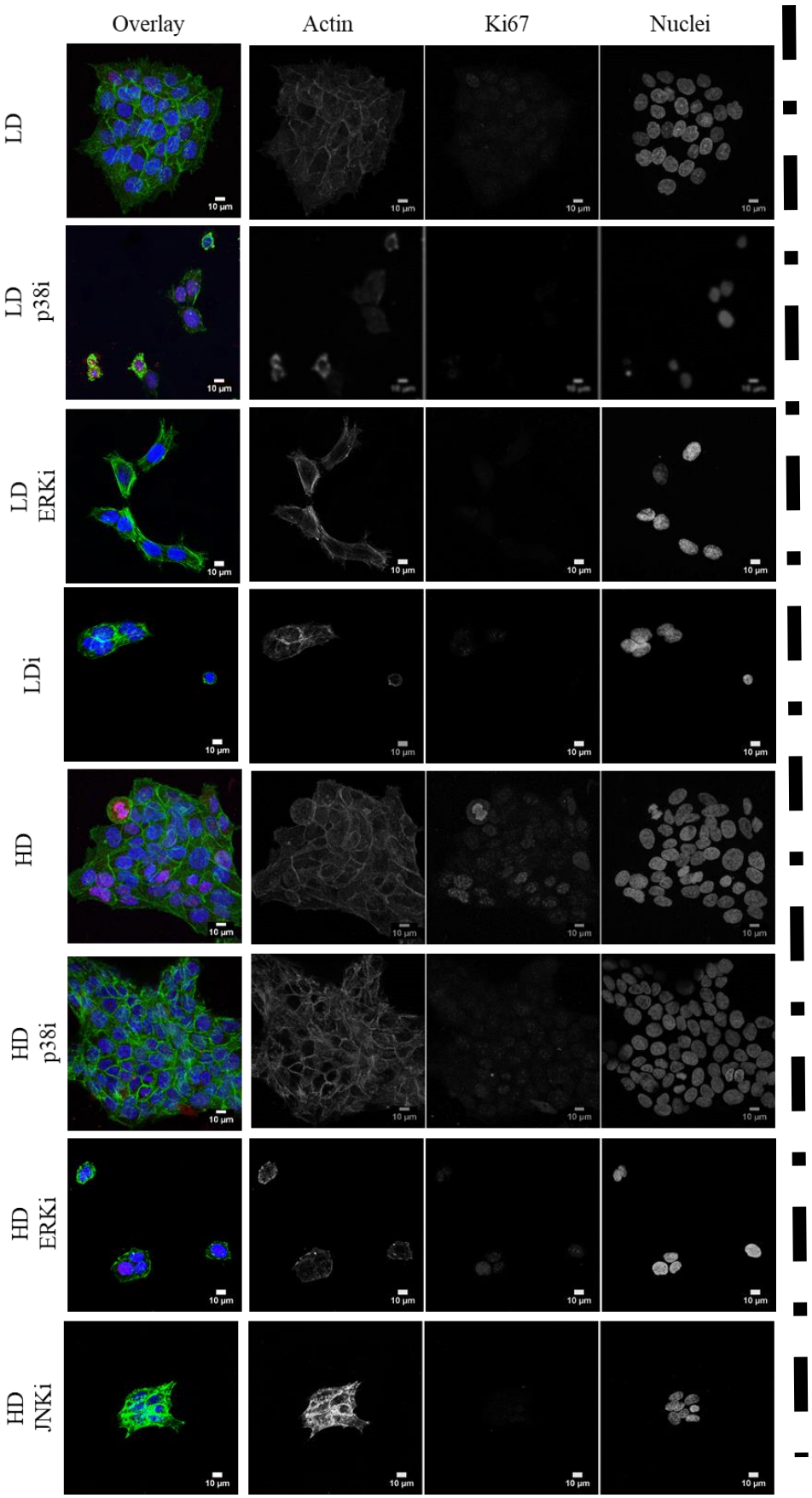

Panel B: HaCaT cells 120h after seeding on collagen.

Figure 5.7:

Confocal images of HaCaTs labelled for Ki67, cultured for 24h or 120h on collagen hydrogels pre- and post-treatment (Panels A-B).

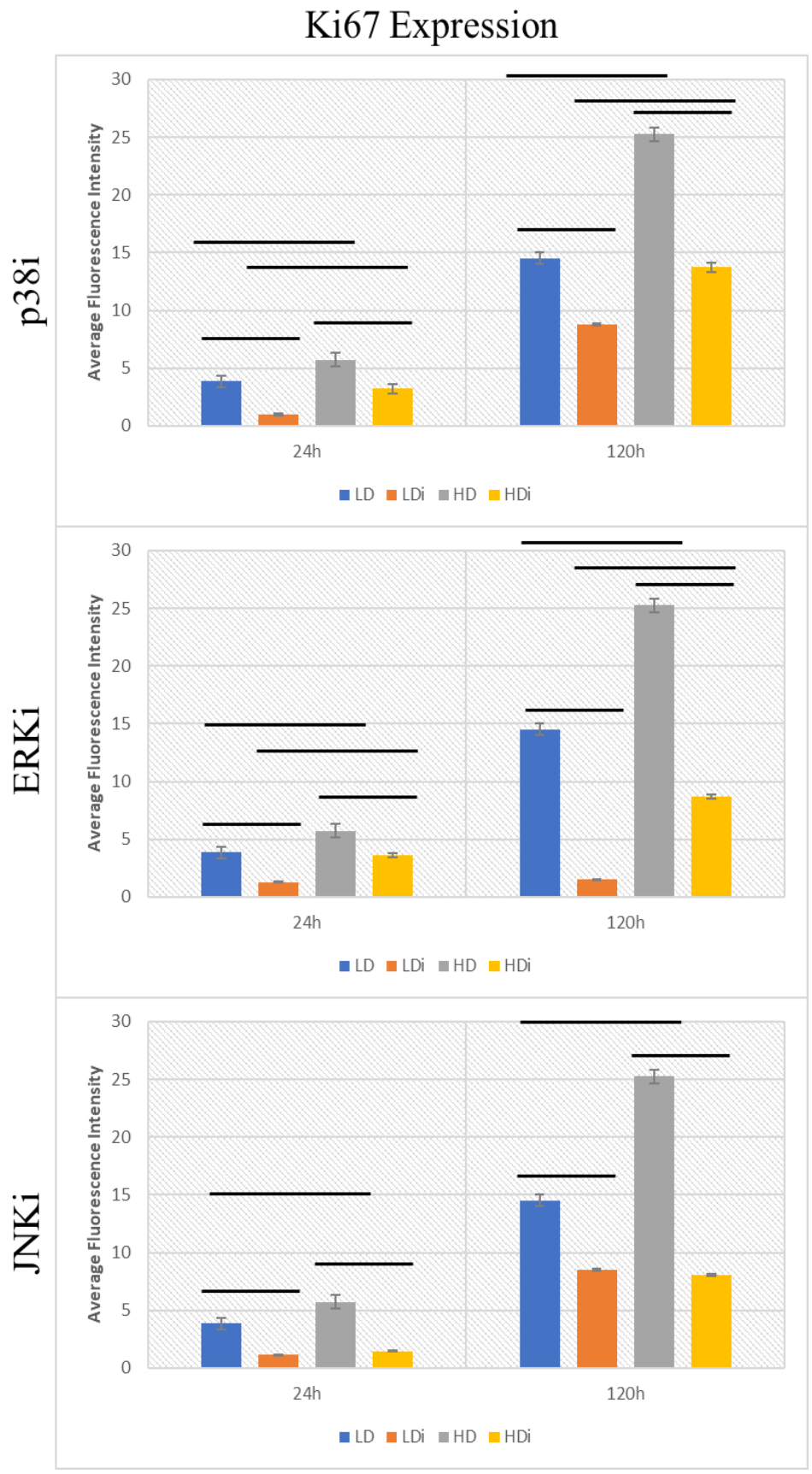

Figure 5.8:

Ki67 Expression in HaCaT cells after either a 24h or 120h treatment. Horizontal bars represent $p<0.0005$ between groups as determined by the students t-test (n=3 with >25 nuclei/n at 24h and >100 nuclei/n at

Visual inspection of images was relatively unhelpful other than to establish whether the labelling process was a success (figure 5.7). The true difficulty lied in analysing the mage in a manner that was unbiased. Despite following the same protocol, due to the great many steps, variations in antibody stock, variations in temperature during antibody incubations and pipetting error (although small) all contribute to variations in levels of background and so to separate the 'wheat from the chaff', a macro was developed that would distinguish 'true signal' from background based on a threshold set. This method of analysis effectively removed human subjectivity and restored all signals to a base line allowing comparisons to be drawn between repeats with true variation being represented as is evident from the small standard error of means derived for each variable and very low P values (<0.005) where differences exist.

Figure 5.8 clearly demonstrates a reduction Ki67 expression after both the 24h and 120h incubation in response to inhibition of p38, ERK and JNK with all exhibiting a significant difference to their untreated counterparts suggesting all three impact upon cell cycle progression. ERK inhibition produced the strongest reduction in Ki67 demonstrating its importance in cell cycle propagation. However, neither p38 inhibition nor ERK inhibition nullified the significant difference between the HD and LD matrices (i.e. p38i LD exhibited significant difference to p38i HD) after either the 24h or 120h incubation implying the density-dependent proliferation advantage is only partly transduced by these MAPKS. JNK has been demonstrated as being a key player in communicating matrix derived proliferation cues with no significant difference being observed between JNKi HD and JNKi LD after both a 24h and a 120h incubation. This abolition of the proliferation advantage produced by the HD/putative low-stiffness collagen matrix, and to a level significantly below the untreated counterparts, strongly placed JNK as a key transducer of collagen density/stiffness derived proliferative cues.

For all the effects described they were exhibited at both the 24h time point and the 120h time point suggesting MAPKs were central to cell-ECM interactions. The effect of p38 inhibition was lessened after a 120h incubation which suggested cell-cell adhesion attenuates the effects of p38 inhibition. A similar effect is also observed for JNK, however the effect of ERK inhibition if amplified which suggested a potential synergy between ERK inhibition and cell-cell adhesion.

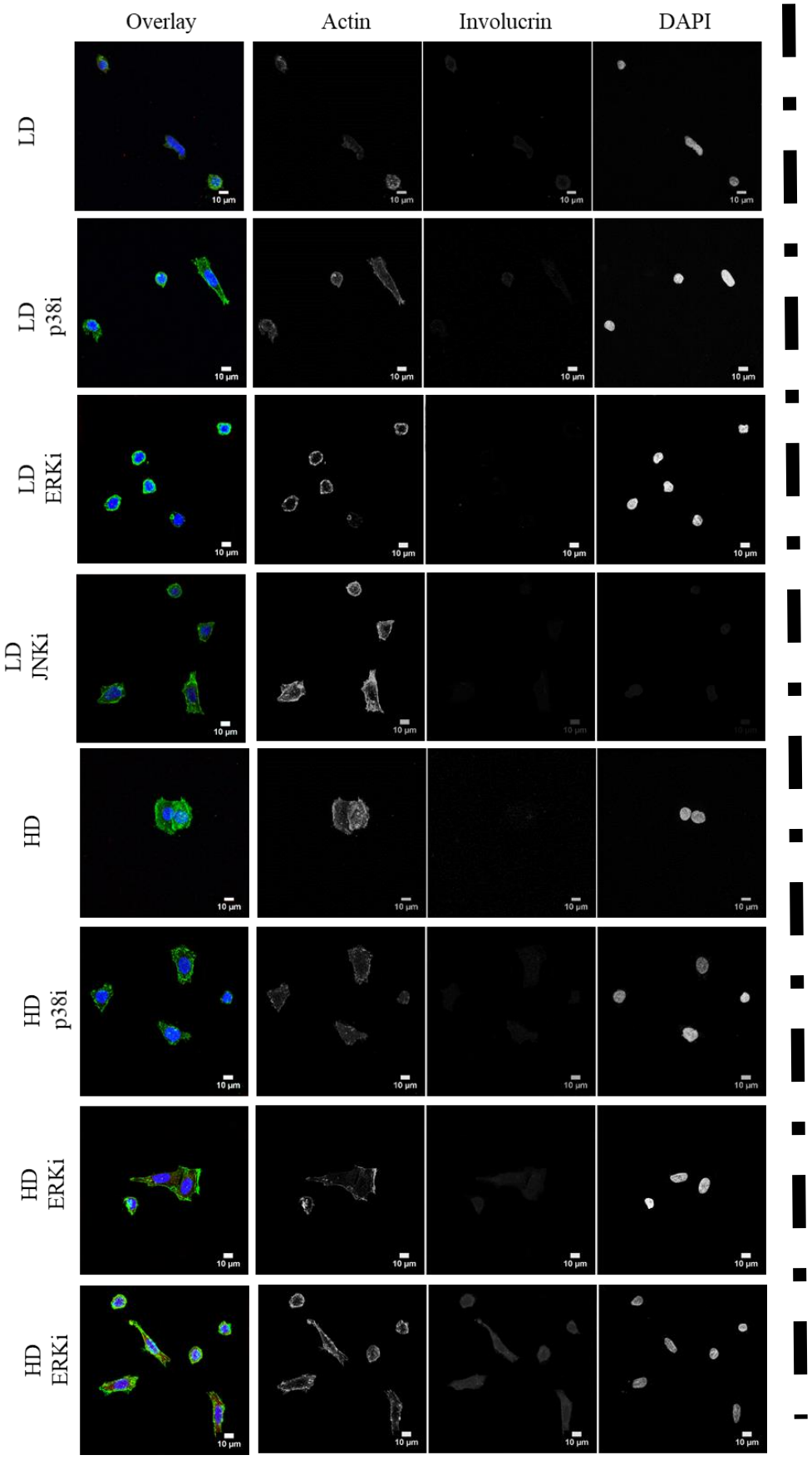

Panel A: HaCaT cells 24h after seeding on collagen.

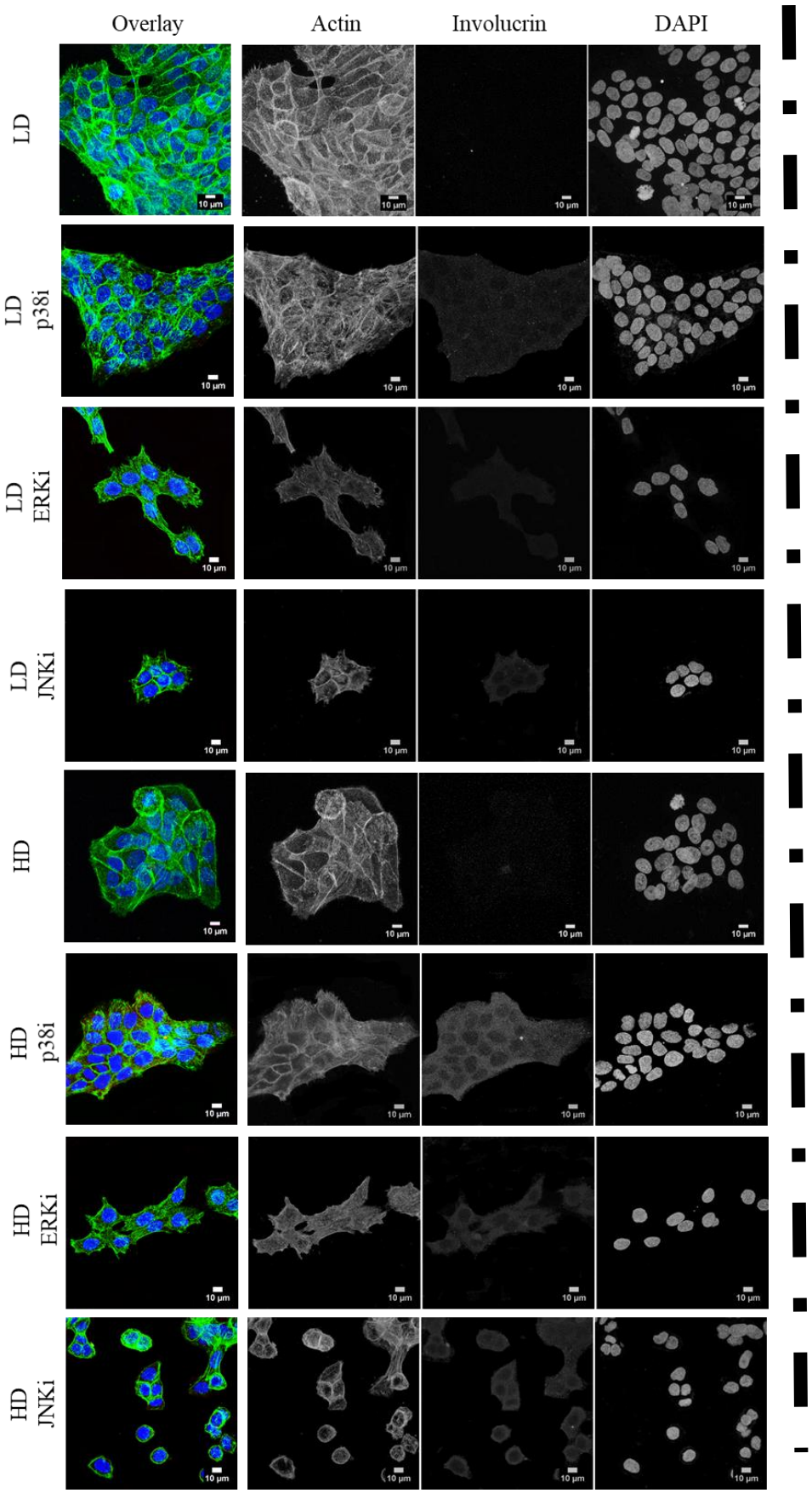

Panel B: HaCaT cells 120h after seeding on collagen.

Figure 5.9:

Confocal images of HaCaTs, labelled for involucrin, cultured for 24h or 120h on collagen hydrogels pre- and post-treatment (Panels A-B).

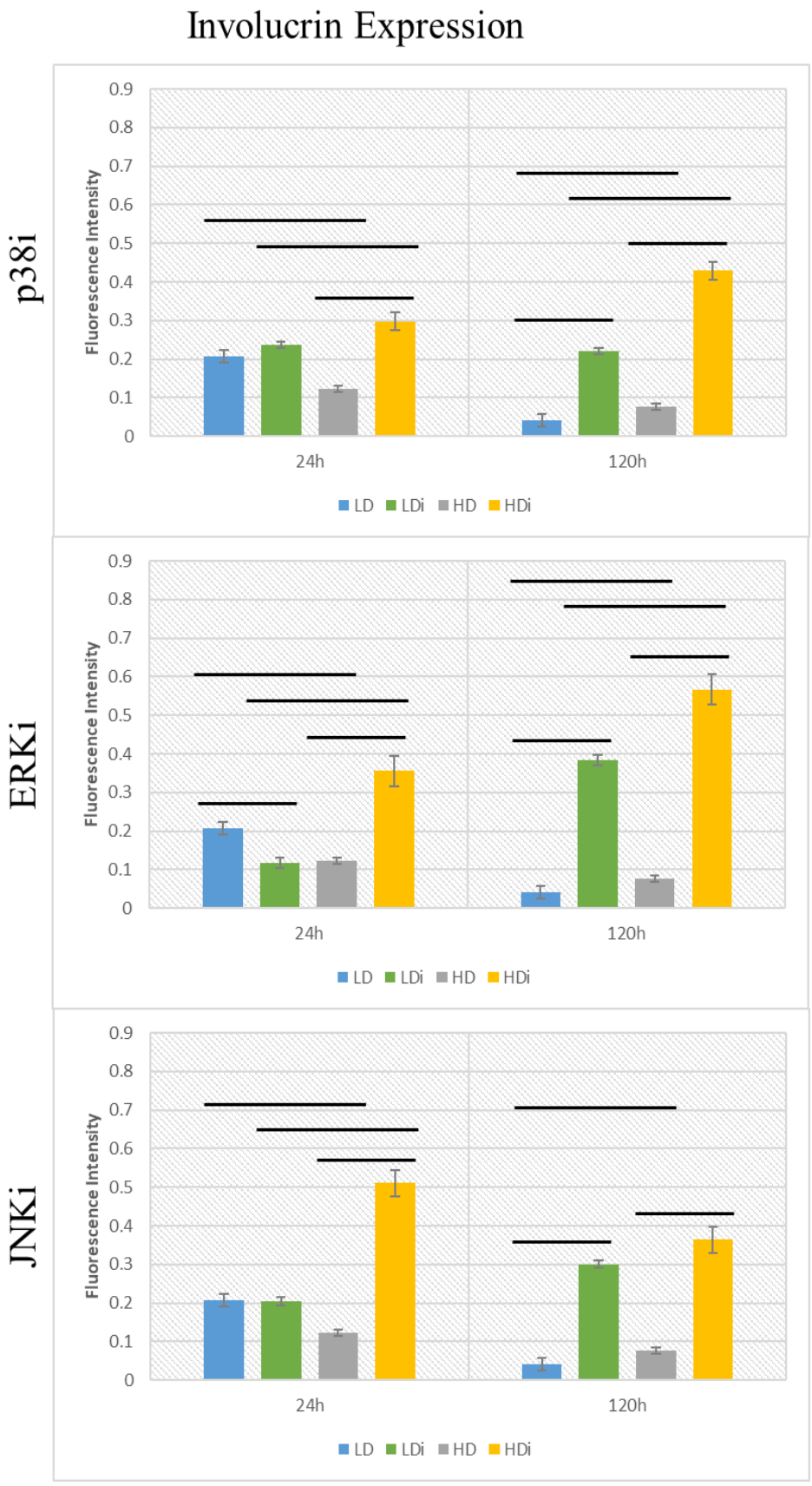

Figure 5.10:

Ki67 Expression in HaCaT cells after either a 24h or 120h treatment. Horizontal bars represent $p<0.0005$ between groups as determined by the students t-test (n=3 with >25 nuclei/n at 24h and >100 nuclei/n at

After a 24h incubation period involucrin significantly increased on the HD matrices for all treatments suggesting a role for all MAPKs in propagating the proliferation advantage conferred by HD matrices (figure 5.10). This was also echoed at the 120h time point for all treatments indicating an importance in mediating the cell-ECM interaction for HD matrices. However, the LD matrices showed varying patterns. p38 exhibited a slight non-significant increase which suggests p38 to be important in mediating the density-dependent proliferation advantage via cell-ECM interactions but still retains a significant difference with p38i HD supporting earlier finding that also suggested this pathway to be acting in parallel with other pathways to achieve the matrix derived proliferation advantage. The reduction of involucrin with ERKi inhibition suggested cells have exited cell cycling and entered a state of quiescence. The retention of the significant difference between the HD and LD matrices post inhibition again suggest this was not the only pathway important in retaining the proliferation advantage over a programme of terminal differentiation. JNK inhibition exhibits no significant changes on the LD matrices suggesting the cells had entered a state of quiescence when considered in conjunction with the significantly reduced ki67 expression.

After 120h a pattern emerged that was complimentary to the equivalents labelled for Ki67. All three treatments produced a significant increase in HaCaTs on both the HD and LD matrices demonstrating the importance of MAPKs in propagating cell cycling in HaCaTs over terminal differentiation in the context of collagen. Of particular note is the nullification of the significant difference between the HD and LD matrices when JNK is inhibited. Again this supports the premise of JNK being central to communicating matrix derived proliferation cues.

A critical observation was that unlike for the Ki67 labelled cells where the same effect was observed at both the 24h and 120h for both HD and LD matrices this was only the case for the HD matrices. This suggests that the density-dependent proliferation advantage is mediated by all three MAPKs and that the differentiation potential is reduced by the cell-ECM interaction and furthermore by the cell-cell interactions. The reduction of involucrin expression in untreated cells after a 120h incubation and increase in treated cells suggest that the cell-cell interactions reduced the differentiation potential causing quiescence, and that this is mediated by all three MAPKs.

5.2.4 High-Density Matrices Produce an Increase in Nuclear Size and a Reduction in Nuclear Circularity

The characteristics of nuclei with respects to circularity and dimensions were quantified to address how changes in collagen substrate impact upon nuclear morphology and how these characteristics correlate with proliferation and differentiation rates. Alterations in nuclear morphology from circularity to size could indicate changes in nuclear stability/arrangement which in turn may have epigenetic impacts that affect rates of proliferation and differentiation. To summarise the finings so far it is clear that increased collagen density leads to increased rates of proliferation, whilst perturbing differentiation in a density dependent manner.

After 24h of incubation there was a significant decrease in circularity of nuclei in cells on the HD matrices compared with the nuclei of cells grown on the LD matrices (figure 5.11). In conjunction there was also a significant increase in the area occupied by nuclei in cells grown on HD matrices. This could indicate an increase in cytoplasmic volume as cells are preparing to divide.

After 120h on the respective substrates the same pattern as at 24h is observed with the highest density matrices exhibiting significantly larger nuclei compared with the LD matrices suggestive of increased cytoplasmic volume and cell spreading (figure 5.11). However, in contrast to the 24h time point the nuclei have increased significantly by three or more microns in both the x- and y-direction. When you consider that the average size of nuclei in HaCaT cells is 8um this increase is substantial. Combined with a reduction in circularity this data could implicate collagen as an extracellular cue that affects nuclear dynamics.

Cells cultured on HD matrices exhibited a significantly higher expression of Ki67 compared with those grown on the low-density matrices. Further to this, cells on HD matrices had significantly larger nuclei compared with those on the low-density matrices (figure 5.11). This further supports the idea of collagen as an extracellular cue that affect nuclear dynamics. When considered in conjunction with the increased levels of Ki67 expression a possible link emerges between cytoskeletal influence over nuclear morphology and the effect of collagen on proliferation.

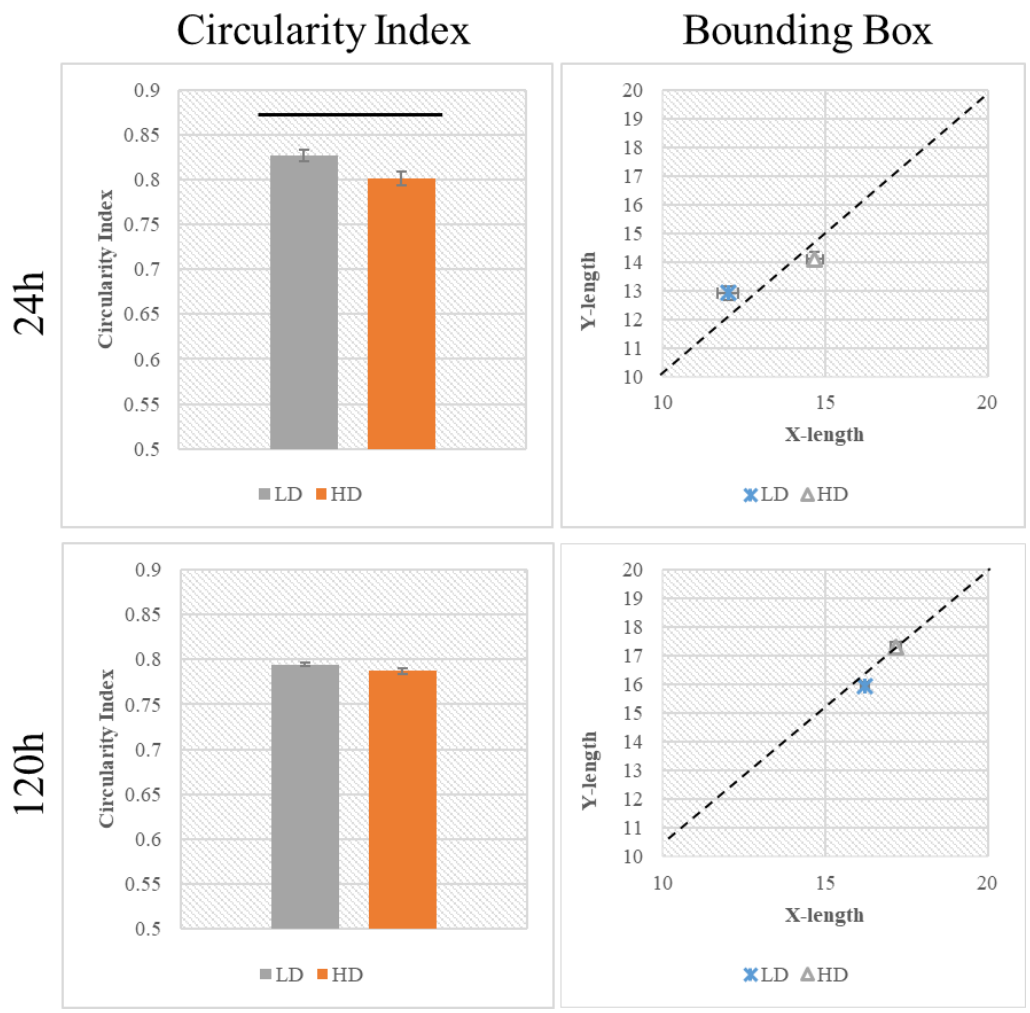

Figure 5.11: Nuclear morphology descriptors for cells cultured on HD and LD matrices. HaCaTs were on either HD or LD matrices and evaluated after either 24h or 120h. Horizontal bars represent a $p<0.005$ as determined by the students t-test.

5.2.5: MAPKs Inhibition Impacts Upon Nuclear Morphology

A link emerged between collagen density, changes in nuclear morphologies and changes in rates of proliferation and differentiation. It has been established that the HD matrices produced increased rates of proliferation and generate significantly larger cross-sectional areas compared with HaCaTs grown on LD matrices. To evaluate how MAPKs may transduce cues that directly or indirectly impact upon nuclear morphology each of the three groups were inhibited for both a 24h and a 120h period in HaCaT cells cultured on either the HD or LD matrices. This was to establish the cell-ECM and cell-cell contact govern nuclear morphology by MAPK signalling.

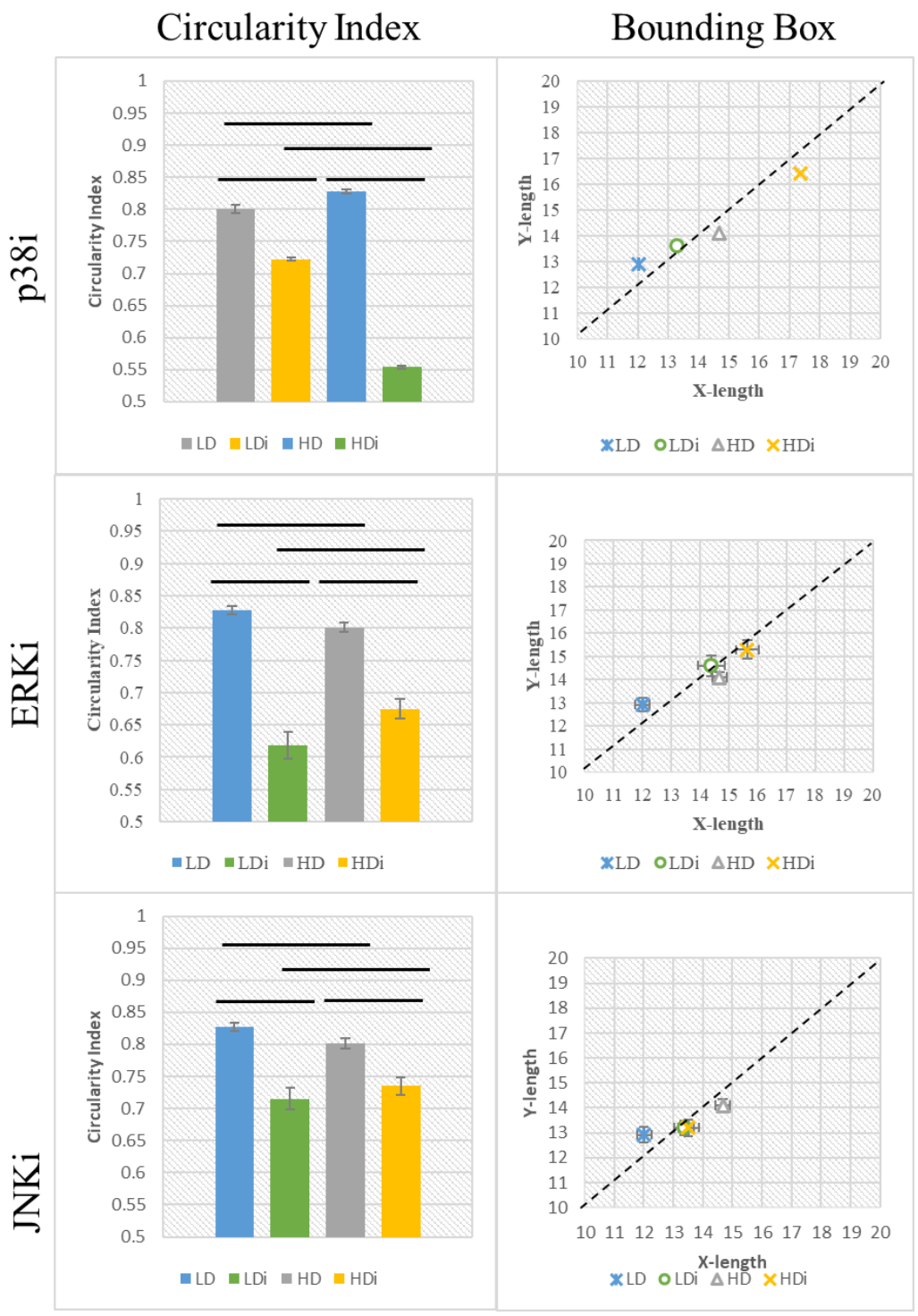

Figure 5.12: Nuclear morphology descriptors for cells cultured on HD and LD matrices after MAPK inhibition. HaCaTs were cultured on either HD or LD matrices and evaluated 24h after the addition p38, ERK or JNK inhibitors. Horizontal bars represent a $p<0.005$ as determined by the students t-test.

Figure 5.12 shows a pronounced reduction in circularity in addition to significant increases in cross-sectional volumes 24h after p38 inhibition for cells on both the HD and LD matrices. This could imply an increase in cell spreading and a reduction in cytosolic volume. The greater loss observed in cells inhibited on the HD matrices further supported the hypothesis that parallel pathways to p38 may be at play in mediating collagen sensing.

After a 24h incubation with ERKi cells cultured on both HD and LD matrices exhibited significant reductions in circularity (figure 5.12). The elongation of nuclei coincides with increased Ki67 expression in cells on both densities supporting earlier correlations noted between loss of circularity and increased rates of proliferation. The observed difference suggested the ERK attenuation to be working in synergy with a collagen density dependent mechanism not yet identified in this study. The loss of circularity is accompanied by an increase in cross-sectional area of nuclei and appears to coincide with increased Ki67 expression (figure 5.12). Interestingly the cells cultured on the LD matrices exhibit a larger increase in cross-sectional area compared the high-density matrices which also exhibits a larger increase in Ki67 expression. This suggested that increased nuclear volume is a characteristic of proliferating cells and that ERK signalling is an enabling factor in propagating cell cycling over terminal differentiation in a collagen density-dependent manner.

After a 24h incubation in the presence of JNKi there was significant reduction in nuclear circularity for HaCaTs grown on both the HD and LD matrices (figure 5.12). This reduction in circularity would suggested JNK signalling to be a factor in modulating nuclear dynamics or in connecting nuclear dynamics with proliferation and differentiation. The significant reduction in circularity coincides with a reduction in Ki67 expression and increased involucrin expression demonstrating a link between nuclear morphology and cell behaviour i.e. cells entering terminal differentiation appear to experience reduced nuclear cross-sectional area and decreased nuclear circularity whilst cycling cells appear to exhibit an increase in nuclear cross-sectional area and increased nuclear circularity. Interestingly the JNKi produced a reduction in nuclear cross-sectional area on the HD matrices and an increase on the LD matrices with both LDi and HDi conditions generating nuclei with almost identical parameters. This suggested ERK to be key in modulating nuclear dynamics resulting from the density-dependent proliferation advantage.

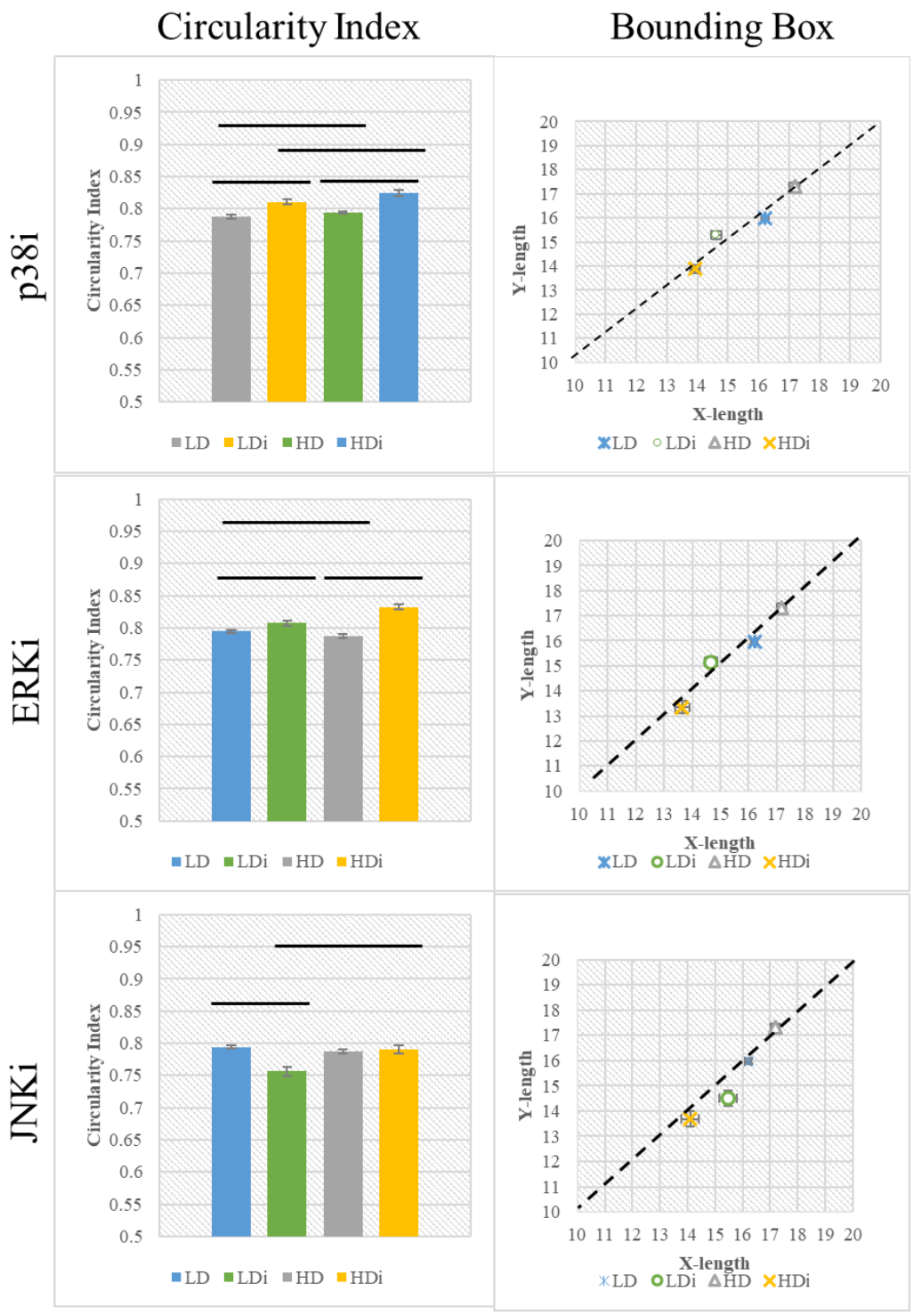

Figure 5.13: Nuclear morphology descriptors for cells cultured on HD and LD matrices after MAPK inhibition. HaCaTs were cultured on either HD or LD matrices and evaluated 120h after the addition p38, ERK or JNK inhibitors. Horizontal bars represent a $p<0.005$ as determined by the students t-test.

After a 120h incubation the same pattern of reduced nuclear circularity is retained however there is a significant reduction in nuclear cross-sectional area as a result of p38 inhibition contrasting with the increased in nuclear volume observed at 24h (figure 5.13). This contraction of the nuclei also occurred as levels of involucrin were increased which implied the contraction to be symptomatic of cells becoming more differentiated as indicated by the increased involucrin expression. There was a significant decrease in nuclear volume in HaCaTs on both HD and LD matrices post treatment with the p38 inhibitor. There is a greater decrease observed in nuclei on the HD matrices (figure 5.13) and a significant difference between cells inhibited on the HD and LD matrices which implied the collagen density-dependent effect was mediated independently of p38 signalling. Notably this was also the case for increased involucrin expression in cells on the HD matrices. This indicated a link between reduced nuclear-cross sectional area and increased involucrin expression that is impacted upon by p38 signalling.

After 120h incubation with the ERKi inhibitor, HaCaT cells exhibited significant increases in circularity (figure 5.13) on both HD and LD matrices. These significant increases correlate with the increased involucrin expression also associated with the inhibition of ERK suggesting increased circularity is associated with cells entering a programme of terminal differentiation. The cross-sectional area of nuclei was reduced in HaCaTs on both HD and LD matrices post treatment compared with their nontreated counterparts. The nuclei of treated HaCaTs on HD matrices exhibit a much greater reduction in nuclear cross-sectional area compared with those treated on LD matrices suggesting ERK signalling to be a factor in linking collagen sensing to nuclear rearrangement. The reduction in cross-sectional area with increased again correlates with increased involucrin expression suggesting that nuclear volume is reduced as cells terminally differentiate.

After a 120h incubation with JNKi a similar correlation was evident with greatly reduced cross-sectional areas corresponding with significant increases of involucrin expression. The circularity however only shows a significant decrease in cells treated on the LD matrices. This suggest that JNK signalling is worked in parallel with other signalling pathways elicited by the collagen that similarly stimulate proliferation over differentiation. There is a negligible difference in cross-sectional area of nuclei in

HaCaTs post 24h treatment. This suggest ERK to be key in modulating nuclear dynamics resulting from the density-dependent proliferation advantage.

5.3 Discussion

5.3.1 Collagen Matrix Density Spatially Restricts HaCaTs-Implications in proliferation and differentiation rates

The evidence provided here demonstrates an increase in Ki67 positive cells with increased collagen fibres per unit area (figure 5.14). Contrary to finding in Connelly et al (2010), there is a clear correlation between the availability of substrate per unit area and Ki67 expression. However, it could be argued that the void sizes within the different matrices produce the same effect as increasing and decreasing the size of the type 1 collage islands. Interestingly the LD matrices elicited a decrease in nuclear cross-sectional area and increase in nuclear circularity indicative of cells undertaking a programme of differentiation. This was described in the Connolly study as cells with a “low shape factor” i.e. higher circularity, and similarly correlated with cells entering a programme of differentiation as indicated by involucrin expression.

This led me to conclude that the LD matrices with larger voids provide cells with a differentiation advantage whilst HD matrices generate a proliferative advantage (figure 5.14). Corroborating the idea that LD collagen has a similar effect to reducing substrate area was the effects observed on the HD matrices which showed similar findings to those by Connely et al with increased rates of proliferation being accompanied by reduced circularity (or “high shape factor”) increased nuclear volume (figure 5.14).

However, it should also be considered that the LD matrices were the result of increased bundling and therefore increased stiffness (Roeder et al. 2002). This would reduce the number of points of contact a cell is able to make with the substrate reducing the number of integrin-ECM interactions resulting in reduced proliferation rates (Gupta et al. 2016; Burns 2012; Schrader et al. 2011). This is perhaps a means of executing substrate restriction and therefore supports findings by Connely et al. To take this further there is a need to evaluate variations in integrin-ECM binding and correlate these against matrix stiffness as determined by atomic force microscopy.

There are several hypothesized routes by which increased integrin binding could mediate increased cellular proliferation. Increased integrin clustering at the membrane has been noted to result increased FAK activity with subsequent increase in ERK1/2 activity and LEF/TCF promotor activity (Lowry et al. 2005; Vuori et al. 1996; D D

Schlaepfer et al. 1998; Stefan Kippenberger et al. 2004; Kolch 2005; X. Wu et al. 2006). Further to this calveolin that is sequestered to the integrin complexes elicit phosphorylation of ERK1/2 via p130 Cas (Aplin et al. 1998; Wary et al. 1998, 1996). The Connely study identifies actin polymerisation as a key driver of differentiation. Descot et al (2009) identifies a pathway where increased F-actin leads to a reduction in total cell G-actin which is linked to upregulation of MAL and increased promoter SRF leading to upregulation of Mig6/Erif1. Mig6/Erif1 inhibits EGFR activity which was found to reduce phosphor-ERK1/2 resulting in reduced TCF activity and loss of the proliferative advantage. Elevated SRF was also documented within the Connely study supporting this. It can be postulated that the increased availability of substrate to HaCaTs promotes increased activation of ERK via FAK, countering the inhibition of EGFR leading to a proliferative advantage on the HD matrices. The proliferative advantage was retained for cells on HD matrices up to 120h after seeding. To clarify the extent to which FAK and availability of G-actin counter one another it would be necessary to asses ERK1/2 activity and TCF/LEF activity in the presence of latrunculin-A and in the presence of a FAK inhibitor. ERK1/2 inhibition alone may allow for the actin driven differentiation advantage to take president. Additionally, inhibition of ERK1/2 in conjunction with latrunculin A may cause a cell to become quiescent as both proliferative and differentiating cues are being supressed. This would highlight FAK and actin as key regulators of cell proliferation and differentiation at the basement membrane.

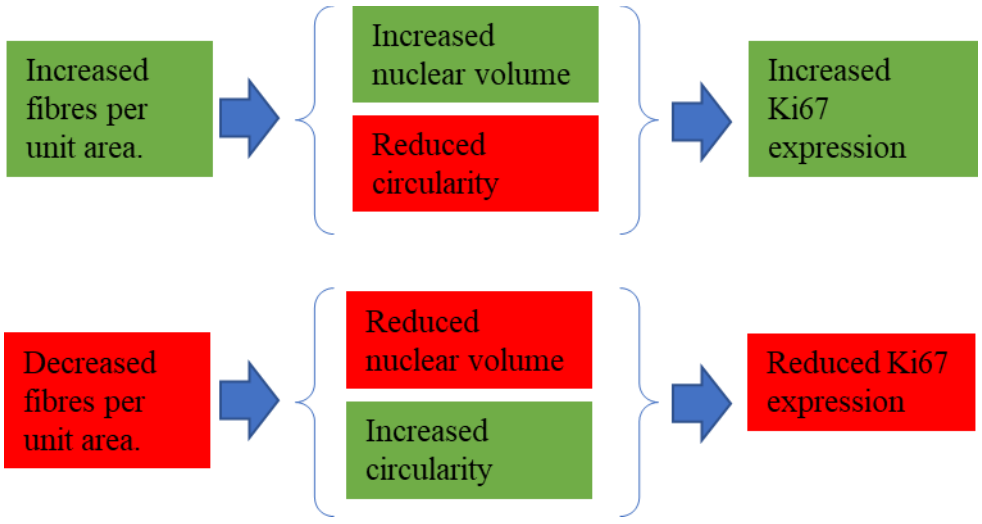

Figure 5.14: Phenotypic outputs manifested in HaCaTs as a result of LD and HD collagen.

5.3.2 p38 Inhibition Suggest Roles Maintenance of the Proliferative Advantage Conferred by High-Density Collagen Substrate in HaCaT Cells

p38 inhibition gave rise to increased involucrin expression with a greater increase exhibited on high-density collagen matrices. In conjunction there was a reduction of Ki67 expression that was independent of collagen density. p38 stimulation produces increased Cyclin D1 activity which complexes with, and activates the cyclin dependent kinases CDK4 and CDK6, which have been demonstrated as important in the G1/S transition of the cell cycle (Schulze et al. 1996; Horsley et al. 2008; Zhu et al. 1996; Moreno-Layseca and Streuli 2014; Mateyak, Obaya, and Sedivy 1999). This suggests that the failure of the cell cycle transition produces a differentiation advantage over a proliferative advantage independent of integrin mediated ERK1/2 induced proliferation. In this way p38 can be seen as important in maintaining the proliferative potential of cells. The fact that the Ki67 rates are reduced to the same level irrespective of collagen density may also suggest a role for p38 in collagen-induced proliferation. This is in conflict with recent findings that utilised transcriptomics and proteomics to demonstrate how the MAPK phosphatase DUSP10 specifically downregulated p38 imparting keratinocytes with increased colony formation capability (Mishra et al. 2017). However, it should be noted that DUSP10 overexpression may well impact upon its specificity as many DUSPs have been found to have a capacity to dephosphorylate several MAPKs (Gazel et al. 2008; Mishra et al. 2017).

The findings here also contradict those made by Dashti et al (2001), whom hypothesized a central role for p38δ as central to propagating proliferation. As the p38 inhibitor is not effective as a p38δ inhibitor it would suggest that p38$\alpha/\beta/\gamma$ is central to maintaining the hypothesized proliferative potential and not p38δ.

The increased cross-section area and loss of circularity was also more prominent for cells on the HD matrices post p38 inhibition which alligns with a proliferation phenotype based on earlier findings. This data suggests the connection between nuclear dynamics and cell fate to be independent of p38 signalling. This may also suggest that ERK counterbalances p38 activity promoting proliferation in support of findings by Zhang et al (2001). As p38 is inhibited pharmacologically there may be a larger pool of phosphor-ERK1/2 available which produces the more extreme proliferation phenotype observed. What is noteworthy however is the initial increase

in Ki67 expression at 24h producing a phenotype that aligns with that produced by DUSP10 inhibition (Mishra et al. 2017). It may well be possible that integrin mediated stimulation of FAK produces the initial Ki67 expression which becomes attenuated with time through reduced G-actin. This could be verified though correlating F-actin abundance at different stages after seeding with phosphor-ERK1/2 activity. The down regulation of ERK1/2 then causes a loss in the proliferative advantage allowing the differentiation advantage to take over in the absence of p38 signalling. The large increase of involucrin after 120h lends support to this hypothesis.

5.3.4 ERK Signalling Could Drives the Proliferative Advantage Gained from High-Density Collagen Matrices

ERK inhibition produced little to no effect on cellular proliferation rates compared with the untreated cells on equivalent matrices. This suggests that integrin mediated ERK signalling as non-essential in driving proliferation in HaCaTs as determined by Ki67 expression. However, when considering nuclear cross-sectional areas there is a notable decrease compared with untreated cells. This observation aligns with a recent study that demonstrates the importance of ERK signalling in cell growth via lack of activation of the transcription factor TIF-1A which is required for RNA Polymerase 1 transcription (Zhao et al. 2003). A possible explanation is that ERK1/2 is phosphorylated by a MAPKK other than MEK1. This also aligns with the differentiation phenotype described in Connely et al (2010). This could suggest that nuclear dynamics are independent of cell-cycling status or that ERK signalling is important in linking the orchestration of nuclear dynamics with cell-cycle status.

Involucrin expression was greatly increased as a result of ERK inhibition which has been noted in several studies involving osteoclasts, adipocytes, muscle stem cells and keratinocytes demonstrating the conserved roll of ERK signalling in propagating a proliferative advantage over a differentiation advantage (C. Ge et al. 2016; Michailovici et al. 2014). What was interesting is that cells incubated with ERKi on high-density collagen matrices exhibited a greater increase of involucrin expression compared with cells treated on low-density matrices. This suggest a collagen-dependent mechanism that promotes a proliferative advantage over a differential advantage that is independent of ERK signalling.

The high-density matrices appear to attenuate the differentiation bias induced by ERK inhibition. This posits two interesting hypotheses. The first is that there may be ERK-independent signalling that retains the proliferative advantage and the second is that the drug concentration used was insufficient to counteract the integrin-mediated stimulation of ERK via FAK/fyn pathway and the discoidin domain 1 receptor (DDR1) stimulated activation of ERK1/2 through collagen 1 binding as observed in lung fibroblast and, head and neck squamous cell carcinomas (Ruiz and Jarai 2011; Silva et al. 2018). What is clear is that in the absence of ERK signalling produces a differentiation advantage for HaCaTs in a collagen density-dependent manner.

5.3.5 JNK Signalling Could Counteract ERK1/2 Mediated Proliferation in HaCaTs

JNK1/2 has been found to ubiquitinate ERK1/2 resulting in proteasomal degradation. It has been implicated in downregulation of LEF/TCF transcription factor activity through loss of β-catenin by ubiquitination through lack of activation by ERK1/2. This produces a concomitant increase of involucrin expression indicative of loss of the proliferative advantage conferred by ERK1/2 signalling (Dashti, Efimova, and Eckert 2001; Tan et al. 2017). The reduced Ki67 expression and increased involucrin expression observed post JNK inhibition supports these findings. The collagen-dependent increase of involucrin expression would further support its involvement in counterbalancing ERK1/2 activation of β-catenin resulting in reduced proliferation rates. More interestingly perhaps, is that the occurrence is collagen density-dependent supporting the hypothesis that increased collagen density could lead to increased integrin clustering at adhesion sites with the concomitant increase in ERK1/2 signalling stimulated via increased FAK and p130Cas activity (Vuori et al. 1996; D D Schlaepfer et al. 1998; Qiming Chen et al. 1996; D'Souza-Schorey, Boettner, and Van Aelst 1998; Pozzi et al. 1998; Becerra-Bayona et al. 2018).

The Connely, 2010 Study concludes that actin driven shape changes drive the terminal differentiation as inhibition of actin polymerisation prevented differentiation of keratinocytes on the smallest of islands. In conjunction with this it was noted that Rho kinase inhibition also prevented actin polymerisation, however MEK1 (JNK1/2 kinase) inhibition did not impact upon differentiation rates suggesting shape induced terminal differentiation was independent of actin induced differentiation. Parallels can be drawn with findings here as JNK inhibition resulted in increased rates of involucrin

expression yet had no effect on nuclear circularity for cells exposed to JNKi on high-density matrices compared with uninhibited cells on HD matrices.

6 Conclusions and Future Outlook

Research into mechanical sensing presents an opportunity to uncover native ECM and cell sensing mechanisms that govern tissue homeostasis and dysregulation. As the field is extraordinarily broad these final conclusions will focus specifically on how findings within this study demonstrate governance of epidermal tissues through mechanical sensing and how structures have developed to maintain tissue homeostasis.

At the basement membrane and the outer root sheath of the follicle there are three main groups of cells; stem cells, transit amplifying cells and cells undergoing programs of terminal differentiation (V. Levy et al. 2005; Snippert et al. 2010; Blanpain and Fuchs 2006b, 2009). Stem cells need to change between quiescence and cell-cycling depending on the demand for epidermal replenishment or stimulation of anagen, and transit amplifying cells need to undergo a finite number of divisions before entering a programme of terminal differentiation where they detach from the basement membrane and begin a programme of terminal differentiation (Connelly et al. 2011; Dupont 2016; Blanpain and Fuchs 2009). This implies the involvement of other cell-regulatory mechanisms that are independent of mechanical sensing. Such mechanisms include epigenetic modification as demonstrated thorough histone acetylation and nuclear envelope transmembrane (NET) protein binding with changes that correspond to chromatin remodelling (M De Ruijter et al. 2003; Y. Li et al. 2011; Ropero and Esteller 2007; X. Wong, Luperchio, and Reddy 2014). Chromosomal restrictions conferred by histone acetylation and chromosomal binding to NET proteins provide a possible explanation for how cells within a niche are able to diverge in cell commitments such as the basement membrane of the skin, bulge of the follicle and hair follicle matrix of anagen follicles.

In understanding how, the different compartments of the hair follicle and dermal collagen contribute to the distribution of force exerted on the pilosebaceous unit during the loading of hair shafts there is opportunity to explore the effects on the propagation of anagen and interfollicular epidermal/dermal homeostasis. Findings presented here demonstrate physical mechanisms employed to prevent deformation of nuclei within regions of the follicle where stem cell populations localise to. Recently biophysical cues have been shown to impact upon histone deacetylase (HDAC)

activity. Mesenchymal stem cells were cultured on extensible silicone matrices. When subjected to stretching there was an increase in nuclear elongation that correlated with reduced HDAC activity and subsequent increase in histone acetylation. Knock-down of lamin A/C abolished mechanical abrogation of HDAC activity (Y. Li et al. 2011). This study demonstrates the importance of amelioration of nuclear deformation in the pilosebaceous unit to preserve stem cell niches. Other studies identified how mechanical stretching caused upregulation of the Ras-like protein Rap1 producing increased p38 activity whilst cellular contraction resulted in upregulation of Ras and upregulation of ERK1/2 and JNK activity (Sawada et al. 2001; Yano et al. 2004). A second study identified the upregulation of ERK1/2 in response to prolonged cell stretching and increased proliferation rates in HaCaT cells (Yano et al. 2004; S Kippenberger et al. 2000). There is a need to analyse the structural changes of lamin A/C as a result of cellular compression in conjunction with HDAC activity, ERK1/2 activity and expression of pro-meiotic genes to unify these theories under the umbrella hypothesis that mechanical compression can drive proliferation through nuclear remodelling and subsequent chromatin remodelling.

The role of the interfollicular collagen may have greater importance other than in follicular anchorage and providing structural integrity that were discussed earlier. An emerging theory is that cellular tension plays a key role in modulating cellular dynamics and, such tensions are conferred by the stiffness of the extracellular matrix (Gosline et al. 2002; Greiner et al. 2013; McBeath et al. 2004; Freeman et al. 2017; Sawada et al. 2001; Raymond et al. 2005). In the case of cells at the basement membrane and non-cycling portion of the dermis there is a rich network of which key structural components comprise collagen and elastin (Muiznieks and Keeley 2013; Tilbury et al. 2014; Gosline et al. 2002). The structural stiffness of these matrices has been shown to alter formation of focal adhesion and formation of actin-stress fibres both of which impact upon cellular proliferation rates and differentiation rates (O. V. Kim et al. 2017; Olson and Nordheim 2010a; Connelly et al. 2010; David D. Schlaepfer et al. 1994; Raymond et al. 2005; J. Koster, Van Wilpe, et al. 2004; Q Chen et al. 1996; Soucy and Romer 2009; Elbediwy et al. 2016; Dupont 2016; Hao et al. 2014). The cell tensioning allows for cells to rapidly sense alterations in their physical environments. This tensioning is also essential for maintenance of homeostasis governing proliferation and differentiation of stem cells. Matrix stiffness

is well established as a means of altering fate of mesenchymal stem cells with specific stiffnesses producing differentiation into osteoblast, fibroblasts, chondrocytes and adipocytes to name a few (Engler et al. 2006; Huebsch et al., n.d.; D. Li et al. 2011; Palomares et al. 2009). Loss of tensioning in the skin could therefore have implications in stem cell renewal and differentiation in the hair follicle and epidermis. Little is understood regarding the mechanisms by which stiffness affects cell fate decision and proliferative potential.

Within this study there is a correlation between nuclear size, circularity and proliferation rates. That is that colonies with a higher proportion of proliferating cells exhibit nuclei that on average are at least 30% larger and exhibit a reduction in circularity. As the collagen matrices manufactured do not exhibit a common fibre orientation, cell spreading should be non-directional leading to circular morphologies if the nuclear dynamics are governed by reorganisation of the actin cytoskeleton dynamics (Y. Li et al. 2011; C S Chen et al. 1997; Connelly et al. 2010). This suggests cells a larger proportion of polarised cells indicative of mitosis, corroborating the effect of high-density collagen on proliferation rates as also found in other studies i.e. increased density (points of contact) produces elevated Ki67 expression (Connelly et al. 2010; Morishima 1999; Olson and Nordheim 2010b; K. K. Lee et al. 2002; Crisp et al. 2006; Osorio and Gomes 2014; Good 2015). The biological importance of this is evident when considering the nucleus contains several meters of genetic material within a volume that could range from 512 um^3 to over 1,728 um^3 (based on the upper and lower limit of nuclear size recorded within this study). It therefore utilises histones and NETs to carefully fold chromosomes to create sufficient space for transcription to occur during normal cell homeostasis. As cells specialise, they only requires access to a specific subset of genes to perform their function which dictates which genes can be transcribed. During cell division the genome must be replicated in its entirety required de-condensation of chromosomes. To accommodate for the unfolding of several meters of genetic material there is a need for nuclear expansion as is implied by findings here. It therefore stands to reason that proliferative cues derived from mechanical sensing must have a capacity to initiate changes in nuclear dynamics and chromosomal remodelling. Further understanding of the interplay between physical cues and epigenetic modification will provide new targets to combat gene dysregulation in a tissue specific manner. The

role of NETs in chromosomal organisation are being characterised more and more as having tissue specific organisations and expressions (X. Wong, Luperchio, and Reddy 2014; Murao et al. 2006; Huh et al. 2003).

The findings here that increased collagen density leads to an upregulation of proliferation in a collagen density-dependant mechanism mediated by p38 and ERK would encourage pursuit of how these particular MAPKs are regulated by hemidesmosomes. This could lead to the uncovering of new targets to combat squamous cells carcinomas that frequently experience dysregulation of hemidesmosomal proteins including plectin and β4 integrin. Plectin is a cytoskeletal linker protein that has also been shown to interact with MAPKs via the α6β4/FAK/p38 pathway (Almeida et al. 2015).

Where the application of understanding cellular behaviour on different densities of collagen is most applicable to technical advancement in the medical field is in wound healing. In understanding how to produce environments that promote cellular growth presents a potential solution to the development of bio-scaffolds and hydrogels that could greatly improve recovery times for patients with large wounds and persistent wounds. This study has succeeded in defining some characteristics that are conducive to propagating cellular proliferation i.e. A high-density matrix. By identifying biosimilars that are synthetic or naturally derived which can be more easily extracted/developed it may be possible to develop new wound healing solutions. The next logical step would be to use atomic force microscopy to define the stiffnesses of the high-density and low-density matrices to understand how these characteristics may also impact upon the phenotype elicited.

At the core of this study is the application of advanced bioimaging. The techniques used, and methods of analysis utilised have a far wider application that has been explored within this thesis. Automated analysis of protein localisation presents a high-throughput screening method to asses protein expression across tissues that could aid greatly in the fields of diagnosis of tissue specific diseases enabling for the use of more targeted treatments. This technique has since been utilised in assessing the homologous recombination potential of ovarian cancer cells (data not yet published) to evaluate the mechanism of potentiation to targeted treatments. The novel means by which SHG signal has been analysed within this thesis provides a new gateway into

characterising of collagenous structures and biological and synthetic structures comprising repeating units that exhibit non-centrosymmetry. This would be highly applicable to industries wanting to characterise matrices for optimal cellular growth, in particular where constructing skin-like models.

7 References

Aberle, H, S Butz, J Stappert, … H Weissig - Journal of cell, and Undefined 1994. 1994. 'Assembly of the Cadherin-Catenin Complex in Vitro with Recombinant Proteins'. *Jcs.Biologists.Org*.

Adams, CL, YT Chen, … SJ Smith - The Journal of cell, and Undefined 1998. 1998. 'Mechanisms of Epithelial Cell–Cell Adhesion and Cell Compaction Revealed by High-Resolution Tracking of E-Cadherin–Green Fluorescent Protein'. *Jcb.Rupress.Org*.

Aharonov, Y., and D. Bohm. 1961. 'Time in the Quantum Theory and the Uncertainty Relation for Time and Energy'. *Physical Review* 122 (5): 1649–58. https://doi.org/10.1103/PhysRev.122.1649.

Akasaka, T, R L van Leeuwen, I G Yoshinaga, M C Mihm, and H R Byers. 1995. 'Focal Adhesion Kinase (P125FAK) Expression Correlates with Motility of Human Melanoma Cell Lines.' *The Journal of Investigative Dermatology* 105 (1): 104–8. https://doi.org/10.1111/1523-1747.ep12313396.

Alam, Hunain, Lalit Sehgal, Samrat T. Kundu, Sorab N. Dalal, and Milind M. Vaidya. 2011. 'Novel Function of Keratins 5 and 14 in Proliferation and Differentiation of Stratified Epithelial Cells'. Edited by Robert David Goldman. *Molecular Biology of the Cell* 22 (21): 4068–78. https://doi.org/10.1091/mbc.e10-08-0703.

Alessi, D R, A Cuenda, P Cohen, D T Dudley, and A R Saltiel. 1995. 'PD 098059 Is a Specific Inhibitor of the Activation of Mitogen-Activated Protein Kinase Kinase in Vitro and in Vivo.' *The Journal of Biological Chemistry* 270 (46): 27489–94.

Alexandrescu, Doru T, C Lisa Kauffman, and Constantin A Dasanu. 2009. 'The Cutaneous Epidermal Growth Factor Network: Can It Be Translated Clinically to Stimulate Hair Growth?' *Dermatology Online Journal* 15 (3): 1.

Almeida, Filipe V., Gernot Walko, James R. McMillan, John A. McGrath, Gerhard Wiche, Asa H. Barber, and John T. Connelly. 2015. 'The Cytolinker Plectin Regulates Nuclear Mechanotransduction in Keratinocytes'. *Journal of Cell Science* 128 (24).

Andl, Thomas, Kyung Ahn, Alladin Kairo, Emily Y Chu, Lara Wine-Lee, Seshamma

T Reddy, Nirvana J Croft, et al. 2004. ‘Epithelial Bmpr1a Regulates Differentiation and Proliferation in Postnatal Hair Follicles and Is Essential for Tooth Development.’ *Development (Cambridge, England)* 131 (10): 2257–68. https://doi.org/10.1242/dev.01125.

Andrä, Kerstin, Iris Kornacker, Almut Jörgl, Michael Zörer, Daniel Spazierer, Peter Fuchs, Irmgard Fischer, and Gerhard Wiche. 2003. ‘Plectin-Isoform-Specific Rescue of Hemidesmosomal Defects in Plectin (–/–) Keratinocytes’. *Journal of Investigative Dermatology* 120 (2): 189–97. https://doi.org/10.1046/J.1523-1747.2003.12027.X.

Ansell, David M., Jennifer E. Kloepper, Helen A. Thomason, Ralf Paus, and Matthew J. Hardman. 2011. ‘Exploring the “Hair Growth–Wound Healing Connection”: Anagen Phase Promotes Wound Re-Epithelialization’. *Journal of Investigative Dermatology* 131 (2): 518–28. https://doi.org/10.1038/JID.2010.291.

Aplin, a E, A Howe, S K Alahari, and R L Juliano. 1998. ‘Signal Transduction and Signal Modulation by Cell Adhesion Receptors: The Role of Integrins, Cadherins, Immunoglobulin-Cell Adhesion Molecules, and Selectins.’ *Pharmacological Reviews* 50 (2): 197–263. https://doi.org/0031-6997/98/5002-0197.

Aragona, Mariaceleste, Sophie Dekoninck, Steffen Rulands, Sandrine Lenglez, Guilhem Mascré, Benjamin D. Simons, and Cédric Blanpain. 2017. ‘Defining Stem Cell Dynamics and Migration during Wound Healing in Mouse Skin Epidermis’. *Nature Communications* 8 (March): 14684. https://doi.org/10.1038/ncomms14684.

Arai, Ayako, Eiichiro Kanda, and Osamu Miura. 2002. ‘Rac Is Activated by Erythropoietin or Interleukin-3 and Is Involved in Activation of the Erk Signaling Pathway’. *Oncogene* 21 (17): 2641–51. https://doi.org/10.1038/sj.onc.1205346.

ARGYRIS, T S, and M E TRIMBLE. 1964. ‘ON THE MECHANISM OF HAIR GROWTH STIMULATION IN WOUND HEALING.’ *Developmental Biology* 9 (April): 230–54.

Auber, L. 2012. ‘VII.—The Anatomy of Follicles Producing Wool-Fibres, with

Special Reference to Keratinization'. *Transactions of the Royal Society of Edinburgh* 62 (01): 191–254. https://doi.org/10.1017/S0080456800009285.

Azreq, Mohammed-Amine El, Maleck Kadiri, Marc Boisvert, Nathalie Pagé, Philippe A Tessier, and Fawzi Aoudjit. 2016. 'Discoidin Domain Receptor 1 Promotes Th17 Cell Migration by Activating the RhoA/ROCK/MAPK/ERK Signaling Pathway.' *Oncotarget* 7 (29): 44975–90. https://doi.org/10.18632/oncotarget.10455.

Azuara-Liceaga, Elisa, Marisol Sandoval, Matilde Corona, Patricio Gariglio, and Esther López-Bayghen. 2004. 'The Human Involucrin Gene Is Transcriptionally Repressed through a Tissue-Specific Silencer Element Recognized by Oct-2.' *Biochemical and Biophysical Research Communications* 318 (2): 361–71. https://doi.org/10.1016/j.bbrc.2004.04.034.

Balasubramanian, Sivaprakasam, and Richard L Eckert. 2007. 'Keratinocyte Proliferation, Differentiation, and Apoptosis--Differential Mechanisms of Regulation by Curcumin, EGCG and Apigenin.' *Toxicology and Applied Pharmacology* 224 (3): 214–19. https://doi.org/10.1016/j.taap.2007.03.020.

Balasubramanian, Sivaprakasam, Tatiana Efimova, and Richard L Eckert. 2002. 'Green Tea Polyphenol Stimulates a Ras, MEKK1, MEK3, and P38 Cascade to Increase Activator Protein 1 Factor-Dependent Involucrin Gene Expression in Normal Human Keratinocytes.' *The Journal of Biological Chemistry* 277 (3): 1828–36. https://doi.org/10.1074/jbc.M110376200.

Baldock, C, A J Koster, U Ziese, M J Rock, M J Sherratt, K E Kadler, C A Shuttleworth, and C M Kielty. 2001. 'The Supramolecular Organization of Fibrillin-Rich Microfibrils.' *The Journal of Cell Biology* 152 (5): 1045–56.

Bancelin, Stéphane, Carole Aimé, Ivan Gusachenko, Laura Kowalczuk, Gaël Latour, Thibaud Coradin, and Marie-Claire Schanne-Klein. 2014. 'Determination of Collagen Fibril Size via Absolute Measurements of Second-Harmonic Generation Signals.' *Nature Communications* 5 (January): 4920. https://doi.org/10.1038/ncomms5920.

Barkhausen, Tanja, Martijn van Griensven, Johannes Zeichen, and Ulrich Bosch. 2003. 'Modulation of Cell Functions of Human Tendon Fibroblasts by Different

Repetitive Cyclic Mechanical Stress Patterns'. *Experimental and Toxicologic Pathology* 55 (2–3): 153–58. https://doi.org/10.1078/0940-2993-00302.

Barnum, Kevin J., and Matthew J. O'Connell. 2014. 'Cell Cycle Regulation by Checkpoints'. *Methods in Molecular Biology*. https://doi.org/10.1007/978-1-4939-0888-2_2.

Barry, S T, H M Flinn, M J Humphries, D R Critchley, and A J Ridley. 1997. 'Requirement for Rho in Integrin Signalling.' *Cell Adhesion and Communication* 4 (6): 387–98. https://doi.org/10.3109/15419069709004456.

Bauer, J S, J Varner, C Schreiner, L Kornberg, R Nicholas, and R L Juliano. 1993. 'Functional Role of the Cytoplasmic Domain of the Integrin Alpha 5 Subunit.' *The Journal of Cell Biology* 122 (1): 209–21. https://doi.org/10.1083/jcb.122.1.209.

Bauman, Tyler M, Tristan M Nicholson, Lisa L Abler, Kevin W Eliceiri, Wei Huang, Chad M Vezina, and William A Ricke. 2014. 'Characterization of Fibrillar Collagens and Extracellular Matrix of Glandular Benign Prostatic Hyperplasia Nodules.' *PloS One* 9 (10): e109102. https://doi.org/10.1371/journal.pone.0109102.

Becerra-Bayona, Silvia M., Viviana R. Guiza-Arguello, Brooke Russell, Magnus Höök, and Mariah S. Hahn. 2018. 'Influence of Collagen-Based Integrin α_1 and α_2 Mediated Signaling on Human Mesenchymal Stem Cell Osteogenesis in Three Dimensional Contexts'. *Journal of Biomedical Materials Research Part A*, May. https://doi.org/10.1002/jbm.a.36451.

Beck, Benjamin, and Cédric Blanpain. 2012. 'Mechanisms Regulating Epidermal Stem Cells.' *The EMBO Journal* 31 (9): 2067–75. https://doi.org/10.1038/emboj.2012.67.

Behrens, J, J P von Kries, M Kühl, L Bruhn, D Wedlich, R Grosschedl, and W Birchmeier. 1996. 'Functional Interaction of Beta-Catenin with the Transcription Factor LEF-1.' *Nature* 382 (6592): 638–42. https://doi.org/10.1038/382638a0.

Bella, Jordi, Jingsong Liu, Rachel Kramer, Barbara Brodsky, and Helen M. Berman. 2006. 'Conformational Effects of Gly–X–Gly Interruptions in the Collagen

Triple Helix'. *Journal of Molecular Biology* 362 (2): 298–311. https://doi.org/10.1016/j.jmb.2006.07.014.

Bennett, B. L., D. T. Sasaki, B. W. Murray, E. C. O'Leary, S. T. Sakata, W. Xu, J. C. Leisten, et al. 2001. 'SP600125, an Anthrapyrazolone Inhibitor of Jun N-Terminal Kinase'. *Proceedings of the National Academy of Sciences* 98 (24): 13681–86. https://doi.org/10.1073/pnas.251194298.

Berditchevski, F, E Gilbert, M R Griffiths, S Fitter, L Ashman, and S J Jenner. 2001. 'Analysis of the CD151-Alpha3beta1 Integrin and CD151-Tetraspanin Interactions by Mutagenesis.' *The Journal of Biological Chemistry* 276 (44): 41165–74. https://doi.org/10.1074/jbc.M104041200.

Bhatt, R. R., J E J Ferrell, Andrea L. Lewellyn, and James L. Maller. 1999. 'The Protein Kinase P90 Rsk as an Essential Mediator of Cytostatic Factor Activity.' *Science* 286 (5443): 1362–65. https://doi.org/10.1126/science.286.5443.1362.

Bialojan, C, and A Takai. 1988. 'Inhibitory Effect of a Marine-Sponge Toxin, Okadaic Acid, on Protein Phosphatases. Specificity and Kinetics.' *The Biochemical Journal* 256 (1): 283–90.

BIRBECK, M S, and E H MERCER. 1957. 'The Electron Microscopy of the Human Hair Follicle. III. The Inner Root Sheath and Trichohyaline.' *The Journal of Biophysical and Biochemical Cytology* 3 (2): 223–30.

Birchmeier, W. 1995. 'E-Cadherin as a Tumor (Invasion) Suppressor Gene.' *BioEssays : News and Reviews in Molecular, Cellular and Developmental Biology* 17 (2): 97–99. https://doi.org/10.1002/bies.950170203.

Blanpain, Cédric, and Elaine Fuchs. 2006a. 'Epidermal Stem Cells of the Skin.' *Annual Review of Cell and Developmental Biology* 22 (January): 339–73. https://doi.org/10.1146/annurev.cellbio.22.010305.104357.

———. 2006b. 'Epidermal Stem Cells of the Skin'. *Annual Review of Cell and Developmental Biology* 22 (1): 339–73. https://doi.org/10.1146/annurev.cellbio.22.010305.104357.

———. 2009. 'Epidermal Homeostasis: A Balancing Act of Stem Cells in the Skin.' *Nature Reviews. Molecular Cell Biology* 10 (3): 207–17.

https://doi.org/10.1038/nrm2636.

Blanpain, Cédric, William E Lowry, H Amalia Pasolli, and Elaine Fuchs. 2006. 'Canonical Notch Signaling Functions as a Commitment Switch in the Epidermal Lineage.' *Genes & Development* 20 (21): 3022–35. https://doi.org/10.1101/gad.1477606.

Bonni, A. 1999. 'Cell Survival Promoted by the Ras-MAPK Signaling Pathway by Transcription-Dependent and -Independent Mechanisms.' *Science* 286 (5443): 1358–62. https://doi.org/10.1126/science.286.5443.1358.

Borradori, Luca, and Arnoud Sonnenberg. 1999. 'Structure and Function of Hemidesmosomes: More Than Simple Adhesion Complexes'. *Journal of Investigative Dermatology* 112 (4): 411–18. https://doi.org/10.1046/j.1523-1747.1999.00546.x.

Botchkarev, V A, N V Botchkareva, M Nakamura, O Huber, K Funa, R Lauster, R Paus, and B A Gilchrest. 2001. 'Noggin Is Required for Induction of the Hair Follicle Growth Phase in Postnatal Skin.' *FASEB Journal : Official Publication of the Federation of American Societies for Experimental Biology* 15 (12): 2205–14. https://doi.org/10.1096/fj.01-0207com.

Boukamp, P, R T Petrussevska, D Breitkreutz, J Hornung, A Markham, and N E Fusenig. 1988. 'Normal Keratinization in a Spontaneously Immortalized Aneuploid Human Keratinocyte Cell Line.' *The Journal of Cell Biology* 106 (3): 761–71. https://doi.org/10.1083/JCB.106.3.761.

Brenner, B, E Gulbins, K Schlottmann, U Koppenhoefer, G L Busch, B Walzog, M Steinhausen, K M Coggeshall, O Linderkamp, and F Lang. 1996. 'L-Selectin Activates the Ras Pathway via the Tyrosine Kinase P56lck.' *Proceedings of the National Academy of Sciences of the United States of America* 93 (26): 15376–81. https://doi.org/10.1073/pnas.93.26.15376.

Brodsky, Barbara, and Anton V. Persikov. 2005. *Molecular Structure of the Collagen Triple Helix*. *Advances in Protein Chemistry*. Vol. 70. Academic Press. https://doi.org/10.1016/S0065-3233(05)70009-7.

Brodsky, Barbara, and John A M Ramshaw. 1997. 'The Collagen Triple-Helix

Structure'. *Matrix Biology* 15: 545–54.

Brooks, P C, S Strömblad, L C Sanders, T L von Schalscha, R T Aimes, W G Stetler-Stevenson, J P Quigley, and D A Cheresh. 1996. 'Localization of Matrix Metalloproteinase MMP-2 to the Surface of Invasive Cells by Interaction with Integrin Alpha v Beta 3.' *Cell* 85 (5): 683–93. https://doi.org/10.1016/s0092-8674(00)81235-0.

Broussard, Joshua A., Ruiguo Yang, Changjin Huang, S. Shiva P. Nathamgari, Allison M. Beese, Lisa M. Godsel, Marihan H. Hegazy, et al. 2017. 'The Desmoplakin–Intermediate Filament Linkage Regulates Cell Mechanics'. Edited by Asma Nusrat. *Molecular Biology of the Cell* 28 (23): 3156–64. https://doi.org/10.1091/mbc.e16-07-0520.

Buhl, A M, N L Johnson, N Dhanasekaran, and G L Johnson. 1995. 'G Alpha 12 and G Alpha 13 Stimulate Rho-Dependent Stress Fiber Formation and Focal Adhesion Assembly.' *The Journal of Biological Chemistry* 270 (42): 24631–34. https://doi.org/10.1074/jbc.270.42.24631.

Burns. 2012. 'Substrate Stiffness Regulates the Proliferation, Migration, and Differentiation of Epidermal Cells' 38 (3): 414–20. https://doi.org/10.1016/J.BURNS.2011.09.002.

Burridge, Keith, and Magdalena Chrzanowska-Wodnicka. 1996a. 'FOCAL ADHESIONS, CONTRACTILITY, AND SIGNALING'. *Annual Review of Cell and Developmental Biology* 12 (1): 463–519. https://doi.org/10.1146/annurev.cellbio.12.1.463.

———. 1996b. 'FOCAL ADHESIONS, CONTRACTILITY, AND SIGNALING'. *Annual Review of Cell and Developmental Biology* 12 (1): 463–519. https://doi.org/10.1146/annurev.cellbio.12.1.463.

Čabrijan, Leo, and Jasna Lipozenčić. 'Adhesion Molecules in Keratinocytes.' *Clinics in Dermatology* 29 (4): 427–31. https://doi.org/10.1016/j.clindermatol.2011.01.012.

Cain, Natalie E., Erin C. Tapley, Kent L. McDonald, Benjamin M. Cain, and Daniel A. Starr. 2014. 'The SUN Protein UNC-84 Is Required Only in Force-Bearing

Cells to Maintain Nuclear Envelope Architecture'. *The Journal of Cell Biology* 206 (2): 163–72. https://doi.org/10.1083/jcb.201405081.

Candi, Eleonora, Rainer Schmidt, and Gerry Melino. 2005. 'The Cornified Envelope: A Model of Cell Death in the Skin'. *Nature Reviews Molecular Cell Biology* 6 (4): 328–40. https://doi.org/10.1038/nrm1619.

Carlson, Mark W, Addy Alt-Holland, Christophe Egles, and Jonathan A Garlick. 2008. 'Three-Dimensional Tissue Models of Normal and Diseased Skin.' *Current Protocols in Cell Biology / Editorial Board, Juan S. Bonifacino ... [et Al.]* Chapter 19 (December): Unit 19.9. https://doi.org/10.1002/0471143030.cb1909s41.

Centuori, Sara M., Cecil J. Gomes, Jesse Trujillo, Jamie Borg, Joshua Brownlee, Charles W. Putnam, and Jesse D. Martinez. 2016. 'Deoxycholic Acid Mediates Non-Canonical EGFR-MAPK Activation through the Induction of Calcium Signaling in Colon Cancer Cells'. *Biochimica et Biophysica Acta (BBA) - Molecular and Cell Biology of Lipids* 1861 (7): 663–70. https://doi.org/10.1016/J.BBALIP.2016.04.006.

Chan, Y, I Anton-Lamprecht, Q C Yu, A Jäckel, B Zabel, J P Ernst, and E Fuchs. 1994. 'A Human Keratin 14 "Knockout": The Absence of K14 Leads to Severe Epidermolysis Bullosa Simplex and a Function for an Intermediate Filament Protein.' *Genes & Development* 8 (21): 2574–87. https://doi.org/10.1101/gad.8.21.2574.

Chang, Chenbei, Bart J L Eggen, Daniel C Weinstein, and Ali H Brivanlou. 2003. 'Regulation of Nodal and BMP Signaling by Tomoregulin-1 (X7365) through Novel Mechanisms.' *Developmental Biology* 255 (1): 1–11.

Chapman, David M. 1997. 'The Nature of Cuticular "ruffles" on Slowly Plucked Anagen Hair Roots'. *Journal of Cutaneous Pathology* 24: 434–39. https://doi.org/10.1111/j.1600-0560.1997.tb00819.x.

Chaudhry, Shazia S., Stuart A. Cain, Amanda Morgan, Sarah L. Dallas, C. Adrian Shuttleworth, and Cay M. Kielty. 2007. 'Fibrillin-1 Regulates the Bioavailability of TGFβ1'. *The Journal of Cell Biology* 176 (3): 355–67. https://doi.org/10.1083/jcb.200608167.

Chaudhuri, Ovijit, Sandeep T. Koshy, Cristiana Branco da Cunha, Jae-Won Shin, Catia S. Verbeke, Kimberly H. Allison, and David J. Mooney. 2014. 'Extracellular Matrix Stiffness and Composition Jointly Regulate the Induction of Malignant Phenotypes in Mammary Epithelium'. *Nature Materials* 13 (10): 970–78. https://doi.org/10.1038/nmat4009.

Chen, C S, M Mrksich, S Huang, G M Whitesides, and D E Ingber. 1997. 'Geometric Control of Cell Life and Death.' *Science (New York, N.Y.)* 276 (5317): 1425–28.

Chen, C Y, R Gherzi, J S Andersen, G Gaietta, K Jürchott, H D Royer, M Mann, and M Karin. 2000. 'Nucleolin and YB-1 Are Required for JNK-Mediated Interleukin-2 MRNA Stabilization during T-Cell Activation.' *Genes Dev.* 14 (10): 1236–48. https://doi.org/10.1101/GAD.14.10.1236.

Chen, Christopher S, John Tan, and Joe Tien. 2004. 'MECHANOTRANSDUCTION AT CELL-MATRIX AND CELL-CELL CONTACTS'. *Annu. Rev. Biomed. Eng* 6: 275–302. https://doi.org/10.1146/annurev.bioeng.6.040803.140040.

Chen, Jianxin, Anthony Lee, Jianhua Zhao, Hequn Wang, Harvey Lui, David I. McLean, and Haishan Zeng. 2009. 'Spectroscopic Characterization and Microscopic Imaging of Extracted and *in Situ* Cutaneous Collagen and Elastic Tissue Components under Two-Photon Excitation'. *Skin Research and Technology* 15 (4): 418–26. https://doi.org/10.1111/j.1600-0846.2009.00381.x.

Chen, Jing, Xiaoqin Zhu, Yahao Xu, Yiyan Tang, Shuyuan Xiong, Shuangmu Zhuo, and Jianxin Chen. 2014. 'Stereoscopic Visualization and Quantification of Auricular Cartilage Regeneration in Rabbits Using Multiphoton Microscopy.' *Scanning* 36 (5): 540–46. https://doi.org/10.1002/sca.21153.

Chen, Q, T H Lin, C J Der, and R L Juliano. 1996. 'Integrin-Mediated Activation of MEK and Mitogen-Activated Protein Kinase Is Independent of Ras [Corrected].' *The Journal of Biological Chemistry* 271 (30): 18122–27. https://doi.org/10.1074/JBC.271.30.18122.

Chen, Qiming, Tsung H. Lin, Channing J. Der, and R. L. Juliano. 1996. 'Integrin-Mediated Activation of MEK and Mitogen-Activated Protein Kinase Is Independent of Ras'. *Journal of Biological Chemistry* 271 (30): 18122–27. https://doi.org/10.1074/jbc.271.30.18122.

Chen, Xiwu, Hongtao Wang, Hong-Jun Liao, Wen Hu, Leslie Gewin, Glenda Mernaugh, Sheng Zhang, et al. 2014. 'Integrin-Mediated Type II TGF-β Receptor Tyrosine Dephosphorylation Controls SMAD-Dependent Profibrotic Signaling'. *The Journal of Clinical Investigation* 124 (8): 3295–3310. https://doi.org/10.1172/JCI71668.

Chen, Yunfeng, Hyunjung Lee, Haibin Tong, Martin Schwartz, and Cheng Zhu. 2017. 'Force Regulated Conformational Change of Integrin AVβ3'. *Matrix Biology* 60: 70–85. https://doi.org/10.1016/j.matbio.2016.07.002.

Chiang, Chin, Ryan Z. Swan, Marina Grachtchouk, Matthew Bolinger, Ying Litingtung, Erin K. Robertson, Michael K. Cooper, et al. 1999. 'Essential Role ForSonic Hedgehogduring Hair Follicle Morphogenesis'. *Developmental Biology* 205 (1): 1–9. https://doi.org/10.1006/DBIO.1998.9103.

Choi, Hee-Jung, and William I. Weis. 2016. 'Purification and Structural Analysis of Desmoplakin'. *Methods in Enzymology* 569 (January): 197–213. https://doi.org/10.1016/BS.MIE.2015.05.006.

Chung, Martin I S, Ming Miao, Richard J Stahl, Esther Chan, John Parkinson, and Fred W Keeley. 2006. 'Sequences and Domain Structures of Mammalian, Avian, Amphibian and Teleost Tropoelastins: Clues to the Evolutionary History of Elastins.' *Matrix Biology : Journal of the International Society for Matrix Biology* 25 (8): 492–504. https://doi.org/10.1016/j.matbio.2006.08.258.

Cicchi, Riccardo, Nadine Vogler, Dimitrios Kapsokalyvas, Benjamin Dietzek, Jürgen Popp, and Francesco Saverio Pavone. 2013. 'From Molecular Structure to Tissue Architecture: Collagen Organization Probed by SHG Microscopy'. *Journal of Biophotonics* 6 (2): 129–42. https://doi.org/10.1002/jbio.201200092.

Clark, E A, and R O Hynes. 1996. 'Ras Activation Is Necessary for Integrin-Mediated Activation of Extracellular Signal-Regulated Kinase 2 and Cytosolic Phospholipase A2 but Not for Cytoskeletal Organization.' *The Journal of Biological Chemistry* 271 (25): 14814–18. https://doi.org/10.1074/JBC.271.25.14814.

Clavel, Carlos, Laura Grisanti, Roland Zemla, Amelie Rezza, Rita Barros, Rachel Sennett, Amin Reza Mazloom, et al. 2012. 'Sox2 in the Dermal Papilla Niche

Controls Hair Growth by Fine-Tuning BMP Signaling in Differentiating Hair Shaft Progenitors'. *Developmental Cell* 23 (5): 981–94.

Clemmensen, O J, B Hainau, and B Hansted. 1991. 'The Ultrastructure of the Transition Zone between Specialized Cells ("Flügelzellen") of Huxley's Layer of the Inner Root Sheath and Cells of the Outer Root Sheath of the Human Hair Follicle.' *The American Journal of Dermatopathology* 13 (3): 264–70.

Commo, S., O. Gaillard, and B.A. Bernard. 2000. 'The Human Hair Follicle Contains Two Distinct K19 Positive Compartments in the Outer Root Sheath: A Unifying Hypothesis for Stem Cell Reservoir?' *Differentiation* 66 (4–5): 157–64. https://doi.org/10.1111/j.1432-0436.2000.660401.x.

Connelly, John T., Julien E. Gautrot, Britta Trappmann, David Wei-Min Tan, Giacomo Donati, Wilhelm T.S. Huck, and Fiona M. Watt. 2010. 'Actin and Serum Response Factor Transduce Physical Cues from the Microenvironment to Regulate Epidermal Stem Cell Fate Decisions'. *Nature Cell Biology* 12 (7): 711–18. https://doi.org/10.1038/ncb2074.

Connelly, John T, Ajay Mishra, Julien E Gautrot, and Fiona M Watt. 2011. 'Shape-Induced Terminal Differentiation of Human Epidermal Stem Cells Requires P38 and Is Regulated by Histone Acetylation.' *PloS One* 6 (11): e27259. https://doi.org/10.1371/journal.pone.0027259.

Corson, Glen M, Noe L Charbonneau, Douglas R Keene, and Lynn Y Sakai. 2004. 'Differential Expression of Fibrillin-3 Adds to Microfibril Variety in Human and Avian, but Not Rodent, Connective Tissues.' *Genomics* 83 (3): 461–72. https://doi.org/10.1016/j.ygeno.2003.08.023.

Cotsarelis, G, T T Sun, and R M Lavker. 1990. 'Label-Retaining Cells Reside in the Bulge Area of Pilosebaceous Unit: Implications for Follicular Stem Cells, Hair Cycle, and Skin Carcinogenesis.' *Cell* 61 (7): 1329–37.

Coulombe, P. A., R. Kopan, and E. Fuchs. 1989. 'Expression of Keratin K14 in the Epidermis and Hair-Follicle: Insights into Complex Programs of Differentiation'. *Journal of Cell Biology* 109 (5): 2295–2312. https://doi.org/10.1083/jcb.109.5.2295.

Coulombe, Pierre A, and Chang-Hun Lee. 2012. ‘Defining Keratin Protein Function in Skin Epithelia: Epidermolysis Bullosa Simplex and Its Aftermath.’ *The Journal of Investigative Dermatology* 132 (3 Pt 2): 763–75. https://doi.org/10.1038/jid.2011.450.

Cribier, Bernard, Bernard Peltre, Edouard Grosshans, Lutz Langbein, and Jürgen Schweizer. 2004. ‘On the Regulation of Hair Keratin Expression: Lessons from Studies in Pilomatricomas.’ *The Journal of Investigative Dermatology* 122 (5): 1078–83. https://doi.org/10.1111/j.0022-202X.2004.22513.x.

Crisp, Melissa, Qian Liu, Kyle Roux, J.B. Rattner, Catherine Shanahan, Brian Burke, Phillip D. Stahl, and Didier Hodzic. 2006. ‘Coupling of the Nucleus and Cytoplasm’. *The Journal of Cell Biology* 172 (1): 41–53. https://doi.org/10.1083/jcb.200509124.

Cuenda, A. 1997. ‘Activation of Stress-Activated Protein Kinase-3 (SAPK3) by Cytokines and Cellular Stresses Is Mediated via SAPKK3 (MKK6); Comparison of the Specificities of SAPK3 and SAPK2 (RK/P38)’. *The EMBO Journal* 16 (2): 295–305. https://doi.org/10.1093/emboj/16.2.295.

Culav, E M, C H Clark, and M J Merrilees. 1999. ‘Connective Tissues: Matrix Composition and Its Relevance to Physical Therapy.’ *Physical Therapy* 79 (3): 308–19.

Cybulsky, A V, and A J McTavish. 1997. ‘Extracellular Matrix Is Required for MAP Kinase Activation and Proliferation of Rat Glomerular Epithelial Cells.’ *Biochemical and Biophysical Research Communications* 231 (1): 160–66. https://doi.org/10.1006/bbrc.1997.6064.

D’Souza-Schorey, C, B Boettner, and L Van Aelst. 1998. ‘Rac Regulates Integrin-Mediated Spreading and Increased Adhesion of T Lymphocytes.’ *Molecular and Cellular Biology* 18 (7): 3936–46. https://doi.org/10.1128/MCB.18.7.3936.

Dan, I, N M Watanabe, and A Kusumi. 2001. ‘The Ste20 Group Kinases as Regulators of MAP Kinase Cascades.’ *Trends in Cell Biology* 11 (5): 220–30.

Dans, Michael, Laurent Gagnoux-Palacios, Pamela Blaikie, Sharon Klein, Agnese Mariotti, and Filippo G. Giancotti. 2001. ‘Tyrosine Phosphorylation of the β_4

Integrin Cytoplasmic Domain Mediates Shc Signaling to Extracellular Signal-Regulated Kinase and Antagonizes Formation of Hemidesmosomes'. *Journal of Biological Chemistry* 276 (2): 1494–1502. https://doi.org/10.1074/jbc.M008663200.

Dashti, S R, T Efimova, and R L Eckert. 2001. 'MEK6 Regulates Human Involucrin Gene Expression via a P38alpha - and P38delta -Dependent Mechanism.' *The Journal of Biological Chemistry* 276 (29): 27214–20. https://doi.org/10.1074/jbc.M100465200.

Deng, Zhili, Xiaohua Lei, Xudong Zhang, Huishan Zhang, Shuang Liu, Qi Chen, Huimin Hu, et al. 2015. 'MTOR Signaling Promotes Stem Cell Activation via Counterbalancing BMP-Mediated Suppression during Hair Regeneration'. *Journal of Molecular Cell Biology* 7 (1): 62–72. https://doi.org/10.1093/jmcb/mjv005.

Denk, Winfried, James H Strickler, and Watt W Webb. 1990. 'Two-Photon Laser Scanning Fluorescence Microscopy'. *Science, New Series* 248 (4951): 73–76.

Descot, Arnaud, Reinhard Hoffmann, Dmitry Shaposhnikov, Markus Reschke, Axel Ullrich, and Guido Posern. 2009. 'Negative Regulation of the EGFR-MAPK Cascade by Actin-MAL-Mediated Mig6/Errfi-1 Induction'. *Molecular Cell* 35 (3): 291–304. https://doi.org/10.1016/j.molcel.2009.07.015.

Ding, Yanning, and Trevor Dale. 2002. 'Wnt Signal Transduction: Kinase Cogs in a Nano-Machine?' *Trends in Biochemical Sciences* 27 (7): 327–29. https://doi.org/10.1016/S0968-0004(02)02137-0.

Donetti, Elena, Elena Boschini, Anna Cerini, Silvia Selleri, Cristiano Rumio, and Isabella Barajon. 2004. 'Desmocollin 1 Expression and Desmosomal Remodeling during Terminal Differentiation of Human Anagen Hair Follicle: An Electron Microscopic Study.' *Experimental Dermatology* 13 (5): 289–97. https://doi.org/10.1111/j.0906-6705.2004.00152.x.

Dudley, D T, L Pang, S J Decker, A J Bridges, and A R Saltiel. 1995. 'A Synthetic Inhibitor of the Mitogen-Activated Protein Kinase Cascade.' *Proceedings of the National Academy of Sciences of the United States of America* 92 (17): 7686–89.

Dupont, Sirio. 2016. ‘Role of YAP/TAZ in Cell-Matrix Adhesion-Mediated Signalling and Mechanotransduction’. *Experimental Cell Research* 343 (1): 42–53. https://doi.org/10.1016/J.YEXCR.2015.10.034.

Dutta, Anindita, Jing Li, Carmine Fedele, Aejaz Sayeed, Amrita Singh, Shelia M Violette, Thomas D Manes, and Lucia R Languino. 2015. ‘Avβ6 Integrin Is Required for TGFβ1-Mediated Matrix Metalloproteinase2 Expression.’ *The Biochemical Journal* 466 (3): 525–36. https://doi.org/10.1042/BJ20140698.

Eckert, Richard L., James F. Crish, Tatiana Efimova, Shervin R. Dashti, Anne Deucher, Frederic Bone, Gautam Adhikary, Guosheng Huang, Ramamurthy Gopalakrishnan, and Sivaprakasam Balasubramanian. 2004. ‘Regulation of Involucrin Gene Expression’. *Journal of Investigative Dermatology* 123 (1): 13–22. https://doi.org/10.1111/J.0022-202X.2004.22723.X.

Efimova, T, P LaCelle, J F Welter, and R L Eckert. 1998. ‘Regulation of Human Involucrin Promoter Activity by a Protein Kinase C, Ras, MEKK1, MEK3, P38/RK, AP1 Signal Transduction Pathway.’ *The Journal of Biological Chemistry* 273 (38): 24387–95. https://doi.org/10.1074/JBC.273.38.24387.

Ehrlich, JS, MDH Hansen, WJ Nelson - Developmental Cell, and Undefined 2002. 2002. ‘Spatio-Temporal Regulation of Rac1 Localization and Lamellipodia Dynamics during Epithelial Cell-Cell Adhesion’. *Elsevier*.

Elbediwy, Ahmed, Zoé I Vincent-Mistiaen, Bradley Spencer-Dene, Richard K Stone, Stefan Boeing, Stefanie K Wculek, Julia Cordero, et al. 2016. ‘Integrin Signalling Regulates YAP and TAZ to Control Skin Homeostasis.’ *Development (Cambridge, England)* 143 (10): 1674–87. https://doi.org/10.1242/dev.133728.

Elliott, K, T J Stephenson, and A G Messenger. 1999. ‘Differences in Hair Follicle Dermal Papilla Volume Are Due to Extracellular Matrix Volume and Cell Number: Implications for the Control of Hair Follicle Size and Androgen Responses.’ *The Journal of Investigative Dermatology* 113 (6): 873–77. https://doi.org/10.1046/j.1523-1747.1999.00797.x.

Engler, Adam J., Shamik Sen, H. Lee Sweeney, and Dennis E. Discher. 2006. ‘Matrix Elasticity Directs Stem Cell Lineage Specification’. *Cell* 126 (4): 677–89. https://doi.org/10.1016/J.CELL.2006.06.044.

English, Jessie, Gray Pearson, Julie Wilsbacher, Jennifer Swantek, Mahesh Karandikar, Shuichan Xu, and Melanie H. Cobb. 1999. ‘New Insights into the Control of MAP Kinase Pathways.’ *Exp. Cell Res.* 253 (1): 255–70.

Favre, Bertrand, Nadja Begré, Jamal-Eddine Bouameur, Prakash Lingasamy, Gloria M. Conover, Lionel Fontao, and Luca Borradori. 2018. ‘Desmoplakin Interacts with the Coil 1 of Different Types of Intermediate Filament Proteins and Displays High Affinity for Assembled Intermediate Filaments’. Edited by Pavel Strnad. *PLOS ONE* 13 (10): e0205038. https://doi.org/10.1371/journal.pone.0205038.

Ferber, A, C Yaen, E Sarmiento, J Martinez - Experimental cell Research, and Undefined 2002. 2002. ‘An Octapeptide in the Juxtamembrane Domain of VE-Cadherin Is Important for P120ctn Binding and Cell Proliferation’. *Elsevier*.

Fine, Jo-David. 2010. ‘Inherited Epidermolysis Bullosa: Past, Present, and Future’. *Annals of the New York Academy of Sciences* 1194 (1): 213–22. https://doi.org/10.1111/j.1749-6632.2010.05463.x.

Foitzik, K, R Paus, T Doetschman, and G P Dotto. 1999. ‘The TGF-Beta2 Isoform Is Both a Required and Sufficient Inducer of Murine Hair Follicle Morphogenesis.’ *Developmental Biology* 212 (2): 278–89. https://doi.org/10.1006/dbio.1999.9325.

Folgueras, Alicia R, Xingyi Guo, H Amalia Pasolli, Nicole Stokes, Lisa Polak, Deyou Zheng, and Elaine Fuchs. 2013. ‘Architectural Niche Organization by LHX2 Is Linked to Hair Follicle Stem Cell Function.’ *Cell Stem Cell* 13 (3): 314–27. https://doi.org/10.1016/j.stem.2013.06.018.

Frank Krumeich. n.d. ‘Properties of Electrons, Their Interactions with Matter and Applications in Electron Microscopy’.

Freeman, Spencer A., Sonja Christian, Pamela Austin, Irene Iu, Marcia L. Graves, Lin Huang, Shuo Tang, Daniel Coombs, Michael R. Gold, and Calvin D. Roskelley. 2017. ‘Applied Stretch Initiates Directional Invasion through the Action of Rap1 GTPase as a Tension Sensor’. *Journal of Cell Science* 130 (1): 152–63. https://doi.org/10.1242/jcs.180612.

Friedl, Peter, Katarina Wolf, and Jan Lammerding. 2011. ‘Nuclear Mechanics during

Cell Migration'. *Current Opinion in Cell Biology* 23 (1): 55–64. https://doi.org/10.1016/J.CEB.2010.10.015.

Frisch, S. M. 1996. 'Control of Adhesion-Dependent Cell Survival by Focal Adhesion Kinase'. *The Journal of Cell Biology* 134 (3): 793–99. https://doi.org/10.1083/jcb.134.3.793.

Fuchs, E, and H Green. 1980. 'Changes in Keratin Gene Expression during Terminal Differentiation of the Keratinocyte.' *Cell* 19 (4): 1033–42.

Fuchs, S. Y., V. Adler, T. Buschmann, Z. Yin, X. Wu, S. N. Jones, and Z. Ronai. 1998. 'JNK Targets P53 Ubiquitination and Degradation in Nonstressed Cells'. *Genes & Development* 12 (17): 2658–63. https://doi.org/10.1101/gad.12.17.2658.

Fuchs, Serge Y., Victor Adler, Matthew R. Pincus, and Ze'ev Ronai. 1998. 'MEKK1/JNK Signaling Stabilizes and Activates P53'. *Proceedings of the National Academy of Sciences* 95 (18).

Füllgrabe, Anja, Simon Joost, Alexandra Are, Tina Jacob, Unnikrishnan Sivan, Andrea Haegebarth, Sten Linnarsson, et al. 2015. 'Dynamics of Lgr6+ Progenitor Cells in the Hair Follicle, Sebaceous Gland, and Interfollicular Epidermis'. *Stem Cell Reports* 5 (5): 843–55. https://doi.org/10.1016/J.STEMCR.2015.09.013.

Gadhari, Neha, Mirren Charnley, Mattia Marelli, Jürgen Brugger, and Matthias Chiquet. 2013. 'Cell Shape-Dependent Early Responses of Fibroblasts to Cyclic Strain'. *Biochimica et Biophysica Acta (BBA) - Molecular Cell Research* 1833 (12): 3415–25.

Gahmberg, Carl G., Susanna C. Fagerholm, Susanna M. Nurmi, Triantafyllos Chavakis, Silvia Marchesan, and Mikaela Grönholm. 2009. 'Regulation of Integrin Activity and Signalling'. *Biochimica et Biophysica Acta (BBA) - General Subjects* 1790 (6): 431–44. https://doi.org/10.1016/j.bbagen.2009.03.007.

Gallant, Nathan D., Kristin E. Michael, and Andrés J. García. 2005. 'Cell Adhesion Strengthening: Contributions of Adhesive Area, Integrin Binding, and Focal

Adhesion Assembly'. *Molecular Biology of the Cell* 16 (9): 4329–40. https://doi.org/10.1091/mbc.e05-02-0170.

García Lopez, M a, a Aguado Martínez, C Lamaze, C Martínez-A, and T Fischer. 2009. 'Inhibition of Dynamin Prevents CCL2-Mediated Endocytosis of CCR2 and Activation of ERK1/2.' *Cellular Signalling* 21 (12): 1748–57. https://doi.org/10.1016/j.cellsig.2009.07.010.

Garcin, Clare L., and David M. Ansell. 2017. 'The Battle of the Bulge: Re-Evaluating Hair Follicle Stem Cells in Wound Repair'. *Experimental Dermatology* 26 (2): 101–4. https://doi.org/10.1111/exd.13184.

Garrod, David, and Martyn Chidgey. 2008. 'Desmosome Structure, Composition and Function'. *Biochimica et Biophysica Acta (BBA) - Biomembranes* 1778 (3): 572–87. https://doi.org/10.1016/J.BBAMEM.2007.07.014.

Gattazzo, Francesca, Anna Urciuolo, and Paolo Bonaldo. 2014. 'Extracellular Matrix: A Dynamic Microenvironment for Stem Cell Niche.' *Biochimica et Biophysica Acta*, January. https://doi.org/10.1016/j.bbagen.2014.01.010.

Gazel, Alix, Tomohiro Banno, Rebecca Walsh, and Miroslav Blumenberg. 2006. 'Inhibition of JNK Promotes Differentiation of Epidermal Keratinocytes.' *The Journal of Biological Chemistry* 281 (29): 20530–41. https://doi.org/10.1074/jbc.M602712200.

Gazel, Alix, Rajiv I. Nijhawan, Rebecca Walsh, and Miroslav Blumenberg. 2008. 'Transcriptional Profiling Defines the Roles of ERK and P38 Kinases in Epidermal Keratinocytes'. *Journal of Cellular Physiology* 215 (2): 292–308. https://doi.org/10.1002/jcp.21394.

Ge, Chunxi, William P. Cawthorn, Yan Li, Guisheng Zhao, Ormond A. MacDougald, and Renny T. Franceschi. 2016. 'Reciprocal Control of Osteogenic and Adipogenic Differentiation by ERK/MAP Kinase Phosphorylation of Runx2 and PPARγ Transcription Factors'. *Journal of Cellular Physiology* 231 (3): 587–96. https://doi.org/10.1002/jcp.25102.

Ge, Yejing, and Elaine Fuchs. 2018. 'Stretching the Limits: From Homeostasis to Stem Cell Plasticity in Wound Healing and Cancer'. *Nature Reviews Genetics* 19

(5): 311–25. https://doi.org/10.1038/nrg.2018.9.

Getsios, Spiro, Arthur C Huen, and Kathleen J Green. 2004. 'Working out the Strength and Flexibility of Desmosomes.' *Nature Reviews. Molecular Cell Biology* 5 (4): 271–81. https://doi.org/10.1038/nrm1356.

Ghazizadeh, S, and L B Taichman. 2001. 'Multiple Classes of Stem Cells in Cutaneous Epithelium: A Lineage Analysis of Adult Mouse Skin.' *The EMBO Journal* 20 (6): 1215–22. https://doi.org/10.1093/emboj/20.6.1215.

Glover, James D., Kirsty L. Wells, Franziska Matthäus, Kevin J. Painter, William Ho, Jon Riddell, Jeanette A. Johansson, et al. 2017. 'Hierarchical Patterning Modes Orchestrate Hair Follicle Morphogenesis'. Edited by Caroline Hill. *PLOS Biology* 15 (7): e2002117. https://doi.org/10.1371/journal.pbio.2002117.

Goetsch, K P, K Kallmeyer, and C U Niesler. 2011. 'Decorin Modulates Collagen I-Stimulated, but Not Fibronectin-Stimulated, Migration of C2C12 Myoblasts.' *Matrix Biology : Journal of the International Society for Matrix Biology* 30 (2): 109–17. https://doi.org/10.1016/j.matbio.2010.10.009.

Good, Matthew C. 2015. 'Turn Up the Volume: Uncovering Nucleus Size Control Mechanisms'. *Developmental Cell* 33: 496–97. https://doi.org/10.1016/j.devcel.2015.05.015.

Gooding, Jane M., Kyoko L. Yap, and Mitsuhiko Ikura. 2004. 'The Cadherin-Catenin Complex as a Focal Point of Cell Adhesion and Signalling: New Insights from Three-Dimensional Structures'. *BioEssays* 26 (5): 497–511. https://doi.org/10.1002/bies.20033.

Göppert-Mayer, Maria. 1931. 'Über Elementarakte Mit Zwei Quantensprüngen'. *Annalen Der Physik* 401 (3): 273–94. https://doi.org/10.1002/andp.19314010303.

Gordon, Marion K., and Rita A. Hahn. 2010. 'Collagens.' *Cell and Tissue Research* 339 (1): 247–57. https://doi.org/10.1007/s00441-009-0844-4.

Gosline, John, Margo Lillie, Emily Carrington, Paul Guerette, Christine Ortlepp, and Ken Savage. 2002. 'Elastic Proteins: Biological Roles and Mechanical Properties.' *Philosophical Transactions of the Royal Society of London. Series B,*

Biological Sciences 357 (1418): 121–32. https://doi.org/10.1098/rstb.2001.1022.

Graves, Lee M., Hedeel I. Guy, Piotr Kozlowski, Min Huang, Eduardo Lazarowski, R. Marshall Pope, Matthew A. Collins, Erik N. Dahlstrand, H. Shelton Earp, and David R. Evans. 2000. 'Regulation of Carbamoyl Phosphate Synthetase by MAP Kinase.' *Nature* 403 (6767): 328–32. https://doi.org/10.1038/35002111.

Greco, Valentina, Ting Chen, Michael Rendl, Markus Schober, H Amalia Pasolli, Nicole Stokes, June Dela Cruz-Racelis, and Elaine Fuchs. 2009. 'A Two-Step Mechanism for Stem Cell Activation during Hair Regeneration.' *Cell Stem Cell* 4 (2): 155–69. https://doi.org/10.1016/j.stem.2008.12.009.

Greiner, Alexandra M, Hao Chen, Joachim P Spatz, and Ralf Kemkemer. 2013. 'Cyclic Tensile Strain Controls Cell Shape and Directs Actin Stress Fiber Formation and Focal Adhesion Alignment in Spreading Cells.' Edited by Pontus Aspenstrom. *PloS One* 8 (10): e77328. https://doi.org/10.1371/journal.pone.0077328.

Gross, S. D., M S Schwab, A L Lewellyn, and J L Maller. 1999. 'Induction of Metaphase Arrest in Cleaving Xenopus Embryos by the Protein Kinase P90Rsk.' *Science* 286 (5443): 1365–67.

Gu, Changkyu, Suma Yaddanapudi, Astrid Weins, Teresia Osborn, Jochen Reiser, Martin Pollak, John Hartwig, and Sanja Sever. 2010. 'Direct Dynamin-Actin Interactions Regulate the Actin Cytoskeleton.' *The EMBO Journal* 29 (21): 3593–3606. https://doi.org/10.1038/emboj.2010.249.

Gu, Li-Hong, and Pierre A. Coulombe. 2007a. 'Keratin Expression Provides Novel Insight into the Morphogenesis and Function of the Companion Layer in Hair Follicles'. *Journal of Investigative Dermatology* 127 (5): 1061–73. https://doi.org/10.1038/SJ.JID.5700673.

Gu, Li-Hong, and Pierre A Coulombe. 2007b. 'Keratin Expression Provides Novel Insight into the Morphogenesis and Function of the Companion Layer in Hair Follicles.' *The Journal of Investigative Dermatology* 127 (5): 1061–73. https://doi.org/10.1038/sj.jid.5700673.

Guasch, Géraldine, Markus Schober, H Amalia Pasolli, Emily Belmont Conn, Lisa

Polak, and Elaine Fuchs. 2007. ‘Loss of TGFbeta Signaling Destabilizes Homeostasis and Promotes Squamous Cell Carcinomas in Stratified Epithelia.’ *Cancer Cell* 12 (4): 313–27. https://doi.org/10.1016/j.ccr.2007.08.020.

Gullberg, Donald E, and Evy Lundgren-Akerlund. 2002. ‘Collagen-Binding I Domain Integrins--What Do They Do?’ *Progress in Histochemistry and Cytochemistry* 37 (1): 3–54. https://doi.org/10.1016/S0079-6336(02)80008-0.

Guo, L, L Degenstein, and E Fuchs. 1996. ‘Keratinocyte Growth Factor Is Required for Hair Development but Not for Wound Healing.’ *Genes & Development* 10 (2): 165–75.

Gupta, Prerak, Gautham Hari Narayana S. N., Uvanesh Kasiviswanathan, Tarun Agarwal, Senthilguru K., Devdeep Mukhopadhyay, Kunal Pal, Supratim Giri, Tapas K. Maiti, and Indranil Banerjee. 2016. ‘Substrate Stiffness Does Affect the Fate of Human Keratinocytes’. *RSC Advances* 6 (5): 3539–51. https://doi.org/10.1039/C5RA19947F.

Gutkind, J S. 2000. ‘Regulation of Mitogen-Activated Protein Kinase Signaling Networks by G Protein-Coupled Receptors.’ *Science’s STKE : Signal Transduction Knowledge Environment* 2000 (40): re1. https://doi.org/10.1126/stke.2000.40.re1.

Gutkind, S J. 2000. ‘Regulation of Mitogen-Activated Protein Kinase Signalling Networks by G-Protein Coupled Receptors [Online] Http://Www.Stke.Org/Cgi/Content/Full/OC_sigtrans;2000/40/Re1’.

Gwak, Jungsug, Sun Gwan Hwang, Hyung-Soon Park, Sang Rak Choi, Sun-Hee Park, Hyunjoon Kim, Nam-Chul Ha, et al. 2012. ‘Small Molecule-Based Disruption of the Axin/β-Catenin Protein Complex Regulates Mesenchymal Stem Cell Differentiation’. *Cell Research* 22 (1): 237–47. https://doi.org/10.1038/cr.2011.127.

Haase, Kristina, and Andrew E Pelling. 2015. ‘Investigating Cell Mechanics with Atomic Force Microscopy.’ *Journal of the Royal Society, Interface* 12 (104): 20140970. https://doi.org/10.1098/rsif.2014.0970.

Hamill, Kevin J., Susan B. Hopkinson, Philip DeBiase, and Jonathan C.R. Jones.

2009. ‘BPAG1e Maintains Keratinocyte Polarity through B4 Integrin–Mediated Modulation of Rac 1 and Cofilin Activities’. Edited by Jean E. Schwarzbauer. *Molecular Biology of the Cell* 20 (12): 2954–62. https://doi.org/10.1091/mbc.e09-01-0051.

Hanakawa, Yasushi, Hong Li, Chenyan Lin, John R Stanley, and George Cotsarelis. 2004. ‘Desmogleins 1 and 3 in the Companion Layer Anchor Mouse Anagen Hair to the Follicle.’ *The Journal of Investigative Dermatology* 123 (5): 817–22. https://doi.org/10.1111/j.0022-202X.2004.23479.x.

Hanks, Steven K., and Thomas R. Polte. 1997. ‘Signaling through Focal Adhesion Kinase’. *BioEssays* 19 (2): 137–45. https://doi.org/10.1002/bies.950190208.

Hao, Jin, Yueling Zhang, Yating Wang, Rui Ye, Jingyi Qiu, Zhihe Zhao, and Juan Li. 2014. ‘Role of Extracellular Matrix and YAP/TAZ in Cell Fate Determination’. *Cellular Signalling* 26 (2): 186–91.

Haque, Farhana, David J Lloyd, Dawn T Smallwood, Carolyn L Dent, Catherine M Shanahan, Andrew M Fry, Richard C Trembath, and Sue Shackleton. 2006. ‘SUN1 Interacts with Nuclear Lamin A and Cytoplasmic Nesprins to Provide a Physical Connection between the Nuclear Lamina and the Cytoskeleton.’ *Molecular and Cellular Biology* 26 (10): 3738–51. https://doi.org/10.1128/MCB.26.10.3738-3751.2006.

Haque, Farhana, Daniela Mazzeo, Jennifer T Patel, Dawn T Smallwood, Juliet A Ellis, Catherine M Shanahan, and Sue Shackleton. 2010. ‘Mammalian SUN Protein Interaction Networks at the Inner Nuclear Membrane and Their Role in Laminopathy Disease Processes.’ *The Journal of Biological Chemistry* 285 (5): 3487–98. https://doi.org/10.1074/jbc.M109.071910.

Haystead, T. A. J., A. T. R. Sim, D. Carling, R. C. Honnor, Y. Tsukitani, P. Cohen, and D. G. Hardie. 1989. ‘Effects of the Tumour Promoter Okadaic Acid on Intracellular Protein Phosphorylation and Metabolism’. *Nature* 337 (6202): 78–81. https://doi.org/10.1038/337078a0.

Heidari, Fatemeh, Abazar Yari, Homa Rasoolijazi, Mansoureh Soleimani, Ahmadreza Dehpoor, Nayereh Sajedi, Sanaz Joulai Veijouye, and Maliheh Nobakht. 2016. ‘Bulge Hair Follicle Stem Cells Accelerate Cutaneous Wound Healing in Rats.’

Wounds : A Compendium of Clinical Research and Practice 28 (4): 132–41.

Hellström, Martin, Sten Hellström, Anna Engström-Laurent, and Ulf Bertheim. 2014. 'The Structure of the Basement Membrane Zone Differs between Keloids, Hypertrophic Scars and Normal Skin: A Possible Background to an Impaired Function.' *Journal of Plastic, Reconstructive & Aesthetic Surgery : JPRAS* 67 (11): 1564–72. https://doi.org/10.1016/j.bjps.2014.06.014.

Herskowitz, Ira. 1995. 'MAP Kinase Pathways in Yeast: For Mating and More.' *Cell* 80 (2): 187–97. https://doi.org/10.1016/0092-8674(95)90402-6.

Heuke, S, N Vogler, T Meyer, D Akimov, F Kluschke, H-J Röwert-Huber, J Lademann, B Dietzek, and J Popp. 2013. 'Multimodal Mapping of Human Skin.' *The British Journal of Dermatology* 169 (4): 794–803. https://doi.org/10.1111/bjd.12427.

Hofmann, Hans, Tilman Voss, Klaus K??hn, and J??rgen Engel. 1984. 'Localization of Flexible Sites in Thread-like Molecules from Electron Micrographs. Comparison of Interstitial, Basement Membrane and Intima Collagens'. *Journal of Molecular Biology* 172 (3): 325–43. https://doi.org/10.1016/S0022-2836(84)80029-7.

Hohl, D. 1990. 'Cornified Cell Envelope.' *Dermatologica* 180 (4): 201–11.

Hong, Zhigang, Jésus A. Cabrera, Saswati Mahapatra, Shelby Kutty, E. Kenneth Weir, and Stephen L. Archer. 2014. 'Activation of the EGFR/P38/JNK Pathway by Mitochondrial-Derived Hydrogen Peroxide Contributes to Oxygen-Induced Contraction of Ductus Arteriosus'. *Journal of Molecular Medicine* 92 (9): 995–1007. https://doi.org/10.1007/s00109-014-1162-1.

Horsley, Valerie, Antonios O Aliprantis, Lisa Polak, Laurie H Glimcher, and Elaine Fuchs. 2008. 'NFATc1 Balances Quiescence and Proliferation of Skin Stem Cells.' *Cell* 132 (2): 299–310. https://doi.org/10.1016/j.cell.2007.11.047.

Hsu, Chao-Kai, Hsi-Hui Lin, Hans I-Chen Harn, Michael W. Hughes, Ming-Jer Tang, and Chao-Chun Yang. 2018. 'Mechanical Forces in Skin Disorders'. *Journal of Dermatological Science* 90 (3): 232–40. https://doi.org/10.1016/J.JDERMSCI.2018.03.004.

Hsu, Ya-Chieh, H. Amalia Pasolli, and Elaine Fuchs. 2011a. 'Dynamics between Stem Cells, Niche, and Progeny in the Hair Follicle'. *Cell* 144 (1): 92–105. https://doi.org/10.1016/J.CELL.2010.11.049.

Hsu, Ya-Chieh, H Amalia Pasolli, and Elaine Fuchs. 2011b. 'Dynamics between Stem Cells, Niche, and Progeny in the Hair Follicle.' *Cell* 144 (1): 92–105. https://doi.org/10.1016/j.cell.2010.11.049.

Huang, Shaohui, Ahmed A Heikal, and Watt W Webb. 2002. 'Two-Photon Fluorescence Spectroscopy and Microscopy of NAD(P)H and Flavoprotein.' *Biophysical Journal* 82 (5): 2811–25. https://doi.org/10.1016/S0006-3495(02)75621-X.

Huber, O, R Korn, J McLaughlin, M Ohsugi, B G Herrmann, and R Kemler. 1996. 'Nuclear Localization of Beta-Catenin by Interaction with Transcription Factor LEF-1.' *Mechanisms of Development* 59 (1): 3–10.

Hubmacher, Dirk, Kerstin Tiedemann, and Dieter P Reinhardt. 2006. 'Fibrillins: From Biogenesis of Microfibrils to Signaling Functions.' *Current Topics in Developmental Biology* 75 (January): 93–123. https://doi.org/10.1016/S0070-2153(06)75004-9.

Huebsch, N, PR Arany, AS Mao, D Shvartsman - Nature materials, and undefined 2010. n.d. 'Harnessing Traction-Mediated Manipulation of the Cell/Matrix Interface to Control Stem-Cell Fate'. *Nature.Com*.

Huelsken, Joerg, Juergen Behrens, Soung Hoo Jeon, Jung-Soo Lee, and Kang-Yell Choi. 2002. 'The Wnt Signalling Pathway.' *Journal of Cell Science* 115 (Pt 21): 3977–78. https://doi.org/10.1242/jcs.00089.

Huelsken, Joerg, Regina Vogel, Bettina Erdmann, George Cotsarelis, and Walter Birchmeier. 2001. 'β-Catenin Controls Hair Follicle Morphogenesis and Stem Cell Differentiation in the Skin'. *Cell* 105 (4): 533–45. https://doi.org/10.1016/S0092-8674(01)00336-1.

Huh, Won-Ki, James V Falvo, Luke C Gerke, Adam S Carroll, Russell W Howson, Jonathan S Weissman, and Erin K O'Shea. 2003. 'Global Analysis of Protein Localization in Budding Yeast.' *Nature* 425 (6959): 686–91.

https://doi.org/10.1038/nature02026.

Hyytiäinen, Marko, Carita Penttinen, and Jorma Keski-Oja. 2004. 'Latent TGF-β Binding Proteins: Extracellular Matrix Association and Roles in TGF-β Activation'. *Critical Reviews in Clinical Laboratory Sciences* 41 (3): 233–64. https://doi.org/10.1080/10408360490460933.

Ibrahim, L, and E A Wright. 1982. 'A Quantitative Study of Hair Growth Using Mouse and Rat Vibrissal Follicles. I. Dermal Papilla Volume Determines Hair Volume.' *Journal of Embryology and Experimental Morphology* 72 (December): 209–24.

Ibrahim, Sherif Abdelaziz, Hebatallah Hassan, and Martin Götte. 2014. 'MicroRNA-Dependent Targeting of the Extracellular Matrix as a Mechanism of Regulating Cell Behavior'. *Biochimica et Biophysica Acta (BBA) - General Subjects*.

Ilić, D, Y Furuta, S Kanazawa, N Takeda, K Sobue, N Nakatsuji, S Nomura, J Fujimoto, M Okada, and T Yamamoto. 1995. 'Reduced Cell Motility and Enhanced Focal Adhesion Contact Formation in Cells from FAK-Deficient Mice.' *Nature* 377 (6549): 539–44. https://doi.org/10.1038/377539a0.

Ip, Y Tony, and Roger J Davis. 1998. 'Signal Transduction by the C-Jun N-Terminal Kinase (JNK) — from Inflammation to Development'. *Current Opinion in Cell Biology* 10 (2): 205–19. https://doi.org/10.1016/S0955-0674(98)80143-9.

Ishida, T, T E Peterson, N L Kovach, B C Berk, S. Kudoh, W. Zhu, T. Kadowaki, and Y. Yazaki. 1996. 'MAP Kinase Activation by Flow in Endothelial Cells. Role of Beta 1 Integrins and Tyrosine Kinases.' *Circulation Research* 79 (2): 310–16. https://doi.org/10.1161/01.res.79.2.310.

Ito, M. 1986. 'The Innermost Cell Layer of the Outer Root Sheath in Anagen Hair Follicle: Light and Electron Microscopic Study.' *Archives of Dermatological Research* 279 (2): 112–19.

———. 1988. 'Electron Microscopic Study on Cell Differentiation in Anagen Hair Follicles in Mice.' *The Journal of Investigative Dermatology* 90 (1): 65–72.

Ito, Mayumi, Kenji Kizawa, Kazuto Hamada, and George Cotsarelis. 2004. 'Hair Follicle Stem Cells in the Lower Bulge Form the Secondary Germ, a

Biochemically Distinct but Functionally Equivalent Progenitor Cell Population, at the Termination of Catagen.' *Differentiation; Research in Biological Diversity* 72 (9–10): 548–57. https://doi.org/10.1111/j.1432-0436.2004.07209008.x.

Ito, Mayumi, Yaping Liu, Zaixin Yang, Jane Nguyen, Fan Liang, Rebecca J Morris, and George Cotsarelis. 2005. 'Stem Cells in the Hair Follicle Bulge Contribute to Wound Repair but Not to Homeostasis of the Epidermis.' *Nature Medicine* 11 (12): 1351–54. https://doi.org/10.1038/nm1328.

Itoh, Toshiki, and Pietro De Camilli. 2006. 'BAR, F-BAR (EFC) and ENTH/ANTH Domains in the Regulation of Membrane-Cytosol Interfaces and Membrane Curvature.' *Biochimica et Biophysica Acta* 1761 (8): 897–912. https://doi.org/10.1016/j.bbalip.2006.06.015.

Jaalouk, Diana E., and Jan Lammerding. 2009. 'Mechanotransduction Gone Awry'. *Nature Reviews Molecular Cell Biology* 10 (1): 63–73. https://doi.org/10.1038/nrm2597.

Jaks, Viljar, Nick Barker, Maria Kasper, Johan H van Es, Hugo J Snippert, Hans Clevers, and Rune Toftgård. 2008. 'Lgr5 Marks Cycling, yet Long-Lived, Hair Follicle Stem Cells.' *Nature Genetics* 40 (11): 1291–99. https://doi.org/10.1038/ng.239.

Jamora, Colin, Ramanuj DasGupta, Pawel Kocieniewski, and Elaine Fuchs. 2003. 'Links between Signal Transduction, Transcription and Adhesion in Epithelial Bud Development.' *Nature* 422 (6929): 317–22. https://doi.org/10.1038/nature01458.

JH-C Wang, Review, and BP Thampatty. 2006. 'An Introductory Review of Cell Mechanobiology'. *Biomechan Model Mechanobiol* 5: 1–16. https://doi.org/10.1007/s10237-005-0012-z.

Jiang, Lichun, Long Wang, Champ P. Chen, Mei-Qing Li, and Xin-Hua Liao. 2017. 'Lgr6 Is Dispensable for Epidermal Cell Proliferation and Wound Repair'. *Experimental Dermatology* 26 (2): 105–7. https://doi.org/10.1111/exd.13187.

Jiao, Shi, Bingci Liu, Ai Gao, Meng Ye, Xiaowei Jia, Fengmei Zhang, Haifeng Liu, Xianglin Shi, and Chuanshu Huang. 2008. 'Benzo(a)Pyrene-Caused Increased

G1–S Transition Requires the Activation of c-Jun through P53-Dependent PI-3K/Akt/ERK Pathway in Human Embryo Lung Fibroblasts'. *Toxicology Letters* 178 (3): 167–75. https://doi.org/10.1016/J.TOXLET.2008.03.012.

Jones, Jonathan C.R., Susan B. Hopkinson, and Lawrence E. Goldfinger. 1998. 'Structure and Assembly of Hemidesmosomes'. *BioEssays* 20 (6): 488–94. https://doi.org/10.1002/(SICI)1521-1878(199806)20:6<488::AID-BIES7>3.0.CO;2-I.

Judah, David, Alena Rudkouskaya, Ryan Wilson, David E Carter, and Lina Dagnino. 2012. 'Multiple Roles of Integrin-Linked Kinase in Epidermal Development, Maturation and Pigmentation Revealed by Molecular Profiling.' *PloS One* 7 (5): e36704. https://doi.org/10.1371/journal.pone.0036704.

Kallunki, T, B Su, I Tsigelny, H K Sluss, B Dérijard, G Moore, R Davis, and M Karin. 1994. 'JNK2 Contains a Specificity-Determining Region Responsible for Efficient c-Jun Binding and Phosphorylation.' *Genes & Development* 8 (24): 2996–3007. https://doi.org/10.1101/gad.8.24.2996.

Kallunki, Tuula, Tiliang Deng, Masahiko Hibi, and Michael Karin. 1996. 'C-Jun Can Recruit JNK to Phosphorylate Dimerization Partners via Specific Docking Interactions.' *Cell* 87 (5): 929–39. https://doi.org/10.1016/S0092-8674(00)81999-6.

Ke, H., R. Harris, J. L. Coloff, J. Y. Jin, B. Leshin, P. M. de Marval, S. Tao, J. C. Rathmell, R. P. Hall, and J. Y. Zhang. 2010. 'The C-Jun NH2-Terminal Kinase 2 Plays a Dominant Role in Human Epidermal Neoplasia'. *Cancer Research* 70 (8): 3080–88. https://doi.org/10.1158/0008-5472.CAN-09-2923.

Keely, Patricia J., John K. Westwick, Ian P. Whitehead, Channing J. Der, and Leslie V. Parise. 1997. 'Cdc42 and Rac1 Induce Integrin-Mediated Cell Motility and Invasiveness through PI(3)K'. *Nature* 390 (6660): 632–36. https://doi.org/10.1038/37656.

Keyse, Stephen M. 2010. 'MAP Kinase Phosphatases'. In *Handbook of Cell Signaling*, 755–69. Elsevier. https://doi.org/10.1016/B978-0-12-374145-5.00097-8.

Khatau, S. B., C. M. Hale, P. J. Stewart-Hutchinson, M. S. Patel, C. L. Stewart, P. C. Searson, D. Hodzic, and D. Wirtz. 2009. 'A Perinuclear Actin Cap Regulates Nuclear Shape'. *Proceedings of the National Academy of Sciences* 106 (45): 19017–22. https://doi.org/10.1073/pnas.0908686106.

Kim, Eun Kyung, and Eui-Ju Choi. 2010. 'Pathological Roles of MAPK Signaling Pathways in Human Diseases'. *Biochimica et Biophysica Acta (BBA) - Molecular Basis of Disease* 1802 (4): 396–405. https://doi.org/10.1016/J.BBADIS.2009.12.009.

Kim, O.V., R.I. Litvinov, J. Chen, D.Z. Chen, J.W. Weisel, and M.S. Alber. 2017. 'Compression-Induced Structural and Mechanical Changes of Fibrin-Collagen Composites'. *Matrix Biology* 60–61 (July): 141–56. https://doi.org/10.1016/J.MATBIO.2016.10.007.

Kim, Soo-Hyun, Jeremy Turnbull, and Scott Guimond. 2011. 'Extracellular Matrix and Cell Signalling: The Dynamic Cooperation of Integrin, Proteoglycan and Growth Factor Receptor.' *The Journal of Endocrinology* 209 (2): 139–51. https://doi.org/10.1530/JOE-10-0377.

Kippenberger, S, A Bernd, S Loitsch, M Guschel, J Müller, J Bereiter-Hahn, and R Kaufmann. 2000. 'Signaling of Mechanical Stretch in Human Keratinocytes via MAP Kinases.' *The Journal of Investigative Dermatology* 114 (3): 408–12. https://doi.org/10.1046/j.1523-1747.2000.00915.x.

Kippenberger, Stefan, Stefan Loitsch, Maike Guschel, Jutta Müller, Yvonne Knies, Roland Kaufmann, and August Bernd. 2005. 'Mechanical Stretch Stimulates Protein Kinase B/Akt Phosphorylation in Epidermal Cells via Angiotensin II Type 1 Receptor and Epidermal Growth Factor Receptor'. *Journal of Biological Chemistry* 280 (4): 3060–67. https://doi.org/10.1074/jbc.M409590200.

Kippenberger, Stefan, Stefan Loitsch, Jutta Müller, Maike Guschel, Roland Kaufmann, and August Bernd. 2004. 'Ligation of the B4 Integrin Triggers Adhesion Behavior of Human Keratinocytes by an "Inside-out" Mechanism'. *Journal of Investigative Dermatology* 123 (3): 444–51. https://doi.org/10.1111/j.0022-202X.2004.23323.x.

Kirsch, AK, V Subramaniam, G Striker, C Schnetter - Biophysical journal, and

undefined 1998. n.d. ‘Continuous Wave Two-Photon Scanning near-Field Optical Microscopy’. *Elsevier*.

Kobielak, Krzysztof, H Amalia Pasolli, Laura Alonso, Lisa Polak, and Elaine Fuchs. 2003. ‘Defining BMP Functions in the Hair Follicle by Conditional Ablation of BMP Receptor IA.’ *The Journal of Cell Biology* 163 (3): 609–23. https://doi.org/10.1083/jcb.200309042.

Kobielak, Krzysztof, Nicole Stokes, June de la Cruz, Lisa Polak, and Elaine Fuchs. 2007. ‘Loss of a Quiescent Niche but Not Follicle Stem Cells in the Absence of Bone Morphogenetic Protein Signaling.’ *Proceedings of the National Academy of Sciences of the United States of America* 104 (24): 10063–68. https://doi.org/10.1073/pnas.0703004104.

Koegel, Heidi, Lukas von Tobel, Matthias Schäfer, Siegfried Alberti, Elisabeth Kremmer, Cornelia Mauch, Daniel Hohl, et al. 2009. ‘Loss of Serum Response Factor in Keratinocytes Results in Hyperproliferative Skin Disease in Mice’. *Journal of Clinical Investigation* 119 (4): 899–910. https://doi.org/10.1172/JCI37771.

Kohn, Wayne D, Cyril M Kay, and Robert S Hodges. 1997. ‘Salt Effects on Protein Stability: Two-Strandedα-Helical Coiled-Coils Containing Inter- or Intrahelical Ion Pairs’. *Journal of Molecular Biology* 267 (4): 1039–52. https://doi.org/10.1006/jmbi.1997.0930.

Kolch, Walter. 2005. ‘Coordinating ERK/MAPK Signalling through Scaffolds and Inhibitors’. *Nature Reviews Molecular Cell Biology* 6 (11): 827–37. https://doi.org/10.1038/nrm1743.

Koster, J., S. Van Wilpe, I. Kuikman, S. H M Litjens, and A. Sonnenberg. 2004. ‘Role of Binding of Plectin to the Integrin B4 Subunit in the Assembly of Hemidesmosomes’ 15 (3): 1211–23. https://doi.org/10.1091/mbc.E03-09-0697.

Koster, J., S. van Wilpe, I. Kuikman, S.H.M. Litjens, and A. Sonnenberg. 2004. ‘Role of Binding of Plectin to the Integrin B4 Subunit in the Assembly of Hemidesmosomes’. *Molecular Biology of the Cell* 15 (3): 1211–23. https://doi.org/10.1091/mbc.e03-09-0697.

Koster, Maranke I., and Dennis R. Roop. 2007. ‘Mechanisms Regulating Epithelial Stratification’. *Annual Review of Cell and Developmental Biology* 23 (1): 93–113. https://doi.org/10.1146/annurev.cellbio.23.090506.123357.

Kourmouli, N, P A Theodoropoulos, G Dialynas, A Bakou, A S Politou, I G Cowell, P B Singh, and S D Georgatos. 2000. ‘Dynamic Associations of Heterochromatin Protein 1 with the Nuclear Envelope.’ *The EMBO Journal* 19 (23): 6558–68. https://doi.org/10.1093/emboj/19.23.6558.

Kowalczyk, Andrew P., Elayne A. Bornslaeger, Suzanne M. Norvell, Helena L. Palka, and Kathleen J. Green. 1998. ‘Desmosomes: Intercellular Adhesive Junctions Specialized for Attachment of Intermediate Filaments’. *International Review of Cytology* 185 (January): 237–302. https://doi.org/10.1016/S0074-7696(08)60153-9.

Koyama, Taro, Kazuhiro Kobayashi, Takanori Hama, Kasumi Murakami, and Rei Ogawa. 2016. ‘Standardized Scalp Massage Results in Increased Hair Thickness by Inducing Stretching Forces to Dermal Papilla Cells in the Subcutaneous Tissue.’ *Eplasty* 16: e8.

Kozel, Beth A., Brenda J. Rongish, Andras Czirok, Julia Zach, Charles D. Little, Elaine C. Davis, Russell H. Knutsen, Jessica E. Wagenseil, Marilyn A. Levy, and Robert P. Mecham. 2006. ‘Elastic Fiber Formation: A Dynamic View of Extracellular Matrix Assembly Using Timer Reporters.’ *Journal of Cellular Physiology* 207 (1): 87–96. https://doi.org/10.1002/jcp.20546.

Kramer, Ruth M., Edda F. Roberts, Suzane L. Um, Angelika G. Börsch-Haubold, Steve P. Watson, Matthew J. Fisher, and Joseph A. Jakubowski. 1996. ‘P38 Mitogen-Activated Protein Kinase Phosphorylates Cytosolic Phospholipase A $_2$ (CPLA $_2$) in Thrombin-Stimulated Platelets’. *Journal of Biological Chemistry* 271 (44): 27723–29. https://doi.org/10.1074/jbc.271.44.27723.

Kulessa, H, G Turk, and B L Hogan. 2000. ‘Inhibition of Bmp Signaling Affects Growth and Differentiation in the Anagen Hair Follicle.’ *The EMBO Journal* 19 (24): 6664–74. https://doi.org/10.1093/emboj/19.24.6664.

Kumar, Sanjay, Peter C. McDonnell, Rebecca J. Gum, Annalisa T. Hand, John C. Lee, and Peter R. Young. 1997. ‘Novel Homologues of CSBP/P38 MAP Kinase:

Activation, Substrate Specificity and Sensitivity to Inhibition by Pyridinyl Imidazoles'. *Biochemical and Biophysical Research Communications* 235 (3): 533–38. https://doi.org/10.1006/bbrc.1997.6849.

Kuo, John. 2008. *Electron Microscopy*. https://doi.org/10.1007/978-1-60327-375-6_54.

Laiho, Lily H., Serge Pelet, Thomas M. Hancewicz, Peter D. Kaplan, and Peter T. C. So. 2005. 'Two-Photon 3-D Mapping of Ex Vivo Human Skin Endogenous Fluorescence Species Based on Fluorescence Emission Spectra'. *Journal of Biomedical Optics* 10 (2): 024016. https://doi.org/10.1117/1.1891370.

Lamarche, Nathalie, Nicolas Tapon, Lisa Stowers, Peter D Burbelo, Pontus Aspenström, Tina Bridges, John Chant, and Alan Hall. 1996. 'Rac and Cdc42 Induce Actin Polymerization and G1 Cell Cycle Progression Independently of P65PAK and the JNK/SAPK MAP Kinase Cascade'. *Cell* 87 (3): 519–29. https://doi.org/10.1016/S0092-8674(00)81371-9.

Langbein, Lutz, Michael a. Rogers, Silke Praetzel, Noriaki Aoki, Hermelita Winter, and Jürgen Schweizer. 2002. 'A Novel Epithelial Keratin, HK6irs1, Is Expressed Differentially in All Layers of the Inner Root Sheath, Including Specialized Huxley Cells (Flügelzellen) of the Human Hair Follicle.' *The Journal of Investigative Dermatology* 118 (5): 789–99. https://doi.org/10.1046/j.1523-1747.2002.01711.x.

Langbein, Lutz, and Jürgen Schweizer. 2005a. 'Keratins of the Human Hair Follicle11This Article Is Dedicated with Gratitude to Werner W. Franke on the Occasion of His 65th Birthday. His Pioneering Work on Epithelial and Hair Keratins Has Been Pivotal to Our Own Investigations in This Field.' *International Review of Cytology* 243: 1–78.

———. 2005b. 'Keratins of the Human Hair Follicle.' *International Review of Cytology* 243 (January): 1–78. https://doi.org/10.1016/S0074-7696(05)43001-6.

Langbein, Lutz, Hiroshi Yoshida, Silke Praetzel-Wunder, David a Parry, and Juergen Schweizer. 2010. 'The Keratins of the Human Beard Hair Medulla: The Riddle in the Middle.' *The Journal of Investigative Dermatology* 130 (1): 55–73. https://doi.org/10.1038/jid.2009.192.

Lange, Dirk, Keiko Funa, Peter ten Dijke, Vladimir Botchkarev, Ralf Paus, and Uwe Wollina. 1998. 'SMAD3, SMAD4 and SMAD7 Expression during Murine Hair Follicle Development and Cycling'. *Journal of Dermatological Science* 16 (March): S75. https://doi.org/10.1016/S0923-1811(98)83447-6.

Lasa, M., K. R. Mahtani, A. Finch, G. Brewer, J. Saklatvala, and A. R. Clark. 2000. 'Regulation of Cyclooxygenase 2 MRNA Stability by the Mitogen-Activated Protein Kinase P38 Signaling Cascade.' *Mol. Cell. Biol.* 20 (12): 4265–74. https://doi.org/10.1128/MCB.20.12.4265-4274.2000.

Lechler, Terry, and Elaine Fuchs. 2005. 'Asymmetric Cell Divisions Promote Stratification and Differentiation of Mammalian Skin.' *Nature* 437 (7056): 275–80. https://doi.org/10.1038/nature03922.

Lee, Chang-Hun, Min-Sung Kim, Byung Min Chung, Daniel J Leahy, and Pierre A Coulombe. 2012. 'Structural Basis for Heteromeric Assembly and Perinuclear Organization of Keratin Filaments'. *Nature Structural & Molecular Biology* 19 (7): 707–15. https://doi.org/10.1038/nsmb.2330.

Lee, Kenneth K., Daniel Starr, Merav Cohen, Jun Liu, Min Han, Katherine L. Wilson, and Yosef Gruenbaum. 2002. 'Lamin-Dependent Localization of UNC-84, A Protein Required for Nuclear Migration in *Caenorhabditis Elegans*'. Edited by Judith Kimble. *Molecular Biology of the Cell* 13 (3): 892–901. https://doi.org/10.1091/mbc.01-06-0294.

Lee, Kyoung-Jin, Yuri Kim, Yeon Ho Yoo, Min-Seo Kim, Sun-Hee Lee, Chang-Gyum Kim, Kyeonghan Park, et al. 2017. 'CD99-Derived Agonist Ligands Inhibit Fibronectin-Induced Activation of B1 Integrin through the Protein Kinase A/SHP2/Extracellular Signal-Regulated Kinase/PTPN12/Focal Adhesion Kinase Signaling Pathway.' *Molecular and Cellular Biology* 37 (14): e00675-16. https://doi.org/10.1128/MCB.00675-16.

Lee, Moonsup, Hong Ji, Yasuhide Furuta, Jae-il Park, and Pierre D McCrea. 2014. 'P120-Catenin Regulates REST and CoREST, and Modulates Mouse Embryonic Stem Cell Differentiation.' *Journal of Cell Science* 127 (Pt 18): 4037–51. https://doi.org/10.1242/jcs.151944.

Lee, T.C., R.L. Kashyap, and C.N. Chu. 1994. 'Building Skeleton Models via 3-D

Medial Surface Axis Thinning Algorithms'. *CVGIP: Graphical Models and Image Processing* 56 (6): 462–78.

Legué, Emilie, and Jean-François Nicolas. 2005. 'Hair Follicle Renewal: Organization of Stem Cells in the Matrix and the Role of Stereotyped Lineages and Behaviors.' *Development (Cambridge, England)* 132 (18): 4143–54. https://doi.org/10.1242/dev.01975.

Levy, L, S Broad, D Diekmann, R D Evans, and F M Watt. 2000. 'Beta1 Integrins Regulate Keratinocyte Adhesion and Differentiation by Distinct Mechanisms.' *Molecular Biology of the Cell* 11 (2): 453–66.

Levy, Vered, Catherine Lindon, Brian D. Harfe, and Bruce A. Morgan. 2005. 'Distinct Stem Cell Populations Regenerate the Follicle and Interfollicular Epidermis'. *Developmental Cell* 9 (6): 855–61. https://doi.org/10.1016/J.DEVCEL.2005.11.003.

Li, Dong, Jiaxi Zhou, Farhan Chowdhury, Jianjun Cheng, Ning Wang, and Fei Wang. 2011. 'Role of Mechanical Factors in Fate Decisions of Stem Cells'. *Regenerative Medicine* 6 (2): 229–40. https://doi.org/10.2217/rme.11.2.

Li, L, L B Margolis, R Paus, and R M Hoffman. 1992. 'Hair Shaft Elongation, Follicle Growth, and Spontaneous Regression in Long-Term, Gelatin Sponge-Supported Histoculture of Human Scalp Skin.' *Proceedings of the National Academy of Sciences of the United States of America* 89 (18): 8764–68.

Li, Li, Steffany A.L. Bennett, and Lisheng Wang. 2012. 'Role of E-Cadherin and Other Cell Adhesion Molecules in Survival and Differentiation of Human Pluripotent Stem Cells'. *Cell Adhesion & Migration* 6 (1): 59–73. https://doi.org/10.4161/cam.19583.

Li, Stephen Yt, Dolores D Mruk, and C Yan Cheng. 2013. 'Focal Adhesion Kinase Is a Regulator of F-Actin Dynamics: New Insights from Studies in the Testis.' *Spermatogenesis* 3 (3): e25385. https://doi.org/10.4161/spmg.25385.

Li, Xing, Lin Zhang, Xinjuan Yin, Zhan Gao, Huanhuan Zhang, Xiaozhuan Liu, Xinjuan Pan, Ning Li, and Zengli Yu. 2014. 'Retinoic Acid Remodels Extracellular Matrix (ECM) of Cultured Human Fetal Palate Mesenchymal Cells

(HFPMCs) through down-Regulation of TGF-β/Smad Signaling'. *Toxicology Letters* 225 (2): 208–15.

Li, Yuan, Julia S. Chu, Kyle Kurpinski, Xian Li, Diana M. Bautista, Li Yang, K.-L. Paul Sung, and Song Li. 2011. 'Biophysical Regulation of Histone Acetylation in Mesenchymal Stem Cells'. *Biophysical Journal* 100 (8): 1902–9. https://doi.org/10.1016/J.BPJ.2011.03.008.

Lim, Xinhong, Si Hui Tan, Ka Lou Yu, Sophia Beng Hui Lim, and Roeland Nusse. 2016. 'Axin2 Marks Quiescent Hair Follicle Bulge Stem Cells That Are Maintained by Autocrine Wnt/β-Catenin Signaling.' *Proceedings of the National Academy of Sciences of the United States of America* 113 (11): E1498-505. https://doi.org/10.1073/pnas.1601599113.

Lin, Hsien-Yi, and Liang-Tung Yang. 2013. 'Differential Response of Epithelial Stem Cell Populations in Hair Follicles to TGF-β Signaling'. *Developmental Biology* 373 (2): 394–406.

List, K, and CC Haudenschild. 2002. 'Matriptase/MT-SP1 Is Required for Postnatal Survival, Epidermal Barrier Function, Hair Follicle Development, and Thymic Homeostasis'. *ONCOGENE*- ….

List, Karin, Roman Szabo, Alfredo Molinolo, Boye Schnack Nielsen, and Thomas H Bugge. 2006. 'Delineation of Matriptase Protein Expression by Enzymatic Gene Trapping Suggests Diverging Roles in Barrier Function, Hair Formation, and Squamous Cell Carcinogenesis.' *The American Journal of Pathology* 168 (5): 1513–25. https://doi.org/10.2353/ajpath.2006.051071.

Litjens, Sandy H.M., José M. de Pereda, and Arnoud Sonnenberg. 2006. 'Current Insights into the Formation and Breakdown of Hemidesmosomes'. *Trends in Cell Biology* 16 (7): 376–83. https://doi.org/10.1016/j.tcb.2006.05.004.

Liu, Feng, Mary Ann Sells, and Jonathan Chernoff. 1998. 'Protein Tyrosine Phosphatase 1B Negatively Regulates Integrin Signaling'. *Current Biology* 8 (3): 173-S2. https://doi.org/10.1016/S0960-9822(98)70066-1.

Liu, Shixuan, Miriam Bracha Ginzberg, Nish Patel, Marc Hild, Bosco Leung, Yen-Chi Chen, Zhengda Li, et al. 2017. 'Size Uniformity of Animal Cells Is Actively

Maintained by a P38 MAPK-Dependent Regulation of G1-Length'. *BioRxiv*, March, 119867. https://doi.org/10.1101/119867.

Lloyd, C. 1995. 'The Basal Keratin Network of Stratified Squamous Epithelia: Defining K15 Function in the Absence of K14'. *The Journal of Cell Biology* 129 (5): 1329–44. https://doi.org/10.1083/jcb.129.5.1329.

Lonsdale-Eccles, J D, K A Resing, R L Meek, and B A Dale. 1984. 'High-Molecular-Weight Precursor of Epidermal Filaggrin and Hypothesis for Its Tandem Repeating Structure.' *Biochemistry* 23 (6): 1239–45.

Loschke, Fanny, Melanie Homberg, and Thomas M. Magin. 2016. 'Keratin Isotypes Control Desmosome Stability and Dynamics through PKCα'. *Journal of Investigative Dermatology* 136 (1): 202–13. https://doi.org/10.1038/JID.2015.403.

Lough, Denver, Hui Dai, Mei Yang, Joel Reichensperger, Lisa Cox, Carrie Harrison, and Michael W Neumeister. 2013. 'Stimulation of the Follicular Bulge LGR5+ and LGR6+ Stem Cells with the Gut-Derived Human Alpha Defensin 5 Results in Decreased Bacterial Presence, Enhanced Wound Healing, and Hair Growth from Tissues Devoid of Adnexal Structures.' *Plastic and Reconstructive Surgery* 132 (5): 1159–71. https://doi.org/10.1097/PRS.0b013e3182a48af6.

Lovett, David B., Nandini Shekhar, Jeffrey A. Nickerson, Kyle J. Roux, and Tanmay P. Lele. 2013. 'Modulation of Nuclear Shape by Substrate Rigidity'. *Cellular and Molecular Bioengineering* 6 (2): 230–38. https://doi.org/10.1007/s12195-013-0270-2.

Lowry, William E, Cedric Blanpain, Jonathan A Nowak, Geraldine Guasch, Lisa Lewis, and Elaine Fuchs. 2005. 'Defining the Impact of Beta-Catenin/Tcf Transactivation on Epithelial Stem Cells.' *Genes & Development* 19 (13): 1596–1611. https://doi.org/10.1101/gad.1324905.

Lu, Wenshu, Maria Schneider, Sascha Neumann, Verena-Maren Jaeger, Surayya Taranum, Martina Munck, Sarah Cartwright, et al. 2012. 'Nesprin Interchain Associations Control Nuclear Size'. *Cellular and Molecular Life Sciences* 69 (20): 3493–3509. https://doi.org/10.1007/s00018-012-1034-1.

Lyman, S, A Gilmore, K Burridge, S Gidwitz, and G C White. 1997. 'Integrin-Mediated Activation of Focal Adhesion Kinase Is Independent of Focal Adhesion Formation or Integrin Activation. Studies with Activated and Inhibitory Beta3 Cytoplasmic Domain Mutants.' *The Journal of Biological Chemistry* 272 (36): 22538–47. https://doi.org/10.1074/JBC.272.36.22538.

M De Ruijter, Annemieke J, Albert H Van Gennip, Huib N Caron, Stephan Kemp, and B P Van Kuilenburg. 2003. 'Histone Deacetylases (HDACs) : Characterization of the Classical HDAC Family'. *Biochem. J* 370: 737–49.

MacDonald, Bryan T., Keiko Tamai, and Xi He. 2009. 'Wnt/β-Catenin Signaling: Components, Mechanisms, and Diseases'. *Developmental Cell* 17 (1): 9–26. https://doi.org/10.1016/J.DEVCEL.2009.06.016.

Machesky, L M, and A Hall. 1997. 'Role of Actin Polymerization and Adhesion to Extracellular Matrix in Rac- and Rho-Induced Cytoskeletal Reorganization.' *The Journal of Cell Biology* 138 (4): 913–26. https://doi.org/10.1083/JCB.138.4.913.

Mainiero, F, C Murgia, K K Wary, A M Curatola, A Pepe, M Blumemberg, J K Westwick, C J Der, and F G Giancotti. 1997. 'The Coupling of Alpha6beta4 Integrin to Ras-MAP Kinase Pathways Mediated by Shc Controls Keratinocyte Proliferation.' *The EMBO Journal* 16 (9): 2365–75. https://doi.org/10.1093/emboj/16.9.2365.

Makino, T., M. Jinnin, F.C. Muchemwa, S. Fukushima, H. Kogushi-Nishi, C. Moriya, T. Igata, A. Fujisawa, T. Johno, and H. Ihn. 2009. 'Basic Fibroblast Growth Factor Stimulates the Proliferation of Human Dermal Fibroblasts via the ERK1/2 and JNK Pathways'. *British Journal of Dermatology* 162 (4): 717–23. https://doi.org/10.1111/j.1365-2133.2009.09581.x.

Maniotis, A J, C S Chen, and D E Ingber. 1997. 'Demonstration of Mechanical Connections between Integrins, Cytoskeletal Filaments, and Nucleoplasm That Stabilize Nuclear Structure.' *Proceedings of the National Academy of Sciences of the United States of America* 94 (3): 849–54. https://doi.org/10.1073/PNAS.94.3.849.

Martín, Humberto, Marta Flández, César Nombela, and María Molina. 2005. 'Protein Phosphatases in MAPK Signalling: We Keep Learning from Yeast'. *Molecular*

Microbiology 58 (1): 6–16. https://doi.org/10.1111/j.1365-2958.2005.04822.x.

Massam-Wu, T., M. Chiu, R. Choudhury, S. S. Chaudhry, A. K. Baldwin, A. McGovern, C. Baldock, C. A. Shuttleworth, and C. M. Kielty. 2010. 'Assembly of Fibrillin Microfibrils Governs Extracellular Deposition of Latent TGF'. *Journal of Cell Science* 123 (17): 3006–18. https://doi.org/10.1242/jcs.073437.

Mater, David Van, Frank T Kolligs, Andrzej A Dlugosz, and Eric R Fearon. 2003. 'Transient Activation of Beta -Catenin Signaling in Cutaneous Keratinocytes Is Sufficient to Trigger the Active Growth Phase of the Hair Cycle in Mice.' *Genes & Development* 17 (10): 1219–24. https://doi.org/10.1101/gad.1076103.

Mateyak, M K, A J Obaya, and J M Sedivy. 1999. 'C-Myc Regulates Cyclin D-Cdk4 and -Cdk6 Activity but Affects Cell Cycle Progression at Multiple Independent Points.' *Molecular and Cellular Biology* 19 (7): 4672–83. https://doi.org/10.1128/MCB.19.7.4672.

Mazza, D., P. Bianchini, V. Caorsi, F. Cella, P. P. Mondal, E. Ronzitti, I. Testa, G. Vicidomini, and A. Diaspro. 2008. 'Non-Linear Microscopy'. In *Biophotonics*, 47–69. Berlin, Heidelberg: Springer Berlin Heidelberg. https://doi.org/10.1007/978-3-540-76782-4_4.

McBeath, Rowena, Dana M Pirone, Celeste M Nelson, Kiran Bhadriraju, and Christopher S Chen. 2004. 'Cell Shape, Cytoskeletal Tension, and RhoA Regulate Stem Cell Lineage Commitment.' *Developmental Cell* 6 (4): 483–95.

McGee, Matthew D., Regina Rillo, Amy S. Anderson, and Daniel A. Starr. 2006. 'UNC-83 Is a KASH Protein Required for Nuclear Migration and Is Recruited to the Outer Nuclear Membrane by a Physical Interaction with the SUN Protein UNC-84'. *Molecular Biology of the Cell* 17 (4): 1790–1801. https://doi.org/10.1091/mbc.e05-09-0894.

McGrath, John A., Biljana Gatalica, Angela M. Christiano, Kehua si, Katsushi Owaribe, James R. McMillan, Robin A.J. Eady, and Jouni Uitto. 1995. 'Mutations in the 180–KD Bullous Pemphigoid Antigen (BPAG2), a Hemidesmosomal Transmembrane Collagen (COL17A1), in Generalized Atrophic Benign Epidermolysis Bullosa'. *Nature Genetics* 11 (1): 83–86. https://doi.org/10.1038/ng0995-83.

Medhurst, Annette L, Daniël O Warmerdam, Ildem Akerman, Edward H Verwayen, Roland Kanaar, Veronique A J Smits, and Nicholas D Lakin. 2008. 'ATR and Rad17 Collaborate in Modulating Rad9 Localisation at Sites of DNA Damage.' *Journal of Cell Science* 121 (Pt 23): 3933–40. https://doi.org/10.1242/jcs.033688.

Mehic, Denis, Latifa Bakiri, Minoo Ghannadan, Erwin F. Wagner, and Erwin Tschachler. 2005. 'Fos and Jun Proteins Are Specifically Expressed During Differentiation of Human Keratinocytes'. *Journal of Investigative Dermatology* 124 (1): 212–20. https://doi.org/10.1111/j.0022-202X.2004.23558.x.

Merrill, B J, U Gat, R DasGupta, and E Fuchs. 2001. 'Tcf3 and Lef1 Regulate Lineage Differentiation of Multipotent Stem Cells in Skin.' *Genes & Development* 15 (13): 1688–1705. https://doi.org/10.1101/gad.891401.

Micallef, Ludovic, Françoise Belaubre, Aline Pinon, Chantal Jayat-Vignoles, Christiane Delage, Marie Charveron, and Alain Simon. 2009. 'Effects of Extracellular Calcium on the Growth-Differentiation Switch in Immortalized Keratinocyte HaCaT Cells Compared with Normal Human Keratinocytes.' *Experimental Dermatology* 18 (2): 143–51. https://doi.org/10.1111/j.1600-0625.2008.00775.x.

Michailovici, Inbal, Heather A Harrington, Hadar Hay Azogui, Yfat Yahalom-Ronen, Alexander Plotnikov, Saunders Ching, Michael P H Stumpf, Ophir D Klein, Rony Seger, and Eldad Tzahor. 2014. 'Nuclear to Cytoplasmic Shuttling of ERK Promotes Differentiation of Muscle Stem/Progenitor Cells.' *Development (Cambridge, England)* 141 (13): 2611–20. https://doi.org/10.1242/dev.107078.

Millar, Sarah E. 2002. 'Molecular Mechanisms Regulating Hair Follicle Development.' *The Journal of Investigative Dermatology* 118 (2): 216–25. https://doi.org/10.1046/j.0022-202x.2001.01670.x.

Minden, A, A Lin, M McMahon, C Lange-Carter, B Derijard, R. Davis, G. Johnson, and M Karin. 1994. 'Differential Activation of ERK and JNK Mitogen-Activated Protein Kinases by Raf-1 and MEKK'. *Science* 266 (5191): 1719–23. https://doi.org/10.1126/science.7992057.

Minden, A, A Lin, T Smeal, B Dérijard, M Cobb, R Davis, and M Karin. 1994. 'C-

Jun N-Terminal Phosphorylation Correlates with Activation of the JNK Subgroup but Not the ERK Subgroup of Mitogen-Activated Protein Kinases.' *Molecular and Cellular Biology* 14 (10): 6683–88. https://doi.org/10.1128/mcb.14.10.6683.

Ming Kwan, Kin, Allen G Li, Xiao-Jing Wang, Wolfgang Wurst, and Richard R Behringer. 2004. 'Essential Roles of BMPR-IA Signaling in Differentiation and Growth of Hair Follicles and in Skin Tumorigenesis.' *Genesis (New York, N.Y. : 2000)* 39 (1): 10–25. https://doi.org/10.1002/gene.20021.

Miralles, Francesc, Guido Posern, Alexia Ileana Zaromytidou, and Richard Treisman. 2003. 'Actin Dynamics Control SRF Activity by Regulation of Its Coactivator MAL'. *Cell* 113 (3): 329–42. https://doi.org/10.1016/S0092-8674(03)00278-2.

Mishima, Kenji, Kazuya Inoue, and Yoshio Hayashi. 2002. 'Overexpression of Extracellular-Signal Regulated Kinases on Oral Squamous Cell Carcinoma.' *Oral Oncology* 38 (5): 468–74.

Mishra, Ajay, Bénédicte Oulès, Angela Oliveira Pisco, Tony Ly, Kifayathullah Liakath-Ali, Gernot Walko, Priyalakshmi Viswanathan, et al. 2017. 'A Protein Phosphatase Network Controls the Temporal and Spatial Dynamics of Differentiation Commitment in Human Epidermis.' *ELife* 6 (October). https://doi.org/10.7554/eLife.27356.

Moreno-Layseca, Paulina, and Charles H. Streuli. 2014. 'Signalling Pathways Linking Integrins with Cell Cycle Progression'. *Matrix Biology* 34 (February): 144–53. https://doi.org/10.1016/J.MATBIO.2013.10.011.

Morishima, Nobuhiro. 1999. 'Changes in Nuclear Morphology during Apoptosis Correlate with Vimentin Cleavage by Different Caspases Located Either Upstream or Downstream of Bcl-2 Action'. *Genes to Cells* 4 (7): 401–14. https://doi.org/10.1046/j.1365-2443.1999.00270.x.

Moriya, Chikako, Masatoshi Jinnin, Keitaro Yamane, Keishi Maruo, Faith C. Muchemwa, Toshikatsu Igata, Takamitsu Makino, Satoshi Fukushima, and Hironobu Ihn. 2011. 'Expression of Matrix Metalloproteinase-13 Is Controlled by IL-13 via PI3K/Akt3 and PKC-δ in Normal Human Dermal Fibroblasts'. *Journal of Investigative Dermatology* 131 (3): 655–61.

https://doi.org/10.1038/jid.2010.361.

Morris, R J, and C S Potten. 1999. ‘Highly Persistent Label-Retaining Cells in the Hair Follicles of Mice and Their Fate Following Induction of Anagen.’ *The Journal of Investigative Dermatology* 112 (4): 470–75. https://doi.org/10.1046/j.1523-1747.1999.00537.x.

Morris, Rebecca J, Yaping Liu, Lee Marles, Zaixin Yang, Carol Trempus, Shulan Li, Jamie S Lin, Janet A Sawicki, and George Cotsarelis. 2004. ‘Capturing and Profiling Adult Hair Follicle Stem Cells.’ *Nature Biotechnology* 22 (4): 411–17. https://doi.org/10.1038/nbt950.

Muiznieks, Lisa D, and Fred W Keeley. 2010. ‘Proline Periodicity Modulates the Self-Assembly Properties of Elastin-like Polypeptides.’ *The Journal of Biological Chemistry* 285 (51): 39779–89. https://doi.org/10.1074/jbc.M110.164467.

———. 2013. ‘Molecular Assembly and Mechanical Properties of the Extracellular Matrix: A Fibrous Protein Perspective.’ *Biochimica et Biophysica Acta* 1832 (7): 866–75. https://doi.org/10.1016/j.bbadis.2012.11.022.

Müller-Röver, S, B Handjiski, C van der Veen, S Eichmüller, K Foitzik, I A McKay, K S Stenn, and R Paus. 2001. ‘A Comprehensive Guide for the Accurate Classification of Murine Hair Follicles in Distinct Hair Cycle Stages.’ *The Journal of Investigative Dermatology* 117 (1): 3–15. https://doi.org/10.1046/j.0022-202x.2001.01377.x.

Murao, K., Y. Kubo, N. Ohtani, E. Hara, and S. Arase. 2006. ‘Epigenetic Abnormalities in Cutaneous Squamous Cell Carcinomas: Frequent Inactivation of the RB1/P16 and P53 Pathways’. *British Journal of Dermatology* 155 (5): 999–1005. https://doi.org/10.1111/j.1365-2133.2006.07487.x.

Murthy, S, J F Crish, T M Zaim, and R L Eckert. 1993. ‘A Dual Role for Involucrin in the Epidermis-Ultrastructural Localization in Epidermis and Hair Follicle in Humans and Transgenic Mice.’ *Journal of Structural Biology* 111 (1): 68–76. https://doi.org/10.1006/jsbi.1993.1037.

Na, Renhua, Ida-Marie Stender, Lixin Ma, and Hans Christian Wulf. 2000.

‘Autofluorescence Spectrum of Skin: Component Bands and Body Site Variations’. *Skin Research and Technology* 6 (3): 112–17. https://doi.org/10.1034/j.1600-0846.2000.006003112.x.

Nanba, D, Y Hieda, and Y Nakanishi. 2000. ‘Remodeling of Desmosomal and Hemidesmosomal Adhesion Systems during Early Morphogenesis of Mouse Pelage Hair Follicles.’ *The Journal of Investigative Dermatology* 114 (1): 171–77. https://doi.org/10.1046/j.1523-1747.2000.00842.x.

Naylor, Elizabeth C, Rachel E B Watson, and Michael J Sherratt. 2011. ‘Molecular Aspects of Skin Ageing.’ *Maturitas* 69 (3): 249–56. https://doi.org/10.1016/j.maturitas.2011.04.011.

Nery, F. C., J. Zeng, B. P. Niland, J. Hewett, J. Farley, D. Irimia, Y. Li, G. Wiche, A. Sonnenberg, and X. O. Breakefield. 2008. ‘TorsinA Binds the KASH Domain of Nesprins and Participates in Linkage between Nuclear Envelope and Cytoskeleton’. *Journal of Cell Science* 121 (20): 3476–86. https://doi.org/10.1242/jcs.029454.

Nikolopoulos, S. N., P. Blaikie, T. Yoshioka, W. Guo, C. Puri, C. Tacchetti, and F. G. Giancotti. 2005. ‘Targeted Deletion of the Integrin 4 Signaling Domain Suppresses Laminin-5-Dependent Nuclear Entry of Mitogen-Activated Protein Kinases and NF- B, Causing Defects in Epidermal Growth and Migration’. *Molecular and Cellular Biology* 25 (14): 6090–6102. https://doi.org/10.1128/MCB.25.14.6090-6102.2005.

Nobes, Catherine D., and Alan Hall. 1999. ‘Rho GTPases Control Polarity, Protrusion, and Adhesion during Cell Movement’. *The Journal of Cell Biology* 144 (6): 1235–44. https://doi.org/10.1083/jcb.144.6.1235.

Novak, A, S C Hsu, C Leung-Hagesteijn, G Radeva, J Papkoff, R Montesano, C Roskelley, R Grosschedl, and S Dedhar. 1998. ‘Cell Adhesion and the Integrin-Linked Kinase Regulate the LEF-1 and Beta-Catenin Signaling Pathways.’ *Proceedings of the National Academy of Sciences of the United States of America* 95 (8): 4374–79. https://doi.org/10.1073/PNAS.95.8.4374.

Nowak, Jonathan A, Lisa Polak, H Amalia Pasolli, and Elaine Fuchs. 2008. ‘Hair Follicle Stem Cells Are Specified and Function in Early Skin Morphogenesis.’

Cell Stem Cell 3 (1): 33–43. https://doi.org/10.1016/j.stem.2008.05.009.

Ohyama, Manabu, Atsushi Terunuma, Christine L Tock, Michael F Radonovich, Cynthia A Pise-Masison, Steven B Hopping, John N Brady, Mark C Udey, and Jonathan C Vogel. 2006. 'Characterization and Isolation of Stem Cell-Enriched Human Hair Follicle Bulge Cells.' *The Journal of Clinical Investigation* 116 (1): 249–60. https://doi.org/10.1172/JCI26043.

Olson, Eric N, and Alfred Nordheim. 2010a. 'Linking Actin Dynamics and Gene Transcription to Drive Cellular Motile Functions.' *Nature Reviews. Molecular Cell Biology* 11 (5): 353–65. https://doi.org/10.1038/nrm2890.

———. 2010b. 'Linking Actin Dynamics and Gene Transcription to Drive Cellular Motile Functions.' *Nature Reviews. Molecular Cell Biology* 11 (5): 353–65.

Oshima, H, A Rochat, C Kedzia, K Kobayashi, and Y Barrandon. 2001. 'Morphogenesis and Renewal of Hair Follicles from Adult Multipotent Stem Cells.' *Cell* 104 (2): 233–45.

Oshimori, Naoki, and Elaine Fuchs. 2012. 'Paracrine TGF-β Signaling Counterbalances BMP-Mediated Repression in Hair Follicle Stem Cell Activation.' *Cell Stem Cell* 10 (1): 63–75. https://doi.org/10.1016/j.stem.2011.11.005.

Osmanagic-Myers, Selma, Martin Gregor, Gernot Walko, Gerald Burgstaller, Siegfried Reipert, and Gerhard Wiche. 2006. 'Plectin-Controlled Keratin Cytoarchitecture Affects MAP Kinases Involved in Cellular Stress Response and Migration'. *The Journal of Cell Biology* 174 (4): 557–68. https://doi.org/10.1083/jcb.200605172.

Osorio, Daniel S., and Edgar R. Gomes. 2014. 'Connecting the Nucleus to the Cytoskeleton for Nuclear Positioning and Cell Migration'. In , 505–20. https://doi.org/10.1007/978-1-4899-8032-8_23.

Ostlund, Cecilia, Eric S Folker, Jason C Choi, Edgar R Gomes, Gregg G Gundersen, and Howard J Worman. 2009. 'Dynamics and Molecular Interactions of Linker of Nucleoskeleton and Cytoskeleton (LINC) Complex Proteins.' *Journal of Cell Science* 122 (Pt 22): 4099–4108. https://doi.org/10.1242/jcs.057075.

Ouspenskaia, Tamara, Irina Matos, Aaron F. Mertz, Vincent F. Fiore, and Elaine Fuchs. 2016. 'WNT-SHH Antagonism Specifies and Expands Stem Cells Prior to Niche Formation'. *Cell* 164 (1–2): 156–69. https://doi.org/10.1016/J.CELL.2015.11.058.

Ozawa, Toshiyuki, Daisuke Tsuruta, Jonathan C.R. Jones, Masamitsu Ishii, Kazuo Ikeda, Teruichi Harada, Yumi Aoyama, Akira Kawada, and Hiromi Kobayashi. 2010. 'Dynamic Relationship of Focal Contacts and Hemidesmosome Protein Complexes in Live Cells'. *Journal of Investigative Dermatology* 130 (6): 1624–35. https://doi.org/10.1038/jid.2009.439.

Padmakumar, V C, Thorsten Libotte, Wenshu Lu, Hafida Zaim, Sabu Abraham, Angelika A Noegel, Josef Gotzmann, Roland Foisner, and Iakowos Karakesisoglou. 2005. 'The Inner Nuclear Membrane Protein Sun1 Mediates the Anchorage of Nesprin-2 to the Nuclear Envelope.' *Journal of Cell Science* 118 (Pt 15): 3419–30. https://doi.org/10.1242/jcs.02471.

Palmer, A, A C Gavin, and A R Nebreda. 1998. 'A Link between MAP Kinase and P34(Cdc2)/Cyclin B during Oocyte Maturation: P90(Rsk) Phosphorylates and Inactivates the P34(Cdc2) Inhibitory Kinase Myt1.' *Embo J.* 17 (17): 5037–47. https://doi.org/10.1093/emboj/17.17.5037.

Palomares, Kristy T. Salisbury, Ryan E. Gleason, Zachary D. Mason, Dennis M. Cullinane, Thomas A. Einhorn, Louis C. Gerstenfeld, and Elise F. Morgan. 2009. 'Mechanical Stimulation Alters Tissue Differentiation and Molecular Expression during Bone Healing'. *Journal of Orthopaedic Research* 27 (9): 1123–32. https://doi.org/10.1002/jor.20863.

Pankov, R, E Cukierman, B Z Katz, K Matsumoto, D C Lin, S Lin, C Hahn, and K M Yamada. 2000. 'Integrin Dynamics and Matrix Assembly: Tensin-Dependent Translocation of Alpha(5)Beta(1) Integrins Promotes Early Fibronectin Fibrillogenesis.' *The Journal of Cell Biology* 148 (5): 1075–90. https://doi.org/10.1083/jcb.148.5.1075.

Park, Jae-il, Si Wan Kim, Jon P. Lyons, Hong Ji, Thi T. Nguyen, Kyucheol Cho, Michelle C. Barton, Tom Deroo, Kris Vleminckx, and Pierre D. McCrea. 2005. 'Kaiso/P120-Catenin and TCF/β-Catenin Complexes Coordinately Regulate

Canonical Wnt Gene Targets'. *Developmental Cell* 8 (6): 843–54. https://doi.org/10.1016/J.DEVCEL.2005.04.010.

Paszek, Matthew J., David Boettiger, Valerie M. Weaver, and Daniel A. Hammer. 2009. 'Integrin Clustering Is Driven by Mechanical Resistance from the Glycocalyx and the Substrate'. Edited by Douglas Lauffenberger. *PLoS Computational Biology* 5 (12): e1000604. https://doi.org/10.1371/journal.pcbi.1000604.

Paus, R, S Müller-Röver, C Van Der Veen, M Maurer, S Eichmüller, G Ling, U Hofmann, K Foitzik, L Mecklenburg, and B Handjiski. 1999. 'A Comprehensive Guide for the Recognition and Classification of Distinct Stages of Hair Follicle Morphogenesis.' *The Journal of Investigative Dermatology* 113 (4): 523–32. https://doi.org/10.1046/j.1523-1747.1999.00740.x.

Paus, R, K S Stenn, and R E Link. 1989. 'The Induction of Anagen Hair Growth in Telogen Mouse Skin by Cyclosporine A Administration.' *Laboratory Investigation; a Journal of Technical Methods and Pathology* 60 (3): 365–69.

Pena, A.-M., M. Strupler, T. Boulesteix, and M.-C. Schanne-Klein. 2005. 'Spectroscopic Analysis of Keratin Endogenous Signal for Skin Multiphoton Microscopy'. *Optics Express* 13 (16): 6268. https://doi.org/10.1364/OPEX.13.006268.

Pereda, José M de, M Pilar Lillo, and Arnoud Sonnenberg. 2009. 'Structural Basis of the Interaction between Integrin A6β4 and Plectin at the Hemidesmosomes'. *The EMBO Journal* 28 (8): 1180–90. https://doi.org/10.1038/emboj.2009.48.

Peters, Eva M J, Marit G Hansen, Rupert W Overall, Motonobu Nakamura, Paolo Pertile, Burghard F Klapp, Petra C Arck, and Ralf Paus. 2005. 'Control of Human Hair Growth by Neurotrophins: Brain-Derived Neurotrophic Factor Inhibits Hair Shaft Elongation, Induces Catagen, and Stimulates Follicular Transforming Growth Factor Beta2 Expression.' *The Journal of Investigative Dermatology* 124 (4): 675–85. https://doi.org/10.1111/j.0022-202X.2005.23648.x.

Petiot, Anita, Francesco J A Conti, Richard Grose, Jean-Michel Revest, Kairbaan M Hodivala-Dilke, and Clive Dickson. 2003. 'A Crucial Role for Fgfr2-IIIb

Signalling in Epidermal Development and Hair Follicle Patterning.' *Development (Cambridge, England)* 130 (22): 5493–5501. https://doi.org/10.1242/dev.00788.

Philpott, M P, M R Green, and T Kealey. 1990. 'Human Hair Growth in Vitro.' *Journal of Cell Science* 97 (Pt 3) (November): 463–71.

Plikus, Maksim V, Julie Ann Mayer, Damon de la Cruz, Ruth E Baker, Philip K Maini, Robert Maxson, and Cheng-Ming Chuong. 2008. 'Cyclic Dermal BMP Signalling Regulates Stem Cell Activation during Hair Regeneration.' *Nature* 451 (7176): 340–44. https://doi.org/10.1038/nature06457.

Polte, T R, and S K Hanks. 1997. 'Complexes of Focal Adhesion Kinase (FAK) and Crk-Associated Substrate (P130(Cas)) Are Elevated in Cytoskeleton-Associated Fractions Following Adhesion and Src Transformation. Requirements for Src Kinase Activity and FAK Proline-Rich Motifs.' *The Journal of Biological Chemistry* 272 (9): 5501–9. https://doi.org/10.1074/JBC.272.9.5501.

Posthaus, Horst, Lina Williamson, Dominique Baumann, Rolf Kemler, Reto Caldelari, Maja M Suter, Heinz Schwarz, and Eliane Müller. 2002. 'Beta-Catenin Is Not Required for Proliferation and Differentiation of Epidermal Mouse Keratinocytes.' *Journal of Cell Science* 115 (Pt 23): 4587–95. https://doi.org/10.1242/jcs.00141.

Pozzi, A, K K Wary, F G Giancotti, and H A Gardner. 1998. 'Integrin Alpha1beta1 Mediates a Unique Collagen-Dependent Proliferation Pathway in Vivo.' *The Journal of Cell Biology* 142 (2): 587–94. https://doi.org/10.1083/JCB.142.2.587.

Qian, Rui-Qing, and Robert W. Glanville. 1997. 'Alignment of Fibrillin Molecules in Elastic Microfibrils Is Defined by Transglutaminase-Derived Cross-Links'. *Biochemistry* 36 (50): 15841–47. https://doi.org/10.1021/bi971036f.

Rabbani, Piul, Makoto Takeo, Weichin Chou, Peggy Myung, Marcus Bosenberg, Lynda Chin, M Mark Taketo, and Mayumi Ito. 2011. 'Coordinated Activation of Wnt in Epithelial and Melanocyte Stem Cells Initiates Pigmented Hair Regeneration.' *Cell* 145 (6): 941–55. https://doi.org/10.1016/j.cell.2011.05.004.

Rabinovitz, Isaac, and Arthur M. Mercurio. 1997. 'The Integrin A6β4 Functions in

Carcinoma Cell Migration on Laminin-1 by Mediating the Formation and Stabilization of Actin-Containing Motility Structures'. *The Journal of Cell Biology* 139 (7): 1873–84. https://doi.org/10.1083/jcb.139.7.1873.

Raghavan, Srikala, Alec Vaezi, and Elaine Fuchs. 2003. 'A Role for Alphabeta1 Integrins in Focal Adhesion Function and Polarized Cytoskeletal Dynamics.' *Developmental Cell* 5 (3): 415–27.

Ramirez, Francesco, and Daniel B Rifkin. 2009. 'Extracellular Microfibrils: Contextual Platforms for TGFbeta and BMP Signaling.' *Current Opinion in Cell Biology* 21 (5): 616–22. https://doi.org/10.1016/j.ceb.2009.05.005.

Ramirez, Francesco, and Lynn Y. Sakai. 2010. 'Biogenesis and Function of Fibrillin Assemblies'. *Cell and Tissue Research* 339 (1): 71–82. https://doi.org/10.1007/s00441-009-0822-x.

Rao, Tata Purushothama, and Michael Kühl. 2010. 'An Updated Overview on Wnt Signaling Pathways: A Prelude for More.' *Circulation Research* 106 (12): 1798–1806. https://doi.org/10.1161/CIRCRESAHA.110.219840.

Rauscher, Sarah, and Régis Pomès. 2012. 'Structural Disorder and Protein Elasticity.' *Advances in Experimental Medicine and Biology* 725 (January): 159–83. https://doi.org/10.1007/978-1-4614-0659-4_10.

Raymond, K., Maaike Kreft, Hans Janssen, Jero Calafat, and Arnoud Sonnenberg. 2005. 'Keratinocytes Display Normal Proliferation, Survival and Differentiation in Conditional 4-Integrin Knockout Mice'. *Journal of Cell Science* 118 (5): 1045–60. https://doi.org/10.1242/jcs.01689.

Reddy, S, T Andl, A Bagasra, M M Lu, D J Epstein, E E Morrisey, and S E Millar. 2001. 'Characterization of Wnt Gene Expression in Developing and Postnatal Hair Follicles and Identification of Wnt5a as a Target of Sonic Hedgehog in Hair Follicle Morphogenesis.' *Mechanisms of Development* 107 (1–2): 69–82.

Rich, Alexander, U S A And, and F H C Crick. 1961. 'The Molecular Structure of Collagen'. *Journal of Molecular Biology* 3: 483–506, IN1–4. https://doi.org/10.1016/S0022-2836(61)80016-8.

Richardson, Gavin D, Hisham Bazzi, Katherine A Fantauzzo, James M Waters,

Heather Crawford, Phil Hynd, Angela M Christiano, and Colin A B Jahoda. 2009. 'KGF and EGF Signalling Block Hair Follicle Induction and Promote Interfollicular Epidermal Fate in Developing Mouse Skin.' *Development (Cambridge, England)* 136 (13): 2153–64. https://doi.org/10.1242/dev.031427.

Ridley, A. J. 2003. 'Cell Migration: Integrating Signals from Front to Back'. *Science* 302 (5651): 1704–9. https://doi.org/10.1126/science.1092053.

RITTY, Timothy M., Thomas J. BROEKELMANN, Claudio C. WERNECK, and Robert P. MECHAM. 2003. 'Fibrillin-1 and −2 Contain Heparin-Binding Sites Important for Matrix Deposition and That Support Cell Attachment'. *Biochemical Journal* 375 (2): 425–32. https://doi.org/10.1042/bj20030649.

Robertson, Ian B., Masahito Horiguchi, Lior Zilberberg, Branka Dabovic, Krassimira Hadjiolova, and Daniel B. Rifkin. 2015. 'Latent TGF-β-Binding Proteins'. *Matrix Biology* 47 (September): 44–53. https://doi.org/10.1016/J.MATBIO.2015.05.005.

Rocha-Azevedo, Bruno da, Frederick Grinnell, W. Matthew Petroll, Kristen Billiar, Bruno da Rocha-Azevedo, and Frederick Grinnell. 2013. 'Fibroblast Morphogenesis on 3D Collagen Matrices: The Balance between Cell Clustering and Cell Migration'. *Experimental Cell Research* 319 (16): 2440–46. https://doi.org/10.1016/j.yexcr.2013.05.003.

Rocha-Azevedo, Bruno da, Chin-Han Ho, and Frederick Grinnell. 2013. 'Fibroblast Cluster Formation on 3D Collagen Matrices Requires Cell Contraction Dependent Fibronectin Matrix Organization'. *Experimental Cell Research* 319 (4): 546–55.

Rodríguez-Berriguete, Gonzalo, Norelia Torrealba, Benito Fraile, Ricardo Paniagua, and Mar Royuela. 2016. 'Epidermal Growth Factor Induces P38 MAPK-Dependent G0/G1-to-S Transition in Prostate Cancer Cells upon Androgen Deprivation Conditions'. *Growth Factors* 34 (1–2): 5–10. https://doi.org/10.3109/08977194.2015.1132712.

Roeder, Blayne A., Klod Kokini, Jennifer E. Sturgis, J. Paul Robinson, and Sherry L. Voytik-Harbin. 2002. 'Tensile Mechanical Properties of Three-Dimensional Type I Collagen Extracellular Matrices With Varied Microstructure'. *Journal of*

Biomechanical Engineering 124 (2): 214. https://doi.org/10.1115/1.1449904.

Rompolas, Panteleimon, and Valentina Greco. 2013. 'Stem Cell Dynamics in the Hair Follicle Niche.' *Seminars in Cell & Developmental Biology*, December. https://doi.org/10.1016/j.semcdb.2013.12.005.

Rompolas, Panteleimon, Kailin R Mesa, and Valentina Greco. 2013. 'Spatial Organization within a Niche as a Determinant of Stem-Cell Fate.' *Nature* 502 (7472): 513–18. https://doi.org/10.1038/nature12602.

Ropero, Santiago, and Manel Esteller. 2007. 'The Role of Histone Deacetylases (HDACs) in Human Cancer'. *Molecular Oncology* 1 (1): 19–25. https://doi.org/10.1016/j.molonc.2007.01.001.

Roth, Shmuel, and Isaac Freund. 1979. 'Second Harmonic Generation in Collagen'. *The Journal of Chemical Physics* 70 (4): 1637–43. https://doi.org/10.1063/1.437677.

Rouillard, Andrew D, and Jeffrey W Holmes. 2012. 'Mechanical Regulation of Fibroblast Migration and Collagen Remodelling in Healing Myocardial Infarcts.' *The Journal of Physiology* 590 (Pt 18): 4585–4602. https://doi.org/10.1113/jphysiol.2012.229484.

Ruiz, Pedro A, and Gabor Jarai. 2011. 'Collagen I Induces Discoidin Domain Receptor (DDR) 1 Expression through DDR2 and a JAK2-ERK1/2-Mediated Mechanism in Primary Human Lung Fibroblasts.' *The Journal of Biological Chemistry* 286 (15): 12912–23. https://doi.org/10.1074/jbc.M110.143693.

Russell, D. 2004. 'Mechanical Stress Induces Profound Remodelling of Keratin Filaments and Cell Junctions in Epidermolysis Bullosa Simplex Keratinocytes'. *Journal of Cell Science* 117 (22): 5233–43. https://doi.org/10.1242/jcs.01407.

Ryle, Cathy M., Dirk Breitkreutz, Hanz-Jurgen Stark, Norbert E. Fusening, Irene M. Leigh, Peter M. Stelnert, and Dennis Roop. 1989. 'Density-Dependent Modulation of Synthesis of Keratins 1 and 10 in the Human Keratinocyte Line HACAT and in Ras-Transfected Tumorigenic Clones'. *Differentiation* 40 (1): 42–54. https://doi.org/10.1111/j.1432-0436.1989.tb00812.x.

Sabapathy, Kanaga, Konrad Hochedlinger, Shin Yuen Nam, Anton Bauer, Michael

Karin, and Erwin F. Wagner. 2004. ‘Distinct Roles for JNK1 and JNK2 in Regulating JNK Activity and C-Jun-Dependent Cell Proliferation’. *Molecular Cell* 15 (5): 713–25. https://doi.org/10.1016/J.MOLCEL.2004.08.028.

Sabatier, Laetitia, Daliang Chen, Christine Fagotto-Kaufmann, Dirk Hubmacher, Marc D. McKee, Douglas S. Annis, Deane F. Mosher, and Dieter P. Reinhardt. 2009. ‘Fibrillin Assembly Requires Fibronectin’. Edited by Jean E. Schwarzbauer. *Molecular Biology of the Cell* 20 (3): 846–58. https://doi.org/10.1091/mbc.e08-08-0830.

Sabatier, Laetitia, Nicolai Miosge, Dirk Hubmacher, Guoqing Lin, Elaine C Davis, and Dieter P Reinhardt. 2011. ‘Fibrillin-3 Expression in Human Development.’ *Matrix Biology : Journal of the International Society for Matrix Biology* 30 (1): 43–52. https://doi.org/10.1016/j.matbio.2010.10.003.

Samarakoon, Rohan, and Paul J. Higgins. 2018. ‘The Cytoskeletal Network Regulates Expression of the Profibrotic Genes PAI-1 and CTGF in Vascular Smooth Muscle Cells’. *Advances in Pharmacology* 81 (January): 79–94. https://doi.org/10.1016/BS.APHA.2017.08.006.

Santos, Mirentxu, Jesús M. Paramio, Ana Bravo, Angel Ramirez, and José L. Jorcano. 2002. ‘The Expression of Keratin K10 in the Basal Layer of the Epidermis Inhibits Cell Proliferation and Prevents Skin Tumorigenesis’. *Journal of Biological Chemistry* 277 (21): 19122–30. https://doi.org/10.1074/jbc.M201001200.

Sassa, T, W W Richter, N Uda, M Suganuma, H Suguri, S Yoshizawa, M Hirota, and H Fujiki. 1989. ‘Apparent "Activation" of Protein Kinases by Okadaic Acid Class Tumor Promoters.’ *Biochemical and Biophysical Research Communications* 159 (3): 939–44.

Sawada, Y., K. Nakamura, K. Doi, K. Takeda, K. Tobiume, M. Saitoh, K. Morita, et al. 2001. ‘Rap1 Is Involved in Cell Stretching Modulation of P38 but Not ERK or JNK MAP Kinase’. *Journal of Cell Science* 114 (6).

Sawant, Mugdha, Nicole Schwarz, Reinhard Windoffer, Thomas M. Magin, Jan Krieger, Norbert Mücke, Boguslaw Obara, et al. 2018. ‘Threonine 150 Phosphorylation of Keratin 5 Is Linked to Epidermolysis Bullosa Simplex and

Regulates Filament Assembly and Cell Viability'. *Journal of Investigative Dermatology* 138 (3): 627–36. https://doi.org/10.1016/j.jid.2017.10.011.

Schaller, M D, J D Hildebrand, J D Shannon, J W Fox, R R Vines, and J T Parsons. 1994. 'Autophosphorylation of the Focal Adhesion Kinase, Pp125FAK, Directs SH2-Dependent Binding of Pp60src.' *Molecular and Cellular Biology* 14 (3): 1680–88. https://doi.org/10.1128/MCB.14.3.1680.

Schlaepfer, D D, M A Broome, and T Hunter. 1997. 'Fibronectin-Stimulated Signaling from a Focal Adhesion Kinase-c-Src Complex: Involvement of the Grb2, P130cas, and Nck Adaptor Proteins.' *Molecular and Cellular Biology* 17 (3): 1702–13. https://doi.org/10.1128/MCB.17.3.1702.

Schlaepfer, D D, and T Hunter. 1997. 'Focal Adhesion Kinase Overexpression Enhances Ras-Dependent Integrin Signaling to ERK2/Mitogen-Activated Protein Kinase through Interactions with and Activation of c-Src.' *The Journal of Biological Chemistry* 272 (20): 13189–95. https://doi.org/10.1074/JBC.272.20.13189.

Schlaepfer, D D, K C Jones, T Hunter, G. van Willigen, H. K. Nieuwenhuis, C. Negrier, J. W. Akkerman, and J. L. Bos. 1998. 'Multiple Grb2-Mediated Integrin-Stimulated Signaling Pathways to ERK2/Mitogen-Activated Protein Kinase: Summation of Both c-Src- and Focal Adhesion Kinase-Initiated Tyrosine Phosphorylation Events.' *Molecular and Cellular Biology* 18 (5): 2571–85. https://doi.org/10.1128/mcb.20.3.779-785.2000.

Schlaepfer, David D., Steven K. Hanks, Tony Hunter, and Peter van der Geer. 1994. 'Integrin-Mediated Signal Transduction Linked to Ras Pathway by GRB2 Binding to Focal Adhesion Kinase'. *Nature* 372 (6508): 786–91. https://doi.org/10.1038/372786a0.

Schlaepfer, David D., and Tony Hunter. 1997. 'Focal Adhesion Kinase Overexpression Enhances Ras-Dependent Integrin Signaling to ERK2/Mitogen-Activated Protein Kinase through Interactions with and Activation of c-Src'. *Journal of Biological Chemistry* 272 (20): 13189–95. https://doi.org/10.1074/jbc.272.20.13189.

Schmidt-Ullrich, Ruth, and Ralf Paus. 2005. 'Molecular Principles of Hair Follicle

Induction and Morphogenesis.' *BioEssays : News and Reviews in Molecular, Cellular and Developmental Biology* 27 (3): 247–61. https://doi.org/10.1002/bies.20184.

Schneider, Maria, Angelika A Noegel, and Iakowos Karakesisoglou. 2008. 'KASH-Domain Proteins and the Cytoskeletal Landscapes of the Nuclear Envelope.' *Biochemical Society Transactions* 36 (Pt 6): 1368–72. https://doi.org/10.1042/BST0361368.

Schönthal, A H. 1998. 'Role of PP2A in Intracellular Signal Transduction Pathways.' *Frontiers in Bioscience : A Journal and Virtual Library* 3 (December): D1262-73.

Schönthal, Axel H. 1995. 'Regulation of Gene Expression by Serine/Threonine Protein Phosphatases'. *Seminars in Cancer Biology* 6 (4): 239–48. https://doi.org/10.1006/scbi.1995.0031.

Schrader, Jörg, Timothy T. Gordon-Walker, Rebecca L. Aucott, Mariëlle van Deemter, Alexander Quaas, Shaun Walsh, Daniel Benten, Stuart J. Forbes, Rebecca G. Wells, and John P. Iredale. 2011. 'Matrix Stiffness Modulates Proliferation, Chemotherapeutic Response, and Dormancy in Hepatocellular Carcinoma Cells'. *Hepatology* 53 (4): 1192–1205. https://doi.org/10.1002/hep.24108.

Schulze, A, K Zerfass-Thome, J Bergès, S Middendorp, P Jansen-Dürr, and B Henglein. 1996. 'Anchorage-Dependent Transcription of the Cyclin A Gene.' *Molecular and Cellular Biology* 16 (9): 4632–38. https://doi.org/10.1128/MCB.16.9.4632.

SCOTT, E J VAN, and T M EKEL. 1958. 'Geometric Relationships between the Matrix of the Hair Bulb and Its Dermal Papilla in Normal and Alopecic Scalp.' *The Journal of Investigative Dermatology* 31 (5): 281–87.

'Second Harmonic Generation'. 1990.

Seltmann, Kristin, Wera Roth, Cornelia Kröger, Fanny Loschke, Marcell Lederer, Stefan Hüttelmaier, and Thomas M. Magin. 2013. 'Keratins Mediate Localization of Hemidesmosomes and Repress Cell Motility'. *Journal of*

Investigative Dermatology 133 (1): 181–90. https://doi.org/10.1038/JID.2012.256.

Sengel, P, and A Mauger. 1976. 'Peridermal Cell Patterning in the Feather-Forming Skin of the Chick Embryo.' *Developmental Biology* 51 (1): 166–71.

Shadwick, R E. 1990. 'Elastic Energy Storage in Tendons: Mechanical Differences Related to Function and Age.' *Journal of Applied Physiology (Bethesda, Md. : 1985)* 68 (3): 1033–40.

Sharma, Guru-Dutt, Jiucheng He, and Haydee E. P. Bazan. 2003. 'P38 and ERK1/2 Coordinate Cellular Migration and Proliferation in Epithelial Wound Healing'. *Journal of Biological Chemistry* 278 (24): 21989–97. https://doi.org/10.1074/JBC.M302650200.

Sheen, Yi-Shuan, Sabrina Mai-Yi Fan, Chih-Chieh Chan, Yueh-Feng Wu, Shiou-Hwa Jee, and Sung-Jan Lin. 2015. 'Visible Red Light Enhances Physiological Anagen Entry in Vivo and Has Direct and Indirect Stimulative Effects in Vitro'. *Lasers in Surgery and Medicine* 47 (1): 50–59. https://doi.org/10.1002/lsm.22316.

Sheppard, C., J. Gannaway, R. Kompfner, and D. Walsh. 1977. 'The Scanning Harmonic Optical Microscope'. *IEEE Journal of Quantum Electronics* 13 (9): 912–912. https://doi.org/10.1109/JQE.1977.1069615.

Shi, Y, F Nikulenkov, J Zawacka-Pankau, H Li, R Gabdoulline, J Xu, S Eriksson, et al. 2014. 'ROS-Dependent Activation of JNK Converts P53 into an Efficient Inhibitor of Oncogenes Leading to Robust Apoptosis'. *Cell Death & Differentiation* 21 (4): 612–23. https://doi.org/10.1038/cdd.2013.186.

Silva, Flavia Amoroso Matos e, Katia Klug, Claudia Malheiros Coutinho-Camillo, Luiz Paulo Kowalski, and Fernando Augusto Soares. 2018. 'Abstract A036: DDR2 Expression Is Associated with Poor Prognosis in Head and Neck Squamous Cell Carcinoma'. *Molecular Cancer Therapeutics* 17 (1 Supplement): A036–A036. https://doi.org/10.1158/1535-7163.targ-17-a036.

Snippert, Hugo J, Andrea Haegebarth, Maria Kasper, Viljar Jaks, Johan H van Es, Nick Barker, Marc van de Wetering, et al. 2010. 'Lgr6 Marks Stem Cells in the Hair Follicle That Generate All Cell Lineages of the Skin.' *Science (New York,*

N.Y.) 327 (5971): 1385–89. https://doi.org/10.1126/science.1184733.

So, Peter T C, Chen Y Dong, Barry R Masters, and Keith M Berland. 2000. 'TWO-PHOTON EXCITATION FLUORESCENCE MICROSCOPY'.

Solovei, Irina, Audrey S. Wang, Katharina Thanisch, Christine S. Schmidt, Stefan Krebs, Monika Zwerger, Tatiana V. Cohen, et al. 2013. 'LBR and Lamin A/C Sequentially Tether Peripheral Heterochromatin and Inversely Regulate Differentiation'. *Cell* 152 (3): 584–98. https://doi.org/10.1016/J.CELL.2013.01.009.

Song, Liang-Li, Yan Cui, Si-Jiu Yu, Peng-Gang Liu, Jun Liu, Xue Yang, Jun-Feng He, and Qian Zhang. 2018. 'Expression Characteristics of BMP2, BMPR-IA and Noggin in Different Stages of Hair Follicle in Yak Skin'. *General and Comparative Endocrinology* 260 (May): 18–24. https://doi.org/10.1016/J.YGCEN.2017.11.016.

Sosa, Brian A., Andrea Rothballer, Ulrike Kutay, and Thomas U. Schwartz. 2012. 'LINC Complexes Form by Binding of Three KASH Peptides to Domain Interfaces of Trimeric SUN Proteins'. *Cell* 149 (5): 1035–47. https://doi.org/10.1016/J.CELL.2012.03.046.

Soucy, Patricia A., and Lewis H. Romer. 2009. 'Endothelial Cell Adhesion, Signaling, and Morphogenesis in Fibroblast-Derived Matrix'. *Matrix Biology* 28 (5): 273–83.

Spinardi, L, Y L Ren, R Sanders, and F G Giancotti. 1993. 'The Beta 4 Subunit Cytoplasmic Domain Mediates the Interaction of Alpha 6 Beta 4 Integrin with the Cytoskeleton of Hemidesmosomes.' *Molecular Biology of the Cell* 4 (9): 871–84. https://doi.org/10.1091/mbc.4.9.871.

Stark, Hans-Jürgen, Michael J Willhauck, Nicolae Mirancea, Karsten Boehnke, Iris Nord, Dirk Breitkreutz, Alessandra Pavesio, Petra Boukamp, and Norbert E Fusenig. 2004. 'Authentic Fibroblast Matrix in Dermal Equivalents Normalises Epidermal Histogenesis and Dermoepidermal Junction in Organotypic Co-Culture.' *European Journal of Cell Biology* 83 (11–12): 631–45. https://doi.org/10.1078/0171-9335-00435.

Starr, D. A. 2003. ‘ANChors Away: An Actin Based Mechanism of Nuclear Positioning’. *Journal of Cell Science* 116 (2): 211–16. https://doi.org/10.1242/jcs.00248.

Starr, D A, G J Hermann, C J Malone, W Fixsen, J R Priess, H R Horvitz, and M Han. 2001. ‘Unc-83 Encodes a Novel Component of the Nuclear Envelope and Is Essential for Proper Nuclear Migration.’ *Development (Cambridge, England)* 128 (24): 5039–50.

Starr, Daniel A., and Heidi N. Fridolfsson. 2010. ‘Interactions Between Nuclei and the Cytoskeleton Are Mediated by SUN-KASH Nuclear-Envelope Bridges’. *Annual Review of Cell and Developmental Biology* 26 (1): 421–44. https://doi.org/10.1146/annurev-cellbio-100109-104037.

Starr, Daniel A. 2011. ‘KASH and SUN Proteins.’ *Current Biology : CB* 21 (11): R414-5. https://doi.org/10.1016/j.cub.2011.04.022.

Stenn, K S, N J Combates, K J Eilertsen, J S Gordon, J R Pardinas, S Parimoo, and S M Prouty. 1996. ‘Hair Follicle Growth Controls.’ *Dermatologic Clinics* 14 (4): 543–58.

Sterk, L M, C A Geuijen, L C Oomen, J Calafat, H Janssen, and A Sonnenberg. 2000. ‘The Tetraspan Molecule CD151, a Novel Constituent of Hemidesmosomes, Associates with the Integrin Alpha6beta4 and May Regulate the Spatial Organization of Hemidesmosomes.’ *The Journal of Cell Biology* 149 (4): 969–82. https://doi.org/10.1083/JCB.149.4.969.

Sterk, Lotus M.Th., Cecile A.W. Geuijen, Lauran C.J.M. Oomen, Jero Calafat, Hans Janssen, and Arnoud Sonnenberg. 2000. ‘The Tetraspan Molecule Cd151, a Novel Constituent of Hemidesmosomes, Associates with the Integrin A6β4 and May Regulate the Spatial Organization of Hemidesmosomes’. *The Journal of Cell Biology* 149 (4): 969–82. https://doi.org/10.1083/jcb.149.4.969.

Stick, Reimer, and Martin W Goldberg. 2010. ‘Oocytes as an Experimental System to Analyze the Ultrastructure of Endogenous and Ectopically Expressed Nuclear Envelope Components by Field-Emission Scanning Electron Microscopy.’ *Methods (San Diego, Calif.)* 51 (1): 170–76. https://doi.org/10.1016/j.ymeth.2010.01.015.

Stoll, Stefan W., Sanjay Kansra, and James T. Elder. 2003. 'Keratinocyte Outgrowth from Human Skin Explant Cultures Is Dependent upon P38 Signaling'. *Wound Repair and Regeneration* 11 (5): 346–53. https://doi.org/10.1046/j.1524-475X.2003.11506.x.

Su, Ping Jung, Wei Liang Chen, Yang Fang Chen, and Chen Yuan Dong. 2011. 'Determination of Collagen Nanostructure from Second-Order Susceptibility Tensor Analysis'. *Biophysical Journal* 100 (8): 2053–62. https://doi.org/10.1016/j.bpj.2011.02.015.

Su, Yi-Xun, Cong-Cong Hou, and Wan-Xi Yang. 2014. 'Control of Hair Cell Development by Molecular Pathways Involving Atoh1, Hes1 and Hes5.' *Gene*, December. https://doi.org/10.1016/j.gene.2014.12.054.

Sun, Yu, Wen-Zhou Liu, Tao Liu, Xu Feng, Nuo Yang, and Hua-Fu Zhou. 2015. 'Signaling Pathway of MAPK/ERK in Cell Proliferation, Differentiation, Migration, Senescence and Apoptosis'. *Journal of Receptors and Signal Transduction* 35 (6): 600–604. https://doi.org/10.3109/10799893.2015.1030412.

Swift, J., I. L. Ivanovska, A. Buxboim, T. Harada, P. C. D. P. Dingal, J. Pinter, J. D. Pajerowski, et al. 2013. 'Nuclear Lamin-A Scales with Tissue Stiffness and Enhances Matrix-Directed Differentiation'. *Science* 341 (6149): 1240104–1240104. https://doi.org/10.1126/science.1240104.

Takeda, Masafumi, Masafumi Mizuide, Masako Oka, Tetsuro Watabe, Hirofumi Inoue, Hiroyuki Suzuki, Toshiro Fujita, Takeshi Imamura, Kohei Miyazono, and Keiji Miyazawa. 2004. 'Interaction with Smad4 Is Indispensable for Suppression of BMP Signaling by C-Ski'. *Molecular Biology of the Cell* 15 (3): 963–72. https://doi.org/10.1091/mbc.e03-07-0478.

Takeo, Makoto, Wendy Lee, and Mayumi Ito. 2015. 'Wound Healing and Skin Regeneration.' *Cold Spring Harbor Perspectives in Medicine* 5 (1): a023267. https://doi.org/10.1101/cshperspect.a023267.

Tamburro, Antonio M, Brigida Bochicchio, and Antonietta Pepe. 2003. 'Dissection of Human Tropoelastin: Exon-by-Exon Chemical Synthesis and Related Conformational Studies.' *Biochemistry* 42 (45): 13347–62. https://doi.org/10.1021/bi034837t.

Tan, Qi, Huan Yang, Enmei Liu, and Hua Wang. 2017. ‘P38/ERK MAPK Signaling Pathways Are Involved in the Regulation of Filaggrin and Involucrin by IL-17’. *Molecular Medicine Reports* 16 (6): 8863–67. https://doi.org/10.3892/mmr.2017.7689.

Tapon, Nicolas, and Alan Hall. 1997. ‘Rho, Rac and Cdc42 GTPases Regulate the Organization of the Actin Cytoskeleton’. *Current Opinion in Cell Biology* 9 (1): 86–92. https://doi.org/10.1016/S0955-0674(97)80156-1.

Tausche, Anne-Kathrin, Mouna Skaria, Lorenz Bohlen, Kristin Liebold, Jurg Hafner, Helmut Friedlein, Michael Meurer, et al. 2003. ‘An Autologous Epidermal Equivalent Tissue-Engineered from Follicular Outer Root Sheath Keratinocytes Is as Effective as Split-Thickness Skin Autograft in Recalcitrant Vascular Leg Ulcers’. *Wound Repair and Regeneration* 11 (4): 248–52. https://doi.org/10.1046/j.1524-475X.2003.11403.x.

Thoreson, MA, PZ Anastasiadis, JM Daniel, RC Ireton - J Cell Biol, and Undefined 2000. 2000. ‘Selective Uncoupling of P120ctn from E-Cadherin Disrupts Strong Adhesion’. *Jcb.Rupress.Org*.

Tiaho, F, G Recher, D Rouède - Optics express, and undefined 2007. n.d. ‘Estimation of Helical Angles of Myosin and Collagen by Second Harmonic Generation Imaging Microscopy’. *Osapublishing.Org*.

Tilbury, Karissa, James Hocker, Bruce L Wen, Nathan Sandbo, Vikas Singh, and Paul J Campagnola. 2014. ‘Second Harmonic Generation Microscopy Analysis of Extracellular Matrix Changes in Human Idiopathic Pulmonary Fibrosis.’ *Journal of Biomedical Optics* 19 (8): 86014. https://doi.org/10.1117/1.JBO.19.8.086014.

Toivola, Diana M, Guo-Zhong Tao, Aida Habtezion, Jian Liao, and M Bishr Omary. 2005. ‘Cellular Integrity plus: Organelle-Related and Protein-Targeting Functions of Intermediate Filaments.’ *Trends in Cell Biology* 15 (11): 608–17. https://doi.org/10.1016/j.tcb.2005.09.004.

Treinies, I, H F Paterson, S Hooper, R Wilson, and C J Marshall. 1999. ‘Activated MEK Stimulates Expression of AP-1 Components Independently of Phosphatidylinositol 3-Kinase (PI3-Kinase) but Requires a PI3-Kinase Signal To Stimulate DNA Synthesis.’ *Mol. Cell. Biol.* 19 (1): 321–29.

https://doi.org/10.1128/MCB.19.1.321.

Treisman, Richard. 1996. ‘Regulation of Transcription by MAP Kinase Cascades.’ *Curr. Opin. Cell Biol.* 8 (2): 205–15. https://doi.org/10.1016/S0955-0674(96)80067-6.

Tsai, Su-Yi, Rachel Sennett, Amélie Rezza, Carlos Clavel, Laura Grisanti, Roland Zemla, Sara Najam, and Michael Rendl. 2014. ‘Wnt/β-Catenin Signaling in Dermal Condensates Is Required for Hair Follicle Formation.’ *Developmental Biology* 385 (2): 179–88. https://doi.org/10.1016/j.ydbio.2013.11.023.

Tscharntke, M., R. Pofahl, A. Chrostek-Grashoff, N. Smyth, C. Niessen, C. Niemann, B. Hartwig, et al. 2007. ‘Impaired Epidermal Wound Healing in Vivo upon Inhibition or Deletion of Rac1’. *Journal of Cell Science* 120 (8): 1480–90. https://doi.org/10.1242/jcs.03426.

Tsuruta, Daisuke, Takashi Hashimoto, Kevin J. Hamill, and Jonathan C.R. Jones. 2011. ‘Hemidesmosomes and Focal Contact Proteins: Functions and Cross-Talk in Keratinocytes, Bullous Diseases and Wound Healing’. *Journal of Dermatological Science* 62 (1): 1–7. https://doi.org/10.1016/j.jdermsci.2011.01.005.

Tsuruta, Daisuke, Susan B. Hopkinson, and Jonathan C.R. Jones. 2003a. ‘Hemidesmosome Protein Dynamics in Live Epithelial Cells’. *Cell Motility and the Cytoskeleton* 54 (2): 122–34. https://doi.org/10.1002/cm.10089.

———. 2003b. ‘Hemidesmosome Protein Dynamics in Live Epithelial Cells’. *Cell Motility and the Cytoskeleton* 54 (2): 122–34. https://doi.org/10.1002/cm.10089.

Tu, Yiping, Sofía Sánchez-Iglesias, David Araújo-Vilar, Loren G. Fong, and Stephen G. Young. 2016. ‘*LMNA* Missense Mutations Causing Familial Partial Lipodystrophy Do Not Lead to an Accumulation of Prelamin A’. *Nucleus* 7 (5): 512–21. https://doi.org/10.1080/19491034.2016.1242542.

Tzaphlidou, Margaret. 2004. ‘The Role of Collagen and Elastin in Aged Skin: An Image Processing Approach.’ *Micron (Oxford, England : 1993)* 35 (3): 173–77. https://doi.org/10.1016/j.micron.2003.11.003.

Vaezi, A, C Bauer, V Vasioukhin, E Fuchs - Developmental Cell, and Undefined

2002. 2002. ‘Actin Cable Dynamics and Rho/Rock Orchestrate a Polarized Cytoskeletal Architecture in the Early Steps of Assembling a Stratified Epithelium’. *Elsevier*.

Valencia, Rocio G., Gernot Walko, Lubomir Janda, Jirka Novacek, Eva Mihailovska, Siegfried Reipert, Kerstin Andrä-Marobela, and Gerhard Wiche. 2013. ‘Intermediate Filament-Associated Cytolinker Plectin 1c Destabilizes Microtubules in Keratinocytes’. Edited by Robert D. Goldman. *Molecular Biology of the Cell* 24 (6): 768–84. https://doi.org/10.1091/mbc.e12-06-0488.

Valente, Andrew J., Lucas A. Maddalena, Ellen L. Robb, Fereshteh Moradi, and Jeffrey A. Stuart. 2017. ‘A Simple ImageJ Macro Tool for Analyzing Mitochondrial Network Morphology in Mammalian Cell Culture’. *Acta Histochemica* 119 (3): 315–26. https://doi.org/10.1016/J.ACTHIS.2017.03.001.

Valle-Pérez, Beatriz del, David Casagolda, Ero Lugilde, Gabriela Valls, Montserrat Codina, Natàlia Dave, Antonio García de Herreros, and Mireia Duñach. 2016. ‘Wnt Controls the Transcriptional Activity of Kaiso through CK1ε-Dependent Phosphorylation of P120-Catenin.’ *Journal of Cell Science* 129 (4): 873. https://doi.org/10.1242/jcs.186288.

Vehviläinen, Piia, Marko Hyytiäinen, and Jorma Keski-Oja. 2009. ‘Matrix Association of Latent TGF-Beta Binding Protein-2 (LTBP-2) Is Dependent on Fibrillin-1’. *Journal of Cellular Physiology* 221 (3): 586–93. https://doi.org/10.1002/jcp.21888.

Versaevel, Marie, Thomas Grevesse, and Sylvain Gabriele. 2012. ‘Spatial Coordination between Cell and Nuclear Shape within Micropatterned Endothelial Cells’. *Nature Communications* 3 (1): 671. https://doi.org/10.1038/ncomms1668.

Vidal, Valerie P.I., Marie-Christine Chaboissier, Susanne Lützkendorf, George Cotsarelis, Pleasantine Mill, Chi-Chung Hui, Nicolas Ortonne, Jean-Paul Ortonne, and Andreas Schedl. 2005. ‘Sox9 Is Essential for Outer Root Sheath Differentiation and the Formation of the Hair Stem Cell Compartment’. *Current Biology* 15 (15): 1340–51. https://doi.org/10.1016/J.CUB.2005.06.064.

Vielmuth, Franziska, Marie-Therès Wanuske, Mariya Y. Radeva, Matthias Hiermaier,

Daniela Kugelmann, Elias Walter, Fanny Buechau, Thomas M. Magin, Jens Waschke, and Volker Spindler. 2018. 'Keratins Regulate the Adhesive Properties of Desmosomal Cadherins through Signaling'. *Journal of Investigative Dermatology* 138 (1): 121–31. https://doi.org/10.1016/j.jid.2017.08.033.

Vielreicher, Martin, Monika Gellner, Ulrike Rottensteiner, Raymund E. Horch, Andreas Arkudas, and Oliver Friedrich. 2017. 'Multiphoton Microscopy Analysis of Extracellular Collagen I Network Formation by Mesenchymal Stem Cells'. *Journal of Tissue Engineering and Regenerative Medicine* 11 (7): 2104–15. https://doi.org/10.1002/term.2107.

Volk, T. 1992. 'A New Member of the Spectrin Superfamily May Participate in the Formation of Embryonic Muscle Attachments in Drosophila.' *Development (Cambridge, England)* 116 (3): 721–30.

Vollmar, B, A M El-Gibaly, C Scheuer, M W Strik, H-P Bruch, and M D Menger. 2002. 'Acceleration of Cutaneous Wound Healing by Transient P53 Inhibition'. *Laboratory Investigation* 82 (8): 1063–71. https://doi.org/10.1097/01.LAB.0000024363.37866.45.

Voorhees, Andrew P, Kristine Y DeLeon-Pennell, Yonggang Ma, Ganesh V Halade, Andriy Yabluchanskiy, Rugmani Padmanabhan Iyer, Elizabeth Flynn, Courtney A Cates, Merry L Lindsey, and Hai-Chao Han. 2015. 'Building a Better Infarct: Modulation of Collagen Cross-Linking to Increase Infarct Stiffness and Reduce Left Ventricular Dilation Post-Myocardial Infarction.' *Journal of Molecular and Cellular Cardiology* 85 (August): 229–39. https://doi.org/10.1016/j.yjmcc.2015.06.006.

Vouillarmet, Julien, and Martine Laville. 2016. 'A Case of Familial Partial Lipodystrophy: From Clinical Phenotype to Genetics'. *Canadian Journal of Diabetes* 40 (5): 376–78. https://doi.org/10.1016/j.jcjd.2015.12.007.

Vuori, K, H Hirai, S Aizawa, and E Ruoslahti. 1996. 'Introduction of P130cas Signaling Complex Formation upon Integrin-Mediated Cell Adhesion: A Role for Src Family Kinases.' *Molecular and Cellular Biology* 16 (6): 2606–13. https://doi.org/10.1128/MCB.16.6.2606.

Waikel, R L, Y Kawachi, P A Waikel, X J Wang, and D R Roop. 2001. 'Deregulated

Expression of C-Myc Depletes Epidermal Stem Cells.' *Nature Genetics* 28 (2): 165–68. https://doi.org/10.1038/88889.

Walko, Gernot, Maria J Castañón, and Gerhard Wiche. 2015. 'Molecular Architecture and Function of the Hemidesmosome.' *Cell and Tissue Research* 360 (2): 363–78. https://doi.org/10.1007/s00441-014-2061-z.

Wang, Ju Guang, Motoi Miyazu, Peng Xiang, Shu Nong Li, Masahiro Sokabe, and Keiji Naruse. 2005. 'Stretch-Induced Cell Proliferation Is Mediated by FAK-MAPK Pathway.' *Life Sciences* 76 (24): 2817–25. https://doi.org/10.1016/j.lfs.2004.10.050.

Wang, Ning, Jessica D. Tytell, and Donald E. Ingber. 2009. 'Mechanotransduction at a Distance: Mechanically Coupling the Extracellular Matrix with the Nucleus'. *Nature Reviews Molecular Cell Biology* 10 (1): 75–82. https://doi.org/10.1038/nrm2594.

Wang, Yu, Guixue Wang, Xiangdong Luo, Juhui Qiu, and Chaojun Tang. 2012. 'Substrate Stiffness Regulates the Proliferation, Migration, and Differentiation of Epidermal Cells'. *Burns* 38 (3): 414–20. https://doi.org/10.1016/j.burns.2011.09.002.

Wang, Zhiling, Pauline Wong, Lutz Langbein, Jürgen Schweizer, and Pierre A Coulombe. 2003. 'Type II Epithelial Keratin 6hf (K6hf) Is Expressed in the Companion Layer, Matrix, and Medulla in Anagen-Stage Hair Follicles.' *The Journal of Investigative Dermatology* 121 (6): 1276–82. https://doi.org/10.1111/j.1523-1747.2003.12644.x.

Wary, Kishore K, Fabrizio Mainiero, Steven J Isakoff, Eugene E Marcantonio, and Filippo G Giancotti. 1996. 'The Adaptor Protein Shc Couples a Class of Integrins to the Control of Cell Cycle Progression'. *Cell* 87 (4): 733–43. https://doi.org/10.1016/S0092-8674(00)81392-6.

Wary, Kishore K, Agnese Mariotti, Chiara Zurzolo, and Filippo G Giancotti. 1998. 'A Requirement for Caveolin-1 and Associated Kinase Fyn in Integrin Signaling and Anchorage-Dependent Cell Growth'. *Cell* 94 (5): 625–34. https://doi.org/10.1016/S0092-8674(00)81604-9.

Wasserman, Jonathan D, Matthew Freeman, and F Matthew. 1998. ‘An Autoregulatory Cascade of EGF Receptor Signaling Patterns the Drosophila Egg.’ *Cell* 95 (3): 355–64. https://doi.org/10.1016/S0092-8674(00)81767-5.

Watt, Fiona M. 1983. ‘Involucrin and Other Markers of Keratinocyte Terminal Differentiation’. *Journal of Investigative Dermatology* 81 (1): S100–103. https://doi.org/10.1111/1523-1747.EP12540786.

Watt, Fiona M. 2002. ‘Role of Integrins in Regulating Epidermal Adhesion, Growth and Differentiation.’ *The EMBO Journal* 21 (15): 3919–26. https://doi.org/10.1093/emboj/cdf399.

Wei, Spencer C., Laurent Fattet, Jeff H. Tsai, Yurong Guo, Vincent H. Pai, Hannah E. Majeski, Albert C. Chen, et al. 2015. ‘Matrix Stiffness Drives Epithelial–Mesenchymal Transition and Tumour Metastasis through a TWIST1–G3BP2 Mechanotransduction Pathway’. *Nature Cell Biology* 17 (5): 678–88. https://doi.org/10.1038/ncb3157.

Wei, Y, X Yang, Q Liu, J A Wilkins, and H A Chapman. 1999. ‘A Role for Caveolin and the Urokinase Receptor in Integrin-Mediated Adhesion and Signaling.’ *The Journal of Cell Biology* 144 (6): 1285–94. https://doi.org/10.1083/JCB.144.6.1285.

Wen, Jessica H., Ludovic G. Vincent, Alexander Fuhrmann, Yu Suk Choi, Kolin C. Hribar, Hermes Taylor-Weiner, Shaochen Chen, and Adam J. Engler. 2014. ‘Interplay of Matrix Stiffness and Protein Tethering in Stem Cell Differentiation’. *Nature Materials* 13 (10): 979–87. https://doi.org/10.1038/nmat4051.

Werner, S, H Smola, X Liao, M T Longaker, T Krieg, P H Hofschneider, and L T Williams. 1994. ‘The Function of KGF in Morphogenesis of Epithelium and Reepithelialization of Wounds.’ *Science (New York, N.Y.)* 266 (5186): 819–22.

Werner, Sabine, and Hans Smola. 2001. ‘Paracrine Regulation of Keratinocyte Proliferation and Differentiation’. *Trends in Cell Biology* 11 (4): 143–46. https://doi.org/10.1016/S0962-8924(01)01955-9.

Wess, T.J. J. 2005. ‘Collagen Fibril Form and Function.’ *Advances in Protein*

Chemistry 70 (January): 341–74. https://doi.org/10.1016/S0065-3233(05)70010-3.

Westwick, J K, Q T Lambert, G J Clark, M Symons, L Van Aelst, R G Pestell, and C J Der. 1997. 'Rac Regulation of Transformation, Gene Expression, and Actin Organization by Multiple, PAK-Independent Pathways.' *Molecular and Cellular Biology* 17 (3): 1324–35. https://doi.org/10.1128/MCB.17.3.1324.

Wilhelmsen, Kevin, Sandy H M Litjens, Ingrid Kuikman, Ntambua Tshimbalanga, Hans Janssen, Iman van den Bout, Karine Raymond, and Arnoud Sonnenberg. 2005. 'Nesprin-3, a Novel Outer Nuclear Membrane Protein, Associates with the Cytoskeletal Linker Protein Plectin.' *The Journal of Cell Biology* 171 (5): 799–810. https://doi.org/10.1083/jcb.200506083.

Williams, Rebecca M., Warren R. Zipfel, and Watt W. Webb. 2005. 'Interpreting Second-Harmonic Generation Images of Collagen I Fibrils'. *Biophysical Journal* 88 (2): 1377–86. https://doi.org/10.1529/BIOPHYSJ.104.047308.

Winter, H, L Langbein, S Praetzel, M Jacobs, M A Rogers, I M Leigh, N Tidman, and J Schweizer. 1998. 'A Novel Human Type II Cytokeratin, K6hf, Specifically Expressed in the Companion Layer of the Hair Follicle.' *The Journal of Investigative Dermatology* 111 (6): 955–62. https://doi.org/10.1046/j.1523-1747.1998.00456.x.

Winzen, R. 1999. 'The P38 MAP Kinase Pathway Signals for Cytokine-Induced MRNA Stabilization via MAP Kinase-Activated Protein Kinase 2 and an AU-Rich Region-Targeted Mechanism.' *Embo J.* 19: 6742–53.

Wong, Pauline, and Pierre A. Coulombe. 2003. 'Loss of Keratin 6 (K6) Proteins Reveals a Function for Intermediate Filaments during Wound Repair'. *The Journal of Cell Biology* 163 (2): 327–37. https://doi.org/10.1083/jcb.200305032.

Wong, Xianrong, Teresa R Luperchio, and Karen L Reddy. 2014. 'NET Gains and Losses: The Role of Changing Nuclear Envelope Proteomes in Genome Regulation'. *Current Opinion in Cell Biology* 28 (June): 105–20. https://doi.org/10.1016/J.CEB.2014.04.005.

Wu, Geng, He Huang, Jose Garcia Abreu, and Xi He. 2009. 'Inhibition of GSK3

Phosphorylation of β-Catenin via Phosphorylated PPPSPXS Motifs of Wnt Coreceptor LRP6'. Edited by Dong-Yan Jin. *PLoS ONE* 4 (3): e4926. https://doi.org/10.1371/journal.pone.0004926.

Wu, Xian-Jie, Jian-Wei Zhu, Jing Jing, Dan Xue, Hai Liu, Min Zheng, and Zhong-Fa Lu. 2014. 'VEGF165 Modulates Proliferation, Adhesion, Migration and Differentiation of Cultured Human Outer Root Sheath Cells from Central Hair Follicle Epithelium through VEGFR-2 Activation in Vitro.' *Journal of Dermatological Science* 73 (2): 152–60. https://doi.org/10.1016/j.jdermsci.2013.10.002.

Wu, Xunwei, Fabio Quondamatteo, Tine Lefever, Aleksandra Czuchra, Hannelore Meyer, Anna Chrostek, Ralf Paus, Lutz Langbein, and Cord Brakebusch. 2006. 'Cdc42 Controls Progenitor Cell Differentiation and Beta-Catenin Turnover in Skin.' *Genes & Development* 20 (5): 571–85. https://doi.org/10.1101/gad.361406.

Xing, YiZhan, Wei Xu, Ke Yang, XiaoHua Lian, and Tian Yang. 2011. 'Immunolocalization of Wnt5a during the Hair Cycle and Its Role in Hair Shaft Growth in Mice'. *Acta Histochemica* 113 (6): 608–12.

Xu, Guang-Kui, Chun Yang, Jing Du, and Xi-Qiao Feng. 2014. 'Integrin Activation and Internalization Mediated by Extracellular Matrix Elasticity: A Biomechanical Model.' *Journal of Biomechanics*, January. https://doi.org/10.1016/j.jbiomech.2014.01.022.

Yadin, David A., Ian B. Robertson, Joanne McNaught-Davis, Paul Evans, David Stoddart, Penny A. Handford, Sacha A. Jensen, and Christina Redfield. 2013. 'Structure of the Fibrillin-1 N-Terminal Domains Suggests That Heparan Sulfate Regulates the Early Stages of Microfibril Assembly'. *Structure* 21 (10): 1743–56. https://doi.org/10.1016/j.str.2013.08.004.

Yamao, Mikaru, Mutsumi Inamatsu, Taro Okada, Yuko Ogawa, Chise Tateno, and Katsutoshi Yoshizato. 2015. 'Enhanced Restoration of in Situ-Damaged Hairs by Intradermal Transplantation of Trichogenous Dermal Cells.' *Journal of Tissue Engineering and Regenerative Medicine*, February. https://doi.org/10.1002/term.1997.

Yang, Leilei, Lijuan Wang, and Xiao Yang. 2009. ‘Disruption of Smad4 in Mouse Epidermis Leads to Depletion of Follicle Stem Cells’. Edited by Jonathan Chernoff. *Molecular Biology of the Cell* 20 (3): 882–90. https://doi.org/10.1091/mbc.e08-07-0731.

Yano, Shoichiro, Mayumi Komine, Manabu Fujimoto, Hitoshi Okochi, and Kunihiko Tamaki. 2004. ‘Mechanical Stretching In Vitro Regulates Signal Transduction Pathways and Cellular Proliferation in Human Epidermal Keratinocytes’. *Journal of Investigative Dermatology* 122 (3): 783–90. https://doi.org/10.1111/J.0022-202X.2004.22328.X.

Yew, Elijah, Christopher Rowlands, and Peter T C So. 2014. ‘Application of Multiphoton Microscopy in Dermatological Studies: A Mini-Review.’ *Journal of Innovative Optical Health Sciences* 7 (5): 1330010. https://doi.org/10.1142/S1793545813300103.

Yu, Juehua, Daniel A. Starr, Xiaohui Wu, Susan M. Parkhurst, Yuan Zhuang, Tian Xu, Rener Xu, and Min Han. 2006. ‘The KASH Domain Protein MSP-300 Plays an Essential Role in Nuclear Anchoring during Drosophila Oogenesis’. *Developmental Biology* 289 (2): 336–45. https://doi.org/10.1016/j.ydbio.2005.10.027.

Yuryev, Mikhail, Dmitry Molotkov, and Leonard Khiroug. 2014. ‘In Vivo Two-Photon Microscopy of Single Nerve Endings in Skin.’ *Journal of Visualized Experiments : JoVE*, no. 90 (January). https://doi.org/10.3791/51045.

Zeltz, Cédric, and Donald Gullberg. 2016. ‘The Integrin-Collagen Connection--a Glue for Tissue Repair?’ *Journal of Cell Science* 129 (4): 653–64. https://doi.org/10.1242/jcs.180992.

Zenz, Rainer, Robert Eferl, Lukas Kenner, Lore Florin, Lars Hummerich, Denis Mehic, Harald Scheuch, Peter Angel, Erwin Tschachler, and Erwin F. Wagner. 2005a. ‘Psoriasis-like Skin Disease and Arthritis Caused by Inducible Epidermal Deletion of Jun Proteins’. *Nature* 437 (7057): 369–75. https://doi.org/10.1038/nature03963.

Zenz, Rainer, Robert Eferl, Lukas Kenner, Lore Florin, Lars Hummerich, Denis Mehic, Harald Scheuch, Peter Angel, Erwin Tschachler, and Erwin F Wagner.

2005b. ‘Psoriasis-like Skin Disease and Arthritis Caused by Inducible Epidermal Deletion of Jun Proteins.’ *Nature* 437 (7057): 369–75. https://doi.org/10.1038/nature03963.

Zhang, Jiwang, Xi C He, Wei-Gang Tong, Teri Johnson, Leanne M Wiedemann, Yuji Mishina, Jian Q Feng, and Linheng Li. 2006. ‘Bone Morphogenetic Protein Signaling Inhibits Hair Follicle Anagen Induction by Restricting Epithelial Stem/Progenitor Cell Activation and Expansion.’ *Stem Cells (Dayton, Ohio)* 24 (12): 2826–39. https://doi.org/10.1634/stemcells.2005-0544.

Zhang, Kai, Wei Ding, Wei Sun, Xiao-jiang Sun, You-zhuan Xie, Chang-qing Zhao, and Jie Zhao. 2016. ‘Beta1 Integrin Inhibits Apoptosis Induced by Cyclic Stretch in Annulus Fibrosus Cells via ERK1/2 MAPK Pathway’. *Apoptosis* 21 (1): 13–24. https://doi.org/10.1007/s10495-015-1180-7.

Zhang, Weitian, Addy Alt-Holland, Alexander Margulis, Yulia Shamis, Norbert E Fusenig, Ulrich Rodeck, and Jonathan A Garlick. 2006. ‘E-Cadherin Loss Promotes the Initiation of Squamous Cell Carcinoma Invasion through Modulation of Integrin-Mediated Adhesion.’ *Journal of Cell Science* 119 (Pt 2): 283–91. https://doi.org/10.1242/jcs.02738.

Zhang, Xiaochang, Rener Xu, Binggen Zhu, Xiujuan Yang, Xu Ding, Shumin Duan, Tian Xu, Yuan Zhuang, and Min Han. 2007. ‘Syne-1 and Syne-2 Play Crucial Roles in Myonuclear Anchorage and Motor Neuron Innervation.’ *Development (Cambridge, England)* 134 (5): 901–8. https://doi.org/10.1242/dev.02783.

Zhang, Yuhang, Thomas Andl, Steven H Yang, Monica Teta, Fei Liu, John T Seykora, John W Tobias, et al. 2008. ‘Activation of Beta-Catenin Signaling Programs Embryonic Epidermis to Hair Follicle Fate.’ *Development (Cambridge, England)* 135 (12): 2161–72. https://doi.org/10.1242/dev.017459.

Zhang, Zhiwen, Feng Wen, Chengjian He, and Jun Yu. 2018. ‘Resveratrol Attenuates Mechanical Compression-Induced Nucleus Pulposus Cell Apoptosis through Regulating the ERK1/2 Signaling Pathway in a Disc Organ Culture.’ *Bioscience Reports* 38 (2): BSR20171703. https://doi.org/10.1042/BSR20171703.

Zhao, Jian, Xuejun Yuan, Morten Frödin, and Ingrid Grummt. 2003. ‘ERK-Dependent Phosphorylation of the Transcription Initiation Factor TIF-IA Is

Required for RNA Polymerase I Transcription and Cell Growth'. *Molecular Cell* 11 (2): 405–13. https://doi.org/10.1016/S1097-2765(03)00036-4.

Zhu, X, M Ohtsubo, R M Böhmer, J M Roberts, and R K Assoian. 1996. 'Adhesion-Dependent Cell Cycle Progression Linked to the Expression of Cyclin D1, Activation of Cyclin E-Cdk2, and Phosphorylation of the Retinoblastoma Protein.' *The Journal of Cell Biology* 133 (2): 391–403. https://doi.org/10.1083/JCB.133.2.391.

Zoumi, Aikaterini, Xiao Lu, Ghassan S Kassab, and Bruce J Tromberg. 2004. 'Imaging Coronary Artery Microstructure Using Second-Harmonic and Two-Photon Fluorescence Microscopy.' *Biophysical Journal* 87 (4): 2778–86. https://doi.org/10.1529/biophysj.104.042887.

Zu, Y L, J Qi, A Gilchrist, G A Fernandez, D Vazquez-Abad, D L Kreutzer, C K Huang, and R I Sha'afi. 1998. 'P38 Mitogen-Activated Protein Kinase Activation Is Required for Human Neutrophil Function Triggered by TNF-Alpha or FMLP Stimulation.' *Journal of Immunology (Baltimore, Md. : 1950)* 160 (4): 1982–89.